

Palladium based catalysts for hydrogenation of various functional groups.

by

Kasabe Mirabai Madhukar
10CC17J26032

A thesis submitted to the
Academy of Scientific & Innovative Research
For the award of the degree of

DOCTOR OF PHILOSOPHY
in
SCIENCE

Under the supervision of
Dr. Shubhangi B. Umbarkar



CSIR-National Chemical Laboratory, Pune



Academy of Scientific and Innovative Research
AcSIR Headquarters, CSIR-HRDC campus
Sector 19, Kamla Nehru Nagar,
Ghaziabad, U.P. – 201 002, India

July 2023

Certificate

This is to certify that the work incorporated in this Ph.D. thesis entitled, "*Palladium based catalysts for hydrogenation of various functional groups.*", submitted by *Kasabe Mirabai Madhukar* to the Academy of Scientific and Innovative Research (AcSIR), in partial fulfillment of the requirements for the award of the Degree of *Doctor of Philosophy in Science*, embodies original research work carried-out by the student. We, further certify that this work has not been submitted to any other University or Institution in part or full for the award of any degree or diploma. Research material(s) obtained from other source(s) and used in this research work has/have been duly acknowledged in the thesis. Image(s), illustration(s), figure(s), table(s) etc., used in the thesis from other source(s), have also been duly cited and acknowledged.



Signature of the Student

Name : Kasabe Mirabai

Date : 28/07/2023

Place : Pune



Signature of the Supervisor

Name : S. B. Umbarkar

Date : 28/07/2023

Place : Pune

STATEMENTS OF ACADEMIC INTEGRITY


I Kasabe Mirabai Madhukar Ph.D. student of the Academy of Scientific and Innovative Research (AcSIR) with Registration No. 10CC17J26032 hereby undertake that, the thesis entitled “Palladium based catalysts for hydrogenation of various functional groups.” has been prepared by me and that the document reports original work carried out by me and is free of any plagiarism in compliance with the UGC Regulations on “*Promotion of Academic Integrity and Prevention of Plagiarism in Higher Educational Institutions (2018)*” and the CSIR Guidelines for “*Ethics in Research and in Governance (2020)*”.


Signature of the Student

Date : 28/07/2023

Place : Pune

It is hereby certified that the work done by the student, under my supervision, is plagiarism-free in accordance with the UGC Regulations on “*Promotion of Academic Integrity and Prevention of Plagiarism in Higher Educational Institutions (2018)*” and the CSIR Guidelines for “*Ethics in Research and in Governance (2020)*”.


Signature of the Supervisor

Name : Dr. S. B. Umbarkar

Date : 28/07/2023

Place : Pune

Acknowledgement

This thesis work would never have been accomplished without the encouragement, love, and support of some incredible people who made this Ph.D. journey a lifetime experience. All the precious moments I have spent in CSIR-NCL, especially in catalysis division, will always be cherished. I want to acknowledge all my teachers, family members, friends, and well-wishers who always motivated me to complete this long journey confidently

*First and foremost, I would like to express my deepest gratitude and respect to my research supervisor **Dr. Shubhangi Umbarkar**, who gave me an opportunity to be a part of her wonderful group. I am deeply indebted to her for constant encouragement, guidance, patience, and support throughout my research tenure in NCL. She always a true mentor whose thoughtful advice always motivated me to keep going during my most difficult times in research as well as in my personal life. Thank you, ma'am, for believing in me and guiding me at every step of my Ph.D. work.*

*I am also profoundly indebted to **Dr. Mohan Dongare**. I acknowledge him for his invaluable suggestions, encouragement and numerous scientific discussions has made a high impact on my thesis.*

*My sincere thanks to former and present Head, Catalysis and Inorganic Chemistry Division **Dr.D. Srinivas, Dr. C. S. Gopinath and Dr. S. Umbarkar** for allowing me to utilise divisional facility. **Former and present Director** of CSIR-NCL for providing infrastructure to carry out the research work and AcSIR is acknowledged for the registration for Ph.D.*

*I take this opportunity to offer my sincere thanks to my DAC members, **Dr. B. Garnaik, Dr. K. Joshi, Dr. A. Kelkar and Dr. SAR Mulla** for their constant evaluation, suggestions and advice during my PhD work.*

*I would like to thank to the technical staff of NCL from whom I always gets help in analysis **Mr. Gholap sir, Mr. Deo sir, Dr. Gaydhankar, Mr. R. Jha sir**. I would also thankful to **Dr. Sunita Barve and Mr. Gati Nayak** for their support in references.*

*I would like to thank to my seniors **Dr. Atul, Dr. Reshma and Dr. Dhananjay** for their constant help, suggestions and support during initial stage of my PhD. I would like*

Acknowledgement

to extend my sincere thanks towards my lab mates, **Dr. Swati, Dr. Deepa, Pravin Sir, Sonali, Vishal, Vitthal, Manali, Swapnali, Pratap, Ajinkya, Vaibhav, Jayesh, Pavan, Ankit** for the cooperative and enthusiastic environment in the lab during the work.

There aren't enough words to recognize my dear friends who helped me at various stages of my work at NCL. I wish to thank, **Dr. Mahesh, Dr. Supriya, Dr. Shweta, Ratanmala, Pushpa, Dr. Raghini, Nagesh, Amrin, Shital**. A special thanks to **Dr. Shweta and Ratanmala** for their guidance and moral support.

I take this occasion to thank all my teachers, specially **Dr. N. N. Bhujbal** and **Dr. M. M. Jagtap** and well-wishers classmates & friends in various stages for their love, encouragement whose names are not mentioned here.

Last but not least, the most integral part of my life, my parents and my family, whose unwavering love and faith allowed me to successfully complete my thesis. I do not have words to express my gratitude to **Mummy and Nana (Pappa)**, who always gave me the freedom, strength, and confidence to achieve my goals. Sincere thanks to my siblings **Dada, Tai and Seema** for taking care of me and making me feel protected. It was their love and affection which keeps me going on the endless path of knowledge. I would like to express my deep felt gratitude to **Mama, Mami and other family members** for their constant help, care and love. I would also like to acknowledge my **in-laws** for their constant support, motivation.

Finally I would like to thank my beloved and steadfast husband **Anil** for his incredible patience, dedication, confidence and support throughout my pursuits. His never-ending love, understanding and care against all odds gave me the courage to complete this work successfully. A special thanks to my cute little daughter **Shirisha** who have directly and indirectly inspired and energized me daily for work.

And ultimately, thanks to **God** for his showers of blessing and granting me the capability to proceed successfully.

.....**Mirabai M. Kasabe**



*“If you spend too much time thinking about a thing,
you’ll never get it done. Make at least one definite move
daily toward your goal.”*

-Bruce Lee

***Dedicated to My Parents
Mummy, Nana, Mama
My beloved husband-Anil & Daughter Shirisha***

CONTENT

List of Abbreviations	i
List of Symbols and Units	iii
List of Schemes	iv
List of Figures	iv
List of Tables	viii

Chapter-1

Introduction

1.1	Introduction	2
1.1.1	Homogeneous catalyst	4
1.1.2	Biocatalyst	5
1.1.3	Heterogeneous catalyst	5
1.2	Hydrogenation	8
1.3	Hydrogenation of some industrial important compound	11
1.4	Palladium metal	16
1.5	Metal-support interactions	17
1.6	Preparation methods of heterogeneous catalysts	19
1.7	Different supports used to disperse Pd for hydrogenation	20
1.8	Different functional supports	28
1.9	Limitations of hydrogenation reactions	32
1.10	Research scope and objectives of the thesis	32
1.11	References	34

Chapter-2

Pd-WO₃/SiO₂: Synthesis, Characterization and Its Catalytic Application for Hydrogenation of Cinnamaldehyde under Ambient Conditions

	Abstract	43
2.1	Introduction	44
2.2	Experimental Section	46
2.2.1	Materials	46
2.2.2	Catalyst Preparation	47
2.2.3	Catalysts characterization	48
2.2.4	Catalytic activity	49
2.3	Results and Discussions	51
2.3.1	Catalyst characterization	51
2.3.2	Catalytic activity for cinnamaldehyde hydrogenation	60
2.3.3	Used catalyst characterization	70
2.4	Possible reaction mechanism of cinnamaldehyde hydrogenation on 1P20WS catalyst	72

CONTENT

2.5	Conclusion	76
2.6	References	76

Chapter-3

Pd-WO₃/SiO₂: Synthesis, Characterization And Its Catalytic Applications For Hydrogenation Of Acetophenone Under Ambient Conditions

	Abstract	81
3.1	Introduction	82
3.2	Experimental Section	84
3.2.1	Materials	84
3.2.2	Catalysts characterization	84
3.2.3	Catalytic activity	85
3.3	Results and Discussions	87
3.3.1	Catalytic activity for acetophenone hydrogenation	87
3.3.2	Characterization of used catalyst	103
3.3.3	Deactivation and regeneration of catalyst	106
3.4	Mechanistic study of AP hydrogenation on 1P20WS catalyst	109
3.5	Conclusions	113
3.6	References	114

Chapter-4

Phenol hydrogenation to cyclohexanol catalysed by palladium supported on CuO/CeO₂

	Abstract	118
4.1	Introduction	119
4.2	Experimental Section	121
4.2.1	Materials	121
4.2.2	Catalyst Preparation	122
4.2.3	Catalysts characterization	122
4.2.4	Catalytic activity	124
4.3	Results and Discussions	125
4.3.1	Catalyst synthesis	125
4.3.2	Catalyst Characterization	125
4.3.3	Catalytic activity for phenol hydrogenation	136
4.4	Characterization of the used catalyst	144
4.5	Plausible Mechanism	147
4.6	Conclusion	151
4.7	References	152

CONTENT

Chapter-5

Summary and Conclusion

Summary and Conclusion	156
Thesis abstract	160
List of papers and patents	161
List of conference attended	162
Published papers	

List of Abbreviations

AMT	Ammonium Meta-Tungstate
AP	Acetophenone
BE	Binding Energy
BET	Brunauer-Emmett-Teller
CE	Cyclohexyl Ethanol
CAL	Cinnamaldehyde
CMK	Cyclohexyl Methyl Ketone
CNF	Carbon Nanofibers
CNT	Carbon Nano Tubes
COL	Cinnamyl Alcohol
DCM	Dichloromethane
DFT	Density Functional Theory
DME	Dimethyl Ether
DRIFTS	Diffuse Reflectance Infrared Fourier Transform Spectroscopy
DTA	Differential Thermal Analysis
EB	Ethylbenzene
EC	Ethyl Cyclohexane
EDAX	Energy Dispersive X-ray Spectroscopy
ES	Ethyl Silicate-40
FID	Flame Ionization Detector
FTIR	Fourier Transformed Infrared
ATIR-FTIR	Attenuated Total Reflection-Fourier Transformed Infrared
GC	Gas Chromatography
GCMS	Gas Chromatography-Mass Spectroscopy
GNP	Graphene Nano-Plates
HCAL	Hydrocinnamaldehyde
HCOL	Hydrocinnamyl Alcohol
HPLC	High Performance Liquid Chromatography
HRTEM	High Resolution Transmission Electron Microscopy
HT	Hydrotalcites
ICP-AES	Induced coupled plasma – Atomic emission spectroscopy
IPA	Isopropanol

MIBK	Methyl Isobutyl Ketone
MSI	Metal Support Interaction
NBR	Nitrile Butadiene Rubber
NCNT	Nitrogen-Functionalized Carbon Nanotube
PE	1-Phenyl Ethanol
PB	Propyl Benzene
PMF	Palladium On Magnesium Fluoride
PXRD	Powder X-Ray Diffraction
PZC	Point of Zero Charge
SMSI	Strong Metal Support Interaction
TEM	Transmission Electron Microscopy
TGA	Thermogravimetric Analysis
THF	Tetrahydrofuran
TOF	Turn Over Frequency
TON	Turn Over Number
TPD	Temperature Programmed Desorption
XPS	X-ray Photoelectron Spectroscopy

List of Symbols & Units

Å	Anstrong Unit
a.u.	Arbitrary Unit
°C	Celsius (unit of measurement for temperature)
cm-1	Wavenumber
Ea	Energy of activation
h	Hour (s)
s	Second (s)
Mol	Mole (s)
nm	Nanometer
ppm	Parts per million
%	Percentage
δ	Chemical shift
ν	Frequency
γ	Gamma
λ	wavelength
α	Alpha
kV	Kilovolt
mA	milliampere
θ	Theta
atm	Atmospheric pressure
mmol	milimole

List of Schemes		
Schemes 2.1	Hydrogenation of cinnamaldehyde	44
Schemes 2.2	Phenprobamate	45
Schemes 2.3	Hydrogenation of CAL on PWS	61
Schemes 3.1	Possible products of acetophenone hydrogenation	82
Schemes 3.2	Acetophenone hydrogenation products using PWS catalysts in methanol solvent	89
Schemes 4.1	Hydrogenation of phenol.	118
Schemes 4.2	Hydrogenation of phenol on 1PCC catalyst	137
Schemes 4.3	Dissociative adsorption of phenol onto catalyst (i) adjacent to a surface hydroxyl, and (ii) at an oxygen vacancy	149
Schemes 4.4	Adsorption of phenol onto catalyst i) perpendicular orientation and ii) parallel orientation	150

List of figures		
Fig. 1.1	Energy profile diagram of catalytic reaction	2
Fig. 1.2	Types of catalysis	3
Fig. 1.3	Different product selectivity from butadiene using Ni based catalyst	4
Fig. 1.4	General mechanism for transmetalation using homogeneous catalysis	5
Fig. 1.5	General mechanism for heterogeneous catalysis	7
Fig. 1.6	The contribution of catalytic processes to the chemical industries and the contribution of heterogeneous catalysis in comparison to other catalytic processes	7
Fig. 1.7	Applications of heterogeneous catalyst	8
Fig. 1.8	Steps involve in the hydrogenation of C=C bond at a catalyst surface	10
Fig. 1.9	Factors affecting and affect by metal-support interaction	19
Fig. 1.10	Hydrogenation of various functional group over Pd/MgF ₂ catalyst	32
Fig. 2.1	XRD spectra of (i) (a) 1P10WS, (b) 1P15WS and (c) 1P20WS, (ii) (a) 20WS, (b) 0.1P20WS, (c) 0.5P20WS, (d) 1P20WS and (e) 2P20WS	52
Fig. 2.2	BET surface area analysis of (a) 0.1P20WS, (b) 0.5P20WS, (c) 1P20WS, (d) 2P20WS, (e) 1P10WS and (f) 1P15WS	54

List of Schemes and Fig.

Fig. 2.3	FTIR spectra of all PWS catalysts in range i) 400 to 4000 cm^{-1} and ii) 400 to 2000 cm^{-1} , (a) 0.1P20WS, (b) 0.5P20WS, (c) 1P20WS, (d) 2P20WS, (e) 1P10WS and (f) 1P15WS	55
Fig. 2.4	XPS spectra related to (A) Pd3d, (B) W4f of a) fresh, b) activated 1P20WS catalyst	56
Fig. 2.5	TEM images of 1P20WS catalyst	57
Fig. 2.6	TEM images of 0.1P20WS catalyst	57
Fig. 2.7	TEM images of 0.5P20WS catalyst	58
Fig. 2.8	TEM images of 2P20WS catalyst	58
Fig. 2.9	TEM images of (a) 1P10WS and (b) 1P15WS catalyst	58
Fig. 2.10	SEM images of (a) 0.1P20WS, (b) 0.5P20WS, (c) 1P20WS, (d) 2P20WS, (e) 1P10WS and (f) 1P15WS catalyst	60
Fig. 2.11	CAL hydrogenation reaction profile with time	64
Fig. 2.12	Effect of Pressure on CAL hydrogenation reaction	65
Fig. 2.13	Effect of temperature on CAL hydrogenation reaction	66
Fig. 2.14	Effect of catalyst loading on the conversion of CAL	67
Fig. 2.15	Recycle study of 1P20WS catalyst for CAL hydrogenation	69
Fig. 2.16	XRD pattern of (a) fresh and (b) used 1P20WS catalysts	71
Fig. 2.17	HRTEM data of fresh 1P20WS catalyst	72
Fig. 2.18	HRTEM data of used 1P20WS catalyst	72
Fig. 2.19	CAL adsorption on Pd ₄ nanocluster through (a) C=C bond and (b) C=O bond; CAL adsorption on Pd (111) surface through (c) C=C bond and (d) C=O bond	74
Fig. 2.20	FTIR spectra of PWS catalysts in the range i) 400 to 4000 cm^{-1} and ii) 500 to 2000 cm^{-1} ; a) authentic CAL and b) CAL adsorbed on 1P20WS	75
Fig. 2.21	Plausible mechanism of CAL hydrogenation on 1P20WS catalyst	76
Fig. 3.1	Time on stream analysis for AP hydrogenation Reaction	90
Fig. 3.2	FTIR spectra of PWS catalysts in the range i) 1300 to 3200 cm^{-1} and ii) 500 to 1000 cm^{-1} ; a) 1P20WS catalyst isolated from reaction mixture after 1 h after subtraction of fresh 1P20WS catalyst, b) 1P20WS catalyst isolated from reaction mixture after 5 h after subtraction of reduced 1P20WS catalyst and	92

List of Schemes and Fig.

	c) support (WO₃/SiO₂) isolated after 5 h reaction time after subtraction of fresh support	
Fig. 3.3	TG/DTA curves of 1P20WS i) fresh catalyst, ii) catalyst isolated after 1 h and iii) used catalyst	93
Fig. 3.4	Effect of solvent on AP hydrogenation	94
Fig. 3.5	Effect of catalyst loading on AP hydrogenation	95
Fig. 3.6	Recycle study of 1P20WS catalyst for acetophenone hydrogenation	102
Fig. 3.7	Conversion of AP after filtration of catalyst	103
Fig. 3.8	XRD pattern of (a) fresh and (b) used 1P20WS catalysts	104
Fig. 3.9	HRTEM data of fresh 1P20WS catalyst	104
Fig. 3.10	HRTEM data of used 1P20WS catalyst	105
Fig. 3.11	Comparisons of TG/DTA curves of 1Pd20WS a) fresh catalyst, b) used catalyst, c) used catalyst calcined at 250°C, and d) used catalyst calcined at 500°C	108
Fig. 3.12	TEM images of 1P20WS catalyst calcined at a) 250°C and b) 500°C	109
Fig. 3.13	Recycle study of 1P20WS catalyst for acetophenone hydrogenation at lower conversion	109
Fig. 3.14	FTIR spectra of (i) a) pure methanol, b) methanol adsorbed on catalyst, (ii) a) AP adsorbed on catalyst, b) pure AP, c) catalyst filtered after 1 h reaction time and d) final reaction mixture adsorbed on reduced catalyst	111
Fig. 3.15	Possible bonding modes of AP adsorption on catalyst i) η^1 configuration and ii) X-sensitive benzene mode	112
Fig. 3.16	Plausible mechanism of AP hydrogenation on 1P20WS catalyst	113
Fig. 4.1	NH₃-TPD for CeO₂, 1%Pd/CeO₂, CC and 1PCC	127
Fig. 4.2	XRD patterns of (a) CeO₂, (b) CC, (c) 0.5PCC, (d) 1PCC and (e) 2PCC	128
Fig. 4.3	BET surface area analysis of (a) 1%Pd/CuO, (b) 1%Pd/CeO₂, (c) CC, (d) 0.5PCC, (e) 1PCC, and (f) 2PCC	130
Fig. 4.4	Raman spectra of (a) CuO, (b) CeO₂, (c) CC, and (d) 1PCC	131
Fig. 4.5	XPS spectra of 1PCC (a) Ce 3d (b) O 1s (c) Cu 2p and d) Pd 3d	133
Fig. 4.6	SEM image of catalyst a) CC, b) 0.5PCC, c) 1PCC, and d) 2PCC	134
Fig. 4.7	TEM image of catalyst a) CC, b) 0.5PCC, c) 1PCC, and d) 2PCC, e) High resolution TEM image of 1PCC, and f) SAED	135

	pattern of 1PCC catalyst.	
Fig. 4.8	The conversion of phenol with time	138
Fig. 4.9	Effect of temperature on phenol hydrogenation	139
Fig. 4.10	Catalyst loading effect on phenol hydrogenation	141
Fig. 4.11	Recycle study of phenol hydrogenation	144
Fig. 4.12	XRD pattern of fresh and used 1PCC catalyst	145
Fig. 4.13	BET surface area analysis of fresh and used 1PCC catalyst	146
Fig. 4.14	TEM images of (a) fresh and (b) used 1PCC catalyst	147
Fig. 4.15	FTIR spectra in the range i) 600 to 4000 cm⁻¹, ii) 650 to 900 cm⁻¹, and iii) 1100 to 1660 cm⁻¹: of a) authentic phenol, and phenol adsorbed on b) CuO, c) CeO₂, d) CC, e) 1%Pd/CuO, f) 1%Pd/CeO₂ and g) 1PCC	148
Fig. 4.16	Plausible Mechanism of phenol hydrogenation over PCC catalyst	151

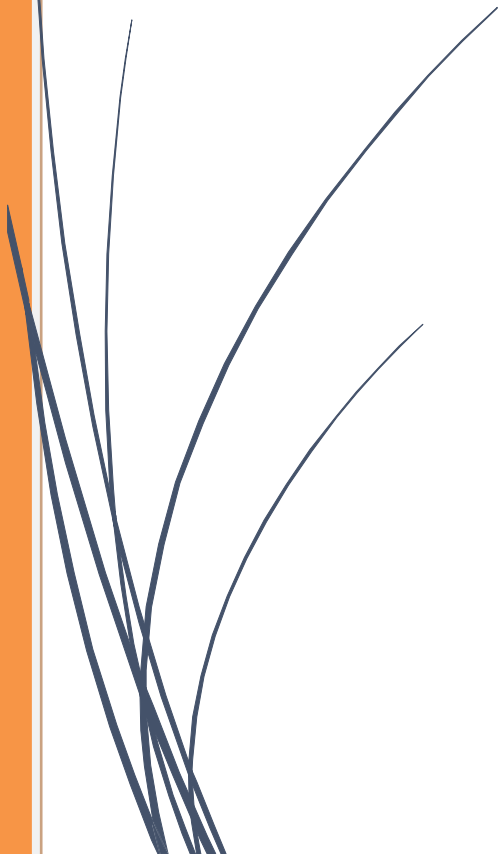
List of Tables

Table 1.1	Difference in homogeneous and heterogeneous catalyst	8
Table 1.2	Industrially important hydrogenated compounds	12
Table 2.1	Nomenclature of all xPd-yWO₃/SiO₂ catalysts	48
Table 2.2	Surface properties of the PWS catalysts	53
Table 2.3	Elemental composition of catalysts by EDAX	60
Table 2.4	The catalyst screening for CAL hydrogenation	62
Table 2.5	Solvent effect on hydrogenation of CAL	63
Table 2.6	Pd loading effect on CAL conversion	68
Table 2.7	Literature survey for hydrogenation of CAL	70
Table 3.1	AP hydrogenation using series of PWS catalysts	88
Table 3.2	Hydrogenation of PE using 1P20WS catalyst	90
Table 3.3	Effect of palladium loading on AP hydrogenation using P20WS catalyst	96
Table 3.4	Hydrogenation of different substituted AP using 1P20WS catalyst	98
Table 3.5	Literature survey for hydrogenation of AP	100
Table 3.6	Recycle study of 1P20WS for styrene hydrogenation	107
Table 4.1	Acidity of the catalysts as determined by NH₃-TPD	126
Table 4.2	Surface properties of the CC catalysts	129
Table 4.3	XPS data for CeO₂, CC and 1PCC	133
Table 4.4	Catalyst screening for phenol hydrogenation	137
Table 4.5	Effect of pressure on phenol hydrogenation	140
Table 4.6	Pd loading effect on phenol hydrogenation	142
Table 4.7	Literature survey for hydrogenation of phenol	142
Table 4.8	Surface characterization of fresh and used 1PCC catalyst	145



Chapter 1

Introduction



1.1 Introduction

The term Catalysis means the process in which the rate of the chemical reaction is accelerated by the addition of a substance that is not consumed in the reaction and the substance is called as a catalyst. The catalyst speeds up the reaction by providing an alternative pathway causing to reduce the activation energy [1]. The eminent Swedish chemist Jöns Jacob Berzelius originally used the word "catalysis" (from the Greek kata-, "down," and lyein, "loosen") in 1835 to link a number of discoveries done by other researcher in the late 18th and early 19th centuries. This includes, the first organic reaction in 1811, that is, the synthesis of sugar from starch which is enhanced by acid. The term catalysis was originated by Scottish chemist Elizabeth Fulhame and explained in a book in 1794 based on her oxidation–reduction experiment. The catalyst accelerates the reaction rate by lowering the reaction's activation energy by providing a different route, as shown in Figure 1.1, without consuming during the reaction. It is used in small quantities, and it can convert a large number of reactant molecules to a desired product.

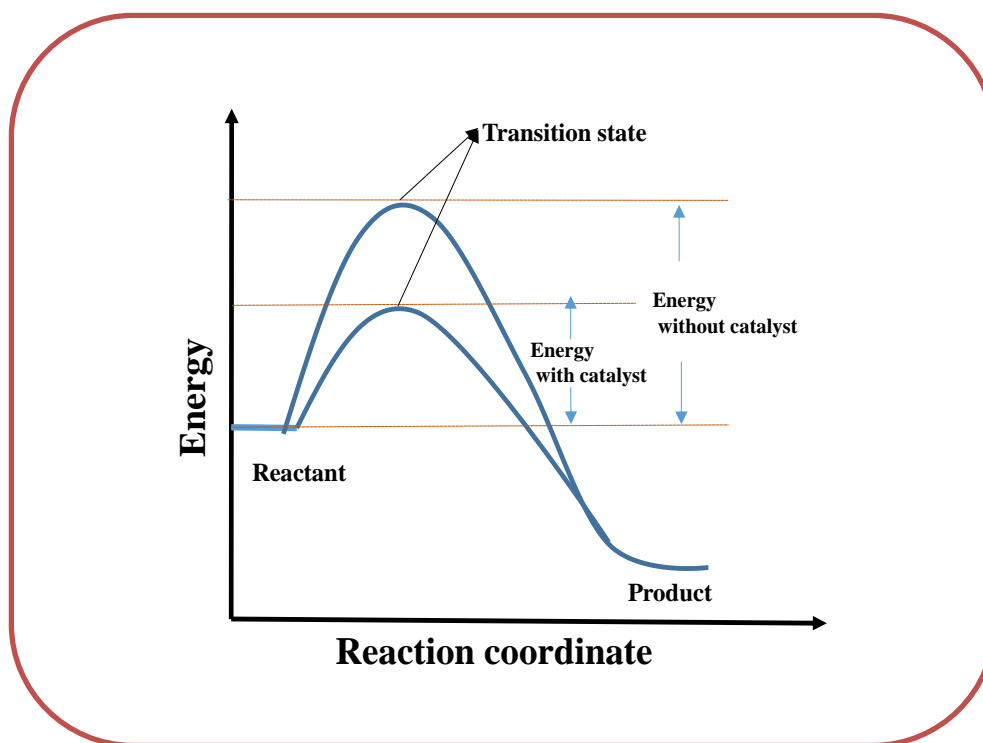


Figure 1.1. Energy profile diagram of catalytic reaction

Catalysis is a multidisciplinary field that involves inorganic chemistry, organic chemistry, materials science, biochemistry, surface science, chemical engineering, bio-engineering, kinetics, and theoretical chemistry. Catalysis is the backbone of most industrial processes; the modern industrialized world would be impossible without catalysts because more than 80 % of the industrial processes which convert raw materials into useful chemicals are based on catalytic technologies. The catalytic production of ammonia fertilizer is the best example of catalysis in everyday life, which is crucial to sustaining the contemporary global population [2]. Nowadays, about fifteen international companies are manufacturing about 100 commercial solid catalysts. Catalyst plays a crucial role in reducing the process cost and also reducing the pollution of the process [3]. The catalyst is vital in lowering many harmful pollutants formed in the process.

The catalyst is divided into three types; homogeneous, heterogeneous, and biocatalyst, as shown in Figure 1.2. The first two are based on the phase of the reactant and catalyst in the mixture during the reaction. Biocatalysts are the catalytic action that occur through the enzymes, and this can be considered as heterologous and homogenous hybrids.

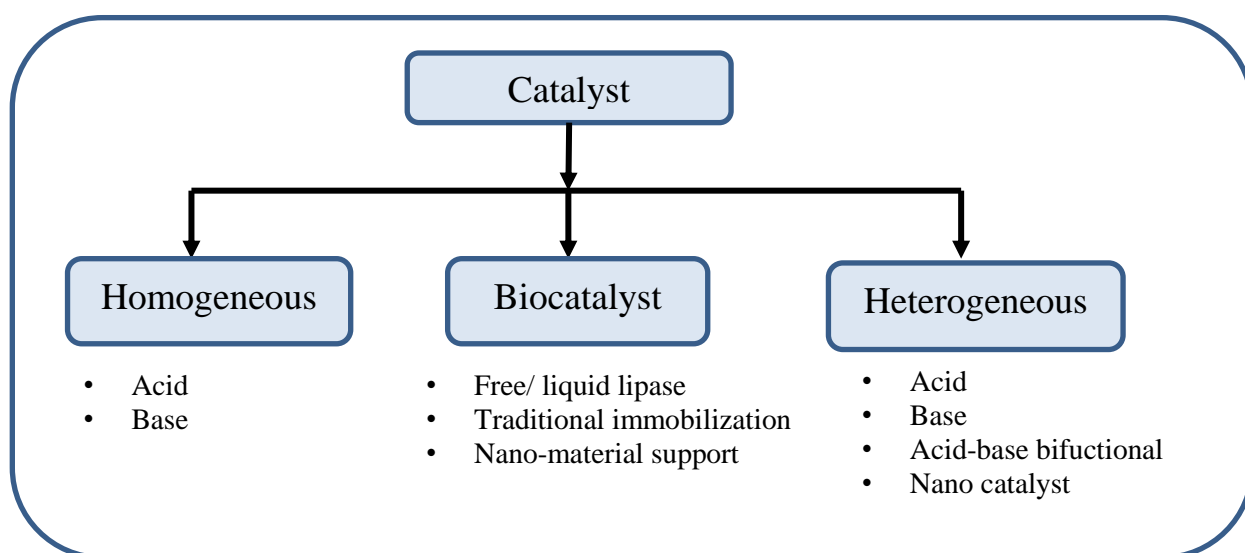


Figure 1.2. Types of catalysis

1.1.1 Homogeneous catalyst

Homogeneous catalysis is the process in which the catalyst is in the same phase as the reactants, mainly in the liquid phase. The catalyst used for this process is known as a homogeneous catalyst. It may be acid, base, metal salts, or a combination of ligand metal complexes (organic or organometallic complexes). Concerning metal complexes, one can tune the catalytic activity of metal to obtain the desired product. This can occur through the electronic interaction between ligands and metals. For example, Ni-based catalysts give different products from butadiene depending on the ligands used with Ni, as shown in Figure 1.3 [4].

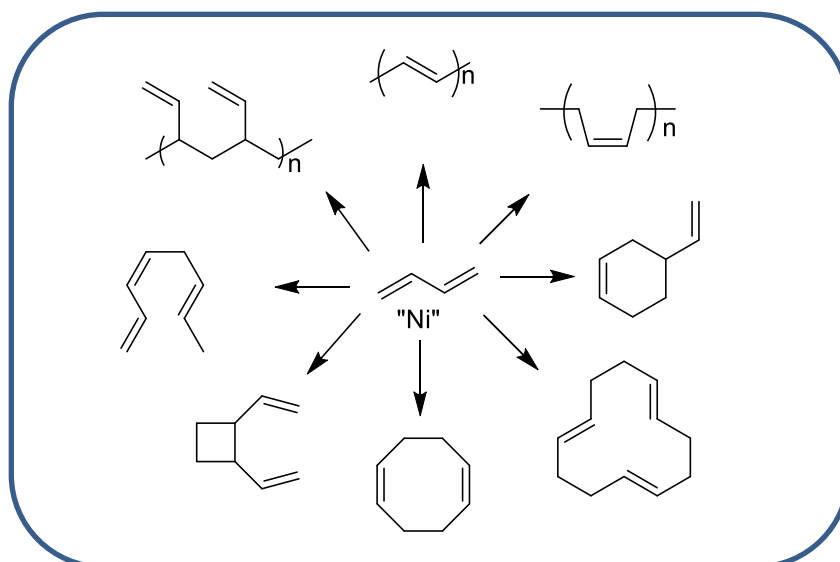


Figure 1.3. Different product selectivity from butadiene using Ni based catalyst

The first commercial process utilizing a homogeneous catalyst (NO - nitric oxide) was developed in the 1750s for the oxidation of SO_2 to SO_3 to produce sulphuric acid in the lead chamber [5]. In the 19th century, there were three crucial homogeneous catalysts- I) In 1938 Co based organometallic complex for hydroformylation which was discovered by Roelen; II) Ziegler–Natta catalysts for the conversion of terminal alkenes to polymer and III) In 1965, Rh based $(\text{RhCl}(\text{PPh}_3)_3)$. Wilkinson investigated the catalyst for the hydrogenation of alkenes. Millions of tons of bulk chemicals are produced by using homogeneous catalytic process examples- oxidation, metathesis, hydroformylation, carbonylation, hydrogenation, and

hydrocyanation. Even though these catalysts are highly efficient in terms of catalytic activity and selectivity, it has major limitation in high catalyst recovery cost and moderate thermal stability. A general mechanism for transmetalation using homogeneous catalysis is given in Figure 1.4.

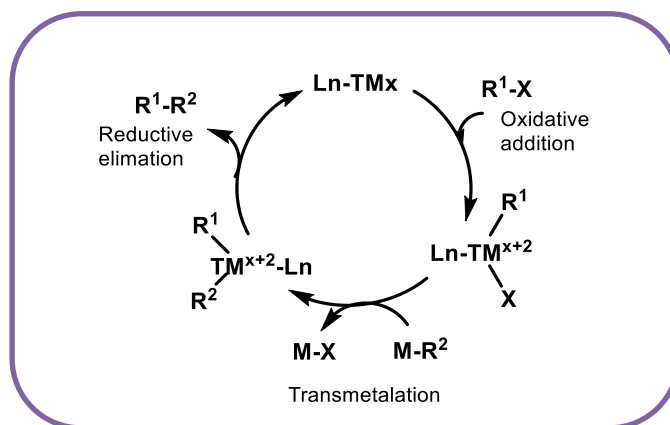


Figure 1.4. General mechanism for transmetalation using homogeneous catalysis

1.1.2 Biocatalyst

Biocatalysts are enzymes obtained from biological sources. These enzymes contain protein which helps to speed up the biological reaction by lowering the activation energy. Most enzymes work in living organisms. Hence it is performed best in water, and is very sensitive to variations in temperature and pH [6]. One of the most distinctive characteristics of biocatalysts is selectivity for initiating and inhibiting their catalytic activity. This distinctive property is due to the enzyme's three-dimensional structure, which is obtained by the intermolecular interaction of many amino acids into proteins. Biocatalysts are biodegradable and work under mild conditions, reducing the formation of side products; thus leading to environmental friendly biocatalysts. The new process of immobilizing enzymes on supports makes biocatalysts more stable and reusable for the reaction [7-8].

1.1.3 Heterogeneous Catalyst

Heterogeneous catalysis is the process in which the reactants and the catalyst are not in same phases. Mostly the catalyst is in the solid phase. This solid catalyst is dispersed in liquid reaction mixture and facilitates the reaction. For gaseous reactants the solid catalyst is

packed in a reactor in the pellet form and the reaction is carried out by passing the gaseous reactant over the solid catalyst. Sometimes a fluidized bed reactors are also used for gas solid reactions to improve the contact between the reactant and catalyst. A general mechanism for heterogeneous catalysis involves three steps, as shown in Figure 1.5. These includes i) the gaseous or liquid reactant from the reaction mixture adsorbed on the catalyst surface, ii) the interaction of adsorbed reactants on the catalyst surface and conversion into the product, iii) the desorption of the product from the catalyst surface [9]. The adsorption of the substrate on the catalyst surface occurs by two adsorption process, one is physisorption and another one is chemisorption. In physisorption, substrate adsorbs on the catalyst surface. Physisorption occurs when the substrate molecule is attracted to atom/ molecules (active site) present on the catalyst surface due to Van Der Waals forces generated between them. Chemisorption occurs when an electronic cloud of substrate molecules overlaps with an electronic cloud of atoms/ molecules (active site) on the catalyst surface. This can take place through one of two different pathways: i) the molecular adsorption pathway in which substrate molecule adsorbs on catalyst surface without breaking of chemical bonds between the atoms ii) the dissociative adsorption pathway in which the substrate (reactant) structure gets affected after the adsorption on the catalyst surface due to the breaking of a chemical bond between the atoms in the substrate molecule in order to form new bonds with the catalyst surface. Chemisorption can be observed over a wide range of temperatures, e.g., hydrogen chemisorption on ZnO-Cr₂O₃ occurs above room temperature. Chemisorption of N₂ on synthetic ammonia-iron catalyst takes place above 400 °C temperature.

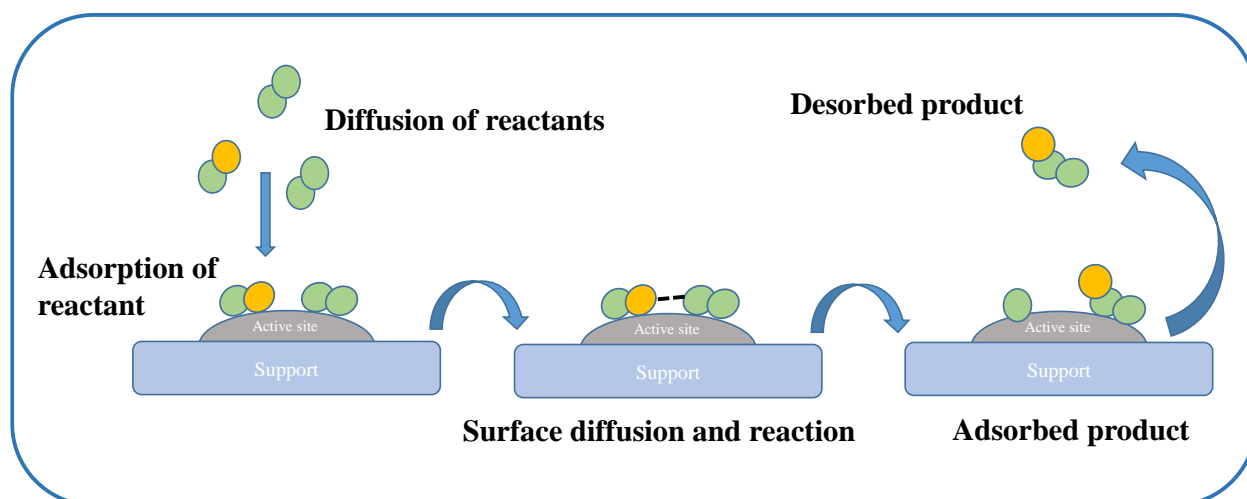


Figure 1.5. General mechanism for heterogeneous catalysis

Almost 85% of industrial production of chemicals are based on various catalytic process. The heterogeneous catalysts are widely used (80%) in the industry to obtain bulk and basic chemicals in large quantities (Figure 1.6) [10]. The heterogeneous catalysts have diverse applications in the field of petrochemical industry to get good quality chemicals and fuels, in the field of energy for its conservation and storage, as well as for rectification of the environment by decreasing the harmful substances. This signifies its essential role in the world economy. The significant difference between homogeneous and heterogeneous catalysts is given in Table 1.1, which makes heterogeneous catalysts more applicable in industry. Heterogeneous catalysts are used in reactions such as oxidation, deNO_x, hydrogenation, photocatalyst, and electrocatalyst, and in producing different fine and bulk pharmaceutical chemicals. (Figure 1.7)

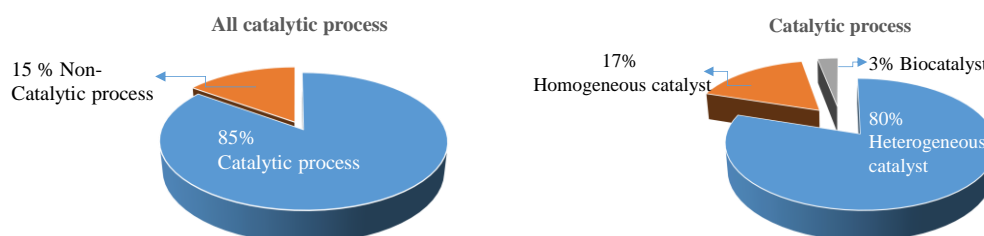


Figure 1.6. The contribution of catalytic processes to the chemical industries and the contribution of heterogeneous catalysis in comparison to other catalytic processes

Table 1.1. Difference in homogeneous and heterogeneous catalyst

Sr. No.	Homogeneous catalyst	Heterogeneous catalyst
1	Low thermal stability	High thermal stability
2	Difficult to recover	Easy to recover
3	High selectivity	Low selectivity
4	Limited application	Wide application

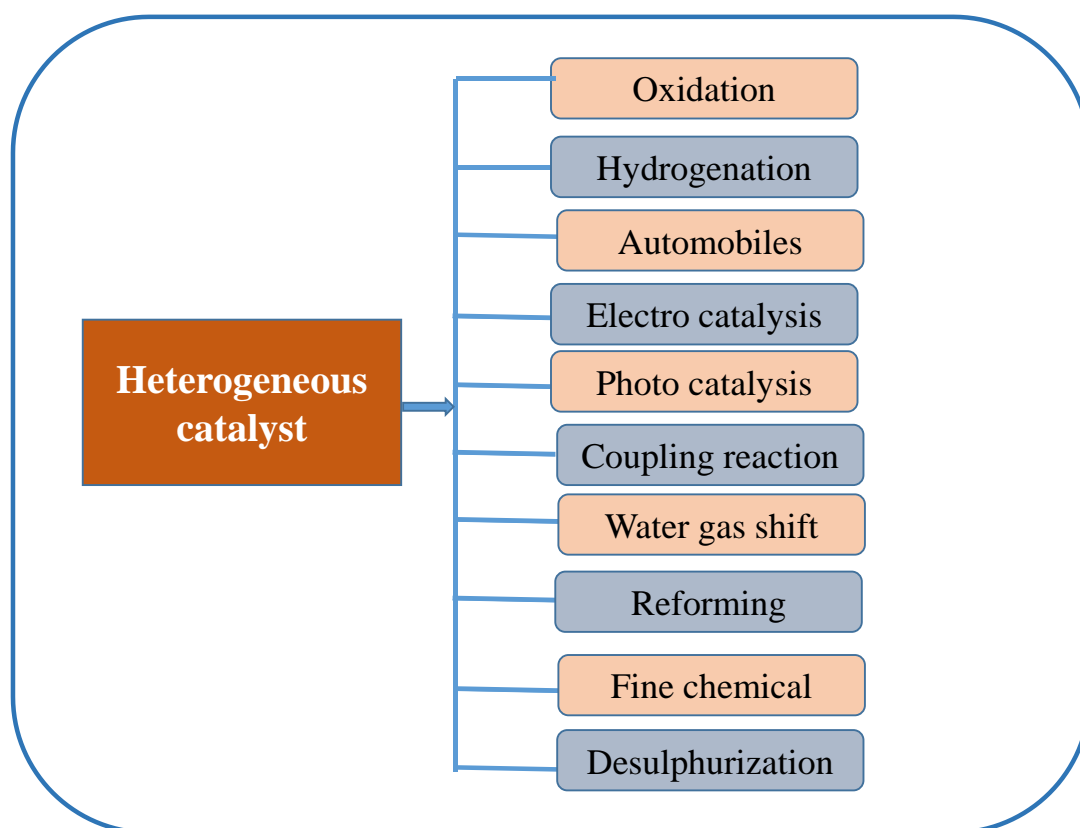


Figure 1.7. Applications of heterogeneous catalyst

1.2 Hydrogenation

In organic synthesis, reduction or hydrogenation is a significant reaction with multiple industrial applications in the food, petrochemical, agricultural, pharmaceutical, etc.

Hydrogenation reaction includes converting an unsaturated compound to a saturated

compound (i.e., double or triple bond to single bond) in the presence of the catalyst. This involves different hydrogenation methods like using metal hydride, transfer hydrogenation, and molecular hydrogen under catalytic conditions. In most industries, metal hydrides such as lithium aluminum hydride (LiAlH_4) at RT or sodium borohydride (NaBH_4) at high temperature are used in a stoichiometric amount as a reducing agent [11]. The transfer hydrogenation method is also used widely. In this method, metal complexes are used as a catalyst and protic solvent as a hydrogen donor, including isopropanol, formaldehyde, formic acid, etc. The activity of these catalysts can be altered by changing the ligand system attached to the metal atom. The real disadvantage of transfer hydrogenation is the inherent reversibility of the reaction, so; this process has a limited scope as it could provide only modest yields of product [12]. Also, using metal hydride reagents causes environmental problems, and the product has no selectivity. It is not useful in the reduction of multifunctional compounds because of non-regioselectivity. Therefore, even if handling H_2 is challenging, catalytic reduction employing molecular H_2 is often employed in the industry. This is clean production method which has excellent atom economy and easy product separation. [13]. Catalytic hydrogenation is the reaction in which molecular hydrogen adds to an unsaturated compound and gives a saturated compound, or sometimes, adding hydrogen causes the molecule to break (this process is known as hydrogenolysis). [12]. Hydrogen acts as a reducing agent, giving its electron in a chemical redox reaction. However, when it reacts with the metal, it behaves as an oxidizing agent. The reaction conditions are mainly based on the type of substrate and catalyst. The central role of the catalyst is to activate the hydrogen molecule and facilitate the reaction between hydrogen and substrate. Both homogeneous and heterogeneous catalysts are used for hydrogenation. Homogenised chemical reactions show a high degree of rate constant and are very selective; however, it is challenging to separate the catalyst from the reaction

mixture. Due to some benefits over homogeneous catalysis, such as (I) regenerability, (II) thermal and mechanical stability, (III) economy, and (IV) appropriate morphological features like high surface area and crystalline nature, heterogeneous catalysts account for nearly 90% of industrial catalytic processes [14]. The mechanism of heterogeneous catalytic hydrogenation was reported by Horiuti-Polanyi [15].

The steps involved in it are as follows and as shown in Figure 1.8.

1. Physisorption of both hydrogen and unsaturated compound on catalyst
2. Hydrogen dissociation into atomic hydrogen and binding of the unsaturated bond to the catalyst (chemisorption)
3. The hydrogen atom transfer from catalyst surface to unsaturated compound which is a reversible step
4. In the next step second hydrogen atom transfers from catalyst surface
5. Desorption of product from catalyst surface

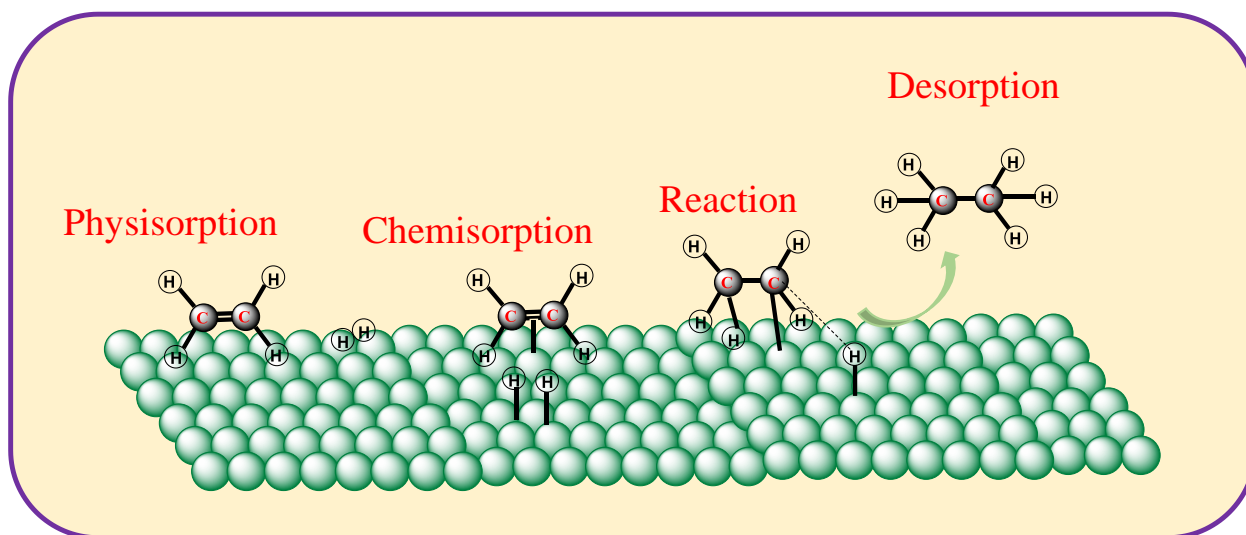


Figure 1.8. Steps involve in the hydrogenation of C=C bond at a catalyst surface

There are different heterogeneous metal catalysts utilized for hydrogenation

including Pd [16], Pt [17], Rh [18], Ir [19], Ni [20, 21], Raney Ni [22], Au [23], Ru [24] and poly-metallic catalysts [25, 26]. Because of the high cost of noble metals, it is dispersed on high surface area supports. This allows more effective and economic usages of the noble metals compared to bulk-metal system. These supports are not only important for the dispersion of metal particles; it also helps in adsorption and desorption of reactants and products, and also affects the catalytic properties of metal particles. As the support plays an important role in the heterogeneous catalyst, many supports are investigated [27] for the hydrogenation such as carbon [28], silica [29], polymeric materials [30], and nanoparticles with magnetism [31]. The chemical and electronic structure of the metal [32] is mainly dependent on the electron transfer [33] by the support and also it has an influence on the adsorption capacity [34].

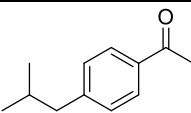
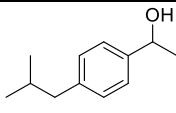
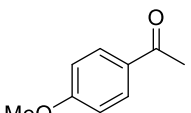
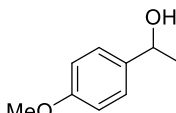
Catalytic hydrogenations generally performed in a variety of methods, including batch-wise or continuous, in the liquid or gas phase. But the liquid phase hydrogenation has an advantage in the higher volume productivity of a hydrogenation system. The capacity to use reaction heat is also higher for the liquid phase because of the larger heat transfer coefficient. [35]. Now a day's liquid phase hydrogenation reaction is getting more attention. [36]. Reactors with fixed beds or those with fluidized beds are often utilized in continuous processes. The selection of an appropriate reactor system is influenced by a number of variables, including the catalyst used, reaction conditions (H_2 pressure, temperature, and solvent), heat production, space-time yield, residence duration, mass-transport phenomena, and financial considerations.

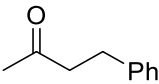
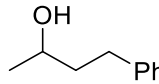
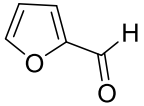
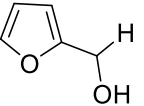
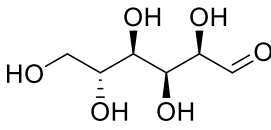
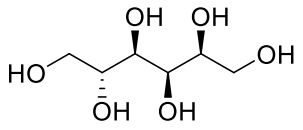
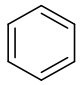
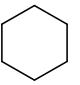
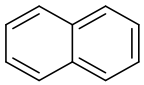
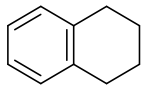
1.3 Hydrogenation of some industrial important compound

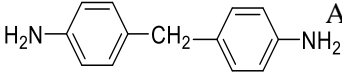
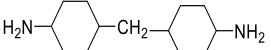
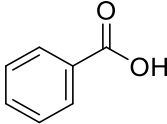
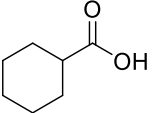
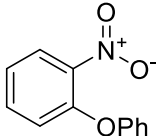
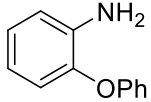
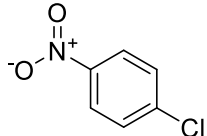
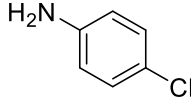
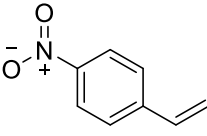
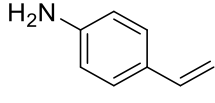
The hydrogenation technique was invented by the French scientist Paul Sabatier. In 1897, he discovered that traces of nickel were responsible for the addition of hydrogen to molecules of gaseous hydrocarbons; later on, this process was known as the Sabatier process.

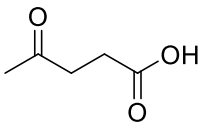
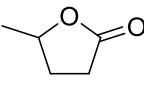
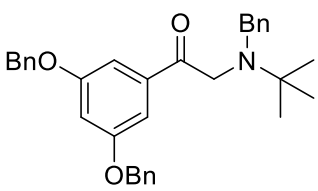
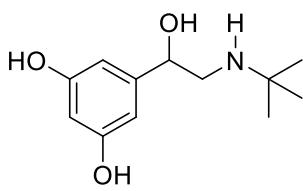
The actual Sabatier process involves the addition of an H₂ molecule to the CO₂ at high temperatures (300-400 °C) in the presence of nickel as a catalyst, producing methane and water. Later, in 1905, Fritz Haber and Carl Bosch discovered the widely accepted Haber-Bosch process. The process transfer the atmospheric nitrogen (N₂) into ammonia (NH₃) by using an iron catalyst under high temperatures (400-500 °C) and H₂ pressures (150-250 bar). The discovery of Raney nickel was found to be revolutionary in hydrogenation. Murray Raney obtained a finely powdered form of nickel from Ni-Al alloy in 1924, which was widely used to for hydrogenation reactions including aromatic ring hydrogenation to alkanes, conversion of nitriles to amines. Hydrogenated products of some compounds are important in various industries, such as food, petrochemical, agricultural, and pharmaceutical industries, are shown in Table 1.2.

Table 1.2. Industrially important hydrogenated compounds (Data from Ullman and Kirk encyclopaedia)

Sr. No	Substrate	Functional group to be reduce	Product	Importance	Existing procedure
1	 1-(4-Isobutylphenyl)ethanone	Ketone	 1-(4-Isobutylphenyl)ethanol	Intermediate in ibuprofen (anti-inflammatory drug)	Raney Ni, high temp and H ₂ pressure
2	 p-Methoxy acetophenone	Ketone	 1-(4-Methoxy phenyl) ethanol	Food additives, flavoring agents	Raney Ni, high temp and H ₂

3	 4-Phenylbutan-2-one	Ketone	 4-Phenylbutan-2-ol	Flavor and fragrance agents	pressure 5%Pt/C, 5-100 °C, 5-50 bar H ₂ pressure
4	 Furfural	Aldehyde	 Furfuryl alcohol	As bio-fuel	10% copper chromate catalyst, 200-300°C, 30 atm H ₂ pressure
5	 Glucose	Aldehyde	 Sorbitol	Use as sugar substitute, as laxative, in mouthwash, toothpaste	Batch fermentation of glucose and fructose by <i>Z. mobilis</i> ,
6	 Benzene	Aromatic	 Cyclohexane	Use in production of adipic acid, Nylon-6	5% Rh/C or 5%Ru/C, 150 °C, 3-50 bar
7	 Naphthalene	Aromatic	 Tetralin	Upgrading of coal liquids and diesel fuels	5% Rh/C or 5%Ru/C, 150 °C, 3-50 bar

8	 4,4'-Methylenedianiline	Aromatic	 4,4'-Methylenebis(cyclohexan-1-amine)	In preparation of polymer	Ru catalyst, 140 °C, 80 bar H ₂ pressure
9	 Benzoic acid	Aromatic	 Cyclohexanecarboxylic acid	Intermediate in synthesis of hexanolactam, praziquantel (parasitic worm infections)	Rh/C
10	 2-Phenoxy nitrobenzene	Nitro	 2-Phenoxyaniline	Intermediate in anti-inflammatory drug	H ₂ - 4bar, 120°, Pd/C (5%-Pd loading)
11	 p-Chloro nitrobenzene	Nitro	 4-Chloroaniline	Precursor for antimicrobial chlorhexidin	Cu or Pd activated C or an oxidic support 90 – 200 °C and 100 – 600 kPa
12	 1-Nitro-4-vinylbenzene	Nitro	 4-Vinylaniline	Used for the production of fine chemicals,	medium-to-high temperature (T > 393 K)

				functionalized and polymers, pigment and pharmaceuticals.	hydrogen pressure ($H_2 > 3$ bar) using noble metal catalysts
13	 Levulinic acid	Acid	 gamma-Valerolactone	Used as fuel additives, food ingredients, pharmaceutical intermediates	Over copper-chromite catalyst, $250^\circ C$ and 200-300 atm pressure
14	Oil Unsaturated fatty acids	Olefins	Alkane Saturated fatty acids	To stabilize the oil and prevent spoilage from oxidation.	Ni-Al alloy catalyst, high temp($150^\circ C$) and pressure
15		Ketone & Debenzylate ion		Intermediate in Terbutaline sulphate drug (used as a short-term asthma treatment)	4 wt % Pd/C catalyst (10% Pd) w.r.t. substrate, 5 bar H_2 , RT, 2 h

Ni and Pd-based catalysts are used in most processes to get hydrogenated products. Nickel is the cheapest element, but due to its poor catalytic activity under ambient conditions, it requires high temperature and high pressure to activate. This makes the process expensive. Palladium metal is less expensive than other noble metals. Also it is more active than non-noble metal. Hence now day's palladium metal-based catalysts are used extensively in industries.

1.4. Palladium metal

Out of six platinum-group (Ru, Rh, Pd, Os, Ir, and Pt) metals, palladium metal is probably more protean and exploited transition metal due to its ability to perform different organic transformations such as cross-coupling, alkylation, arylation, cyclization, oxidation, hydrogenation, radical reaction, petroleum cracking [37-38], fine chemical synthesis [39], etc. Also, it is 2-3 times cheaper than other platinum-group metals. It also has a typical electronic configuration for its outermost shell ($\text{Pd-}4d^{10} 5s^0$), which is different from the other group elements ($\text{Ni-}3d^9 4s^1$, $\text{Pt-}5d^9 6s^1$, $\text{Os-}6d^9 7s^1$ or $6d^8 7s^2$), which makes its properties different from the other. It is less dense and has a low melting point than others. Palladium has a special and significant feature that makes it a highly effective catalytic element in hydrogenation reactions. This includes the quick adsorption of large amounts of hydrogen gas to generate palladium hydride (PdH). Palladium absorbs significant amounts of hydrogen under normal conditions (room temperature and atmospheric pressure). These adsorbed hydrogen atoms occupy the interstitial octahedral positions of the face-centered cubic lattice [40]. In 2001 Schlapbach et al. reported temperatures and equilibrium pressures vital in forming different metal hydrides [41]. Except for Pd, other metals require high temperatures and pressure to form metal hydride. To form a metal hydride, dissociation of the H_2 molecule is a necessary step. Except for Pd, other metal needs energy inputs to overcome the activation barrier, which leads to high H_2 pressure and elevated temperature. In Pd-based catalytic

processes, reaction conditions are frequently mild, which leads to good yields and high chemo-, regio-, and stereoselectivity. Other advantages of using palladium are the need for a catalytic quantity, excellent selectivity, ease of handling, no need for a pre-treatment step, and in most situations, simple catalyst recovery.

Most of the time, palladium and other noble metals are dispersed on supports with larger surface area to reduce the cost of the process. Support plays an important role and has various advantages. Firstly, it reduces the price of the catalyst by reducing the quantity of costly active metal. High metal dispersion on support increases the available metal surface area, which is directly proportional to the catalytic performance. The support gives mechanical strength to the catalyst by stabilizing the metal particles. Sometimes it provides new active sites in reaction to activate substrate molecules; it may be acidic or basic, or bifunctional. However, based on the materials used, the supports can affect the electronic properties of the active metal, alter the amount of active sites, or influence the morphological structure of the metal crystallites. This interaction of support with metal is known as metal support interaction. The strength of these metal-support interactions can have a significant impact on the catalytic activity of the catalyst.

1.5 Metal-support interactions

The discovery of metal support interaction (MSI) has started a very crucial research topic in catalysis as it helps understand the electronic properties and geometrical structures of metal catalysts. [42, 43]. In 1979, Tauster and co-workers reported that H₂ and CO chemisorption decreased on metal from group 8 supported on TiO₂ with an increase in reduction temperature [34]. Detail characterization showed that the decrease of this sorption is not correlated with an agglomeration of metal particles, while attributed to the interaction of support with metal particles. Due to these MSI, support suboxide species encapsulated the metal nanoparticles to lower the high surface energy of particles under reducing conditions.

This cause to decrease in the chemisorption capability of the metal particle by blocking the accessibility of H₂ and CO molecules to particles. For a variety of metal-supported catalyst systems, the MSI has been mostly used as a technique to increase stability [44-46], find out catalytic mechanism [47, 48], improve activity [49, 50], and prop up the selectivity [49-52]. Particularly, the interfacial sites perform an important role by bridging the metal species and support. To learn more information on the MSI, one would like to read related reviews [53-56]. Boaro et al. used different CeO₂-supported catalysts for important CO₂ reduction processes and explained the role of ceria in reactions. Cerium-based catalysts shows a strong metal support interaction (SMSI) due to CeO₂ reducibility. This interaction causes the enhancement of the reducing ability of the metal and support metal due to the hydrogen spillover mechanism. An oxygen vacancy in CeO₂ causes surface imperfections which leads to promoting the anchoring of metal particles over the surface, which gives high metal dispersion [57]. Meriaudeau et al. compared the SMSI impact on Pt supported on TiO₂ and CeO₂ [58]. They used gas chromatography to evaluate the outcomes of H₂ chemisorption and examine the byproducts of hydrogenation processes on carbon molecules. It observed significant differences in the hydrogen and CO chemisorption capacities as well as the hydrogenolysis selectivity between the two systems. Despite the similarity in the reduction process, which involves the creation of Ti³⁺ (Ce³⁺) ions and oxygen vacancies, but the authors proposed that these oxides exhibit distinct mechanisms for the SMSI impact. In a related study, Datye et al. employed HRTEM to compare the SMSI impact on Pt/TiO₂ and Pt/CeO₂ [59]. The findings supported the aforementioned hypothesis, as the presence of a capping layer was detected only in the TiO₂-supported catalyst. The distinctive surface structure and electronic characteristics play a crucial in the substantial modulation of metal-oxide interactions. More specifically, various surface sites such as cations, anions, and vacancies on oxides offer diverse anchoring sites for bonding with metal species. However, due to the

diverse electronic properties and coordination structures of these surface sites, the bonding properties between metal species and different surface sites are distinct, resulting in a varied apparent MSI. The presence of single Pt atoms supported in Fe₂O₃, ZnO, and γ -Al₂O₃ illustrates that the Turnover Frequency (TOF) of individual Pt atoms in CO oxidation increases with the rising redox ability of the supports under identical reaction conditions [60]. This underscores how the unique surface structure and electronic properties effectively modulate metal-oxide interactions, influencing the catalytic behavior in a manner that is contingent upon the specific characteristics of the supporting material. Because of high chemical stability and total surface area of carbon based catalysts such as carbon nanotubes and graphene, have found widespread application in a variety of industrially significant chemical reactions, including liquid phase hydrogenation, photo catalytic reactions, and electrochemical reactions. Strong covalent s-bonds hold the sp²-hybridized carbon in graphitic structures together in a basal plane. Only weak bonding to metal species in contact with the plane is permitted by the carbon p-orbitals, which extend normal to the basal plane. Consequently, because the carbon atoms in the basal plane are too inert to form a bonding contact with metal species, it is challenging to induce MSI in a perfect carbon support [61]. The strength of the MSI of metal supported catalyst depends on different variables including the nature of the metal, nature of support material, precursors used to prepare metal and support, the preparation method of the catalyst. (Figure 1.9)

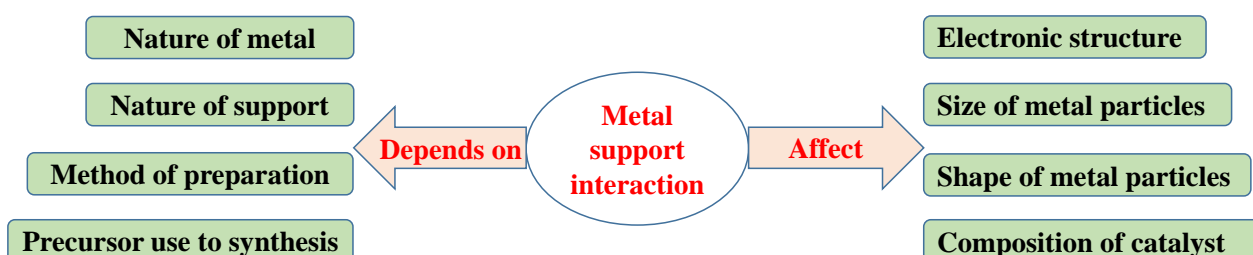


Figure 1.9. Factors affecting and affect by metal-support interaction

1.6 Preparation methods of heterogeneous catalysts

The selection of synthesis method of catalyst and conditions used for pre-treatment plays important role in determining the catalytic performance of catalyst. These factors directly affect the surface area of metal, dispersion, particle size and morphological structures. These parameters control the catalytic activity, selectivity of products, and stability of the catalyst. Hence during selection of catalyst preparation method, it is crucial to consider required material texture which must be on knowledge of chemistry of the intended catalysed reaction. There are some methods for catalyst preparation which includes i) precipitation method [62], ii) impregnation method [63], and iii) chemical deposition method [64]. The precipitation method is generally used in industries for metal oxide synthesis. The catalyst prepared by using impregnation method is more feasible because of its benefits of good particle size, fast recovery and reagent savings. Previously our group has worked on the hydrogenation of nitro group in nitrobenzene by the palladium-supported on magnesium hydroxyl fluoride catalyst produced via impregnation method (1PMF-imp) and data was compared with similar catalyst composition prepared by the precipitation method (1PMF-ppt) under identical reaction conditions. Using 1PMF-imp, 99% conversion of the nitrobenzene during hydrogenation was accomplished in 2 hours at ambient temperature and atmospheric pressure. On the other hand, employing 1PMF-ppt in 2 hours, only 25% conversion was achieved. In light of this, 1PMF-imp's catalytic activity was superior. This might be due to trapping of the palladium inside the bulk of the catalyst added to a catalyst using the precipitation method and result in poor metal dispersion since it was added to the same pot during the precipitation process.

Hence out of these preparation methods impregnation method is widely used method. Palladium is typically supported on different supports such as carbon, metal oxide, zeolites, polymers, etc. by impregnation method.

1.7 Different supports used to disperse Pd for hydrogenation

The strength of MSI is affected by the nature of the support. The catalytic performance of catalysts is frequently altered by the use of various supports as supports have distinct physical and chemical characteristics, such as thermal stability, acid-base properties, large surface area. Mostly the choice of the support depends on the type of reactions. For instance, in an oxidation reaction, the point of zero charge (PZC) of the support is used to determine which support to use for Pd particles [65]. The following is the order of PZC of various typical supports: $\text{MoO}_3 > \text{Nb}_2\text{O}_3 > \text{SiO}_2 > \text{TiO}_2 > \text{CeO}_2 > \text{ZrO}_2 > \text{Co}_3\text{O}_4 > \text{Al}_2\text{O}_3 > \text{activated carbon} \approx \text{carbon black} > \text{graphene oxide}$. Cationic metal precursor adsorb best on negatively charged surfaces because MoO_3 or NbO_3 have strong acidic PZC, whereas the metal particles adsorb on the reduced state supports like carbon with high PZC.

Some of the common supports used to disperse palladium for hydrogenation of various industrially important compound are discussed below.

a) Palladium on carbon

Carbon is a widely used support material that first found use in catalytic chemistry because of its high surface area and more adsorption capability. Palladium on carbon is a common catalyst for hydrogenation and hydrogenolysis of different functional groups [66-68]. Generally, it is commercially available as a black powder with 5% to 10% Pd supported on carbon. Typically, the Pd/C catalyst is used as dry or as a solid that is 50% wet with water. A wet catalyst is safer to handle because of the pyrophoric nature of Pd/C. Recently, the exhaustive progress of catalytic hydrogenation techniques has increased researchers' interest in the production of highly active Pd on various carbon materials includes activated carbon, carbon nanotube (CNT) [69], carbon nanofibers (CNF), carbon nano globules (CNGs) [69], graphene nano-plates (GNP) [70], nitrogen-functionalized carbon nanotube (NCNT) [71], phosphorus-doped carbon [68]. R. Mironenko summarized some of the previous prior

methods to control the catalytic characteristics of Pd/C catalysts with variations of the carbon materials and palladium precursors [67]. The structure, morphology, and surface chemistry of various carbon materials differ from one another. As a result, depending on the type of carbon support selected, the production of palladium clusters and NPs, as well as their catalytic characteristics, might differ dramatically. When Pd/C catalysts are being prepared, the formation of active sites is controlled by a different variables such as the nature of carbon material, palladium precursor, method of preparation, and pre-treatment of catalyst. Since none of the parameters may be taken into account separately, it is not always possible to predict how each one will affect the generation of catalytically active structures. The difficult task of nanoscale design may be made simpler by reducing the number of stages during the catalyst synthesis. Even though the Pd/C catalyst is a more active and robust catalyst for the reduction of various function groups, it has some disadvantages such as handling it is difficult due to its pyrophoric nature, Pd particles agglomeration, reduction–carbideization of Pd²⁺ to Pd carbides (PdC_x) and Pd leaching [72].

b) Palladium on metal oxide

There are two types of metal oxides i) reducible metal oxide, and ii) non-reducible metal oxide based on their chemical behaviors. Reducible oxides are the material that can change the oxidation state of metal easily. When surface oxygen is removed, the excess electron is left on the metal which is redistributed on empty levels of the cation by changing its oxidation state leading to a lower band gap < 3eV. The transition-metal oxides involve WO₃, TiO₂, CeO₂, NiO, and Fe₂O₃ are examples of reducible oxides. Non-reducible oxides are chemically inert and stoichiometrically stable. These oxides do not lose oxygen easily due to the intrinsic resistance (high band gap > 3eV) to change the oxidation state of that corresponding metal cation, for example- Al₂O₃, SiO₂, hydrotalcite, etc. A survey of the literature shows palladium dispersed on SiO₂ [73], Al₂O₃ [74, 75], MgO [76, 77], ZnO [78,

79], ZrO₂ [80, 81], CeO₂ [82, 83], WO₃ [84, 85], MoO₃ [86], and TiO₂ [87, 88] has good catalytic activity for hydrogenation various functional groups. Ye Gou et al. has reported the Pd/NiO catalyst for acetophenone hydrogenation under reaction conditions of 1.5 MPa H₂ pressure, and 80 °C [89]. The reactions were performed on three different Pd/NiO (Pd shape is different hexagonal or triangular Pd/NiO, octahedral Pd/NiO, and cubic Pd/NiO) catalysts under identical reaction conditions and the catalytic activity and selectivity was compared. The order of catalytic activity followed cubic Pd/NiO > octahedral Pd/NiO > hexagonal or triangular Pd/NiO. This may be due to the shape and size of the catalyst. As compared to others, cubic Pd was the smallest in size, which led to a highly active catalyst since there are more catalytically active sites available for the reaction. Patel et al. used ployaniline-coated celite as support to dispersed Pd metal [90]. This catalyst was used for the chemoselective hydrogenation reaction of olefins and imines. It showed prominent catalytic activity under ambient conditions. Due to the basic nature of celite further hydrogenation was avoided and the catalyst became highly chemoselective. Unsupported Pd nanoparticles as well as Pd supported on a variety of supports, including activated carbon, graphene oxide Al₂O₃, SiO₂, TiO₂, and SiC, were prepared and used for the hydrogenation of cinnamaldehyde. [91]. The Pd particle size was affected by changing the precursors, calcination and reduction temperature, and the SMSI effect. From the results, it was concluded that the C=C bond selective hydrogenation was observed over smaller Pd particles while larger Pd particles were responsible for the C=O bond selective hydrogenation and it was also confirmed from DFT calculation. Thus, it is confirmed that support is crucial for tuning the reaction selectivity. Pd/ZrO₂ and PdO/ZrO₂ composites, consisting of nanoparticles of Pd or PdO, were synthesized by a novel one-step approach [80]. These exhibited efficient catalytic activity in the reduction of acetophenone (AP) under aqueous conditions at both 1 bar and 10 bar of H₂ pressure. When compared to Pd or PdO nanoparticles that were not supported, the presence

of zirconia led to a significant enhancement in catalytic activity. While unsupported PdO primarily produced ethylbenzene (EB) through hydrogenation, the PdO/ZrO₂ composite displayed exceptional regioselectivity towards 1-phenyl ethanol (PE), which was maintained even during recycling. Similarly, the Pd/ZrO₂ composite exhibited higher regioselectivity to PE compared to unsupported Pd nanoparticles. In the hydrogenation of substituted acetophenones, both PdO and zirconia contributed to a high selectivity towards alcohol products. L. Zhang investigated the potential size-based SMSI phenomenon in Pd/ZnO catalysts [79]. In this study, hexagonal ZnO nanoplates were employed as support to disperse Pd nanoparticles of varying sizes (ranging from 1.6 to 7.9 nm) by using the atomic layer deposition (ALD) technique. These Pd/ZnO catalysts showed size-based SMSI behaviour during subsequent hydrogen (H₂) reduction at high temperatures, with the bigger Pd particles (2.5 nm) displaying a stronger tendency to be encapsulated by ZnO than the smaller particles. For the CO₂ reduction, the Pd/ZnO catalysts which having bigger Pd nanoparticles demonstrated significantly higher turnover frequencies (TOFs) with selectivity towards CH₃OH compared to smaller (1.6 nm) Pd/ZnO catalysts. These observed variations in catalytic efficiency were related to the varying degrees of Pd-ZnO interface formation induced by the size-dependent SMSI phenomenon.

Zhang et al. successfully developed a controlled synthesis method for silica hollow microspheres with a distinctive rough surface (RS) resembling a moonscape and a macroporous structure (MS) [73]. This synthesis was achieved using the (water-oil-water) three-phase emulsion technique. These materials were used to disperse Pd metal. The catalytic performance of the synthesized catalyst was evaluated for the hydrogenation of NBR (nitrile butadiene rubber). The Pd/N-RS catalyst exhibited remarkable activity for hydrogenation with maintaining 92% of its original performance even after five recycles, surpassing the performance of the Pd/N-MS catalyst. The enhanced reusability of the Pd/N-

RS catalyst can be related to its unique rough surface (moonscape-like), which effectively mitigates diffusion limitations and promotes the rapid desorption of NBR/HNBR molecules from the catalyst support surface. This process allows the re-exposure of active sites, thereby preserving high hydrogenation activity. The results of this research highlights the significance of the rational design of support morphology and structure in improving NBR hydrogenation activity. Zeolite is an excellent support with abundant pores. Wang et al. showed an innovative approach for achieving selective hydrogenation of furfural utilizing a core-shell Pd@S-1 (silicalite-1) zeolite catalyst, which allows for precise control of the wettability of the zeolite sheath [92]. Considerable changes were observed in the diffusion behavior of several molecules by appropriately adjusting the hydrophilicity of the zeolite micropores. Specifically, the Pd@S-1-OH catalysts, derived by silanol group's functionalization on the zeolite, demonstrated exceptional catalytic performance, stability, and selectivity in the hydrogenation of furfural to furan. These findings highlight the profound influence of zeolite micropore hydrophilicity on the hydrogenation process and emphasize the potential for tailoring catalyst properties through the control of wettability for enhanced reaction outcomes.

c) *Palladium on mixed oxide*

In chemistry, an oxide with cations of different chemical elements or a single element in multiple oxidation states is known as a mixed oxide. The term is typically used to describe solid ionic compounds that have two or more elemental cations and the oxide anion O^{2-} , for example- ilmenite ($FeTiO_3$), perovskite ($CaTiO_3$) and garnet ($Fe_3Al_2Si_3O_{12}$). These are natural mixed oxide minerals. Examples of synthetic mixed oxides are ZnO-ZrO₂, CeO₂-ZrO₂, ZnO-SiO₂, CuO-CeO₂, etc. It should be emphasized that the textural and structural characteristics of metal oxide can be considerably improved by adding another metal oxide to it. Even small amounts of metal or metal oxide can increase the thermal stability and catalytic

activity of metal oxide through the formation of a substitutional solid solution and SMSI. There are several reports based on a modification of metal oxide by the addition of metal or metal oxide [93-100]. Vikanova et al. developed Pt-based catalysts supported on synthesized $\text{CeO}_2\text{-ZrO}_2$ (CZ) mixed oxides for the acetophenone hydrogenation showing remarkable catalytic activity under milder conditions [101]. Over a 1% Pt/CZ catalyst, the entire conversion of the substrate was accomplished in 2 hours, which is half compared to the catalysts supported on CeO_2 , TiO_2 , and CZ commercial supports. These results, which were in line with the data from the TPR analysis, noted that hydrogen adsorption was enhanced in 1% Pt/CZ catalysts, which was attributed to the enhanced hydrogen spillover effect. However, this variation in catalytic activities of these catalysts for acetophenone hydrogenation shows that the synthesis process of the support has a significant impact on their performance. Hydride formation on palladium metal supported on SiO_2 (Pd/SiO_2) catalyst was studied, and the results were compared with ZnO-promoted Pd/SiO_2 catalyst [102]. At temperatures above and around 523 K, the pure Pd/SiO_2 catalyst is physically less stable and more prone to sintering and silicide production, which eventually leads to the creation of Pd_2Si alloy at temperatures 200°C lower than for the ZnO-promoted Pd/SiO_2 catalyst (PdZn alloy state). Methanol generation from CO_2 hydrogenation was studied on Cu-ZnO, Cu-ZrO₂, and Cu-ZnO-ZrO₂ [96]. The combined results of the DRIFTS (diffuse reflectance infrared Fourier transform spectroscopy) experiment and DFT (Density functional theory) calculation reveal that the CO_2 adsorption and conversion take place at the ZnO-ZrO₂ interfaces, while metallic Cu is also required to promote H_2 dissociation and serve as a source of hydrogen. The XPS and TPD results showed that the interaction between ZnO and ZrO₂ leads to the formation of oxygen vacancies which were the active sites to adsorbed CO_2 molecule. The impact of the ZnO/SiO₂ ratio on the structural characteristics and catalytic performance of Cu/ZnO and Cu/SiO₂ catalysts for ester hydrogenation in water [99]. This

ratio affects the water tolerance of Cu/SiO₂ and Cu/ZnO catalysts. A significant improvement in water resistance without sacrificing conversion was achieved by adding the right amount of ZnO to Cu/SiO₂ catalysts, which led to a decrease in the reaction temperature. Simultaneously, SiO₂ was added to Cu/ZnO catalysts to successfully reduce agglomeration by serving as a partition material and preventing Cu/ZnO agglomeration. However, the addition of ZnO had a negative impact on the dispersion of copper in Cu/SiO₂, which led to a quick decline in the stability of the catalyst as a result of excessive sintering brought on by the ZnO presence. With increasing SiO₂ content, the copper dispersion in Cu/ZnO catalysts first increased but later declined. The Cu/ZnO catalyst's activity was lowered, and it deactivated quickly, as a result of the excessive addition of SiO₂. This study demonstrated that the Cu/SiO₂ and Cu/ZnO catalysts both benefited from the correct addition of 5% ZnO and 5% SiO₂, respectively. Regalbuto et al. characterized Pt/WO₃/SiO₂ catalysts by XRD, CO chemisorption, and XPS [103]. The data showed that WO₃ controlled the Pt crystallite size, in part by lowering the creation of bulk PtCl₂ precursor. Shift in Pt-electron binding energy (due to charge transfer) and also CO chemisorption data indicated that the catalyst showed strong metal-support interaction. An effective bifunctional catalyst (Pd metal supported on Zn⁺²-Cr⁺³ mixed oxide) for the one-step synthesis of methyl isobutyl ketone (MIBK) from acetone and H₂ in both gas and liquid phases [104]. Acetone is condensed into mesityl oxide using an acid catalyst, and then it is hydrogenated to produce MIBK. The Cr-rich oxides showed the higher surface area and good Pd dispersion. 0.3% Pd/Zn-Cr (1:1) catalyst showing an intermediate acid site and acid strength. This catalyst showed good acetone conversion and selectivity for MIBK.

d) Palladium on metal fluorides

Metal fluorides are the common source of fluorides utilized in the synthesis of cryolite and aluminum. Metal fluorides are usually solid crystalline materials. Calcium fluorides

naturally occur. Solid metal fluoride catalysts have been discovered to be more effective and stable than metal oxide for a few heterogeneously catalyzed processes. Metal fluorides are significantly more Lewis acidic than metal oxides and halides because the most electronegative fluorine atom causes acidity on the central metal. The catalyst 1%Pt/MgF₂ was six times more active than 1%Pt/Al₂O₃ for *o*-chloronitrobenzene hydrogenation [105]. The metal fluoride synthesized by a one-pot fluoro-lytic sol-gel method was used to dispersed Pd metal and subsequently used for the hydrogenation of various functional groups such as olefins [106], oil hydrogenation [107], nitro-aromatics [108], imine and aromatics. In *n*-pentane hydro isomerization processes, Pd-Cu/HS-AlF₃ (HS = high surface area) catalysts showed better activity than the Pd-Cu/C catalyst [109]. The platinum supported on binary Mg-Co fluorides was tested for *o*-chloronitrobenzene (*o*-CNB) hydrogenation [110]. Binary magnesium-cobalt fluorides form solid solutions since the ionic radius of Co²⁺ approximates that of Mg²⁺, which causes the substitution of Co²⁺ into the MgF₂ rutile-type structure. This results in Mg-Co fluorides having more surface area, surface acidity, and nitrobenzene adsorption capacity than their fluorides. It has a significant effect on the activity of *o*-CNB hydrogenation. On Pt/MgCoF catalyst surface, *o*-CNB adsorbs at centers of metal-support boundary through (1) nitrogen of nitro group to Pt centers (electron-rich center) (2) oxygen atoms of the nitro group to Mg²⁺ ions (electron-deficient center).

From all the above discussion it can be conclude that on the surfaces of catalyst, cations, and anions have been referred to as acid-base pairs [111]. Metal ions behave as Lewis or Brønsted acids in heterogeneous catalytic systems, whereas counter ions exhibit basic characteristics. A significant amount of Brønsted acidity may be present in the hydroxyl groups on the surface. The free electron pairs of the species that have been adsorbed may be taken up by the exposed coordinatively unsaturated cations to show Lewis acidity. Hence, all supports discussed above can be categorized into three functional categories, such as neutral,

basic, and acidic supports. There are different acidic supports (zeolites, γ -Al₂O₃, CeO₂, TiO₂, ZrO₂, Nb₂O₅, MgF₂), basic supports (MgO, CaO, BaF₂, hydrotalcite) and neutral supports (SiO₂, CN, α -Al₂O₃) used to disperse metal as per the requirement of reaction.

1.8 Different functional supports

a) Neutral supports

The non-reducible oxides are chemically inert and stoichiometrically stable. These oxides do not lose oxygen easily due to the intrinsic resistance (high band gap $> 3\text{eV}$) to change the oxidation state of that corresponding metal cation. These non-reducible oxides such as Al₂O₃, SiO₂, etc., and carbon, and graphene oxides are the neutral supports which does not contribute in the reaction.

b) Basic supports

The examples of solid bases are metal and mixed oxides, supported alkali or alkaline earth oxides, hydrotalcites, zeolites, basic clays, phosphates, anion exchangers, supported amides and imines, and impregnated carbons. In basic support generally metal oxide -OH group and oxide ion on the surface are a Brønsted and a Lewis base, respectively. Typical examples of metal oxide solid bases are BaO, MgO, CaO, and SrO. Metal oxide becomes more basic with increasing ionic radius, decreasing charge, and decreasing electronegativity of metal ion. Basicity of mixed oxides is relatively understudied, but variety of reactions carried out with solid bases as summarized by Ono and Hattori [112]. The conversion of acetone to methyl isobutyl ketone is performed by Cu, Pd, and Ni supported on MgO, hydrotalcites, etc [113, 114]. One fundamental challenge associated with the utilization and handling of basic catalysts (especially those of a more basic nature) is the existence of acidic contaminants in the surrounding atmosphere. Basic catalysts can become quickly and perhaps irreversibly contaminated by water and CO₂.

c) Acidic supports

In genuine metal oxides, the surface-exposed coordinatively unsaturated cation behaves as a Lewis acid, while the surface-exposed hydrogen of -OH behaves as a Brønsted (or protonic) acid. As ionic radius decreases, charge rises, and electronegativity of metal ions increases, metal oxide generally gets more acidic (both acid intensity and acid quantity). So, from extremely acidic to very basic, metal oxides are ordered according to their acid intensity as follows: $\text{RuO}_4 > \text{MoO}_3, \text{WO}_3 > \text{ZrO}_2 > \text{Cr}_2\text{O}_3, \text{Al}_2\text{O}_3 > \text{MgO} > \text{CaO} > \text{BaO} > \text{Na}_2\text{O}$

The catalytic reduction of carbon monoxide (CO) was examined using Pd dispersed on different materials such as Al_2O_3 , SiO_2 , ZrO_2 , and TiO_2 [115]. The choice of support material exerted a significant influence on both the catalysts' activity and selectivity. Pd/ Al_2O_3 predominantly produced dimethyl ether (DME), methanol formation favored over Pd/ SiO_2 , methane generated over Pd/ TiO_2 , and Pd/ ZrO_2 yielded methanol as the main product. Higher CO conversions on Pd/ ZrO_2 and Pd/ TiO_2 were attributed to the formation of cationic palladium species due to MSI. The substantial formation of DME over Pd/ Al_2O_3 was ascribed to the support metal oxide's acidity. X-ray photoelectron spectroscopy (XPS) analysis revealed the interaction between palladium and the support for Pd/ ZrO_2 and Pd/ TiO_2 , which demonstrated a slightly positive palladium oxidation state because of strong contact between the Pd metal and the support material. Due to the existence of the Pd-support interface, the Pd/ ZrO_2 catalyst showed outstanding activity and selectivity towards methanol. In another study, palladium supported on MgO, hydrotalcites (HT), and Al_2O_3 synthesized and used for the partial hydrogenation of acetylene, aiming to find the influence of support nature on electronic density of Pd, and catalytic performance [116]. It showed that the Pd/HT catalyst exhibited the highest acetylene conversion compared to Pd catalysts supported on Al_2O_3 and MgO. CO pulse and CO-IR analysis revealed that the Pd/HT catalyst exhibited the highest Pd metal dispersion (34.6%) over support among the three catalysts. This was further confirmed by HRTEM and TPR profile. XPS and CO-IR techniques revealed different electronic

densities of supported Pd. The catalyst Pd/HT showed a blue shift in CO-IR and an increase in binding energy (BE) showing that decrease in the electronic density of the supported Pd due to the acidic sites on HT. Conversely, the Pd/MgO catalyst showed red shift and decreased BE suggested that the electronic density of Pd increased due to the basic sites. Pd²⁺ species adsorb onto the basic sites (O₂). Subsequently, upon reduction, the acid sites promote the redistribution of Pd atoms, resulting in the generation of numerous low-coordinated Pd particles, thereby enhancing the dispersion of the catalyst. These clearly show that the acidity of supports plays a vital role in catalyst performance and the selectivity of products.

Previously our group has synthesized palladium supported on magnesium fluoride by a sol-gel route and used for the selective hydrogenation of variety of functional groups of different compounds under ambient reaction conditions as shown in Figure 1.10 [106-108]. Fluorine in MgF₂ produces a higher Lewis acidity on magnesium metal which stabilized the active palladium species by metal support interaction. The synthesis of the catalyst requires 40 % HF which may raise some safety and environmental concerns. The combination of two distinct weakly acidic metal oxides frequently leads to the creation of highly acidic mixed oxides. Amorphous and crystalline SiO₂-Al₂O₃ serve as prime illustrations of this process, wherein potent Brønsted (or protonic) acids are generated. Additional instances include the pairing of TiO₂-SiO₂ and SO₄-ZrO₂. Moreover, the manipulation of basicity can be achieved through the synthesis of mixed oxides. In certain scenarios, coexistence of acidic and basic sites on the metal oxides surfaces play a remarkable role in achieving exceptional catalytic performance.

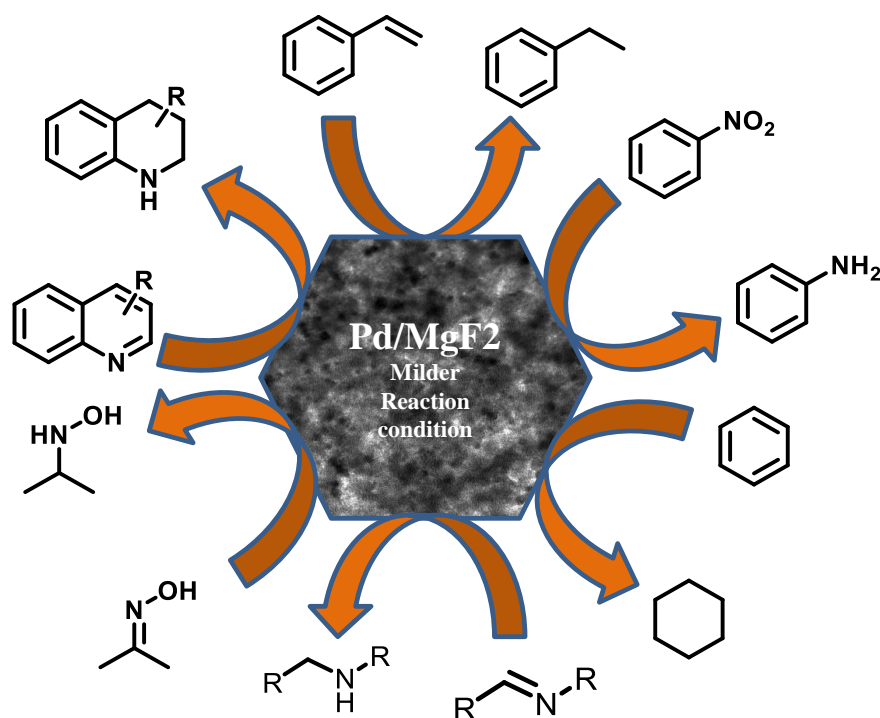


Figure 1.10. Hydrogenation of various functional group over Pd/MgF₂ catalyst.

Previously our group has used a WO₃/SiO₂ (WS) catalyst for nitration reaction instead of conc. H₂SO₄ [117]. The WO₃/SiO₂ catalyst was synthesized by sol-gel method with changing WO₃ loading ranging from 1 to 30 wt%. The sol-gel technique has resulted in the generation of well dispersed WO₃ nano-particles of 2-5 nm size on a high surface area mesoporous silica and showed higher acidity. One of other active mixed metal oxide discussed above i.e. CuO/CeO₂ which previously our group has used for oxidation reaction for the conversion of CO to CO₂. CuO/CeO₂ were synthesized by the co-precipitation method, which caused structural defects in the CeO₂ lattice. The dispersion of palladium metal onto these mixed oxides was carried out to examine the interaction between the Pd metal and the oxides. Subsequently, these catalysts were employed in a range of significant industrial hydrogenation reactions.

1.9 Limitations of hydrogenation reactions

Presently, the significance of hydrogenation reactions in industries has experienced a tremendous increase due to their diverse applications in different fields. Numerous research

groups are actively striving to achieve hydrogenation products under mild conditions for enhanced economic feasibility. Traditional hydrogenation processes predominantly operate at high pressures and temperatures. However, elevated temperatures can result in metal agglomeration, leading to a decrease in catalytic activity. Consequently, several research groups are dedicated to developing catalytic systems that can replace these harsh reaction conditions with ambient conditions for hydrogenation processes [118]. Furthermore, the use of catalysts with high noble metal loading contributes to the costliness of the process. The leaching of noble metals poses a significant challenge for many industries, as it leads to a decrease in metal content and subsequently reduces catalytic activity. Overcoming these limitations is a primary focus for numerous industries and research groups. Therefore, keeping these limitations in mind, the thesis aims to achieve several specific objectives, thus paving the way for advancements in the field of hydrogenation.

1.10 Research scope and objectives of the thesis

The elementary reaction steps in catalysis are heavily influenced by multiple parameters, including the shape, size, and electronic properties of individual particles, and their interfacial interactions. Consequently, the macroscopic catalytic behavior can be understood as the collective result of interactions between reactants, intermediates, and products with the micro(nano)scopic coordination environment of surface atoms, which involves geometric arrangements, electronic confinement, interfacial effects, and other factors. Manipulating these parameters can significantly impact the local surface structure and chemistry, thereby exerting profound effects on catalysis. However, it is important to note that due to the intricate interplay between structural and chemical factors, uncovering the fundamental origin of catalytic performance poses considerable challenges. Considering the role of Pd based catalysts in diverse heterogeneous catalytic reactions and problems involved in catalytic hydrogenation reaction our group has investigated the Pd supported catalyst on metal

fluorides which showed a very high catalytic activity of Pd in various organic reaction. However, there is apprehension of using metal fluorides as supports due to the associated hazards while synthesizing these catalysts. Hence the goal of this thesis is to synthesize Pd based catalysts supported on acidic metal oxides and to correlate its catalytic activity for various hydrogenation reactions. To achieve the above-mentioned goals, Pd-supported WO_3/SiO_2 and CuO/CeO_2 , both having Lewis and Brønsted acidic properties, have been analyzed in the present study. Palladium dispersed on high acidic support may hydrogenate most of industrially important compounds in organic synthesis at ambient conditions. By keeping this in mind, few objectives are set for the thesis work as follows-

- Synthesis of Pd- WO_3/SiO_2 catalysts with different Pd loading on WO_3/SiO_2 support with varying acidity by changing WO_3 loading
- Synthesis of Pd- CuO/CeO_2 catalysts with different Pd loading
- Characterization of all synthesized catalysts to understand the characteristics of the catalysts
- To check catalytic activity of both catalysts for hydrogenation of different industrially important compounds
- To optimize the reaction conditions to optimize the yields of desired product and study the recyclability of the catalysts
- To study mechanistic aspect and establish catalyst structure-activity correlation

1.11 References

1. E. Roduner, *Chem. Soc. Rev.*, **2014**, 43, 8226-8239.
2. V. Smil, *Nature*, **1999**, 400, 415.

3. Jens Hagen, Economic Importance of Catalysts, <https://doi.org/10.1002/9783527684625.ch17>
4. P.W.N.M. van Leeuwen, Reference Module in Chemistry, Molecular Sciences and Chemical Engineering. 2016, <https://doi.org/10.1016/B978-0-12-409547-2.11101-1>.
5. K. Kakaei, M. D. Esrafil, A. Ehsani Chapter 1 - Introduction to Catalysis, Interface Science and Technology, **2019**, 27, 1-21.
6. V. Schie MMCH, Spöring J-D, Bocola M, Domínguez de María P, D. Rother, *Green Chem.*, **2021**, 23, 3191-3206.
7. H. J. Federsel, T. S. Moody, S. J. C. Taylor, *Molecules*, **2021**, 26, 2822.
8. A. Bhangale, L. B. Kathryn, A. G. Richard, *Macromol.*, **2012**, 45, 7000-7008.
9. M. Bowker, *Top. Catal.*, **2016**, 59, 663-670.
10. F. Poovan, V. G. Chandrashekhar, K. Natte, R. V. Jagadeesh, *Catal. Sci. Technol.*, **2022**, 12, 6623–6649.
11. M. B. Smith, J. March, March's Advanced Organic Chemistry: Reactions, Mechanisms and Structure, 6th ed.; Wiley:New York, 2007. b) J. Clayden, N. Greeves, S. Warren, Organic Chemistry, 2nd ed.; Oxford University Press: New York, 2012; p 155.
12. R. W. Johnstone, A. H. Wilby, *Chem. Rev.*, **1985**, 85, 129-170.
13. F.T. Zangeneh, S. Sahebdehfar, M.T. Ravanchi, *J. Nat. Gas Chem.* **2011**, 20, 219–231.
14. G.Ertl, H. Knozinger, J. Weitkamp, Handbook of heterogeneous catalysis, Wiley-VCH, Weinheim, **1997**.
15. Gallezot, Pierre. "Hydrogenation - Heterogeneous" in Encyclopedia of Catalysis, Volume 4, ed. Horvath, I.T., John Wiley & Sons, 2003, Jump up^*Horiuti, Iurô; Polanyi, M. (1934)*.

16. P. Sangeetha, K. Shanthi, K.S.R. Rao, B. Viswanathan, P. Selvam, *Appl. Catal. A*, **2009**, 353, 160–165.
17. G.C. Torres, E.L. Jablonski, G.T. Baronetti, A.A. Castro, S.R. de Miguel, O.A. Scelza, M.D. Blanco, M.A. Pena Jimenez, J.L.G. Fierro, *Appl. Catal. A*, **1997**, 161, 213–226.
18. R. M. Magdalene, E.G. Leelamani, N. M. Nanje Gowda, *J Mol. Catal. A Chem.*, **2004**, 223, 17–20.
19. E. Auer, M. Gross, P. Panster, K. Takemoto, *Catal. Today*, **2001**, 65, 31–37.
20. J. Relvas, R. Andrade, F.G. Freire, F. Lemos, P. Araujo, M. J. Pinho, C.P. Nunes, F.R. Ribeiro, *Catal. Today*, **2008**, 133, 828–835.
21. H. Li, Q. Zhao, H. Li, *J. Mol. Catal. A Chem.*, **2008**, 285, 29–35.
22. G.S. Samuelsen, V.L. Garik, G.B.L. Smith, *J. Am. Chem. Soc.*, **1950**, 72, 3872–3874.
23. F. Cardenas-Lizana, S. Gomez-Quero, N. Perret, M. Keane, *Gold Bull.*, **2009**, 42, 124–132.
24. A. Tijani, B. Coq, F. Figueras, *Appl. Catal.*, **1991**, 76, 255–266.
25. F. Cardenas-Lizana, D. Lamey, S. Gomez-Quero, N. Perret, L. Kiwi-Minsker, M.A. Keane, *Catal. Today*, **2011**, 173, 53–61.
26. T. Joseph, K. V. Kumar, A.V. Ramaswamy, S.B. Halligudi, *Catal. Commun.*, **2007**, 8, 629–634.
27. J. M. Campelo, D. Luna, R. Luque, J. M. Marinas, A. A. Romero, *ChemSusChem.*, **2009**, 2, 18–45.
28. E. Garcia-Bordeje, M. F. R. Pereira, M. Ronningc, D. Chenc, *SPR Catal.*, **2014**, 26, 72–108.
29. R. Ciriminna, A. Fidalgo, V. Pandarus, F. Beland, L. M. Ilharco, M. Pagliaro, *Chem. Rev.*, **2013**, 113, 6592–6620.

30. E. Merino, E. Verde-Sesto, E. M. Maya, M. Iglesias, F. Sanchez, A. Corma, *Chem. Mater.*, **2013**, 25, 981–988.
31. Q. M. Kainz, O. Reiser, *Acc. Chem. Res.*, **2014**, 47, 667– 677.
32. J. Li, J. L. Chen, W. Song, J. L. Liu, W. J. Shen, *Appl. Catal. A*, **2008**, 334, 321– 329.
33. X. Y. Liu, M. H. Liu, Y. C. Luo, C. Y. Mou, S. D. Lin, H. K. Cheng, J. M. Chen, J. F. Lee, T. S. Lin, *J. Am. Chem. Soc.*, **2012**, 134, 10251–10258.
34. S. J. Tauster, S. C. Fung, R. L. Garten, *J. Am. Chem. Soc.*, **1978**, 100, 170– 175.
35. M. Turáková, T. Salmi, K. Eränen, J. Wärnä, D. Yu. Murzin, M. Králik, *Appl. Catal. A General*, **2015**, 499, 66–76.
36. S. Gomez, C. Torres, J.L.G. Fierro, C.R. Apesteguia, P. Reyes, *J. Chil. Chem. Soc.*, **2012**, 57, 1194–1198.
37. S. N. Basahel, A. H.A. Medkhali, M. Mokhtar, K. Narasimharao, *Catal. Today*, **2022**, 399, 81-93.
38. W. Nabgan, B. Nabgan, T. A. T. Abdullah, M. Ikram, A. H. Jadhav, A. A. Jalil, M. W. Ali, *ACS Omega*, **2022**, 7, 3324–3340.
39. M. S. Christodoulou, E. M. Beccalli, S. Giofrè, *Catalysts* **2020**, 10, 634, <https://doi.org/10.3390/catal10060634>.
40. L. Cser, *Appl. Phys. Lett.*, **2004**, 85, 1149-1151.
41. L. Schlapbach, A. Züttel, *Nature*, **2001**, 414, 353-358.
42. L. Wang, J. Zhang, Y. Zhu, S. Xu, C. Wang, C. Bian, X. Meng, F.-S. Xiao, *ACS Catal.*, **2017**, 7, 7461-7465.
43. J. Dong, Q. Fu, Z. Jiang, B. Mei, X. Bao, *J. Am. Chem. Soc.*, **2018**, 140, 13808-13816.
44. H. Tang, J. Wei, F. Liu, B. Qiao, X. Pan, L. Li, J. Liu, J. Wang, T. Zhang, *J. Am. Chem. Soc.*, **2016**, 138, 56-59.

45. H. Tang, F. Liu, J. Wei, B. Qiao, K. Zhao, Y. Su, C. Jin, L. Li, J. J. Liu, J. Wang, T., *Angew. Chem. Int. Ed.*, **2016**, 55, 10606-10611.
46. J. Lee, S.P. Burt, C.A. Carrero, A.C. Alba-Rubio, I. Ro, B.J. O'Neill, H.J. Kim, D.H.K. Jackson, T.F. Kuech, I. Hermans, J.A. Dumesic, G.W. Huber, *J. Catal.*, **2015**, 330, 19-27.
47. J.C. Matsubu, S. Zhang, L. DeRita, N.S. Marinkovic, J.G. Chen, G.W. Graham, X. Pan, P. Christopher, *Nat. Chem.* **2017**, 9, 120-127.
48. S. Bonanni, K. Ait-Mansour, W. Harbich, H. Brune, *J. Am. Chem. Soc.* **2012**, 134, 3445-3450.
49. M. Vannice, *J. Catal.* **1979**, 56, 236-248.
50. P. Sonstrom, D. Arndt, X. Wang, V. Zielasek, M. Baumer, *Angew. Chem. Int. Ed.* **2011**, 50, 3888-3891.
51. S. Oh, Y.K. Kim, C.H. Jung, W.H. Doh, J.Y. Park, *Chem. Commun.*, **2018**, 54, 8174-8177.
52. S. Zhang, Z. Xia, T. Ni, Z. Zhang, Y. Ma, Y. Qu, *J. Catal.*, **2018**, 359, 101-111.
53. T.W. van Deelen, C. Hern Mejía, K.P. de Jong, *Nat. Catal.* **2019**, 2, 955-970.
54. L. Liu, A. Corma, *Chem. Rev.*, **2018**, 118, 4981-5079.
55. L. Zhang, M. Zhou, A. Wang, T. Zhang, *Chem. Rev.*, **2020**, 120, 683-733.
56. I. Ro, J. Resasco, P. Christopher, *ACS Catal.* **2018**, 8, 7368-7387.
57. Boaro, S. Colussi, A. Trovarelli, *Front. Chem.*, **2019**, 7, 28, <https://doi.org/10.3389/fchem.2019.00028>.
58. P. Meriaudeau, O. H. Ellestad, M. Dufaux, C. Naccache, *J. Catal.* **1982**, 75, 243-250.
59. A. K. Datye, D. S. Kalakkad, M. H. Yao, D.J. Smith, *J. Catal.* **1995**, 155, 148-153.
60. Y. Lou, J. Liu, *Ind. Eng. Chem. Res.* **2017**, 56, 6916-6925.
61. S.A. Park, D.S. Kim, T.-J. Kim, Y.-T. Kim, *ACS Catal.* **2013**, 3, 3067-3074.

62. Y. Wang, B. B. Chen, M. Crocker, *Catal. Commun.*, **2015**, 59, 195-200.
63. M. Y. Kim, K. Lee, M. Choi, *J. Catal.*, **2014**, 319, 232-238.
64. C. W. Kuo, B. K. Chen, Y. H. Tseng, *J Taiwan Inst. Chem. Eng.*, **2012**, 43, 798- 805.
65. J. R. Regalbuto, *Synthesis of Solid Catalysts*, Wiley-VCH Verlag GmbH & Co. KGaA, **2009**, 33.
66. R. M. Mironenko, O. B. Belskaya, V. P. Talsi, V. A. Likholobov, *J. Catal.*, **2020**, 389, 721–734.
67. R. M. Mironenko, O. B. Belskaya, V. A. Likholobov, *Catal. Today*, **2020**, 357, 152–165.
68. R. Xiong, W. Zhao, Z. Wang, M. Zhang, *Mol. Catal*, **2021**, 500, 111332-111340.
69. R.M. Mironenko, O.B. Belskaya, T.I. Gulyaeva, A.I. Nizovskii, A.V. Kalinkin, V.I. Bukhtiyarov, A.V. Lavrenov, V.A. Likholobov, *Catal. Today*, **2015**, 249,145–152.
70. S. Capelli, S. Cattaneo, M. Stucchi, B. D. Vandegehuchte, A. Chiericato, A. Villa, L. Prati, *Catalysts*, **2022**, 12, 251-563.
71. S. Yasmin, N. Roy, M. H. Kabir, S. Jeon, *Appl. Surf. Sci. Advances*, **2022**, 9, 100235-100245.
72. A. O. Saumell, R. Mariscal, J. Iglesias, P. Maireles-Torres, M. L. Granados, *Sustain. Energy Fuels*, **2022**, 6, 5160–5176.
73. P. Zhang, H. Zhang, S. Wang, X. Lei, J. Yang, Z. Li, H. Zhu, X. Bao, P. Yuan, *J Mater Sci.*, **2020**, 55, 12876–12883.
74. T. Fovanna, M. Nachtegaal, A. H. Clark, O. Krocher, D. Ferri, *ACS Catal.* **2023**, 13, 3323–3332.
75. D. Lee, J. Choi, Y. Lee, J. M. Lee, *Chem. Eng. Res. Des.*, **2021**, 172, 264–279.
76. P. Claus, H. Berndt, C. Mohr, J. Radnik, E. Shin, M. A. Keane, *J. Catal.*, **2000**, 192, 88–97.

77. M. Krause, M. D. Rötzer, A. S. Crampton, M. Huber, U. Heiz, *J. Chem. Phys.* **2019**, 151, 244304.
78. J. Song, S. Liu, C. Yang, G. Wang, H. Tian, Z. Zhao, R. Mu, J. Gong. *Appl. Catal. B: Environmental*, **2020**, 263, 118367-118376.
79. L. Zhang, X. Liu, H. Wang, L. Cao, C. Huang, S. Li, X. Zhang, Q. Guan, X. Shao, J. Lu, *Catal. Sci. Technol.*, **2021**, 11, 4398-4405.
80. W. Alsalahi, W. Tylus A. M. Trzeciak, *Dalton Trans.*, **2021**, 50, 10386–10393.
81. K. N. Patil, D. Prasad, J. T. Bhanushali, B. Kakade, A. H. Jadhav, B. M. Nagaraja *New J. Chem.*, **2021**, 45, 5659–5681.
82. P. J. Naik, Y. An, S. L. Sedinkin, H. Masching, D. Freppon, E. A. Smith, V. Venditti, I. I. Slowing, *ACS Catal.* **2021**, 11, 10553–10564.
83. L. L.R. Vono, C. Broicher, K. Philippot, L. M. Rossi, *Catal. Today*, **2021**, 381, 126–132.
84. J. Liu, T. Zhang, T. Liu, K. Liu, X. Tan, X. Yu, Q. Zhao, *J. Alloys Compod.*, **2023**, 932, 167577.
85. N. Xue, R. Yu, C. Yuan, X. Xie, Y. Jiang, H. Zhou, T. Cheang, A. Xu, *RSC Adv.*, **2017**, 7, 2351–2357.
86. M. Wen, S. Song, Q. Liu, H. Yin, K. Mori, Y. Kuwahara, G. Li, T. An, H. Yamashita, *Appl. Catal. B: Environmental*, **2021**, 282, 119511-119519.
87. O. F. Aldosari, S. Iqbal, P. J. Miedziak, G. L. Brett, D. R. Jones, X. Liu, J. K. Edwards, D. J. Morgan, D. K. Knight, G. J. Hutchings, *Catal. Sci. Technol.*, **2016**, 6, 234–242.
88. J. Sittikun, Y. Boonyongmaneerat, P. Weerachawanasak, P. Praserttham, J. Panpranot, *Reac. Kinet. Mech. Cat.*, **2014**, 111, 123–135.
89. Gou, X. Liang, B. Chen, *Catal. Today*, **2013**, 216, 200–204.


90. H. A. Patel, M. Rawat, A. L. Patel, A. V. Bedekar, *Appl. Organometal Chem.* **2019**; e4767, <https://doi.org/10.1002/aoc.4767>.
91. F. Jiang, J. Cai, B. Liu, Y. Xua, X. Liu, *RSC Adv.*, **2016**, 6, 75541-75551.
92. C. Wang, Z. Liu, L. Wang, X. Dong, J. Zhang, G. Wang, S. Han, X. Meng, A. Zheng, F. Xiao, *ACS Catal.*, **2018**, 8, 474–481.
93. W. Shen, G. A. Tompsett, R. Xing, W. Curtis Conner Jr., George W. Huber, *J. Catal.*, **2012**, 286, 248–259.
94. S. M. Kim, H. Lee, J. Y. Park, *Catal Lett.*, **2015**, 145, 299–308.
95. A.M. Venezia, V. L. Parola, B. Pawelec, J.L.G. Fierro, *Appl. Catal. A: General*, **2004**, 264, 43–51.
96. Y. Wang, S. Kattel, W. Gao, K. Li, P. Liu, J. G. Chen, H. Wang, *Nature Commun.* **2019**, 10, 1166 <https://doi.org/10.1038/s41467-019-09072-6>.
97. M. Kim, S. Choi, *J. Nanomater.*, **2009**, 2009, doi:10.1155/2009/302919
98. Z. Han, C. Tang, F. Sha, S. Tang, J. Wang, C. Li, *J. Catal.*, **2021**, 396, 242–250
99. Z. Chen, S. Wei, X. Zhao, D. Wang, J. Chen, *New J. Chem.*, **2020**, 44, 14560-14567
100. J. Xu, X. Guo, Y. Guan, P. Wu, *Chin. Chem. Lett.*, **2022**, 33, 349-353.
101. K. V. Vikanova, E. A. Redina, G. I. Kapustin, N. A. Davshan, L. M. Kustov, *Russ. J. Phys. Chem. A*, **2019**, 93, 231–235.
102. B. Jenewein, S. Penner, H. Gabasch, D. Wang, A. Gericke, R. Schlögl, K. Hayek, *J. Catal.*, **2006**, 241, 155-161.
103. J. R. Regalbuto, T. H. Fleisch, E. E. Wolf, *J. Catal.*, **1987**, 107, 114-128.
104. F. Al-Wadaani, Elena F. Kozhevnikova, Ivan V. Kozhevnikov *J. Catal.*, **2008**, 257, 199–205.
105. M. Zieliński, M. Pietrowski, A. Kiderys, M. Kot, E. Alwin, *J. Fluorine Chem.*, **2017**, 195, 18-25.

106. V. R. Acham, A. V. Biradar, M. K. Dongare, E. Kemnitz, S. B. Umbarkar, *ChemCatChem.*, **2014**, 6, 3182 – 3191
107. V. Acham, S. Umbarkar, M. Dongare, E. Kemnitz, *Adv. Porous Mater.*, **2006**, 4, 31-38.
108. R. S. Kokane, V. R. Acham, A. B. Kulal, E. Kemnitz, M. K. Dongare, S. B. Umbarkar, *Chemistry Select.*, **2017**, 2, 10618 –10627.
109. O. Machynsky, E. Kemnitz, Z. Karpinski, *ChemCatChem.*, **2014**, 6, 592–602.
110. M. Pietrowski, M. Zielinski, E. Alwin, I. Gulaczyk, R. E. Przekop, M. Wojciechowska, *J. Catal.*, **2019**, 378, 298–311.
111. R. L. Burwell Jr., G. L. Haller, K. C. Taylor, J. F. Read, *Adv. Synth. Catal.*, **1969**, 29, 1.
112. Y. Ono, H. Hattori, *Solid Base Catalysis*, TIT Press, Tokyo, Springer, Heidelberg, **2011**.
113. M. Varga, A. Molnar, G. Mulas, M. Mohai, I. Bertoti, G. Cocco, *J. Catal.*, **2002**, 206, 71-81.
114. Y. Z. Chen, C. M. Hwang, C. W. Liaw, *Appl. Catal., A*, **1998**, 169, 207-214.
115. W. Shen, M. Okumura, Y. Matsumura, M. Haruta, *Appl. Catal. A: General*, **2001**, 213, 225–232.
116. Y. He, J. Fan, J. Feng, C. Luo, P. Yang, D. Li, *J. Catal.*, **2015**, 331, 118–127.
117. A.B. Kulal, M. K. Dongare, S. B. Umbarkar, *Appl. Catal. B; Environmental*, **2016**, 182, 142-152.
118. W. Yang, Z. Gao, X. Liu, C. Ma, X. Ding, W. Yan, *Fuel*, **2019**, 243, 262-270.



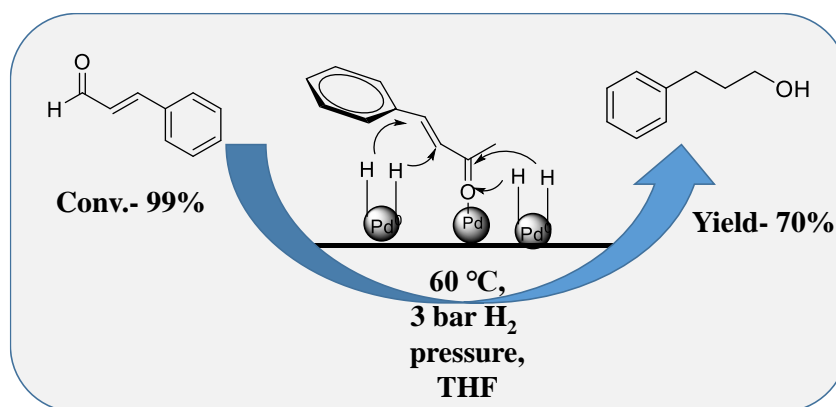
Chapter 2

***Pd-WO₃/SiO₂: Synthesis,
Characterization and Its Catalytic
Application for Hydrogenation of
Cinnamaldehyde under Ambient
Conditions***



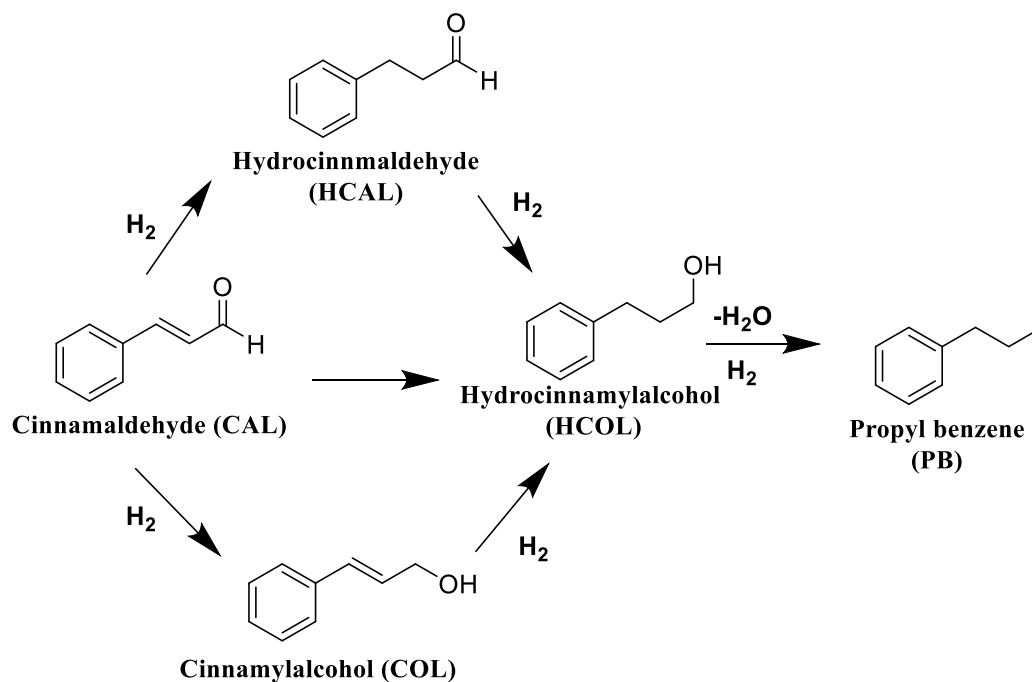
Abstract

A series of palladium supported on WO_3/SiO_2 mixed oxide with different Pd loading (0.1, 0.5, 1, and 2 wt %) were synthesized by wet impregnation of palladium on WO_3/SiO_2 prepared by sol-gel method and characterized by various physico-chemical techniques. The detailed characterization revealed the formation of $Pd/WO_3/SiO_2$ catalyst with high Pd dispersion (36%) on acidic support WO_3/SiO_2 . This catalyst has shown very high efficiency for hydrogenation of cinnamaldehyde at 60 °C and 3 bar H_2 pressure. Using 1%Pd- WO_3/SiO_2 hydrogenation of cinnamaldehyde was achieved with 99% conversion and 70% hydrocinnamyl alcohol selectivity under ambient condition. Selective hydrogenation of cinnamaldehyde to hydrocinnamyl alcohol has been attributed to the high dispersion and large particle size of Pd on WO_3/SiO_2 acidic support. The catalyst was successfully recycled for three times without any loss in catalytic activity. Mechanistic studies using FTIR analysis showed the adsorption of cinnamaldehyde on 1%Pd- WO_3/SiO_2 catalyst through C=O group. Dissociative adsorption of hydrogen molecule takes place on reduced Pd on WO_3/SiO_2 support, into two hydrogen atom. These hydrogen atoms react with the adsorbed cinnamaldehyde molecule and transfer it to hydrocinnamyl alcohol.

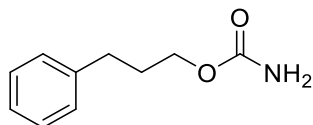


2.1 Introduction

Hydrogenation is an important organic reaction, which has valuable industrial applications in the production of fine chemicals, flavors, agrochemicals, fragrances, and pharmaceutical industry. Catalytic hydrogenation of cinnamaldehyde (CAL) is an important reaction in chemical industry. CAL is α, β -unsaturated aldehyde which contains C=C and C=O conjugated system. Due to the hydrogenation of C=C and C=O bond it gives different hydrogenated products such as hydrocinnamaldehyde (HCAL), cinnamyl alcohol (COL), 3-phenyl propanol or hydrocinnamyl alcohol (HCOL) and propyl benzene (PB) as shown in Scheme 2.1. All the products are important in chemical industries. Among this HCOL is used as food flavoring agent, in the preparation of essence. It is usually used to make peach, apricot, watermelon, plum, watermelon, strawberry, and walnut and hazelnut essences. It is a key intermediate in medicine, proformiphen (Phenprobamate) which is a central skeletal muscle relaxant (Scheme 2.2).



Scheme 2.1. Hydrogenation of cinnamaldehyde



Scheme 2.2. Phenprobamate

Variety of homogeneous and heterogeneous catalysts have been reported for selective hydrogenation of CAL to HCAL and COL [1-8], but very few are reported for HCOL under ambient condition. Till date, both non-noble metal (e. g., Fe, Ni, Co and Cu) and noble metal (e. g., Pt, Pd, Ru, and Ir) nanoparticles (NPs) have been used as efficient catalysts to produce HCOL [9-13]. Some studies have reported the effect of metal (Pt, Rh, and Ru) particle size on selective hydrogenation of CAL [3, 5, 14-16]. In 1990 Giroir-Fendler et al. ascribed the particle size of metals affect the directional effect of the phenyl ring [17]. According to the authors, the phenyl group is repulsed by the metal surface preventing the C=C bond approach the metal surface. As a result, only the C=O bond can approach the metal, resulting in high selectivity for C=O bond hydrogenated products. On the other hand, phenyl group does not interact with the metal surface of microscopic particles, thus both the C=O and C=C bonds can approach the metal surface and undergo hydrogenation. Galvagno et al. [18] reported that the proportion of corners, edges, and faces revealed to the substrate varies as a function of particle size. Different catalytic characteristics can be found in atoms in varied crystallographic locations, resulting in different activities and selectivity. Ma et al. reported 3%Pt/CNTs (carbon nanotubes) catalyst which completely hydrogenate both C=C and C=O bonds on CAL to obtain HCOL, with selectivity about 80% at 80 °C and 30 bar H₂ pressure after longer reaction time (12 h) [19]. Asedegbega-Nieto et al. have carried out CAL hydrogenation on bimetallic catalyst Ru–Cu and Ni– Cu supported on graphite [20]. The reactions were performed over monometallic catalysts (Ru and Ni/graphite) and bimetallic catalysts (Ru-Cu and Ni-Cu/graphite) with varying metal percentage. For Ru-

Cu/graphite series, the monometallic 2Ru/graphite catalyst gave both saturated products (HCAL and COL) and unsaturated alcohol (HCOL). At the lower Cu content (2Ru0.3Cu/graphite) the selectivity for COL is high while when the Cu content increased (2Ru0.9Cu/graphite) the selectivity for HCOL increased. In case of Ni-Cu Series there is no significant change in selectivity. 1.2%Pt/SiO₂ catalyst prepared by impregnation and hydrogen reduction method was used for the hydrogenation of CAL [21]. The catalyst revealed the high activity and selectivity to HCOL (60%) at 10 bar H₂ and 80 °C in 2 h. S. Chang et al. used Pt/graphite to perform the hydrogenation of CAL under milder reaction conditions (60 °C, 3bar H₂ pressure, 4 h) [22]. 2% Pt/graphite gave 6% CAL conversion with 83% selectivity of HCOL. When Pt loading reached 4%, the conversion of CAL increased to 97% with 97% selectivity for HCOL. Even though the reaction conditions are efficient for commercial process, but the higher metal loading makes process expensive. Therefore, it is highly desired to develop the active catalyst to get saturated alcohol (HCOL).

Previously, we have synthesized palladium supported on magnesium hydroxyl fluoride Pd-MgF₂·*x*(OH)_{*x*} catalysts which showed very high efficiency for selective hydrogenation of various olefins/nitro-aromatics under ambient conditions [23, 24]. The high activity was attributed to the acidity of the support which enhanced metal-support interaction and Pd dispersion thus leading to activation of hydrogen under ambient conditions. To study the effect of different acidic supports with tunable acidity on Pd dispersion, metal-support interaction and in turn on hydrogenation activity, we prepared a series of WO₃/SiO₂ solid acid catalysts by simple sol-gel method with varying WO₃ loading for supporting Pd and its activity for CAL hydrogenation.

2.2 Experimental Section

2.2.1 Materials

All the reagents such as palladium acetate, ammonium meta-tungstate (AMT), ethyl silicate-40 (ES-40) and sodium salt of cinnamaldehyde, hydrocinnamaldehyde, 3-phenyl propanol and propyl benzene and solvents such as methanol, ethanol, THF, toluene were procured from Molychem India, Chemplast, Chennai, Sigma Aldrich and used as such without further purification.

2.2.2 Catalyst Preparation

The support WO_3/SiO_2 (WS) with different WO_3 loadings (10, 15, and 20 wt% WO_3 loading on SiO_2) was synthesized by previously reported method [25], using ES-40 as silica precursor and ammonium meta-tungstate (AMT) as WO_3 precursor, respectively by sol-gel technique. Subsequently, palladium (0.1%, 0.5%, 1%, and 2 wt%) was loaded on WS support by simple impregnation method.

The typical synthesis procedure for 20% WO_3/SiO_2 (20WS) and 1%Pd20WS (1P20WS) is described below:

(a) Synthesis of 20WS

Ammonium meta-tungstate (AMT) (5.31 g) was dissolved in 10 mL distilled water and added drop wise into dry IPA solution (35 ml) of ES-40 (50.0 g) with constant stirring. To this solution 3 mL dil. NH_4OH (2.5%) solution was added and stirred until the formation of white gel. This resultant gel was air dried and calcined at 500 °C in air for 5 h.

(b) Synthesis of 1P20WS

The calcined support 20WS (5 g) was dispersed in 50 mL methanol. Solution of palladium acetate (0.105 g) in mixture of methanol (10 mL) and acetone (10 mL) was added drop wise to the slurry of 20WS with constant stirring. This slurry was stirred for 2 h. The solvent was removed on rotary evaporator. The solid was dried at 100 °C and calcined at 250 °C in air for 5 h. Similarly, all the catalysts with different palladium loadings (0.1, 0.5 and 2%) supported on 20WS were

prepared. Similarly, 1% Pd loaded catalysts on 10WS and 15WS support were also prepared. The nomenclature for the catalysts is specified below in Table 2.1.

Table 2.1. Nomenclature of all xPd-yWO₃/SiO₂ catalysts

Sr. No.	Catalyst name	Wt% of Pd	Wt% of WO ₃
		x	y
1	0.1P20WS	0.1	20
2	0.5P20WS	0.5	20
3	1P20WS	1	20
4	2P20WS	2	20
5	1P15WS	1	15
6	1P10WS	1	10

2.2.3 Catalysts characterization

(a) X-ray Diffraction analysis

All the synthesized catalysts were characterized by X-ray diffraction method using PAN analytical X'Pert Pro Dual Goniometer diffractometer. The diffractometer consists of X'celerator solid state detector with CuK α ($\lambda=1.5406\text{\AA}$, 40kV, 30mA) radiation and a Ni filter. The X-ray diffraction pattern of the sample was collected in the range of $2\theta = 20-80^\circ$ with a step size of 0.02° and a scan rate of 4° min^{-1} .

(b) BET surface area measurements

The Brunauer–Emmett–Teller (BET) specific surface area of the catalyst was determined by N₂ sorption method at -196°C , using Auto-sorb Quanta Chrome equipment. The sample was pretreated at 200°C under vacuum prior to N₂ adsorption.

(c) Chemisorption studies

The chemisorption study of H₂ was carried out using Qudrasorb instrument. The catalyst sample (0.15 g) was pretreated at 250 °C with 10 °C min⁻¹ heating rate, for 2 h. The catalyst was reduced at 400 °C in hydrogen for 2 h. The analysis was carried out at 30 °C, with the help of stoichiometry of 1:2 of palladium and H₂.

(d) Fourier Transform Infrared Spectroscopic studies

The Fourier transform infrared (FTIR) spectra of the samples were recorded on a Thermo Nicolet Nexus 670 IR instrument using DTGS detector. KBr pellet method was used for preparation of samples with a resolution of 4 cm⁻¹ in the range of 4000-400 cm⁻¹ and 100 scans.

(e) XPS analysis

X-ray photoelectron spectroscopy (XPS) measurements for all the catalysts were carried out using Thermo K-alpha spectrometer using micro focused and monochromatic Al K α radiation with energy 1486.6 eV. The samples were degassed at 300K for 4 h in a vacuum chamber. Charge compensation was done with the help of electron flood gun. The calibration is done with respect to binding energy (BE) values by referring standard C 1s peak (284.6 eV) of contaminant carbon.

(f) Electron microscopy

The morphology of the samples were determined using scanning electron microscopy (SEM) on a FEI quanta 200 3D dual beam ESEM instrument having thermionic emission tungsten filament in the 3 nm range at 30 kV. The particle size was determined using transmission electron microscopy (TEM) and analysis was done on a Tecnai G2-20 FEI instrument operating at an accelerating voltage of 300 kV. Before analysis, the powder samples were ultrasonically dispersed in isopropanol, and deposited on a carbon coated copper grid, dried in air before TEM analysis.

2.2.4 Catalytic activity

(a) Hydrogenation of Cinnamaldehyde

The catalytic hydrogenation of CAL was carried out in 50 mL two necked round bottom flask at room temperature and 1 atm pressure of H₂. Initially the catalyst (1P20WS) (0.1g) was reduced *in-situ* in ethanol (15 mL) by bubbling H₂ (10 mL/min) for 15 min before each catalytic reaction. Then CAL (1 g) was added to the flask. The reaction mixture was stirred at room temperature with H₂ gas continuously bubbling through the reaction mixture. The analysis was periodically carried out on gas chromatography Shimadzu equipped with a HP-5 column (30 mm × 0.25 mm × 0.25 μm) and FID detector. Conversion of CAL was calculated based upon the GC by external calibration method, where substrate conversion = [moles of substrate reduced]/[Initial moles of substrate used] × 100. The product identification was carried out by comparing authentic standard samples in GC. For pressure effect, the hydrogenation was performed in a 50 mL high-pressure autoclave of Amar make. The reactor was charged with a known quantity of catalyst, 15 mL THF, and substrates. Before starting the reaction the reactor was purged with hydrogen three times, and then the reactor was filled with desired pressure of hydrogen. The reactor was heated to the required temperature of the reaction. Once the temperature was attained the stirring of the reactor was started and the reaction was carried out for 2-8 h. After completion of the reaction the stirring was stopped, and the reactor was cooled down to room temperature. The reactor was depressurized and the analysis of the reaction mixture was carried out.

(b) Procedure for catalyst recycles study

The catalyst recycle study was carried out using 1P20WS catalyst for CAL hydrogenation under optimized reaction conditions [1 g CAL, 0.10 g catalyst (10 wt% catalyst with respect to substrate), 15.0 mL THF, 3 bar H₂ pressure, 60 °C, t-8 h]. After 8 h of the reaction, the catalyst was separated from the reaction mixture by centrifugation; the separated catalyst was washed with methanol for

2-3 times. Further, the washed catalyst was dried in an oven at 80 °C. This dried catalyst was used for the next reaction with the same charge. Again the same procedure was repeated for the next three cycles.

2.3. Results and Discussions

2.3.1 Catalyst characterization

A series of Pd-WO₃/SiO₂ (PWS) catalysts with Pd loading ranging from 0.1 to 2 wt% on 20% WO₃/SiO₂ (20WS) were prepared by wet impregnation method using palladium acetate as palladium pre-cursor. To study the effect of support acidity on catalyst activity, we have also prepared catalysts with 1% Pd loading on 10% WS and 15% WS. The acid strength of the WO₃/SiO₂ supports with varying WO₃ loading is shown in Table 2.2 [25]. Increase in the acidity from 0.34 to 0.56 mmol NH₃/g was observed with increase in the WO₃ loading from 10 to 20%, with maximum acidity for 20WS (0.56 mmol/g) [25].

(a) X-ray diffraction studies

The X-ray diffraction pattern of all the prepared catalysts were analysed for its crystalline phases and the information is provided in Figure 2.1. The XRD pattern showed all the characteristic peaks for monoclinic crystalline WO₃ phases, at 23.1, 23.6, 24.2, 26.6, 28.8 and 33.5° corresponding to (002), (020), (220) and (202) planes. The XRD patterns also indicate the crystalline nature of WO₃ phase with underlying broad peak for amorphous silica centered at 24°. The intensities and positions of the peaks are in accordance with the literature (JCPDS no. 43-1035). However, no peaks corresponding to the palladium were observed in the XRD pattern of the catalysts even for 2% Pd loading, probably due to low palladium loading and high dispersion on the support.

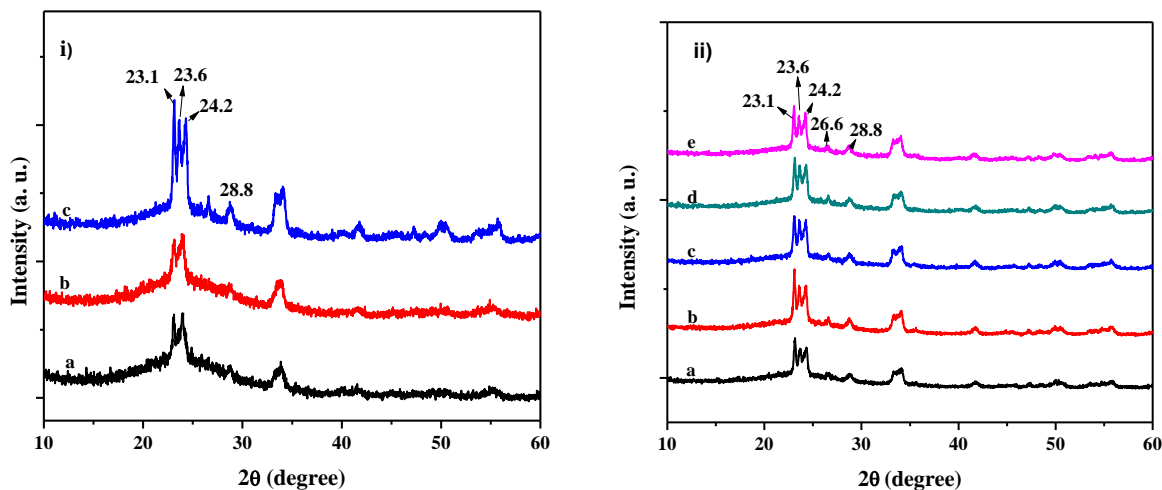


Figure 2.1. XRD pattern of (i) (a) 1P10WS, (b) 1P15WS and (c) 1P20WS, (ii) (a) 20WS, (b) 0.1P20WS, (c) 0.5P20WS, (d) 1P20WS and (e) 2P20WS

(b) BET surface area analysis

The surface area of the support and metal dispersion of the Pd loaded catalysts was determined using BET method and chemisorption respectively, which is given in Table 2.2. The surface area for the supports decreased with increasing WO_3 loading from $553 \text{ m}^2/\text{g}$ for 10WS to $289 \text{ m}^2/\text{g}$ for 20WS. Similarly, there was a decrease in surface area from $289 \text{ m}^2/\text{g}$ with increasing palladium loading, such as 278, 274, 264, and $255 \text{ m}^2/\text{g}$ respectively for 0.1P20WS, 0.5P20WS, 1P20WS, and 2P20WS catalysts. There was no specific trend observed in pore size and pore volume. The adsorption-desorption isotherms of all the Pd loaded catalysts are shown in Figure 2.2, which showed type IV isotherm pattern for all the catalysts confirming its mesoporous nature. The metal dispersion was calculated from the H_2 chemisorption. Very high Pd dispersion on acidic support (Table 2.2) was observed; 0.1P20WS showed maximum Pd dispersion of 40% followed by 0.5P20WS (38%), 1P15WS (37%), and 1P20WS (36%).

Table 2.2. Surface properties of the PWS catalysts

Sr. No.	Catalyst	Surface area, (m ² /g)	Pore size, (Å)	Pore volume, (cc/g)	Pd Dispersion, (%)	NH ₃ Desorbed, mmol/g
1	10WS	553	20	0.56	-	0.34
2	1P10WS	489	16	0.38	33	-
3	15WS	438	44	0.96	-	0.35
4	1P15WS	394	30	0.59	37	-
5	20WS	289	36	0.53	-	0.56
6	0.1P20WS	278	26	0.35	40	-
7	0.5P20WS	274	22	0.30	38	-
8	1P20WS	264	24	0.31	36	-
9	2P20WS	255	15	0.34	33	-

(c) Fourier Transform Infrared spectroscopy

The FTIR spectra of PWS catalysts were studied using KBr pellet method (Figure 2.3). Very strong band between 1300-1000 cm⁻¹ for Si-O-Si appeared mainly due to asymmetric stretching, symmetric stretching and bending vibrations, whereas, W=O_t and W-O-W stretching were observed as weak bands at 959 and 806 cm⁻¹. The bands at 467 cm⁻¹ are assigned to O-Si-O bending vibrations. The band at 1630 cm⁻¹ can be attributed to surface hydroxyl groups.

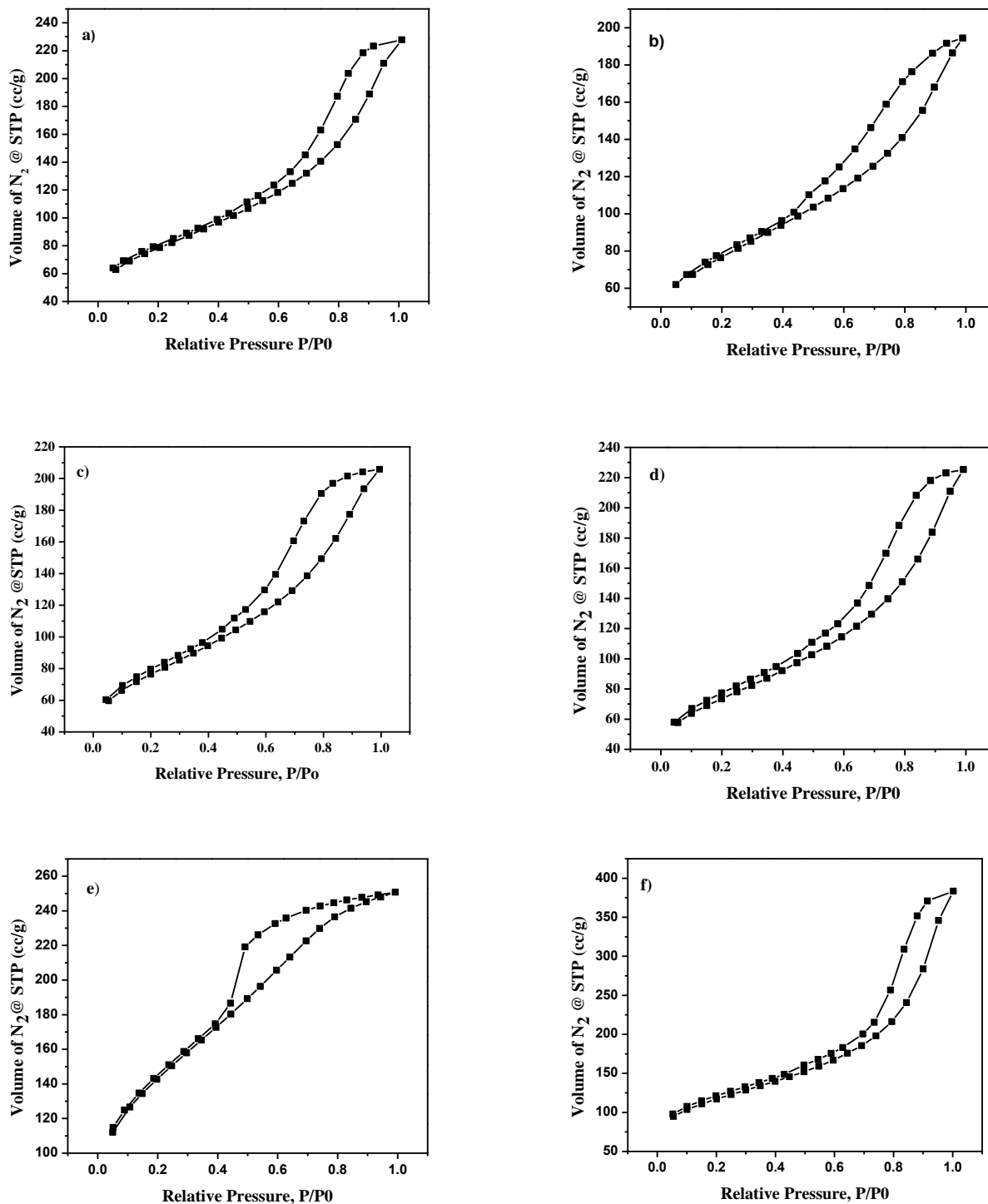


Figure 2.2. BET surface area analysis of (a) 0.1P20WS, (b) 0.5P20WS, (c) 1P20WS, (d) 2P20WS, (e) 1P10WS and (f) 1P15WS

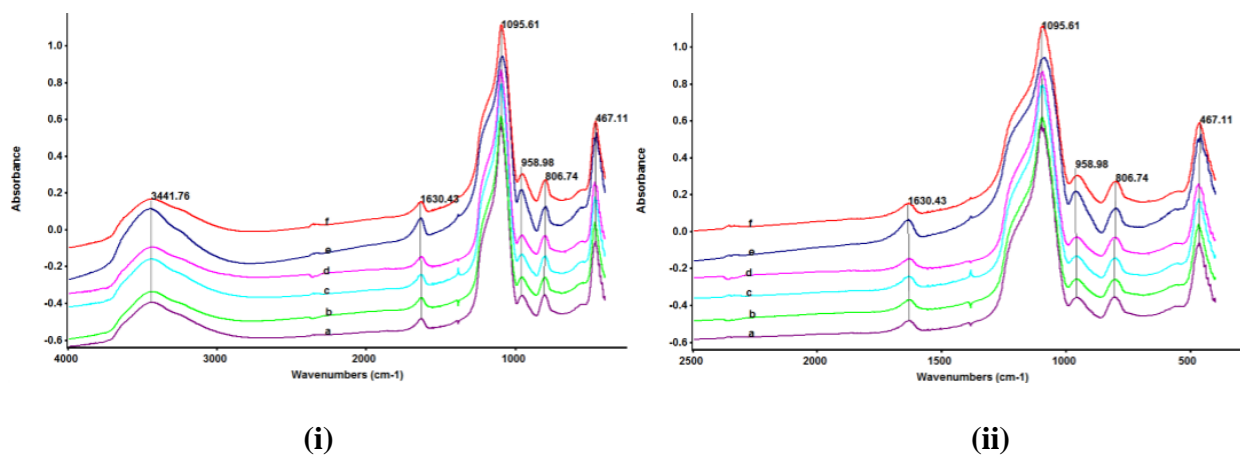


Figure 2.3. FTIR spectra of all PWS catalysts in the range i) 400 to 4000 cm^{-1} and ii) 400 to 2000 cm^{-1} , (a) 0.1P20WS, (b) 0.5P20WS, (c) 1P20WS, (d) 2P20WS, (e) 1P10WS and (f) 1P15WS

(d) X-ray Photoelectron Spectroscopy

X-ray photoelectron spectroscopy (XPS) was utilized to determine the electronic state of palladium in fresh, and activated (reduced in H_2 atmosphere) catalysts (Figure 2.4A). Palladium 3d core level spectrum of the catalyst with the binding energy (BE) of the Pd 3d_{5/2} peak at 335.1 eV, corresponding to metallic palladium, while, Pd3d_{3/2} peaks at 336.7 eV and 336.4 eV, corresponding to Pd⁺² phase was observed in the fresh catalyst indicating presence of both Pd(0) and Pd(+2). However, only metallic palladium species (Pd 3d_{5/2} at 335.1 eV) was observed in the activated catalyst, due to complete reduction of Pd²⁺ to Pd⁰, in presence of hydrogen under ambient conditions. This indicates very facile reduction of Pd (+2) to Pd (0) at room temperature and atmospheric pressure. Figure 2.4(B) represents W4f core level spectra, where doublet can be deconvoluted into pair of peaks with binding energies at 35.1-35.7 eV for W 4f_{7/2} and 37.3-37.8 eV for W 4f_{5/2}, respectively. These peaks can be attributed to +6 oxidation state of tungsten by comparing with earlier literature [26].

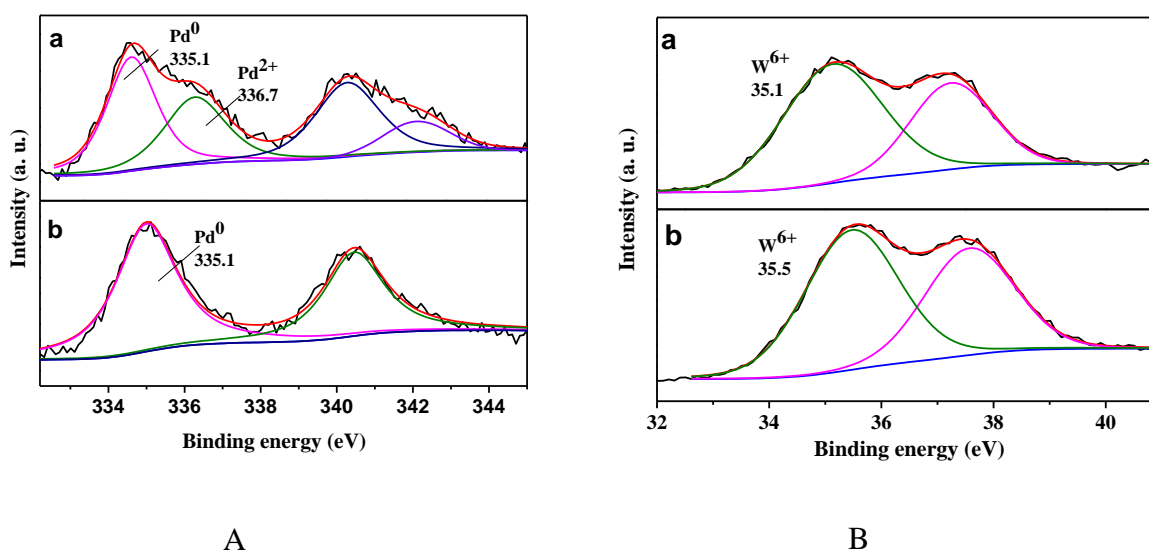


Figure 2.4. XPS spectra related to (A) Pd3d, (B) W4f of a) fresh, b) activated 1P20WS catalyst

(e) TEM Analysis

The palladium particle size was determined using the TEM analysis (Figure 2.5 to 2.9). The catalyst prepared by the impregnation method showed very high dispersion of the palladium particles. Most of the Pd particles were found to be in range of 12-18 nm though the particle size distribution ranged up to 25 nm. The tungsten and palladium particles were distinguished by characteristics d spacing values. Palladium nano-particles were found to be in (111) plane as confirmed by characteristics d spacing of 0.23 nm [27]. The particle size distribution is given as Figure inset. The particle size distribution ranges over 5-25 nm, however, maximum particles are in the range of 12 nm - 18 nm.

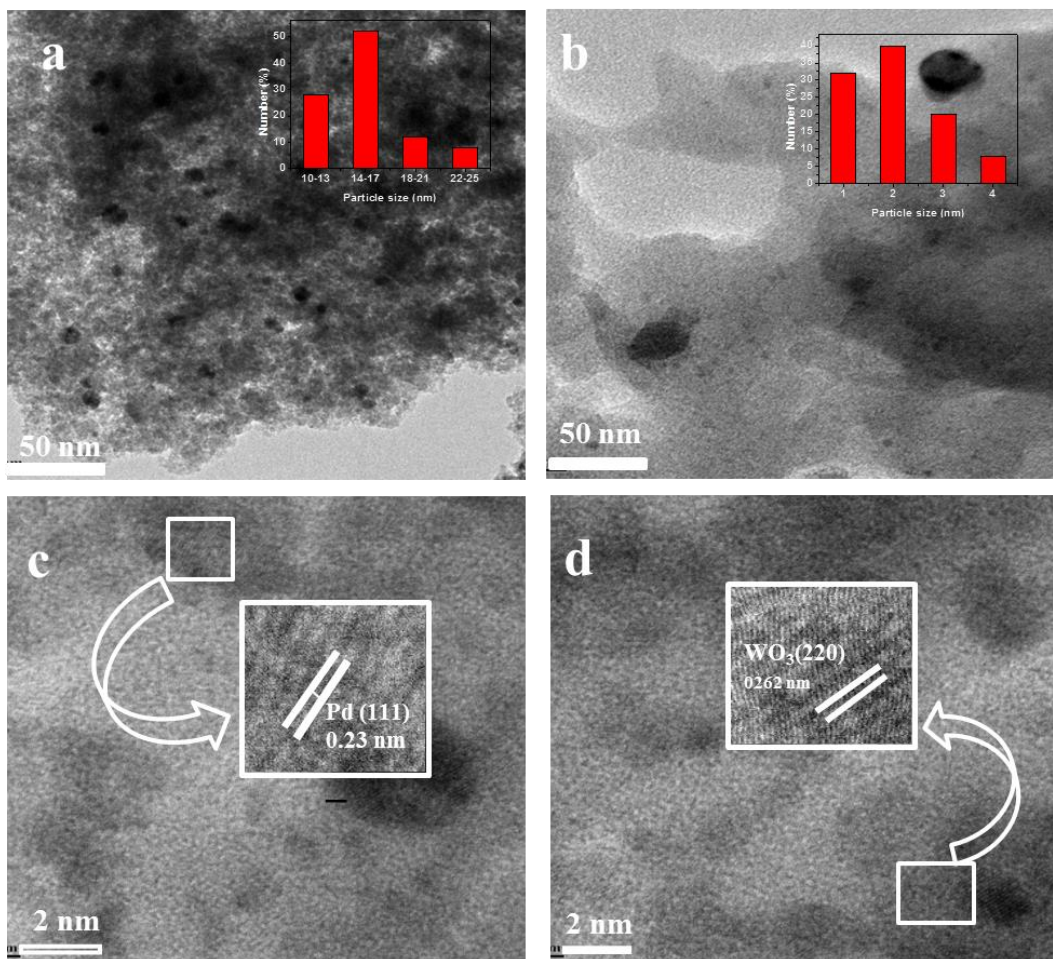


Figure 2.5. TEM images of 1P20WS catalyst

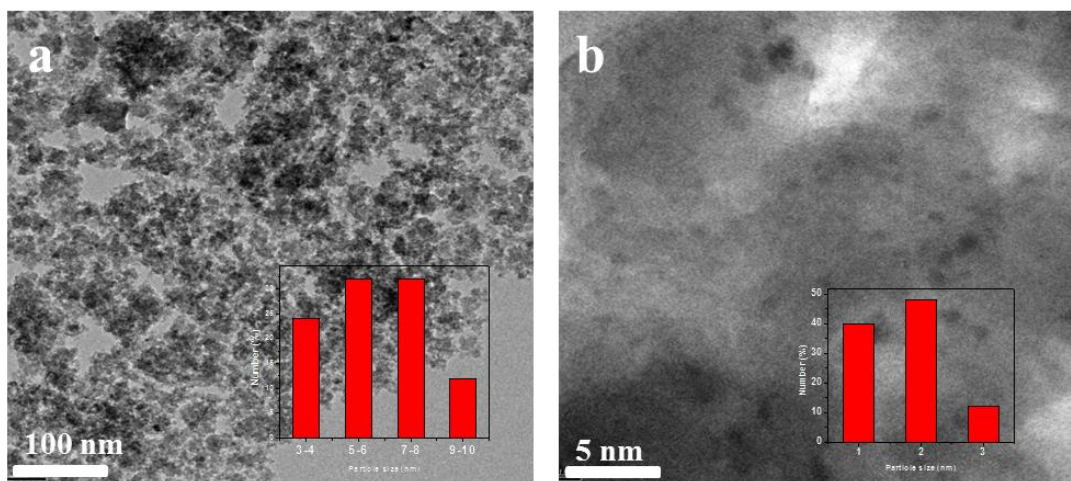


Figure 2.6. TEM images of 0.1P20WS catalyst

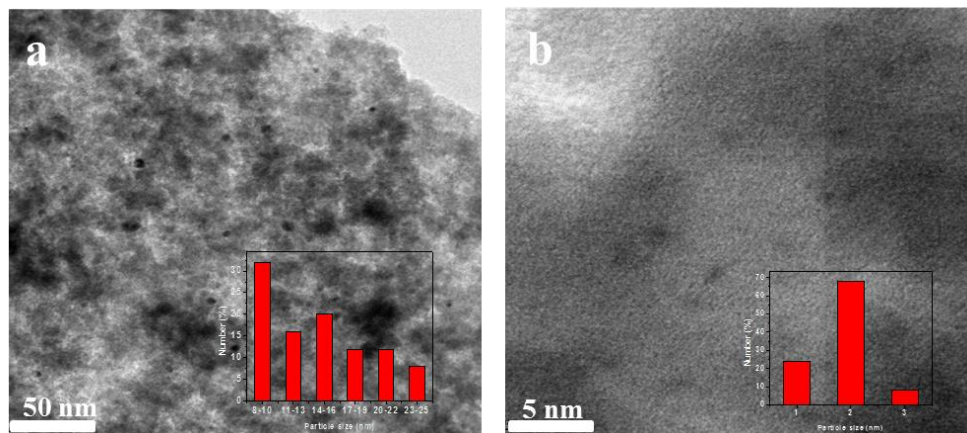


Figure 2.7. TEM images of 0.5P20WS catalyst

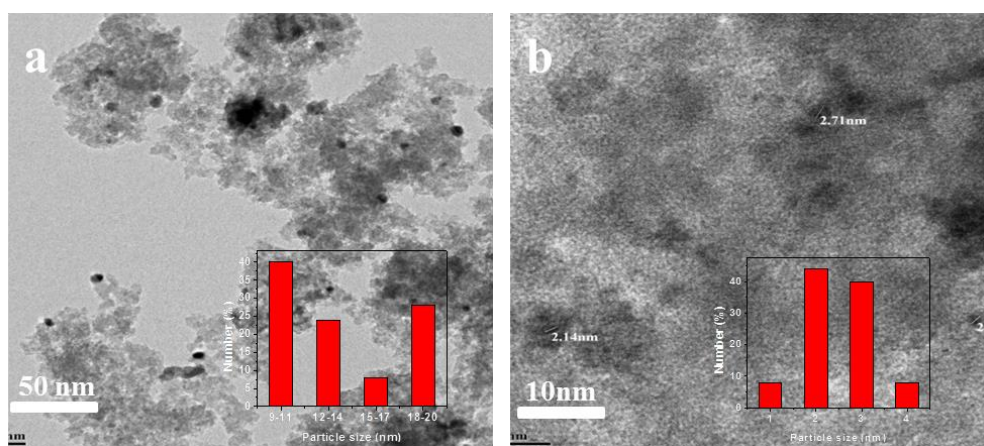


Figure 2.8. TEM images of 2P20WS catalyst

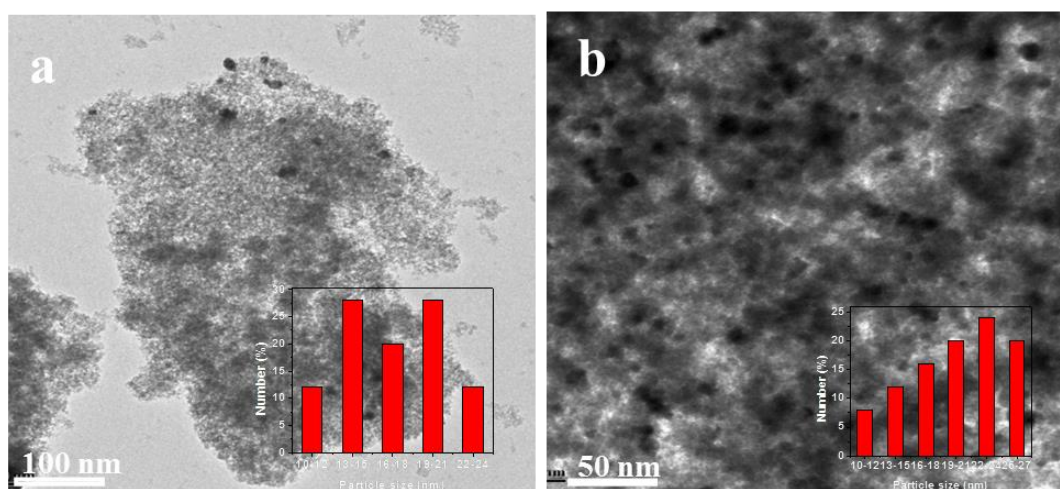


Figure 2.9. TEM images of (a) 1P10WS and (b) 1P15WS catalyst

As previously reported [25], the formation of very small particles of WO_3 (2-5 nm) dispersed on SiO_2 are formed due to sol gel preparation method. The loaded palladium has formed nano sheets on WS support as confirmed from Figure 2.5c. The catalysts showed very high metal dispersion (36%) compared to the literature reports. Palladium dispersion on commercial carbon of very high surface area ($1400 \text{ m}^2/\text{g}$) was reported to be only 30% for 1% Pd loading [28]. The Pd (3%) dispersed on high surface area carbon ($844 \text{ m}^2/\text{g}$) used for nitrobenzene hydrogenation showed only 12.4% Pd dispersion [29]. The high metal dispersion can be attributed to the formation of palladium nano-sheets on the surface. This observation is in agreement with our previous work where Pd nano sheets formation was observed on acidic $\text{MgF}_{2-x}(\text{OH})_x$ support [23].

(f) SEM analysis

SEM images of all the prepared catalysts are shown in Figure 2.10. All the catalysts showed almost similar morphology and particle size with some particles in the range of 10-20 μm and some very small particles of $<5 \mu\text{m}$. Elemental analysis of catalysts carried out by EDAX technique is presented in Table 2.3.

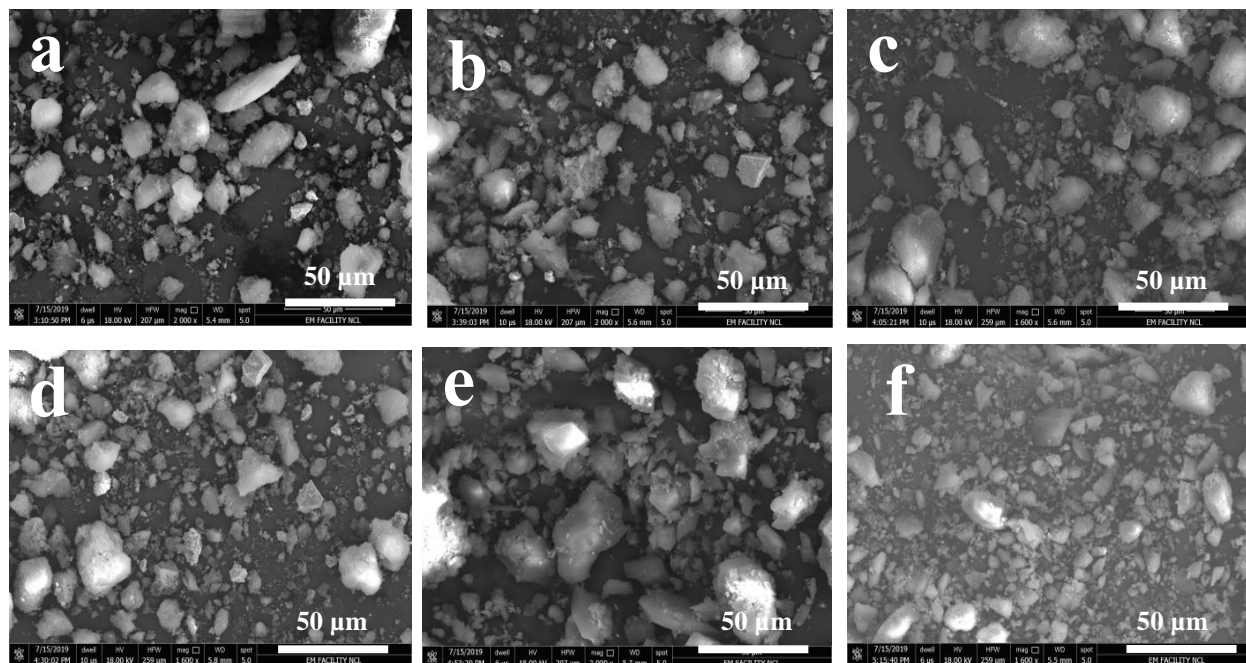


Figure 2.10. SEM images of (a) 0.1P20WS, (b) 0.5P20WS, (c) 1P20WS, (d) 2P20WS, (e) 1P10WS and (f) 1P15WS catalyst

Table 2.3. Elemental composition of catalysts by EDAX

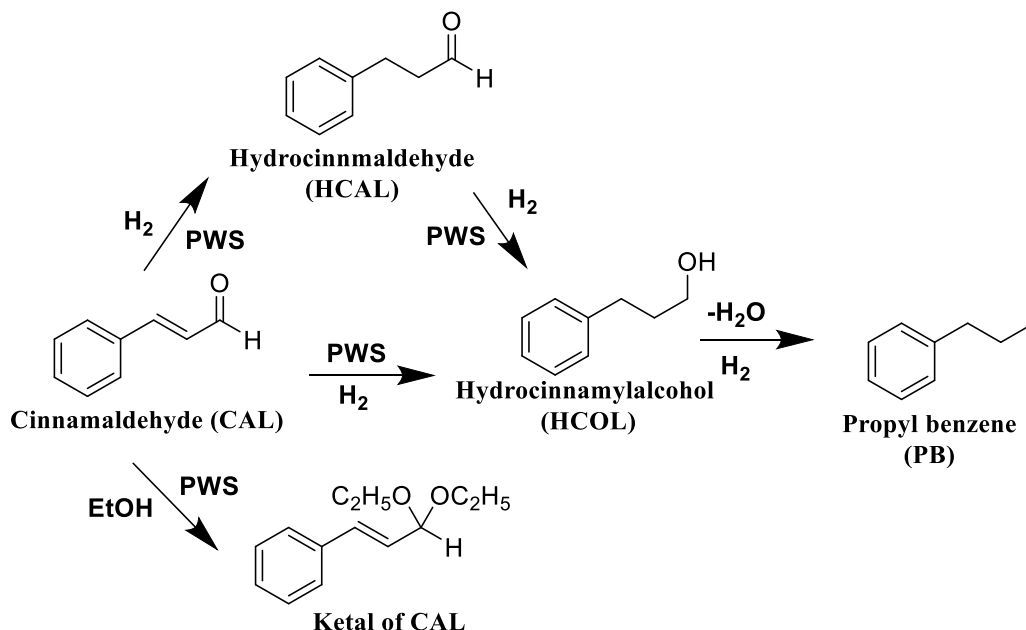
Entry	Catalyst	Elemental Composition (%)			
		Pd	W	Si	O
1	0.1P20WS	0.22	4.17	37.49	58.12
2	0.5P20WS	0.32	2.86	35.46	61.36
3	1P20WS	1.43	6.20	35.29	57.08
4	2P20WS	1.62	14.06	24.71	59.62
5	1P10WS	0.78	6.68	30.63	61.73
6	1P15WS	0.97	16.50	36.18	46.73

2.3.2 Catalytic activity for Cinnamaldehyde hydrogenation

(a) Catalysts screening

The catalytic performance of the palladium supported on WO_3/SiO_2 catalyst was evaluated

for hydrogenation of CAL initially in ethanol at room temperature and atmospheric pressure by continuous bubbling hydrogen gas (10-12 ml/min) through the reaction mixture. There were three hydrogenated products obtained such as HCAL, HCOL, and PB. Along with these hydrogenated products ethyl ketal of CAL was also obtained because the reaction was carried out in ethanol as shown in Scheme 2.3.



Scheme 2.3. Hydrogenation of CAL on PWS catalyst

For comparison, the reaction was carried out using support (20WS) under identical reaction conditions. As expected, the reaction showed very low conversion of CAL (9%) with lower yield (1%) for hydrogenated product HCAL and high (8%) for ketal of CAL (Table 2.4, entry 1). To study the effect of individual components of the support, the reaction was carried out using 1%Pd/SiO₂ and 1%Pd/WO₃ catalyst also; it gave 26% and 22% CAL conversion respectively (Table 2.4, entry 2-3). To study the effect of support acidity on CAL hydrogenation, reaction was also performed using 1P10WS, 1P15WS, and 1P20WS under same reaction condition (Table 2.4, entry 4-6). The catalytic activity increased with increasing the acidity of the support. As mention

above the acidity trend for the support is as follows: 20WS > 15WS > 10WS. As the acidity of 1P20WS catalyst was high it gave high CAL conversion of 93%. While 1P15WS, and 1P10WS catalyst gave 79%, and 63% CAL conversion respectively. The very high activity under ambient condition of the catalysts can be attributed to the very high Pd dispersion on acidic support. This observation is in agreement with our previous results for hydrogenation of styrene under ambient conditions using 1%Pd/MgF_{2-x}(OH)_x, where very high activity was attributed to very high Pd dispersion (48%) and formation of Pd nano sheets on acidic MgF_{2-x}(OH)_x support [23]. Similarly in case of PWS catalysts Pd nano sheet formation was observed on WS support (Figure 2.5. to 2.9.) explaining the high activity of the catalyst for hydrogenation of CAL under ambient conditions. As the rate of hydrogenation is high for 1P20WS, high yield for hydrogenated products was obtained. Almost 40% yield was obtained for HCOL.

Table 2.4. The catalyst screening for CAL hydrogenation

Sr. No.	Catalyst	Time h	Conv. %	Yield PB	Yield HCAL	Yield HCOL	Yield ketal of CAL
1	20WS	8	09	-	1	-	8
2	1Pd/SiO ₂	8	26	-	2	1	23
3	1Pd/WO ₃	8	22	-	2	-	20
4	1P10WS	8	63	2	6	11	44
5	1P15WS	8	79	4	14	27	34
6	1P20WS	8	93	4	17	40	32

Reaction condition- CAL (1 g), 10 wt % catalyst w.r.t. substrate, 15 ml solvent (ethanol), H₂ bubbling, temp-RT.

(b) Solvent effect on Cinnamaldehyde hydrogenation

The effect of various solvents on the hydrogenation of CAL and the yield of hydrogenated products was studied using the polar (methanol, ethanol, and Tetrahydrofuran (THF)) and nonpolar solvents (toluene), and the results are shown in Table 2.5. A very high CAL conversion was obtained in polar solvents with the better yield of HCOL as compared to the nonpolar solvents. The higher rate of hydrogenation in the polar solvent may be due to a high dipole moment, high dielectric constant, and also high hydrogen donor ability of polar solvents [30, 31]. In methanol and ethanol, higher CAL conversion (>99% and 93% respectively) was obtained but due to acidic support the rate of ketal formation was higher than the rate of hydrogenation. Hence in both solvent the yield of ketal of CAL was high as compare to hydrogenated products. In THF 62% CAL conversion was obtained with 47% yield of HCOL. In nonpolar solvent toluene; CAL conversion was 59% with 32% yield for HCOL. In THF good CAL conversion (62%) with high yield (47%) for HCOL was obtained, hence THF was used as solvent for further parametric study.

Table 2.5. Solvent effect on hydrogenation of CAL

Sr. No.	Solvent	Time h	Conv. %	Yield PB	Yield HCOL	Yield HCOL	Ketal of CAL
1	Methanol	8	>99	3	4	22	68
2	Ethanol	8	93	4	17	40	32
3	THF	8	62	6	9	47	-
4	Toluene	8	59	6	21	32	-

Reaction condition- CAL (1 g), 10 wt % catalyst w.r.t. substrate (1P20WS), 15 ml solvent, H₂

bubbling, temp- RT.

(c) Time profile study for Cinnamaldehyde hydrogenation

The reaction profile and yield of products over time was carried out in THF and the result is shown in Figure 2.11. The result showed constant increase in CAL conversion with time, despite the less initial activity with 1P20WS catalyst. The yield of the products HCOL, HCAL, and PB also gradually increased with time. At 1h the yield of HCOL was 5%, which increased to 75% after 12h.

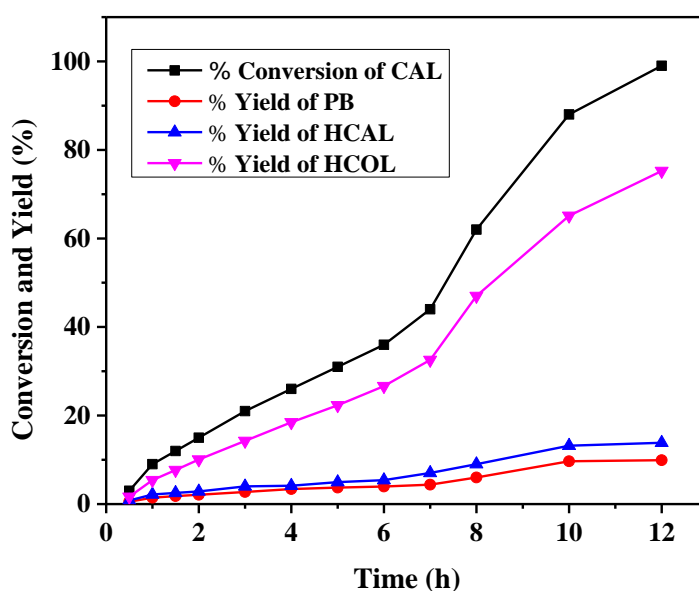


Figure 2.11. CAL hydrogenation reaction profile with time

Reaction condition- CAL (1 g), 10 wt % catalyst w.r.t. substrate (1P20WS), 15 ml solvent (THF), H₂ bubbling, temp- RT.

(d) Pressure effect on Cinnamaldehyde hydrogenation

To find the effect of pressure on CAL hydrogenation, the reaction was carried out at 3bar hydrogen pressure and room temperature. The results were compared with reaction under ambient reaction conditions and the data is shown in Figure 2.12. It shows that with increase in the pressure from 1 to 3 bar the conversion of CAL increased from 62 to 75% and yield from

47 to 53% after 8h. This increase in the reaction rate is attributed to the higher concentration of hydrogen in same volume at higher H₂ pressure which, leads to increase in the solubility of hydrogen.

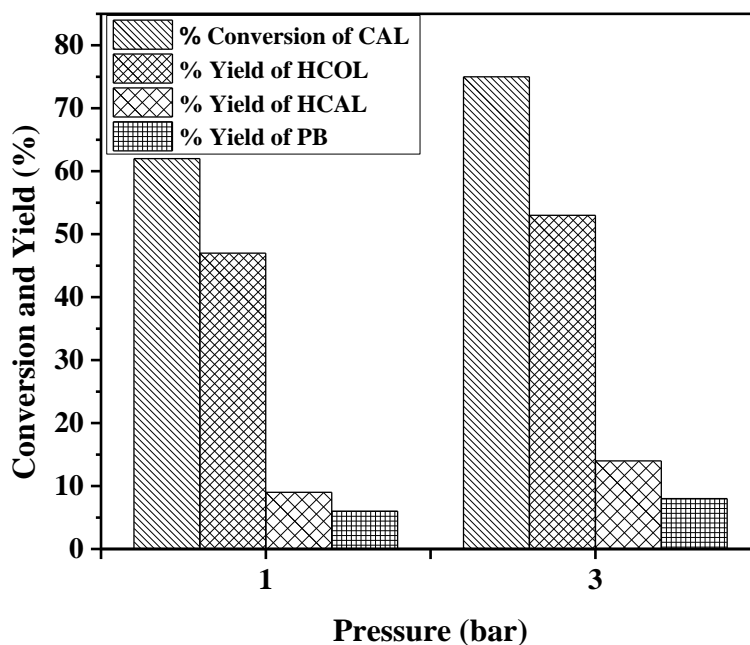


Figure 2.12. Effect of Pressure on CAL hydrogenation reaction

Reaction condition- CAL (1 g), 10 wt % catalyst w.r.t. substrate (1P20WS), 15 ml solvent (THF), temp- RT, time-8h.

(e) Temperature effect on Cinnamaldehyde hydrogenation

In addition to pressure, reaction temperature is also an important factor in investigation of activity of PWS catalyst for CAL hydrogenation. To explore the effect of temperature on CAL hydrogenation, the reactions were performed at RT (30 °C) and 60 °C. The results are shown in Figure 2.13. At 30 °C temperature, 75% conversion of CAL was obtained within 8h with 52% yield of HCOL. As expected the CAL conversion increased, with an increase in the temperature. At 60 °C almost 99% conversion of CAL was observed with 70% yield of HCOL in 8h.

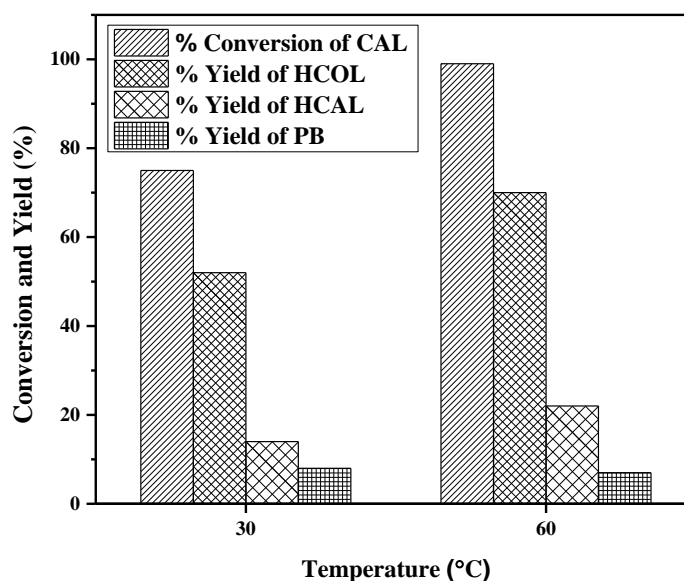


Figure 2.13. Effect of temperature on CAL hydrogenation reaction

Reaction condition- CAL (1 g), 10 wt % catalyst w.r.t. substrate (1P20WS), 15 ml solvent

(THF), 3bar H₂ pressure, time-8h.

(f) Catalyst loading effect on Cinnamaldehyde hydrogenation

To find out the role of the catalyst loading on CAL hydrogenation, reactions were performed at different catalyst loadings such as 5, 10 and 15 wt % with respect to CAL and results are shown in Figure 2.14. As catalyst loading increased gradually from 5 to 15 wt. % with respect to CAL, the conversion gradually increased from 37 to 99%, with HCOL yield from 24 to 72% after 8h. At higher catalyst loading (15 wt. %) 99% CAL conversion was observed with in 5h with 59% yield of HCOL. This can be attributed to the number of active sites with increase in the catalyst charge, which leads to an increase in the conversion.

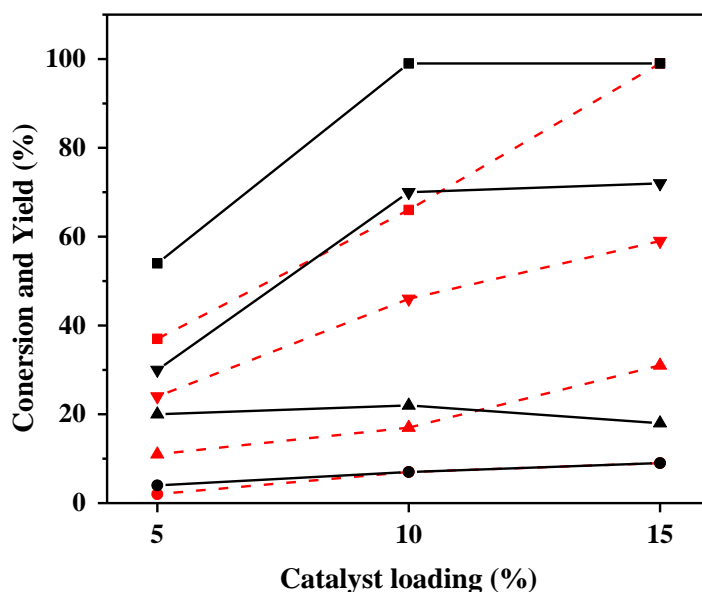


Figure 2.14. Effect of catalyst loading on the conversion of CAL

Reaction condition- CAL (1 g), catalyst (1P20WS), 15 ml solvent (THF), 3 bar H₂ Pressure, temp-60 °C; red dash line-5h; black solid line- 8h; ■conversion of CAL, ▼yield of HCOL, ▲ yield of HCOL and ● yield of PB.

(g) Pd loading effect on Cinnamaldehyde hydrogenation

To study the effect of Pd metal loading on CAL hydrogenation, we controlled Pd loading to 0.5, 1, and 2 wt% by varying the amount of Pd precursor during catalyst synthesis, and reaction results are shown in Table 2.6. As Pd loading was increased, CAL conversion also increased because the active sites increased in the reaction medium. The 0.5P20WS catalyst showed 60% CAL conversion with 28% yield of HCOL, which increased to 99% conversion and 70% yield for 1P20WS catalyst in 8h. With increase in further Pd loading, the time required for complete conversion of CAL decreased from 8 h for 1P20WS catalyst to 5h for 2P20WS catalyst (2% Pd loading). 2P20WS catalyst shows 99% CAL conversion with 61% yield of HCOL after 5h. After 8h the yield of HCOL increased to 75%. The result shows that there is no considerable increase

in yield of HCOL with increasing Pd loading from 1 to 2% in catalyst. So for further recycle study we used 1P20WS catalyst.

Table 2.6. Pd loading effect on CAL conversion

Sr. No.	Catalyst loading wt%	Time h	Conv. %	Yield PB	Yield HCAL	Yield HCOL
1	0.5	2	31	1	16	14
		8	60	2	30	28
2	1	2	42	3	11	28
		8	99	7	22	70
3	2	2	74	7	24	44
		5	99	8	30	61
		8	99	11	13	75

Reaction condition- CAL (1 g), catalyst 10 wt % wrt substrate, 15 ml solvent (THF), 3 bar H₂ Pressure, temp-60 °C.

(h) Recycle study

The recycle study of catalyst was performed with 1P20WS catalyst after separating it from the reaction mixture by centrifugation, washing with solvent and drying in oven at 100 °C. The three cycles were performed using same charge and optimized reaction conditions. The results are shown in Figure 2.15. From result we concluded that the catalyst shows good stability up to three runs with similar yield of HCOL. Additionally, to check Pd leaching in reaction mixture, ICP-AES analysis was carried out and the results showed no Pd leaching in the reaction mixture.

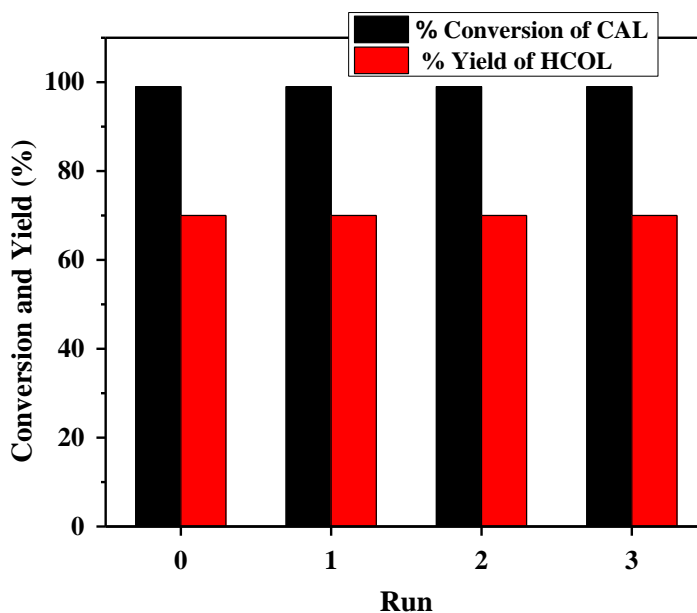


Figure 2.15. Recycle study of 1P20WS catalyst for CAL hydrogenation

Reaction condition- CAL (1 g), 1P20WS catalyst 10 wt % wrt substrate, 15 ml solvent (THF), 3 bar H₂ Pressure, temp-60 °C, time-8h.

There are very few reports, for the selective hydrogenation of CAL to HCOL. Some are shown in Table 2.7. In 2006, Ru-Cu supported on graphite with 2 wt % Ru and 0.9 wt % Cu loading has shown hydrogenation of CAL at 50 °C and 50 bar hydrogen pressure. Catalyst gave 100% conversion of CAL with 50% selectivity of HCOL [20]. Y. Qian reported Pt support on carbon nano-tubes for CAL hydrogenation which showed very good selectivity for HCOL (80%) [19]. Though the selectivity is good, the pressure required for conversion is high (30 bar) and also the Pt loading is high in the catalyst (3 wt %). This may lead to economic concerns. 1% Platinum supported on silica is also reported for same reaction at milder reaction conditions such as 80 °C and 10 bar H₂ pressure [21]. But the catalyst showed very low CAL conversion (38%) with lower (35%) selectivity for HCOL. When the present work was compared with previous literature, the 1P20WS catalyst was found to be superior with 99% CAL conversion with 70% yield of HCOL

under milder reaction condition such as 60 °C temperature and 3 bar hydrogen pressure at lower (1%) palladium loading.

Table 2.7. Literature survey for hydrogenation of CAL

Sr. No.	Catalyst	Catalyst Loading wrt substrate	Solvent	Temp °C	Pressure bar	Time h	Conv. % of CAL	Select. HCOL	Ref.
1	2Ru0.9Cu/graphite	-	IPA	50	50	6	100	50	[20]
2	3%Pt/CNTs	5 wt%	IPA	80	30	12	100	80	[19]
3	1%Pt/SiO ₂	5 wt%	IPA	80	10	2	38	35	[21]
4	5%Ni- 0.5%Pd/CeO ₂ /ZrO ₂	5 wt%	IPA	100	20	8	100	99.9	[32]
5	4% Pt/graphite	15wt%	IPA	60	5	4	97	95	[22]
6	5%Pd/C	5wt%	Dioxane	80	1 atm.	55	100	60	[12]
7	Pd/ZnO	10wt%	Toluene	80	40	1	100	30	[33]
8	Ni-Ag/TiO ₂	15wt%	MeOH	80	20	1	76	40	[34]
9	1P20WS	10wt%	THF	60	3	8	99	70	Present work

2.3.3. Used catalyst characterization

(a) XRD analysis

The powder X-ray diffraction pattern of fresh and used 1P20WS catalysts are shown in Figure 2.16. There was no changes observed in the diffraction pattern of used catalyst compared to fresh catalyst and it completely matched with the XRD pattern of monoclinic crystalline structure of WO₃.

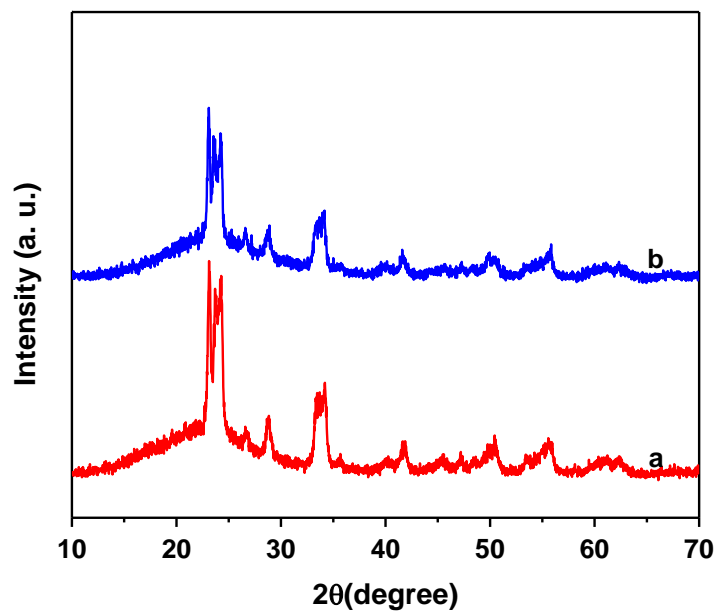


Figure 2.16. XRD pattern of (a) fresh and (b) used 1P20WS catalysts

(b) HRTEM analysis

To study the morphological change in used catalyst, HRTEM analysis of fresh and used catalyst was performed and the results are presented in Figure 2.17 and 2.18. The HRTEM results showed no change in the particle size and also no change in the elemental composition of fresh and used 1P20WS catalyst. The XRD and HRTEM data of used catalyst confirmed no changes in the structure of the used catalyst.

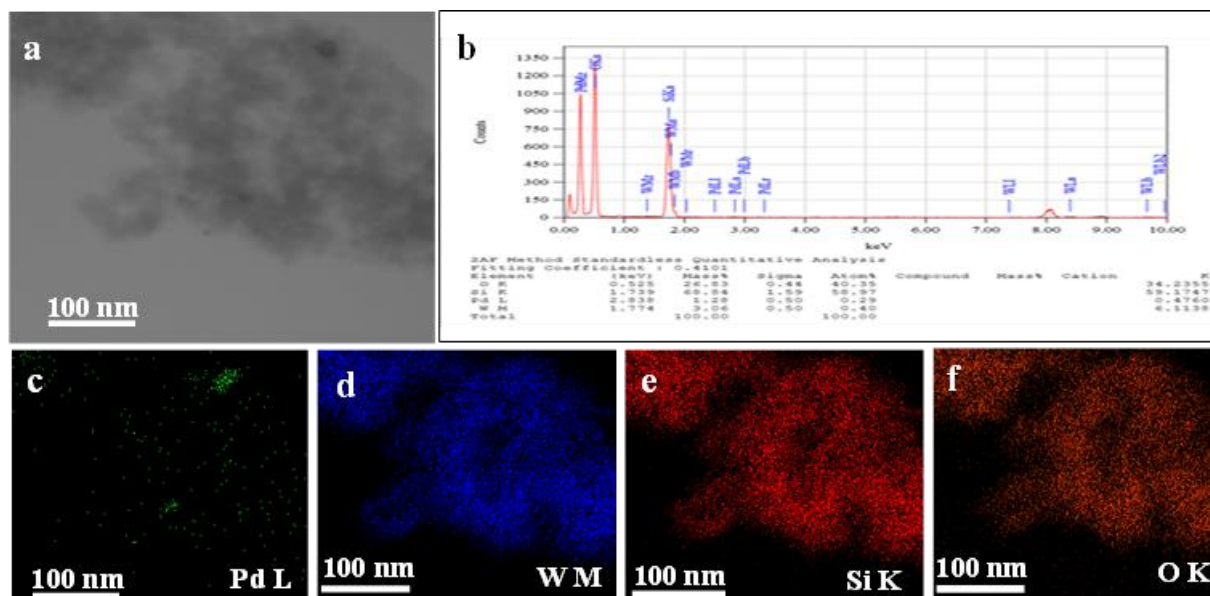


Figure 2.17. HRTEM data of fresh 1P20WS catalyst

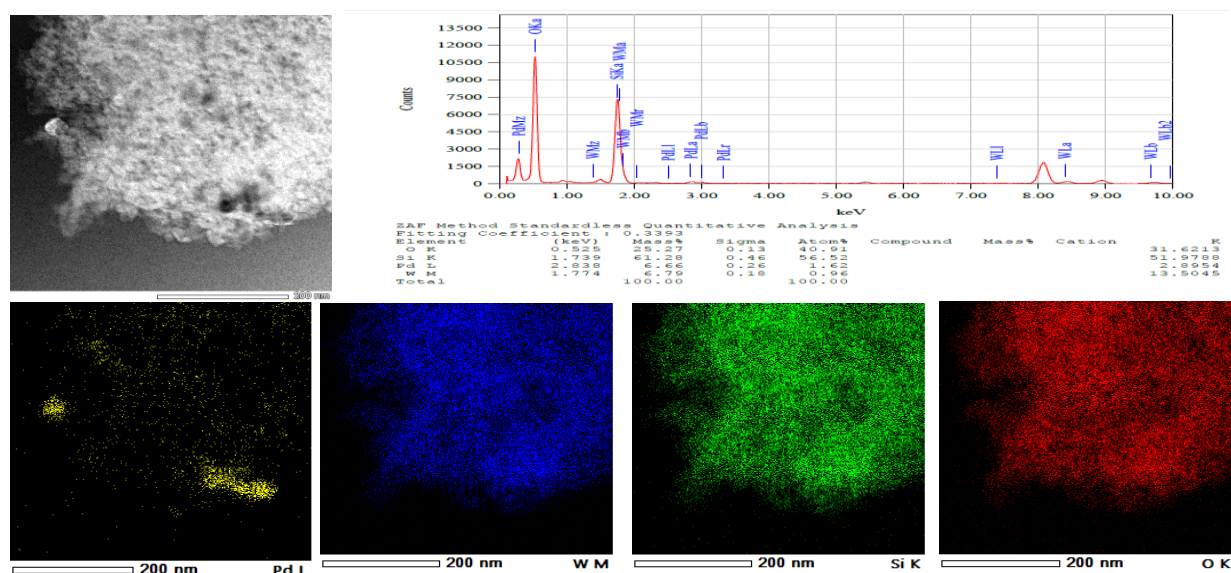


Figure 2.18. HRTEM data of used 1P20WS catalyst

2.4. Possible reaction mechanism of cinnamaldehyde hydrogenation on 1P20WS catalyst

The present 1P20WS catalyst is active for selective hydrogenation of CAL to HCOL. Mechanistic aspects for hydrogenation of CAL on 1P20WS catalyst were studied by survey of the previous literature reports and using FTIR spectroscopy. Literature survey showed that the product selectivity for hydrogenation of α , β -unsaturated carbonyl compounds is depending on d-band

width of metal [35, 36]. According to the Huckel calculations, metal having narrower d-band width shows more interaction with C=C bond compare to C=O bond [37]. The d-band width order for different metals is Pd < Pt < Os. It means the adsorption of C=C bond is more feasible over Pd based catalyst. Hence Pd metal based catalysts shows excellent activity for the selective hydrogenation of CAL into HCAL [38-41]. However, a literature review also showed that the selectivity of CAL hydrogenation also depends on the metal particle size [42, 43]. To study the effect of particle size of Pd on selective hydrogenation of CAL, Jiang and co-worker reported selective hydrogenation of CAL on Pd/TiO₂ catalysts reduced at different temperature such as 250, 450 and 600 °C. As reduction temperature increased the Pd particle size increased from 2 nm to 4 nm. The selectivity of HCOL increased for large particle sized catalyst which were explained on basis of DFT calculation. The smaller Pd particles (Pd₄) required less adsorption energy to adsorb C=C bond as compare to the C=O bond whereas the adsorption of C=O bond is feasible on the larger Pd particles (Pd (111) surface) [44] as shown in Figure 2.19. To lower the steric hindrance on large particle (flat surface), the CAL adsorbed through C=O bond which leads to increase in the HCOL yield. Thus it was concluded that the particle size of Pd particles highly influence the selectivity of CAL hydrogenation.

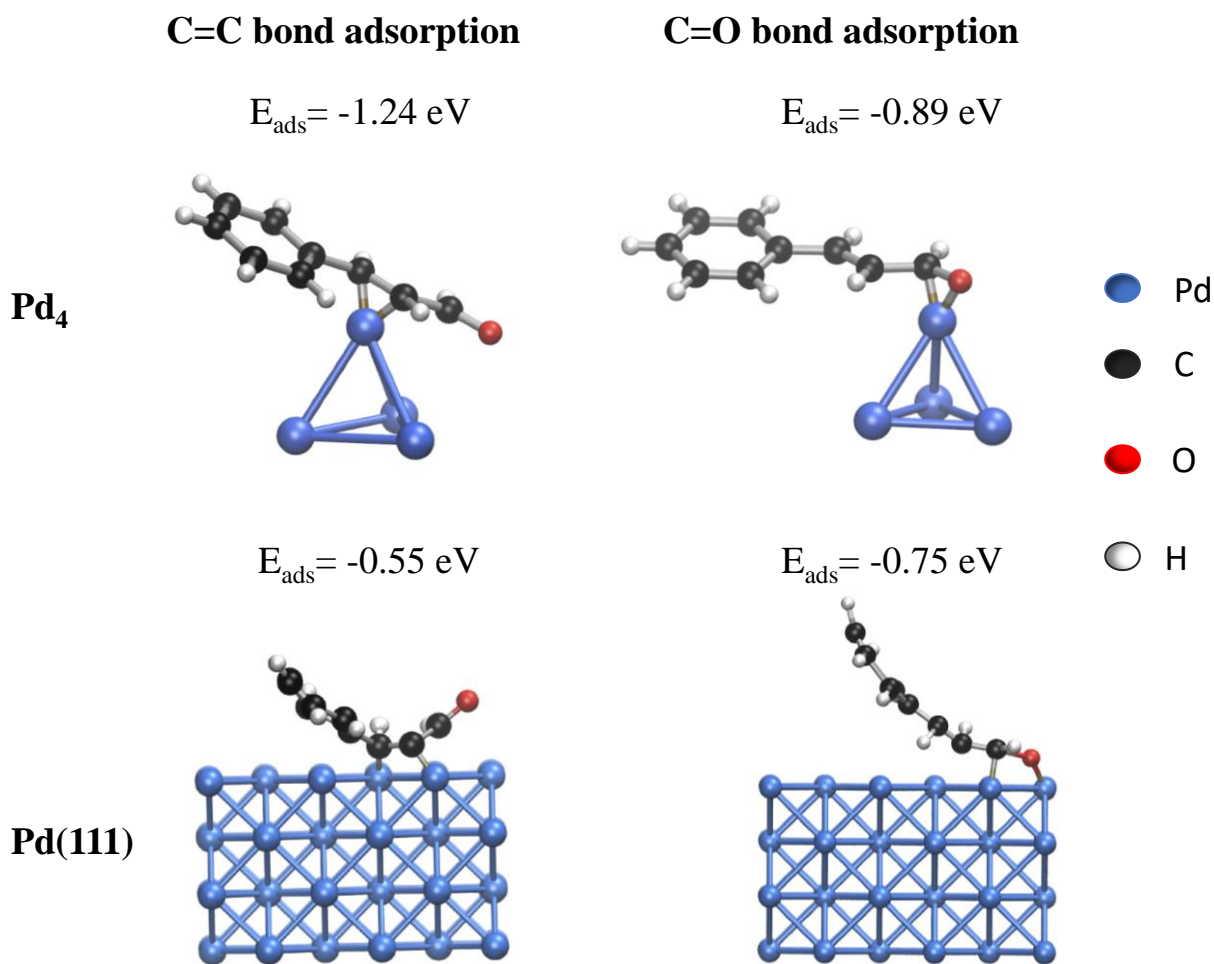


Figure 2.19. CAL adsorption on Pd₄ nanocluster through (a) C=C bond and (b) C=O bond; CAL adsorption on Pd (111) surface through (c) C=C bond and (d) C=O bond. E_{ads} - the corresponding adsorption energy [44].

In present study, TEM analysis showed that the particle size of Pd metal is in range of 12 to 18 nm and the selectivity of HCOL is high. From above literature review and present result, there is a possibility of the adsorption of CAL on 1P20WS catalyst through C=O bond. To confirm the orientation of CAL on 1P20WS catalyst, FTIR spectra of authentic CAL and CAL-adsorbed on 1P20WS catalysts were recorded. The results are shown in Figure 2.20. FTIR spectrum of authentic CAL (Figure 2.20. a) showed peaks at 1624 and 1670 cm^{-1} ascribed to the stretching vibrations of C=C bond and C=O bond respectively. The spectrum of CAL adsorbed on catalyst

showed red shift in C=O stretching vibrations peak from 1670 to 1673 cm^{-1} . This red shift in C=O stretching vibrations may be ascribed to the decrease in bond length due to interaction with catalyst surface. This observation confirmed the adsorption of CAL over 1P20WS, through C=O group of CAL.

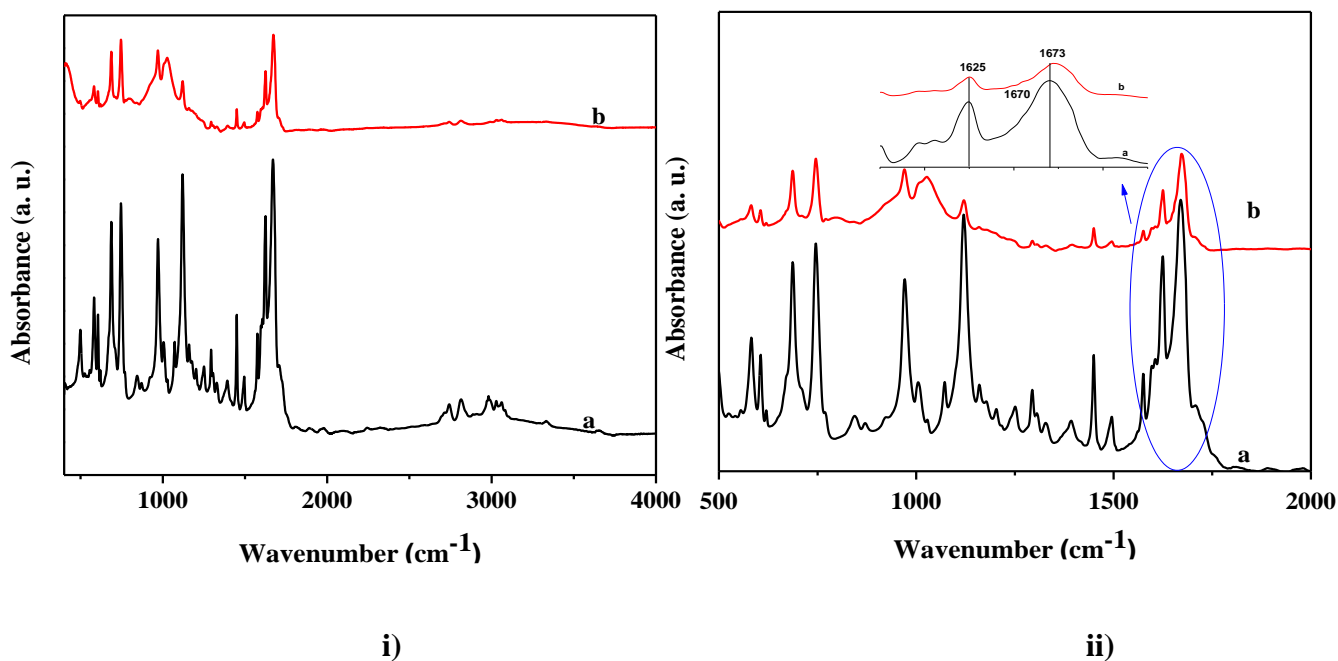


Figure 2.20. FTIR spectra of PWS catalysts in the range i) 400 to 4000 cm^{-1} and ii) 500 to 2000 cm^{-1} ; a) authentic CAL and b) CAL adsorbed on 1P20WS.

Based on the previous reports and FTIR study, the proposed mechanism for the CAL hydrogenation is given in Figure 2.21. The dissociative adsorption of hydrogen molecule takes place on Pd and convert into two hydrogen atom (B) [45]. These hydrogen atoms react with adsorbed CAL molecule and convert to saturated products (C).

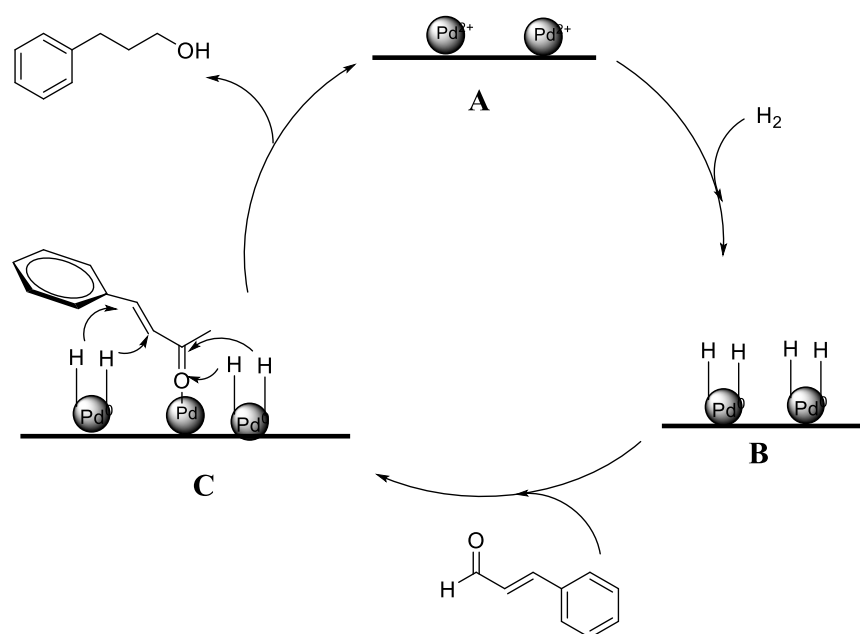


Figure 2.21. Plausible mechanism of CAL hydrogenation on 1P20WS catalyst

2.5 Conclusion

WO₃/SiO₂ was used as an acidic support for palladium to prepare efficient hydrogenation catalyst. Due to the acidic nature of support, catalysts showed strong metal support interaction and high Pd metal dispersion which was confirmed by BET and TEM analysis. This catalyst has shown high efficiency for cinnamaldehyde hydrogenation under milder reaction conditions (3 bar H₂ Pressure, 60 °C temperature). The catalyst was successfully recycled without any palladium leaching which is attributed to strong metal support interaction of Pd metal with WO₃/SiO₂ support. Mechanistic aspects using detailed FTIR spectroscopic analysis revealed activation of cinnamaldehyde on catalyst through C=O group to lower steric hindrance, leading to reduction of both unsaturated bonds (C=C and C=O) into 3-phenyl propanol.

2.6 References

1. A. S. Nagpure, P. Gogoi, S. V. Chilukuri, *Chem Asian J.*, **2021**, *16*, 2702–2722.

2. M. Stucchi, F. Vasile, S. Cattaneo, A. Vomeri, A. B. Hungria, L. Prati, *Eur. J. Org. Chem.*, **2022**, 40, 9-20.
3. Y. Menga, S. Xiab, X. Zhouc, G. Pan, *Chem. Phys. Lett.*, **2020**, 740, 137049, doi.org/10.1016/j.cplett.2019.137049
4. X. Chen, H. Cao, X. Chen, Y. Du, J. Qi, J. Luo, M. Armbrüster, C. Lia, *ACS Appl. Mater. Interfaces*, **2020**, 12, 18551–18561.
5. J. Su, W. Shi, X. Liu, L. Zhang, S. Cheng, Y. Zhang, G. A. Botton, B. Zhang, *J. Catal.*, **2020**, 388, 164–170.
6. B. Chen, X. Yang, X. Zeng, M. Yang, J. Xiao, L. Fan, Z. Huang, F. Zhao, G. Zhan, *Mol. Catal.*, **2020**, 493, 111069, doi.org/10.1016/j.mcat.2020.111069
7. Z. Weng, F. Zaera, *ACS Catal.*, **2018**, 8, 8513–8524.
8. C. Dietrich, D. Schild, W. Wang, C. Kübel, S. Behrens, *Z. Anorg. Allg. Chem.*, **2017**, 643, 120–129.
9. S. Bhogeswararao, V. P. Kumar, K. V. R. Chary, D. Srinivas, *Catal. Lett.*, **2013**, 143, 1266–1276.
10. S. Bhogeswararao, D. Srinivas, *J. Catal.*, **2012**, 285, 31–40.
11. M. J. Ledoux, R. Vieira, C. Pham-Huu, N. Keller, *J. Catal.*, **2003**, 216, 333–342.
12. C. Pham-Huu, N. Keller, M. J. Ledoux, L. J. Charbonniere, R. Ziessel, *Chem. Commun.*, **2000**, 1871–1872.
13. C. Pham-Huu, N. Keller, G. Ehret, L.c.J. Charbonniere, R. Ziessel, M. J. Ledoux, *J. Mol. Catal. A: Chem.*, **2001**, 170, 155–163.
14. M. Lashdaf, J. Lahtinen, M. Lindblad, T. Venalainen, A.O.I. Krause, *Appl. Catal. A*, **2004**, 276, 129–137.

15. A. J. Plomp, H. Vuori, A. Outi I. Krause, K. P. de Jong, J. H. Bitter, *Appl. Catal. A*, **2008**, 351, 9–15.
16. L. Mercadante, G. Neri, C. Milone, A. Donato, S. Galvagno, *J. Mol. Catal. A: Chem.*, **1996**, 105, 93–101.
17. A. Giroir-Fendler, D. Richard, P. Gallezot, *Catal. Lett.*, **1990**, 5, 175–182.
18. S. Galvagno, G. Capannelli, G. Neri, A. Donato, R. Pietropaolo, *J. Mol. Catal.*, **1991**, 64, 237–246.
19. H. Ma, L. Wang, L. Chen, C. Dong, W. Yu, T. Huang, Y. Qian, *Catal. Commun.*, **2007**, 8, 452–456.
20. E. Asedegbega-Nieto, B. Bachiller-Baeza, A. Guerrero-Ruíz, I. Rodríguez- Ramos, *Appl. Catal. A-Gen.*, **2006**, 300, 120–129.
21. D. Wang, Y. Zhu, *J. Chem.*, **2018**, Article ID 5608243, 7 pages
doi.org/10.1155/2018/5608243.
22. S. Chang, S. Meng, X. Fu, S. Zhang, X. Zheng, S. Chen, *Chem. Select.*, **2019**, 4, 2018 – 2023.
23. V. R. Acham, A. V. Biradar, M. K. Dongare, E. Kemnitz, S. B. Umbarkar, *ChemCatChem.*, **2014**, 6, 3182–3191.
24. R. S. Kokane, V. R. Acham, A. B. Kulal, E. Kemnitz, M. K. Dongare, S. B. Umbarkar, *Chemistry Select.*, **2017**, 1, 1–11.
25. A.B. Kulal, M. K. Dongare, S. B. Umbarkar, *Appl. Catal B; Environmental*, **2016**, 182, 142–152.
26. C. D. Wagner, The NIST X-ray photoelectron spectroscopy database, *NIST technical note 1289*, **1991**, 30.
27. Y. Yu, Y. Zhao, T. Huang, H. Liu, *Pure Appl. Chem.*, **2009**, 81, 2377–2385.

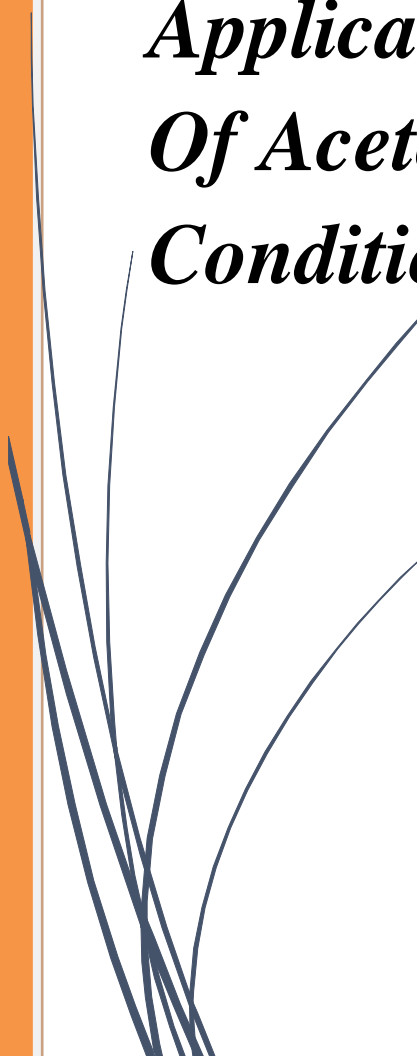
28. K. V. R. Chary, D. Naresh, V. Vishwanathan, M. Sadakane, W. Ueda, *Catal. Commun.*, **2007**, 8, 471-477.
29. M. Turáková, T. Salmi, K. Eränen, J. Wärna, D. Y. Murzin, M. Králik, *Appl. Catal. A*, **2015**, 499, 66-76.
30. H. Yoshida, Y. Onodera, S. Fujita, H. Kawamori, M. Arai, *Green Chem.*, **2015**, 17, 1877-1883.
31. M. J. Kamlet, J. M. Abboud, M. A. Abraham, R. W. Taft, *J. Org. Chem.*, **1983**, 48, 2877-2887.
32. S. Bhogeswararao, V. P. Kumar, K. V. R. Chary, D. Srinivas, *Catal. Lett.*, **2013**, 143, 1266-1276.
33. S. Fujita, H. Mitani, C. Zhang, K. Li, F. Zhao, M. Araia, *Mol. Catal.*, **2017**, 442, 12-19.
34. M. G. Prakash, R. Mahalakshmy, K. R. Krishnamurthy, B. Viswanathan, *Catal. Today*, **2016**, 263, 105-111.
35. P. Maki-Arvela, J. Hajek, T. Salmi, D. Y. Murzin, *Appl. Catal. A*, **2005**, 292, 1-49.
36. Y. A. Ryndin, C. C. Santini, D. Prat and J. M. Basset, *J. Catal.*, **2000**, 190, 364-373.
37. F. Delbecq, P. Sautet, *J. Catal.*, **1995**, 152, 217-236.
38. D. Das, K. Pal, J. Llorca, M. Dominguez, S. Colussi, A. Trovarelli, A. Gayen, *Kinet., Mech. Catal.*, **2017**, 122, 135-153.
39. Y. Zhao, M. Liu, B. Fan, Y. Chen, W. Lv, N. Lu, R. Li, *Catal. Commun.*, **2014**, 57, 119-123.
40. J. Yu, L. Yan, G. Tu, C. Xu, X. Ye, Y. Zhong, W. Zhu, Q. Xiao, *Catal. Lett.*, **2014**, 144, 2065-2070.

41. Q. F. Wu, C. Zhang, B. Zhang, X. R. Li, Z. Ying, T. Liu, W. W. Lin, Y. C. Yu, H. Y. Cheng and F. Y. Zhao, *J. Colloid Interface Sci.*, **2016**, 463, 75–82.
42. H. J. Wei, C. Gomez, J. J. Liu, N. Guo, T. P. Wu, R. Lobo- Lapidus, C. L. Marshall, J. T. Miller, R. J. Meyer, *J. Catal.*, **2013**, 298, 18–26.
43. X. F. Yang, A. Q. Wang, X. D. Wang, T. Zhang, K. L. Han, J. Li, *J. Phys. Chem. C*, **2009**, 113, 20918–20926.
44. F. Jiang, J. Cai, B. Liu, Y. Xua, Xiaohao Liu, *RSC Adv.*, **2016**, 6, 75541–75551.
45. K. N. Patil, D. Prasad, J. T. Bhanushali, B. Kakade, A. H. Jadhav, B. M. Nagaraja *New J. Chem.*, **2021**, 45, 5659–5681



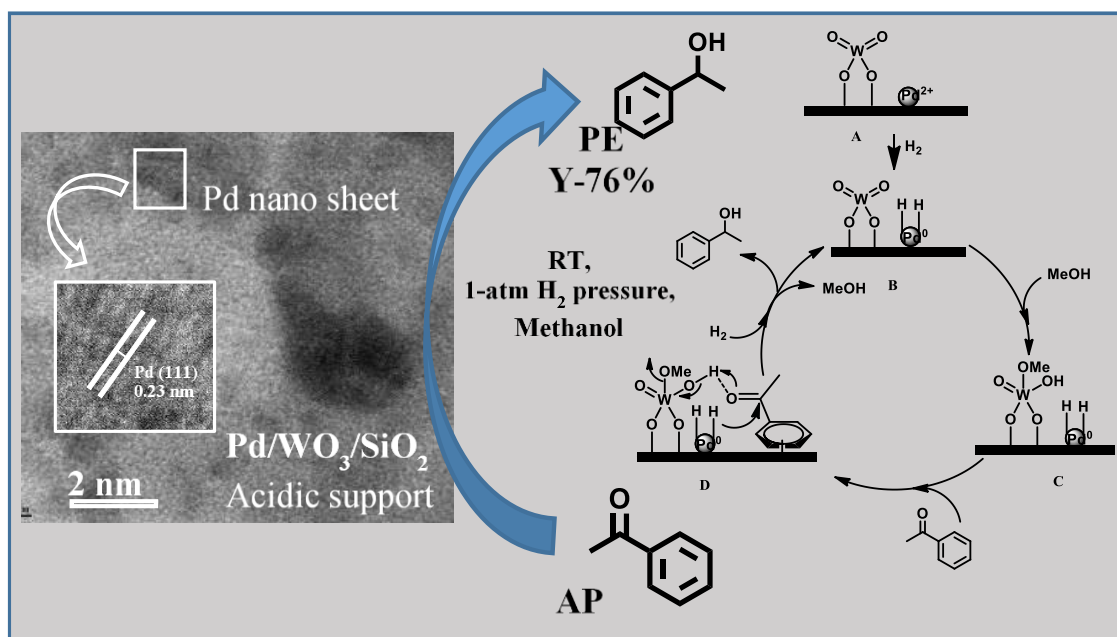
Chapter 3

***Pd-WO₃/SiO₂: Synthesis,
Characterization And Its Catalytic
Applications For Hydrogenation
Of Acetophenone Under Ambient
Conditions***



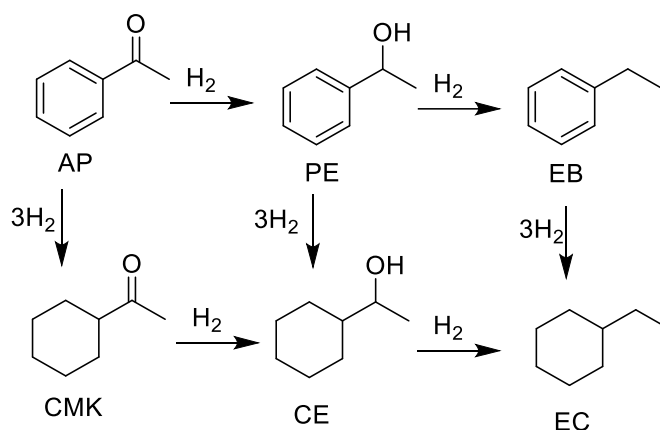
Abstract

Selective hydrogenation of acetophenone to 1-phenylethanol is an important reaction in pharmaceutical and fragrance industries. In-house prepared 1%Pd-WO₃/SiO₂ acidic catalyst showed very high efficiency for acetophenone hydrogenation under ambient conditions with 92% conversion and 76% yield for 1-phenylethanol. The detailed characterization revealed formation of Pd nanosheets (12-18 nm) on acidic support leading to very high Pd dispersion (36%). Selective hydrogenation under milder reaction conditions has been correlated to the high dispersion of Pd on WO₃/SiO₂ acidic support. Variation in support acidity showed increase in catalytic activity with increase in the support acidity. Detailed FTIR analysis revealed dissociative activation of methanol on WO₃ moiety to form CH₃O-W and W-O-H and activation of acetophenone by hydrogen bonding with W-OH. Due to oligomerisation of 1-phenylethanol on catalyst surface, no recycle was possible. The catalyst deactivation was substrate specific. The same catalyst could be efficiently recycled for styrene hydrogenation under ambient conditions.



3.1 Introduction

Catalytic hydrogenation of acetophenone (AP) to produce 1-phenylethanol (PE) is specifically very important due to the applications of PE as perfumery chemical, also an important building block for styrene monomer [1-3]. This reaction includes different side reactions such as the ring hydrogenation, hydrogenolysis of the produced alcohol to aromatic saturated compound. The possible products of AP hydrogenation are shown in Scheme 3.1. The hydrogenation of carbonyl group gives PE and ethylbenzene (EB) as possible products and ring hydrogenation gives cyclohexyl methyl ketone (CMK), cyclohexyl ethanol (CE) and ethyl cyclohexane (EC).



Scheme 3.1. Possible products of acetophenone hydrogenation

Generally, hydrogenation of AP has been investigated over both noble and non-noble transition metals such as Pd, Pt, Rh, Ru, Ni, Cu, Ag, Co and Mg with different supports such as Al₂O₃, SiO₂, zeolites, NiO, CNTs (carbon nano tubes) and polymer matrix under different liquid- or gas-phase reaction conditions [4-19]. R. K. Marella prepared biomorphic MgO/C and used to disperse Cu with different loading. These catalysts were used for catalytic coupling of dehydrogenation of 1, 4-BDO and hydrogenation of AP in one step [8]. 10Cu/C-MgO showed good catalytic activity, with 95% AP conversion and 99% selectivity for PE at 225°C. In US006046369A patent, 63% CuO/SiO₂ catalyst was used for production of PE by AP

hydrogenation at temperature in the range of 60-215 °C and H₂ pressure range of 10 to 50 bar using fixed bed flow reactor [20]. Commercially, this reaction is carried out in liquid phase using supported Ni or Raney Ni doped with Cr or Co catalysts [21]. Among the non-noble metals, Ni based catalysts are widely studied for AP hydrogenation. In 2019, Costa et.al reported 5% NiP/MSNS (mesoporous silica nano spheres) catalyst for AP hydrogenation with 30% conversion and 95% selectivity for PE at 80 °C and 10 bar H₂ pressure [22]. Recently Lin and co-worker prepared Ni/C magnetic catalysts and successfully used it in AP hydrogenation with excellent AP conversion (99%) and 99% selectivity for PE [7]. Under ambient conditions non-noble metal based catalysts gives very poor conversion of AP because of lower catalytic activity of metals under such mild conditions. If the temperature and pressure is increased to increase conversion of AP, variable quantities of by products such as CMK, CE and EC are obtained because of reduction of phenyl ring at high pressure and temperature [23, 24].

While on noble metals such as Pt, Rh and Ru hydrogenation can occur under ambient reaction conditions, high cost of the noble metals is an issue of concern along with selectivity for desired product due to undesired by-product formation [11-14]. Pt based catalysts hydrogenate both carbonyl group as well as phenyl ring of AP with identical rate hence similar quantities of PE and CMK are formed, which further hydrogenate to CE [11, 12]. Ruthenium based catalysts are known to reduced mostly phenyl ring of AP, and hence it gives lower selectivity for PE [13, 14]. Palladium is reported for selective hydrogenation of AP to PE and EB under ambient reaction conditions with relative low cost [15-17]. Wang et al. have shown the selectivity difference between hydrogenation of AP over Pd-supported on carbon nanotubes and commercial activated carbons. The yield of PE for Pd/CNTs catalyst (94.2%) was significantly higher than Pd/ACs (47.9%) at 60 °C [25]. Y. Gou and co-workers have achieved higher conversion (80-92%) by

applying shape controlled phenomenon for Pd-supported on sheet-like NiO catalysts at 80 °C and 1.5 MPa pressure of H₂ in 3h [26]. In addition, Jun Huang et al. have reported an excellent study of tunable acidity, which is essential for developing more efficient catalysts in terms of Pd/silica–alumina for greener chemical processes [27].

After successful hydrogenation of cinnamaldehyde using palladium supported on WO₃/SiO₂ reported in the previous chapter, the same catalyst was used to perform the hydrogenation of AP and the results are reported in this chapter.

3.2 Experimental Section

3.2.1 Materials

All the reagents such as palladium acetate, ammonium meta-tungstate (AMT), ethyl silicate-40 (ES-40), acetophenone, and all the solvents (methanol, ethanol, ethyl acetate, toluene, hexane) of AR grade quality, were procured from Molychem India, Chemplast, Chennai, Sigma Aldrich, and Thomas Baker Chemicals, India and used as such without further purification.

3.2.2 Catalysts characterization

(a) X-ray Diffraction analysis

Fresh and used catalyst were characterized by X-ray diffraction method using PAN analytical X'Pert Pro Dual Goniometer diffractometer. The diffractometer consists of X'celerator solid state detector with CuK α ($\lambda=1.5406\text{\AA}$, 40kV, 30mA) radiation and a Ni filter. The X-ray diffraction pattern of the sample was collected in the range of $2\theta = 20-80^\circ$ with a step size of 0.02° and a scan rate of 4° min^{-1} .

(b) Electron microscopy

The morphology of the samples were determined using scanning electron microscopy (SEM) on a FEI quanta 200 3D dual beam ESEM instrument having thermionic emission tungsten filament in the 3 nm range at 30 kV. The particle size was determined using

transmission electron microscopy (TEM) and analysis was done on a Tecnai G2-20 FEI instrument operating at an accelerating voltage of 300 kV. Before analysis, the powder samples were ultrasonically dispersed in isopropanol, and deposited on a carbon coated copper grid, dried in air before TEM analysis.

(c) TGA/DTA analysis

Mass % loss was determined through TGA-analysis on Diamond -TG/DTA. The catalyst samples were first treated at 30 °C to 800 °C at 10 °C/min in air to determine the mass loss due to carbon deposits.

(d) Fourier Transform Infrared Spectroscopic studies

The Fourier transform infrared (FT-IR) spectra of the fresh and used catalyst were recorded on a Thermo Nicolet Nexus 670 IR instrument using DTGS detector. KBr pellet method was used for preparation of samples with a resolution of 4 cm⁻¹ in the range of 4000-400 cm⁻¹ and 100 scans. Mechanistic aspect was also studied using FTIR spectroscopy.

3.2.3 Catalytic activity

(a) Hydrogenation of acetophenone

The catalytic hydrogenation of AP was carried out in 50 mL two necked round bottom flask at room temperature and 1 atm pressure of H₂. Initially the catalyst (1P20WS) (0.1g) was reduced *in-situ* in methanol (15 mL) by bubbling H₂ (10 mL/min) for 15 min before each catalytic reaction. Then AP (1 g, 8.3 mmol) was added to the flask. The reaction mixture was stirred at room temperature with H₂ gas continuously bubbling through the reaction mixture. The reaction was monitored by GC using GC-Perkin Elmer equipped with HP-FFAP column (30 m X 0.25 mm X 1 μm) and flame ionization detector (FID). Conversion of AP was calculated based on the GC-FID results, where substrate conversion = [moles of substrate reacted] / [Initial moles

of substrate used] \times 100 and the selectivity of products was calculated by [total moles of the product formed] / [total moles of substrate converted] \times 100. The product identification was carried out by comparing authentic standard samples in GC and GCMS.

(b) Catalyst recyclability

The catalyst recycle study was carried out using 1P20WS catalyst for AP hydrogenation under optimized reaction conditions [1 g AP, 0.1 g catalyst, 15 mL methanol as solvent, bubbling H₂, at room temperature (27 °C) for 4 h]. After completion of the reaction, the catalyst was separated from the reaction mixture by centrifugation. Then catalyst was washed with methanol for 2-3 times and dried in an oven at 60 °C. This dried catalyst was used for further recycle study of the catalyst.

(c) Recycle study for styrene hydrogenation

Recycle study for styrene hydrogenation was carried out using 1P20WS catalyst under similar condition [1 g styrene, 0.1 g catalyst, 15 mL methanol as solvent, bubbling H₂, at room temperature (27 °C) for 4 h]. After completion of the reaction, the catalyst was separated from the reaction mixture by centrifugation. Then catalyst was washed with methanol for 2-3 times and dried in an oven at 60 °C. This dried catalyst was used for further recycle study of the catalyst.

(d) Leaching Test

The leaching of Pd in the reaction mixture under the identical reaction conditions was analysed by filtration method and ICP method. AP (1 g), and catalyst (0.1 g), was stirred in 15.0 mL methanol solvent by bubbling H₂ at room temperature (27 °C) for 2 h after reducing the catalyst. After 2 h the catalyst was separated from the reaction mixture by centrifugation, and the reaction mixture was further allowed to react under identical reaction conditions without catalyst.

ICP-AES analysis of reaction mixture was carried out to detect any palladium leaching if any in the reaction.

3.3. Results and Discussions

3.3.1 Catalytic activity for acetophenone hydrogenation

(a) Catalyst screening

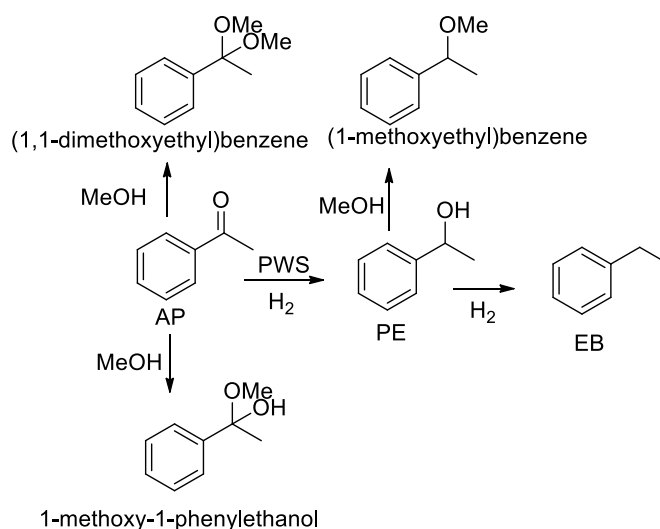
Initially the catalytic activity of 1% Pd loaded on different supports (WS with different WO₃ loading) for AP hydrogenation was evaluated at room temperature and atmospheric hydrogen pressure (8-10 mL/min) in methanol solvent. For comparison blank reaction without catalyst as well as 1% Pd loaded on separately SiO₂ and WO₃ was also carried out. As expected the blank reaction gave very poor conversion (~1%) after 5 h (Table 3.1, entry 1) indicating necessity of the catalyst for AP hydrogenation under ambient conditions. The AP conversion after 5 h was 92, 45 and 26% for 1P20WS, 1P15WS and 1P10WS respectively, whereas the PE yield was 76, 25 and 15% respectively. This trend in conversion and yield is in accordance with the acidity of the support. The acidity trend for the support follows: 20WS > 15WS > 10WS (Table 2.2). As explained in previous chapter (section 2.3.2.a) high activity of the catalysts under ambient condition can be attributed to the very high Pd dispersion on acidic support. To study the contribution of individual SiO₂ and WO₃ in the catalytic activity, 1% Pd loaded separately on SiO₂ and WO₃ was used for AP hydrogenation under identical conditions and indeed the difference in the activity was observed. Though the conversion after 5 h was almost similar 24 and 23 % (Table 3.1, entry 5 and 6) for Pd/SiO₂ and Pd/WO₃ respectively, the PE yield was significantly different. PE yield was 12% and 6% for Pd/WO₃ and Pd/SiO₂ respectively confirming role of acidity in catalytic activity. In the hydrogenation reaction using PWS catalysts, apart from PE other products formed were EB and hemiketal and ketal of AP as well as

methyl ether of PE as shown in Scheme 3.2. Ethylbenzene formation can be explained by sequential dehydration of PE to styrene and subsequent hydrogenation. Palladium is well known for dehydration reaction [28]. The reaction solvent used was methanol hence, acid catalyzed hemiketal and ketal formation with AP takes place in presence of acidic WS support. Similarly acid catalyzed etherification of PE takes place with solvent methanol leading to undesired by-product formation. The reaction was monitored with time to study the concentration time profile.

Table 3.1: AP hydrogenation using series of PWS catalysts

Sr. No.	Catalyst	Time (h)	Conv. (%)	%Yield of			TON	TOF(h ⁻¹)
				PE	EB	Others		
1	Blank	5	1	<1	-	-	-	-
2	1P20WS	1	42	14	<1	-	-	1102
		5	92	76	7	2	2374	-
3	1P15WS	1	29	5	<1	3	-	471
		5	45	25	1	4	707	-
4	1P10WS	1	15	3	-	1	-	454
		5	26	15	<1	3	776	-
5	Pd/SiO ₂	1	16	1	-	-	-	248
		5	24	6	-	-	372	-
6	Pd/WO ₃	1	8	4	-	-	-	313
		5	23	12	-	-	983	-

Reaction conditions - 1g AP (8.3 mmol), 10 wt % catalyst w.r.t. substrate, 15 ml solvent (methanol), 1atm H₂ pressure, RT.



Scheme 3.2. Acetophenone hydrogenation products using PWS catalysts in methanol solvent

(b) Concentration time profile for acetophenone hydrogenation

The AP hydrogenation was monitored with time to follow the change in PE yield with AP conversion (Figure 3.1). The results showed that initially with increase in AP conversion, only PE was formed. After 300 min the AP conversion increased further, though with decrease in PE yield with corresponding increase in EB formation due to dehydration of PE and subsequent hydrogenation to EB. However, the decrease in PE yield (~10%) did not match with corresponding increase in the yield of EB (~2%). This may be due to the possibility of polymerization of PE on catalyst surface [29]. To confirm the oligomerisation of PE, a control experiment was performed for hydrogenation of PE under identical reaction conditions and the results showed (Table 3.2) that after 5h the PE conversion was 35% with 7% yield of EB and 1% other products. These results confirmed oligomerisation of PE on catalyst surface under reaction conditions.

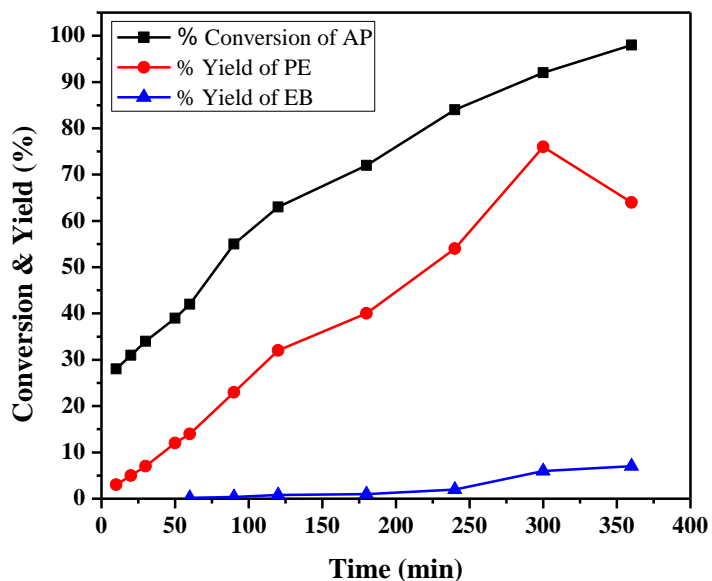


Figure 3.1. Time on stream analysis for AP hydrogenation

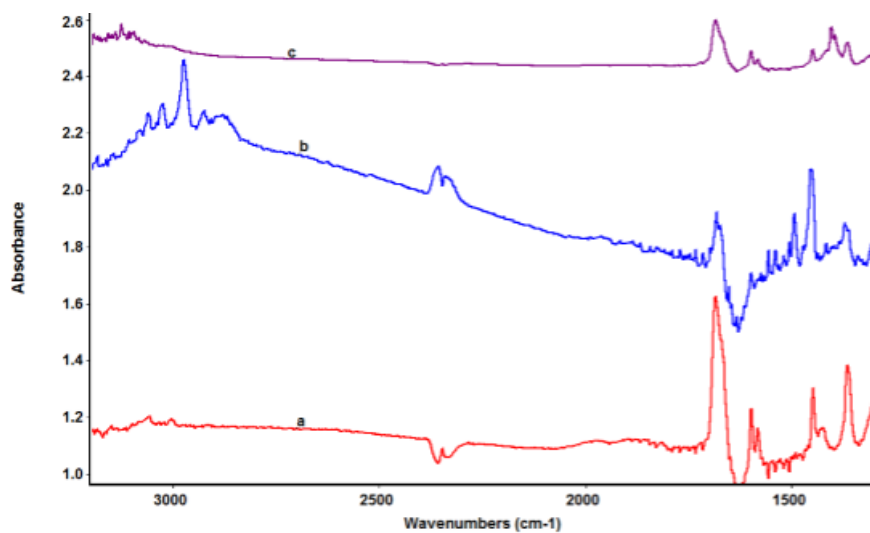
Reaction condition- 1g AP, 10 wt% 1P20WS catalyst w.r.t. AP, Methanol-15 ml, 1-atm H₂ pressure, RT.

Table 3.2: Hydrogenation of PE using 1P20WS catalyst

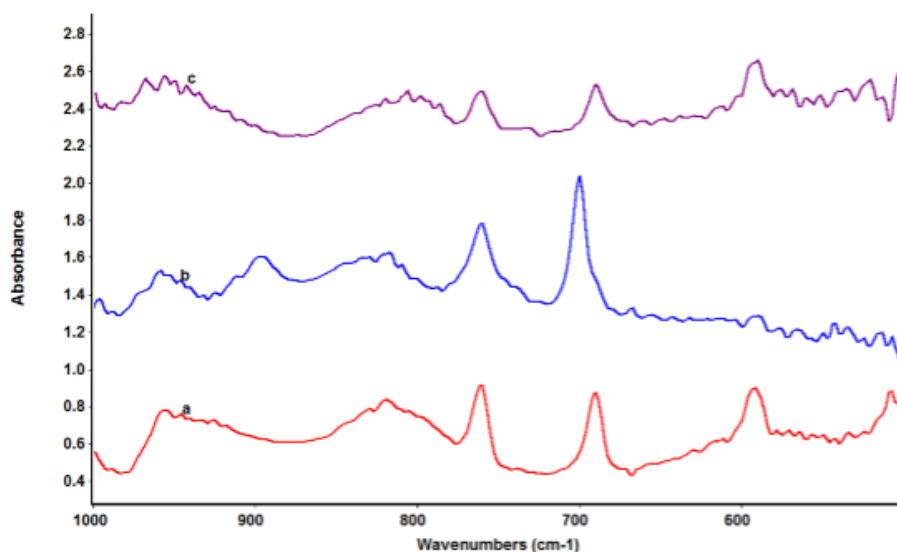
Sr. No.	Time (h)	Conv. (%)	Yield (%)	
			EB	other
1	1	7	1	<2
2	2	9	3	<1
3	3	13	4	<1
4	4	26	5	<1
5	5	35	7	<1

Reaction conditions - 1g PE, 10 wt % 1P20WS catalyst w.r.t. PE, Methanol-15 ml, 1-atm H₂ pressure, RT.

It was also observed that initially up to 1h of reaction time, the total yield of all the products was significantly lower than the conversion. This could be due to strong physisorption of AP on the catalyst surface. Initial difference in conversion and yield may be attributed to induction period during which only acetophenone adsorption onto the catalyst surface was observed. Later the yield of the products increased with increase in the conversion. To confirm this fact the catalyst was separated from the reaction after 1h and characterized by FTIR and TGA analysis (Figure 3.2 and 3.3). Indeed, the FTIR spectrum clearly showed presence of carbonyl and aromatic peaks for AP at 1683 and 800-900 cm^{-1} respectively as shown in Figure 3.2. Additionally only support, 20WS was subjected to the identical reaction conditions for 5 h and the FTIR was recorded after filtration. The spectrum (Figure 3.2iic) also showed presence of strongly adsorbed AP indicating the acidic nature of the support to contribute to the adsorption of the AP on the catalyst surface. The TGA analysis (Figure 3.3) also indicated weight loss and presence of exotherm in catalyst separated after 1 h and 5h indicating presence of physisorbed organics on catalyst surface. Hence the concentration-time profile along with FTIR and TG-DTA analysis of the catalyst separated after 1 and 5 h indicated initial adsorption of AP on the catalyst surface and later the oligomerisation of PE on the catalyst surface giving rise to difference in the AP conversion and total yield of the products as analysed by GC.



i)



ii)

Figure 3.2. FTIR spectra of PWS catalysts in the range i) 1300 to 3200 cm⁻¹ and ii) 500 to 1000 cm⁻¹; a) 1P20WS catalyst isolated from reaction mixture after 1 h after subtraction of fresh 1P20WS catalyst, b) 1P20WS catalyst isolated from reaction mixture after 5 h after subtraction of reduced 1P20WS catalyst and c) support (WO₃/SiO₂) isolated after 5 h reaction time after subtraction of fresh support

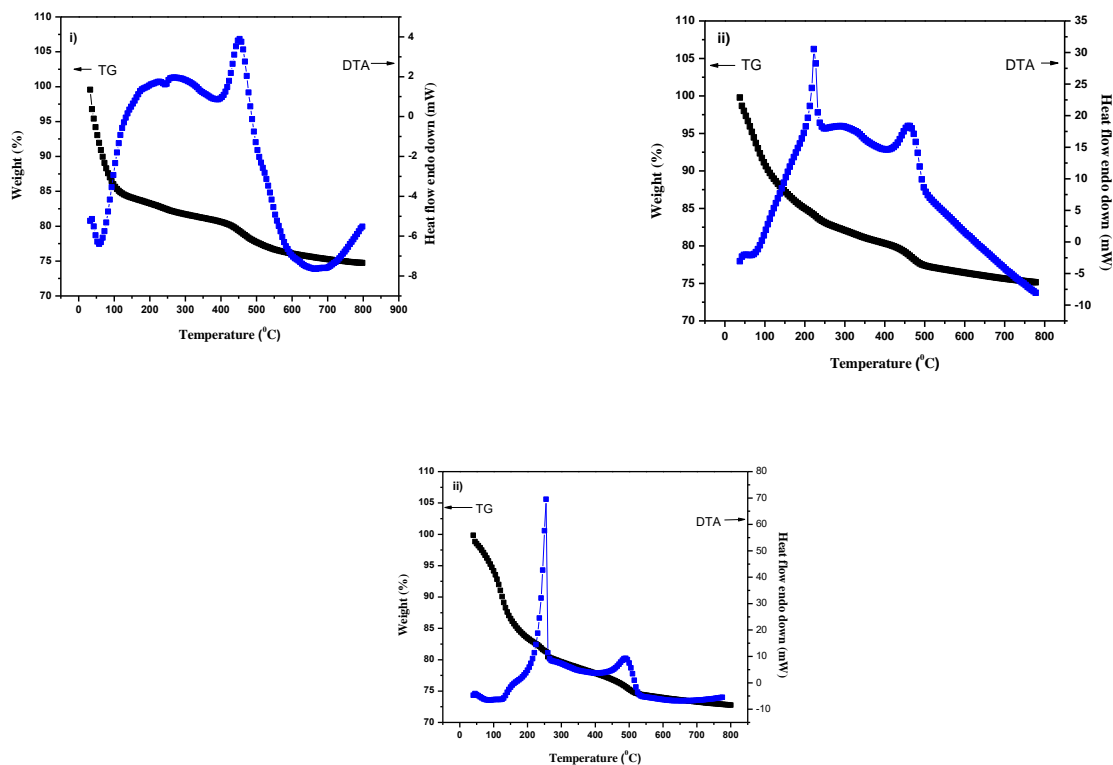


Figure 3.3. TG/DTA curves of 1P20WS i) fresh catalyst, ii) catalyst isolated after 1 h and iii) used catalyst

(c) Effect of solvent

The effect of different solvents on AP conversion and PE yield was studied using a range of polar (methanol, ethanol), nonpolar solvents (hexane, toluene) and the results are shown in Figure 3.4. In case of polar solvents the conversion was 92% and 65% for methanol and ethanol with 78% and 58% PE yield, respectively. In case of non-polar solvents like hexane and toluene AP conversion was 67% and 37%, however, PE yield was significantly lower for both the solvents with 42% and 30%, respectively. Very high AP conversion was obtained in polar solvents with the better yield of PE as compared to the non-polar solvents. This may be due to high dipole moment, high dielectric constant and also high hydrogen donor ability of polar

solvents [30]. High AP conversion and PE yield was observed in case of methanol solvent, this may be attributed to the polarization and activation of C=O bond. In case of protic solvent, due to the hydrogen bonding, the chances of hydrogenolysis of C-OH reduces which leads to the higher yield of PE compared to EB. In case of non-polar solvents as they have the low dipole moment and no hydrogen donor ability, the catalytic activity is low compared to the polar solvents. As there is no possibility of hydrogen bonding, this may further lead to the hydrogenolysis of C-OH bond faster than the polar solvents resulting in high yield of EB compared to the polar solvents.

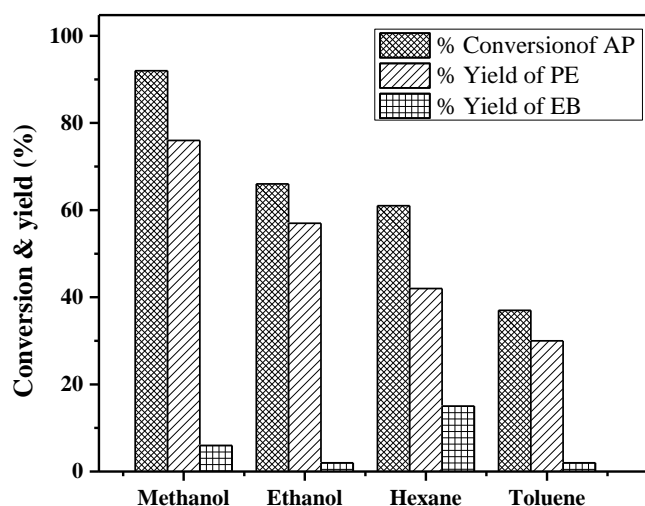


Figure 3.4. Effect of solvent on AP hydrogenation

Reaction conditions - 1g AP (8.3 mmol), 10 wt % 1P20WS catalyst w.r.t. substrate, 15 ml solvent, 1atm H₂ pressure, RT, time-5h.

(d) Effect of catalyst loading

The effect of catalysts loading on AP conversion and PE yield was studied (Figure 3.5). It is very clear from the results that with increase in the catalyst loading gradually from 5 to 10 wt% the PE conversion after 5 h increased from 68 to 92%, whereas for 15% catalyst loading almost 98% conversion was achieved in only 3 h. The PE yield increased from 28 to 78% for 5

and 10 wt% catalyst loading respectively, however, with further increase in the catalyst loading to 15%, decreased the PE yield to 52% with formation of 4% EB, 1% each of methyl ether of PE, ketal and hemiketal. This decrease in the PE yield with increase in the catalyst loading to 15% may be attributed to the higher oligomerisation of PE on catalyst surface. As, the conversion and yield was maximum for 10 wt % catalyst loading, further optimization was carried out using same catalyst loading (10 wt% with respect to AP).

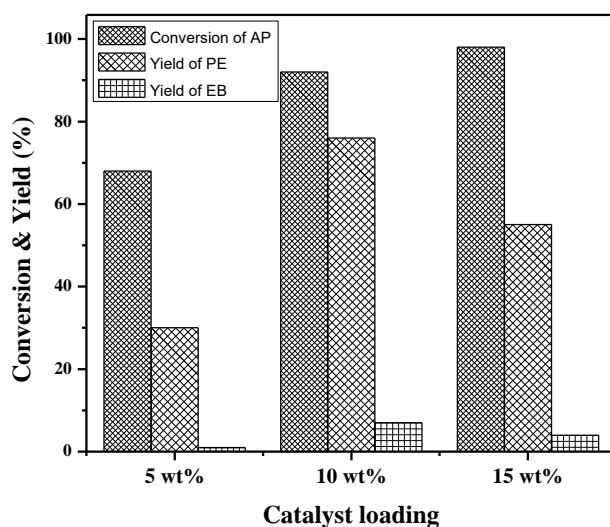


Figure 3.5. Effect of catalyst loading on AP hydrogenation

Reaction condition- 1g AP (8.3 mmol), 1P20WS catalyst, 15 ml solvent (methanol), 1atm H₂ pressure, RT, time- 5h (for 15 wt% time- 3h).

(e) Effect of palladium loading

The effect of Pd loading on 20WS support was studied for AP hydrogenation and the results are summarized in Table 3.3. When Pd loading was gradually increased from 0.1% to 1% on 20WS support, there was a gradual increase in AP conversion from 30 to 92 % and yield of PE from 5% to 76% after 5 h. When Pd loading was further increased to 2% there was increase in the conversion (96%), however, with decrease in the PE yield (72%) after 3h. This can be

attributed to accelerated dehydration of PE to styrene (3%) and subsequent hydrogenation to EB (5%) due to high Pd loading. Recent reports confirmed that palladium is responsible for dehydration reactions [28]. Acid catalyzed (20WS) etherification of PE with methanol (8%) was also observed leading to further decrease in the PE yield.

Table 3.3: Effect of palladium loading on AP hydrogenation using P20WS catalyst

Sr. No.	Palladium loading	Time (h)	Conv. (%)	% Yield of			TON	TOF h ⁻¹
				PHE	EB	Others		
1	0 (WS)	1	11	-	-	2	-	-
		5	18	-	-	4	-	-
2	0.1 %	1	25	1	-	2	-	6111
		5	30	5	-	4	6746	-
3	0.5 %	1	33	4	-	2	-	2222
		5	49	31	1	3	3252	-
4	1 %	1	42	14	1	-	-	1102
		5	92	76	7	2	2374	-
5	2 %	1	46	28	1	1	-	647
		3	96	72	5	11	1359	-

Reaction condition- 1g AP (8.3 mmol), 10 wt % catalyst w.r.t. substrate, 15 ml solvent (methanol), 1atm H₂ pressure, RT.

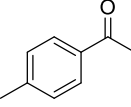
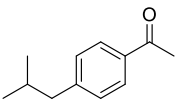
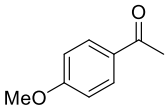
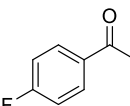
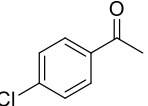
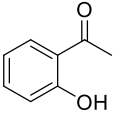
(f) Effect of different substituents on aromatic ring of Acetophenone

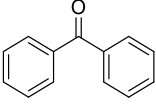
To establish the wider applicability of the catalyst, hydrogenation of various substituted acetophenone including some industrially important substrates was carried out using 1P20WS catalyst in methanol solvent (Table 3.4) under optimized conditions. The rate of hydrogenation is affected by electronic and steric effects of substituents on aromatic ring. The rate of

hydrogenation was high for AP with electron donating groups than for unsubstituted AP except for 2-hydroxy acetophenone. The hydrogenation of *p*-methyl acetophenone was very fast with 34% conversion after 1 h with 97% selectivity for 1-(4-methyl phenyl) ethanol with high TOF 728 h^{-1} (Table 3.4, entry 1). As steric effect of alkyl substituted group increased, the rate of hydrogenation decreased. Hence the rate of hydrogenation of *p*-alkyl acetophenone over 1P20WS decreased in order *p*-Me > *p*-*i*-Bu (Table 3.4, entry 1 and 2). Hydrogenation of 4-isobutyl acetophenone gives 1-(4-isobutyl phenyl) ethanol, which is an intermediate in the synthesis of ibuprofen drug. This drug is used as non-steroidal and anti-inflammatory (NSAI) drug to reduce swelling and inflammation. Nickel based catalysts have been reported previously for this hydrogenation, however at high temperature (100-140 °C) and high pressure (2 - 6 MPa) [31], whereas using present catalyst, the hydrogenation of 4-isobutyl acetophenone could be achieved under ambient conditions with 82% conversion and 91% selectivity after 4 h with very high TOF of 301 h^{-1} (Table 3.4, entry 2). In case of *p*-methoxy acetophenone, 95% conversion was obtained after 5 h, but with lower selectivity (43%) for corresponding PE (Table 3.4, entry 3). Due to electron donating effect of *p*-methoxy group, along with dehydration of PE to EB, it also gave methyl ether of corresponding PE decreasing the selectivity for desired product. In case of *para*-fluro and *para*-chloroacetophenone, the conversion obtained was 80% and 73%, respectively (Table 3.4, entry 4 and 5). However, the selectivity for corresponding PE was very low in case of *para*-chloroacetophenone; due to facile Pd catalyzed hydro dechlorination. Generally, palladium-based catalysts are well known for hydro-dehalogenation. The hydrogenation of *p*-chloroacetophenone gave only 22% 1-(4-chloro phenyl) ethanol along with 53% dechlorinated EB and acetophenone. There was no conversion in case of *ortho*-hydroxyacetophenone; this may be due to *ortho*-steric effect of -OH group and/or higher stability

of the substrate due to intramolecular hydrogen bonding (Table 3.4, entry 6). The hydrogenation of benzophenone was also carried out using 1P20WS catalyst, however with very slow rate, may be due to steric effect of two phenyl ring in molecule. It gave only 19% conversion of benzophenone with 88% selectivity for biphenyl methanol after 4h (Table 3.4, entry 7).

Table 3.4: Hydrogenation of different substituted AP using 1P20WS catalyst

Sr. No.	Substrate	Time h	Conv. %	% Selectivity of Product			TON	TOF h ⁻¹
				PE	EB	Other		
1	 p-Methyl acetophenone	1	34	97	3	-	-	728
		5	96	86	10	4	2056	-
2	 p-Isobutyl acetophenone	1	18	100	-	-	-	301
		5	82	91	8	1	1371	-
3	 p-Methoxy acetophenone	1	19	63	11	26	-	371
		5	95	43	39	18	1855	-
4	 p-Fluoroacetophenone	1	16	100	-	-	-	340
		5	80	97	3	-	1698	-
5	 p-Chloroacetophenone	1	30	23	53	24	-	572
		5	73	22	53	25	1392	-
6	 o-Hydroxy acetophenone	5	No reaction	-	-	-	-	-

7		1	6	83	-	17	-	97
	Benzophenone	5	19	88	-	12	307	-

Reaction conditions- Substrate (8.3 mmol), 10 wt % catalyst w.r.t. substrate, 15 ml solvent (methanol), 1-atm H₂ pressure, RT, time-5h.

There are several reports published on hydrogenation of AP using different transition metal based catalysts, and some of the work is summarized in Table 3.5. From the literature reports it is very clear that hydrogenation of AP is carried out at higher temperatures and/or high pressures. For hydrogenation under milder conditions high noble metal loading was needed. Copper supported on SiO₂ catalyst is reported for 100% conversion of AP at high temperature and pressure [32]. Platinum supported on alumina with 1 wt% platinum loading has shown good catalytic activity for hydrogenation of AP at room temperature and atmospheric pressure [33]. The catalyst Pt/K-N-COF/SiO₂ gave almost 100% AP conversion with 96% selectivity for PE at 60 °C and 20 bar H₂ pressure [6]. Though, Pt based catalysts have provided very high conversion of AP, significantly higher cost of platinum is an issue of concern. Palladium supported on carbon [34, 35] and carbon nanotubes [25] has shown very high catalytic activity for AP hydrogenation at lower temperature and pressure within a short period of time, however at high palladium loading (up to 5%). Sodium promoted 5%Pd/C catalyst has shown 100% AP conversion with 96.4% selectivity for PE at 20 bar hydrogen pressure and 70 °C [36] Palladium and co-metal on carbon (PdCFe and PdCLi) studied to analyze the effect of bimetallic system on reaction rate of hydrogenation of aromatic group or carbonyl group and hydrodeoxygenation [5]. Here 1PdC3Li showed 62% AP conversion with 62% selectivity for PE. Hydrogenation of AP with 97% conversion and 100% selectivity at very high temperature (160 °C) and 10 bar pressure has been reported using Ag-OMS-2 catalyst [37]. Pd/NiO catalyst has yielded only 19 %

conversion [26], for hydrogenation of AP. Nickel and cobalt based catalysts required high temperature (80-180 °C) and high pressures (10-30 bar) for hydrogenation of AP [22, 38, 39]. Compared to the literature report the present catalyst 1P20WS has provided efficient AP hydrogenation under ambient conditions. The hydrogenation of AP was carried out at atmospheric pressure and room temperature using 1P20WS catalyst with very high conversion (92%) and PE yield (76%). The high catalytic activity of PWS catalyst can be correlated to very high surface area, mesoporous nature and high acidity of the catalyst leading to formation of Pd nano sheets and in turn very high Pd dispersion on the catalyst surface.

Table 3.5: Literature survey for hydrogenation of AP

Sr. No.	Catalyst	Solvent	Temp °C	Pressure	Time min	Conv. %	Sel. PE %	Ref.
1	6.8% Cu/SiO ₂	IPA	90	20bar(total) 18.7 (H ₂)	300	100	>99	[31]
2	1%Pt/Al ₂ O ₃	MeOH	RT	0.6 MPa	24 h	89	98	[32]
3	Pt/K-N-COF/SiO ₂	EtOH	60	20 bar	90	100	96	[6]
4	5% Pd/C	H ₂ O/CO ₂	40	3 MPa	45	100	95	[33]
5	3% Pd/CNTs	EtOH	60	10 ml/min	240	95	97	[24]
6	1PdC3Li	EtOH	200	100 ml/min	-	62	62	[5]
7	15%Ag-OMS-2	IPA	160	10 bar	180	97	100	[36]
8	1% Pd/NiO	EtOH	80	1.3 MPa	180	19	92	[25]
9	5% Pd/C	Water + CO ₂	80	CO ₂ -1MPa H ₂ - 4MPa	60	80	100	[34]
10	5 wt % Pd/SA	n-hexane	60	-	5	12	100	[26]

11	Na-5%Pd/C	EtOH	30-70	20 bar	2-9 h	100	96.4	[35]
12	80% Ni ₂ P/Al ₂ O ₃	EtOH,	180	3MPa	-	100	95.6	[37]
13	5% NiP/MSNS	n- heptane	80	1MPa	-	30	95	[21]
14	16.7% Co/Mordernite	Water	100	2 MPa	360	99.9	100	[38]
15	1P20WS	MeOH	RT	10 ml/min	300	92	76 (yield)	Present work

(g) Recycle study

The recyclability of the 1P20WS catalyst was tested for AP hydrogenation and the results are shown in Figure 3.6. The AP conversion for fresh catalyst was 95%, which decreased to 60% for second use with simultaneous decrease in the PE yield from 78 to 49% (recycle 1). The results showed non recyclability of the 1P20WS catalyst for AP hydrogenation. To understand the reason for catalyst deactivation, Pd leaching was analyzed by ICP and the used catalyst was additionally characterized in details.

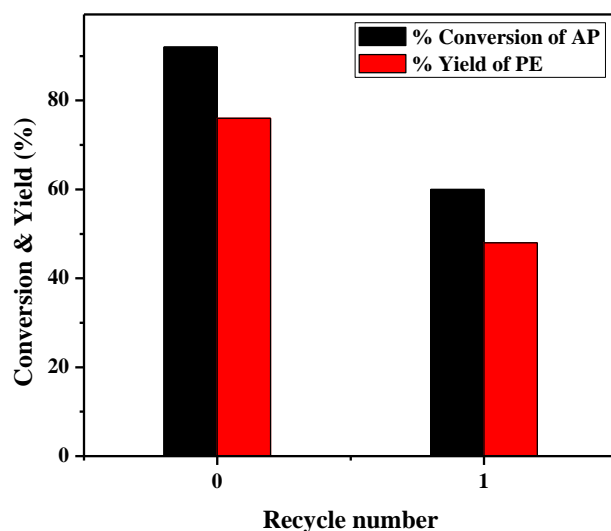


Figure 3.6. Recycle study of 1P20WS catalyst for acetophenone hydrogenation

Reaction conditions- 1g AP (8.3 mmol), 10 wt % catalyst w.r.t. substrate, 15 ml solvent (methanol), 1atm H₂ pressure, RT, time-5h.

h) Leaching Test and ICP analysis of reaction mixture

After completion of 50% reaction, the catalyst was filtered and the reaction mixture without catalyst was allowed to react further for 4 h under identical reaction conditions (Figure 3.7). Even after additional 4 h reaction, there was no increase in the conversion indicating no Pd leaching in the reaction. Additionally ICP analysis of the reaction mixture indicated no Pd in the liquid reaction mixture, confirming almost no leaching of the Pd from the catalyst surface (0.53 ppm). Hence used catalyst was further characterized in details to understand the cause of deactivation.

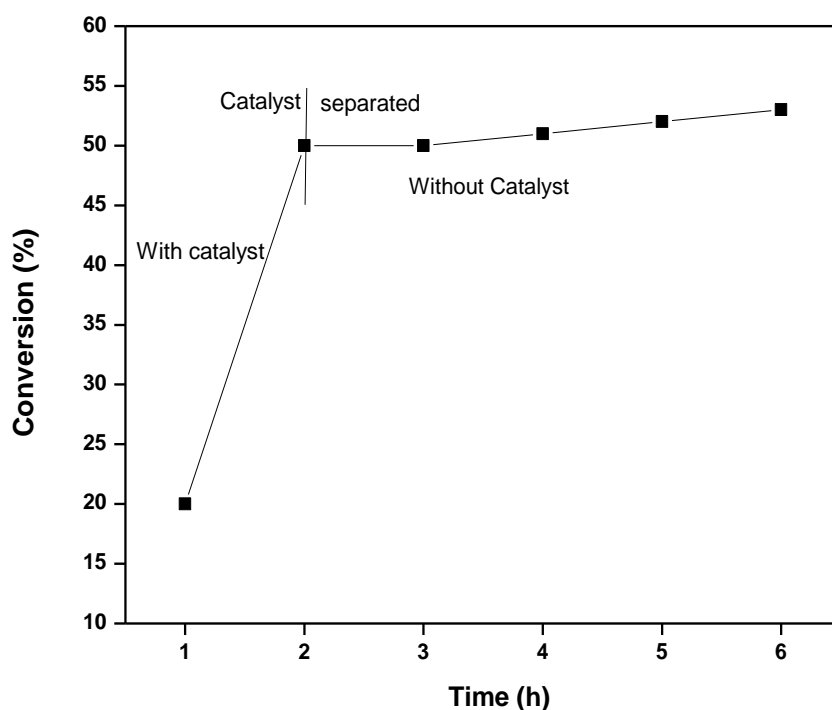


Figure 3.7. Conversion of AP after filtration of catalyst

Reaction condition- 1g AP (8.3 mmol), 10 wt % catalyst w.r.t. substrate, 15 ml solvent (methanol), 1atm H₂ pressure, RT, time-after filtration reaction continued for 4h.

3.3.2 Characterization of used catalyst

a) XRD analysis

The powder X-ray diffraction pattern of fresh and used catalysts are shown in Figure 3.8. No change in the diffraction pattern of used catalyst was observed compared to fresh catalyst. However, the intensity of the WO₃ peaks in used catalyst has decreased compared to fresh catalyst indicating more amorphous nature of the used catalyst.

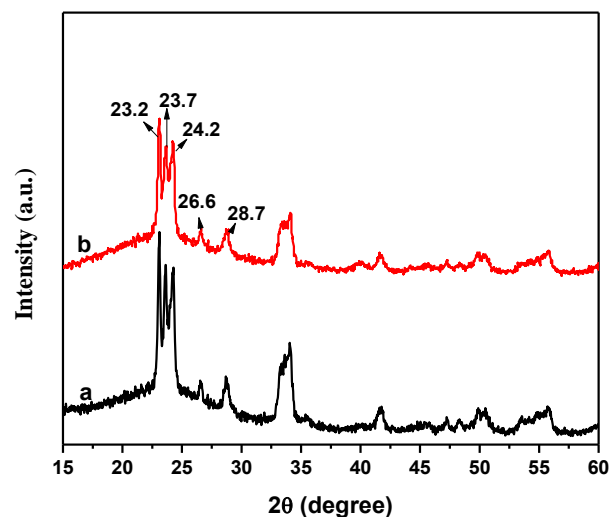


Figure 3.8. XRD pattern of (a) fresh and (b) used 1P20WS catalysts

b) HRTEM analysis

The HRTEM analysis of fresh and used catalyst is presented in Figure 3.9 and 3.10. The HRTEM image showed no change in the particle size of fresh and used catalyst. The particle size was found to be in the range of ~12-15 nm. Also, no change in the elemental composition in fresh and used catalyst was observed confirming no leaching of Pd in reaction mixture.

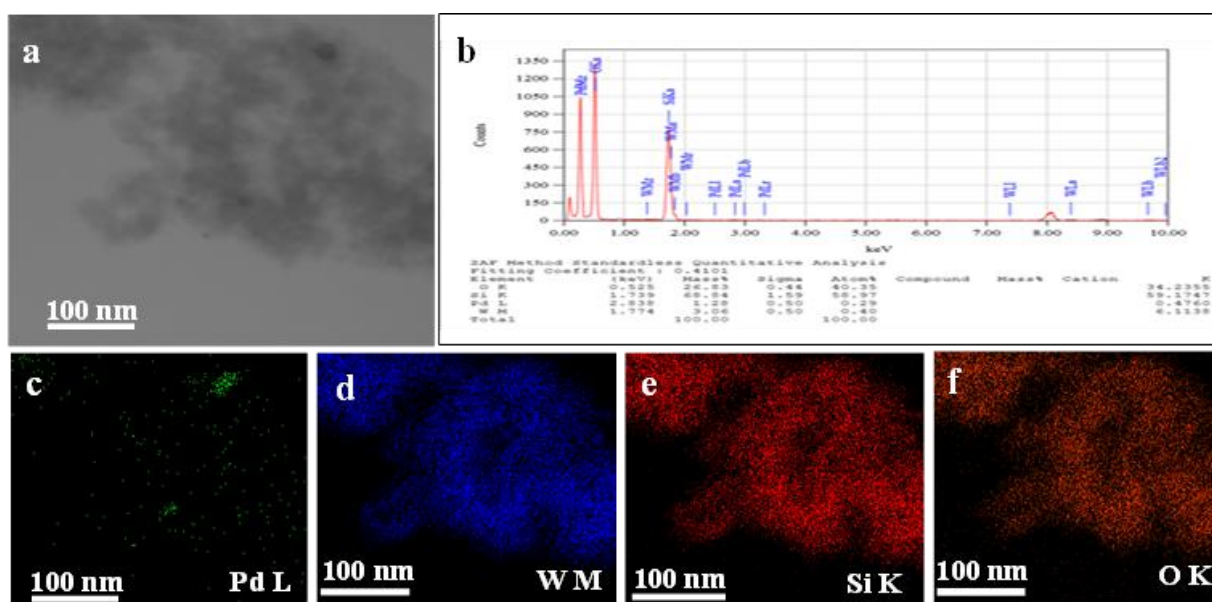


Figure 3.9. HRTEM data of fresh 1P20WS catalyst

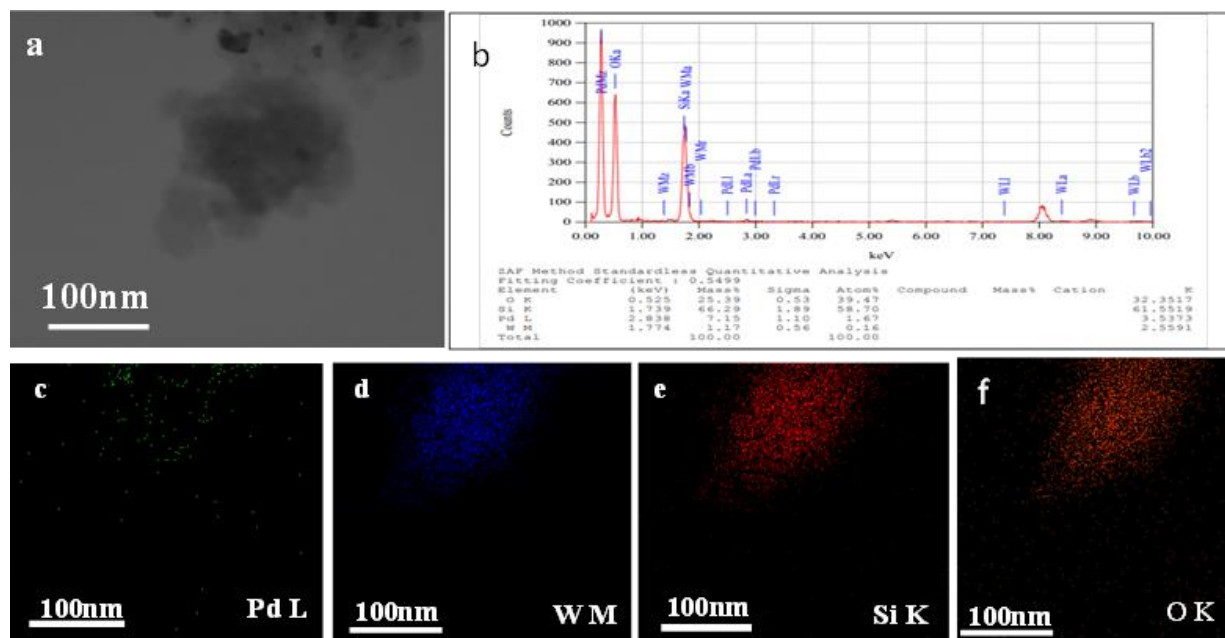


Figure 3.10. HRTEM data of used 1P20WS catalyst

c) TG/DTA analysis

The TG/DTA curves of fresh and used catalysts are shown in Figure 3.3. The results showed the total weight loss in fresh and used catalysts to be about 25 and 27 wt% respectively, however the weight loss in the temperature range of 30-100 °C for physisorbed water was 13.9 % and 5.7% respectively for fresh and used catalyst indicating higher physisorbed water on fresh catalyst. The weight loss in the temperature range of 100-250 °C for physisorbed organics was significantly higher for used catalyst (12.5%) compared to fresh catalyst (3.3%) indicating strong adsorption of organic moieties like reactant/products on the catalyst surface contributing for catalyst deactivation. This is also supported by highly intense exothermal observed in DTA analysis at 256 °C for used catalyst (heat flow 70 mW) compared to fresh catalyst (heat flow 4 mW) confirming combustion of organics at that temperature.

3.3.3 Deactivation and regeneration of catalyst

From above characterization of used catalyst, it is clear that there is no change in the morphology of used catalyst. In 2015, C. H. Bartholomew discussed different reasons for catalyst deactivation in the review article [40]. One of the reasons is strong chemisorption of species on catalytic sites which block active sites for catalytic reaction. Also in previous reports for hydrogenation of 4-isobutyl acetophenone, significant catalyst deactivation was observed due strong adsorption of oligomer deposits from reactants or products. These oligomers were obtained due to undesired side reactions. Adsorption of oligomer on catalyst causes to loss of activity of catalyst by blocking the active sites [29]. In present work, TGA of used catalyst showed strong adsorption of reactant and products on catalyst contributing to the catalyst deactivation. The oligomerisation of the PE was confirmed by hydrogenation of PE under identical conditions where significant difference in PE conversion and product yield was observed on catalyst surface as shown in Table 3.2. To confirm that the deactivation and non-recyclability of 1P20WS catalyst is substrate specific for only AP hydrogenation due to tendency of the product PE to undergo oligomerisation on catalyst surface, this catalyst was used for hydrogenation of styrene and subsequent recycle study (Table 3.6). The results clearly indicated very high efficiency of the catalyst 1P20WS for recycle in hydrogenation of styrene to EB. Hence this catalyst can be recycled efficiently for the hydrogenation reactions where the substrate, product or intermediate does not adsorb very strongly or oligomerise on the catalyst surface.

Table 3.6: Recycle study of 1P20WS for styrene hydrogenation

Sr. No.	Run	Conversion (%)	Selectivity (%) EB
1	0	81	100
2	1	80	100
3	2	81	100
4	3	81	100

Reaction conditions - 1g styrene, 10 wt % catalyst (1P20WS) w.r.t. substrate, 15 ml solvent (methanol), 1-atm H₂ pressure, RT, time-4h.

The regeneration of catalyst is a process to reinstate the catalytic activity of used catalyst by washing or thermal treatment to remove adsorbed species. To remove the adsorbed material, spent catalyst was washed with methanol and DCM. Washing of catalyst with methanol and DCM did not significantly enhance the catalytic activity. HRMS data of DCM filtrate showed that, the filtrate contained polymeric compounds which having m/z in range of 500 to 1460. This confirmed the polymerization of products on catalyst due side reaction. For thermal treatment catalyst was calcined at 250 and 500°C and used to perform reaction under optimized conditions. However, it did not improve the catalytic activity. For 250°C calcined catalyst 42% AP conversion was obtained while for 500°C calcined catalyst only 8% AP conversion was obtained. The conversion was very low so, the TGA and TEM analysis was done for these catalysts. TGA analysis showed almost all the absorbed material on catalyst was removed by calcination (Figure 3.11). The weight loss in the temperature range of 100-250 °C for physisorbed organics for used catalyst was 12.5%, which was reduced to 3.3% and 2.6% for used catalyst calcined at 250°C and at 500°C respectively. The particle size of palladium was increased to 15-25 nm and 29-35

nm for 250 and 500°C calcined catalyst respectively as confirmed by TEM analysis (Figure 3.12). Thus it was confirmed that on thermal treatment adsorbed material was removed but due to exothermicity of the combustion and high temperature agglomeration of palladium particles was observed. Recycle study was done at lower (25%) AP conversion (at 1h) for five catalytic run and results are shown in Figure 3.13. The result showed that catalyst could be recycled for 5 run without losing the catalytic activity at lower before the oligomerisation of the formed product PE.

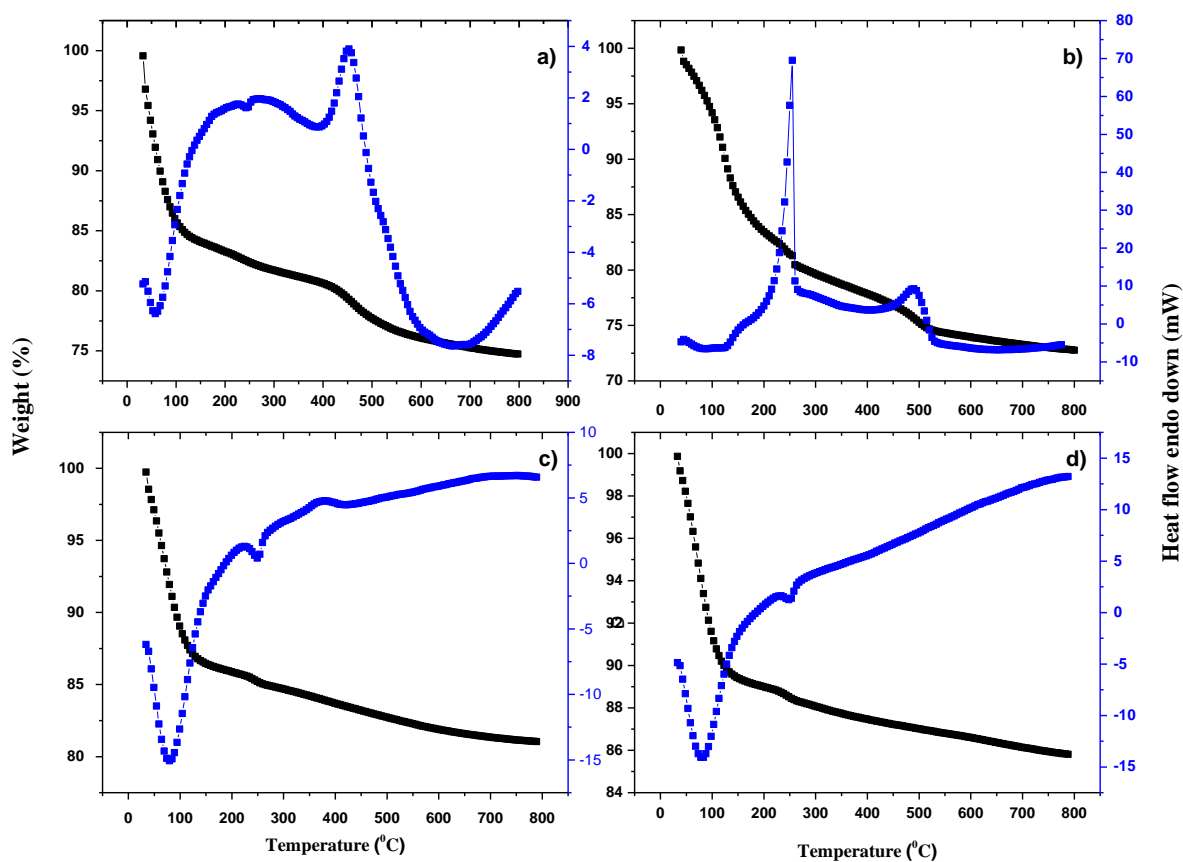


Figure 3.11. Comparisons of TG/DTA curves of 1P20WS a) fresh catalyst, b) used catalyst, c) used catalyst calcined at 250°C, and d) used catalyst calcined at 500°C

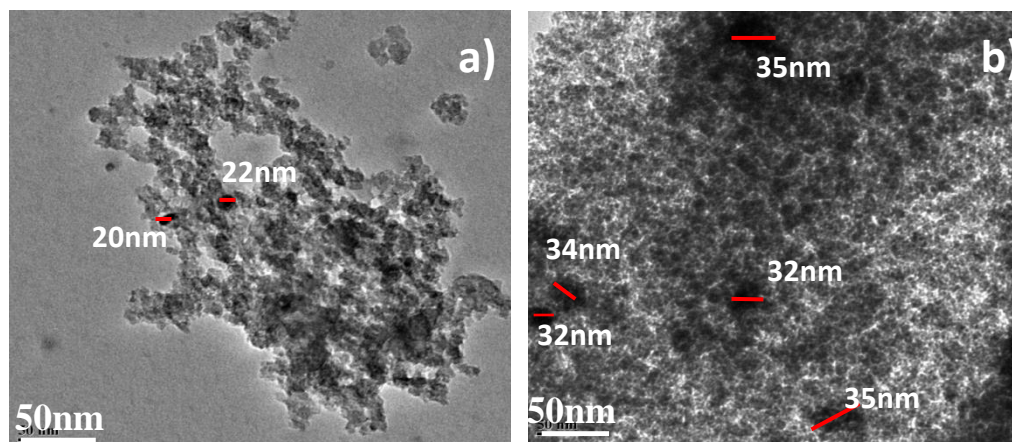


Figure 3.12. TEM images of 1P20WS catalyst calcined at a) 250°C and b) 500°C

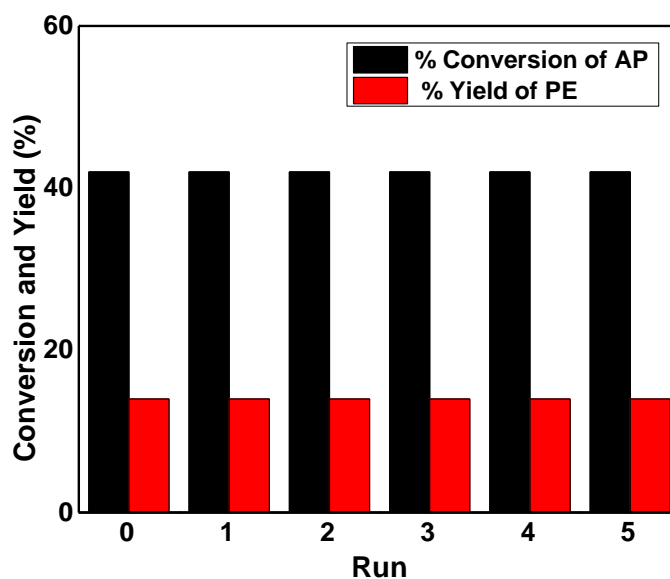


Figure 3.13. Recycle study of 1P20WS catalyst for acetophenone hydrogenation at lower conversion (1h), Reaction conditions- 1g AP (8.3 mmol), 10 wt % catalyst w.r.t. substrate, 15 ml solvent (methanol), 1atm H₂ pressure, RT, time-1h.

3.4 Mechanistic study of AP hydrogenation on 1P20WS catalyst

The mechanism of AP hydrogenation over 1P20WS catalyst was studied by analyzing interaction of reactant/product, solvent methanol and reaction mixture on catalyst (pre-reduced in hydrogen) surface. To study the interaction of adsorbed species on catalyst surface, all spectra

have been reported after subtraction of neat catalyst (reduced). A drop of methanol, AP, or final reaction mixture was placed on the catalyst wafer and FTIR spectrum was recorded. All FTIR spectra are shown in Figure 3.14. FTIR spectrum of pure methanol (Figure 3.14 a) showed peaks at 1447 and 3338 cm^{-1} for bending and stretching vibrations of Me-O-H group respectively. The spectrum of methanol adsorbed on catalyst surface showed the disappearance of peak at 1447 cm^{-1} with appearance of peak at 1643 cm^{-1} which can be attributed to formation of surface hydroxyl groups (Figure 3.14b). The appearance of broad peak centered around 3500 cm^{-1} also indicated the formation of surface hydroxyl groups by dissociation of MeO-H bond to form MeO- and surface -OH groups. It indicated dissociative adsorption of methanol on WO_3 group to form W-OMe and W-OH [41]. To find out the interaction of AP with catalyst surface, AP was adsorbed on catalyst (pre-reduced) wafer and the FTIR spectrum was recorded. The difference spectrum was compared with authentic AP (Figure 3.14iia). Also the FTIR spectrum of catalyst filtered after 1 h reaction time (Figure 3.14iic) was recorded. The final reaction mixture was adsorbed on catalyst wafer (Figure 3.14iid) and compared with authentic AP spectrum (Figure 3.14iib). There was no shift observed in spectrum of adsorbed AP in carbonyl region on catalyst surface (Figure 3.14iia) compared to authentic AP indicating no direct activation of AP on catalyst surface through carbonyl group. However, catalyst filtered after 1 h (Figure 3.14iic) and final reaction mixture (Figure 3.14iid) showed shift in two peaks i.e. 1265 to 1270 cm^{-1} and 1359 to 1365 cm^{-1} (Figure 3.14iic and d). Jun Huang and co-workers reported that the band at 1697 cm^{-1} is attributed to the stretching vibration of AP when adsorbed on Pd by η^1 coordination (Figure 3.15i), whereas AP adsorbed on the catalyst surface by the X-sensitive benzene mode (Figure 3.15ii) showed a band at 1276 cm^{-1} [27]. The band at 1365 cm^{-1} is attributed to bending mode of CH_3 . This clearly indicated the adsorption of AP on catalyst surface through aromatic

ring and not through carbonyl group. The spectrum of final reaction mixture also showed very marginal shift in carbonyl and from 1683 to 1680 cm^{-1} . The marginal shift may be due to activation of carbonyl group of AP by surface hydroxyl groups through hydrogen bonding.

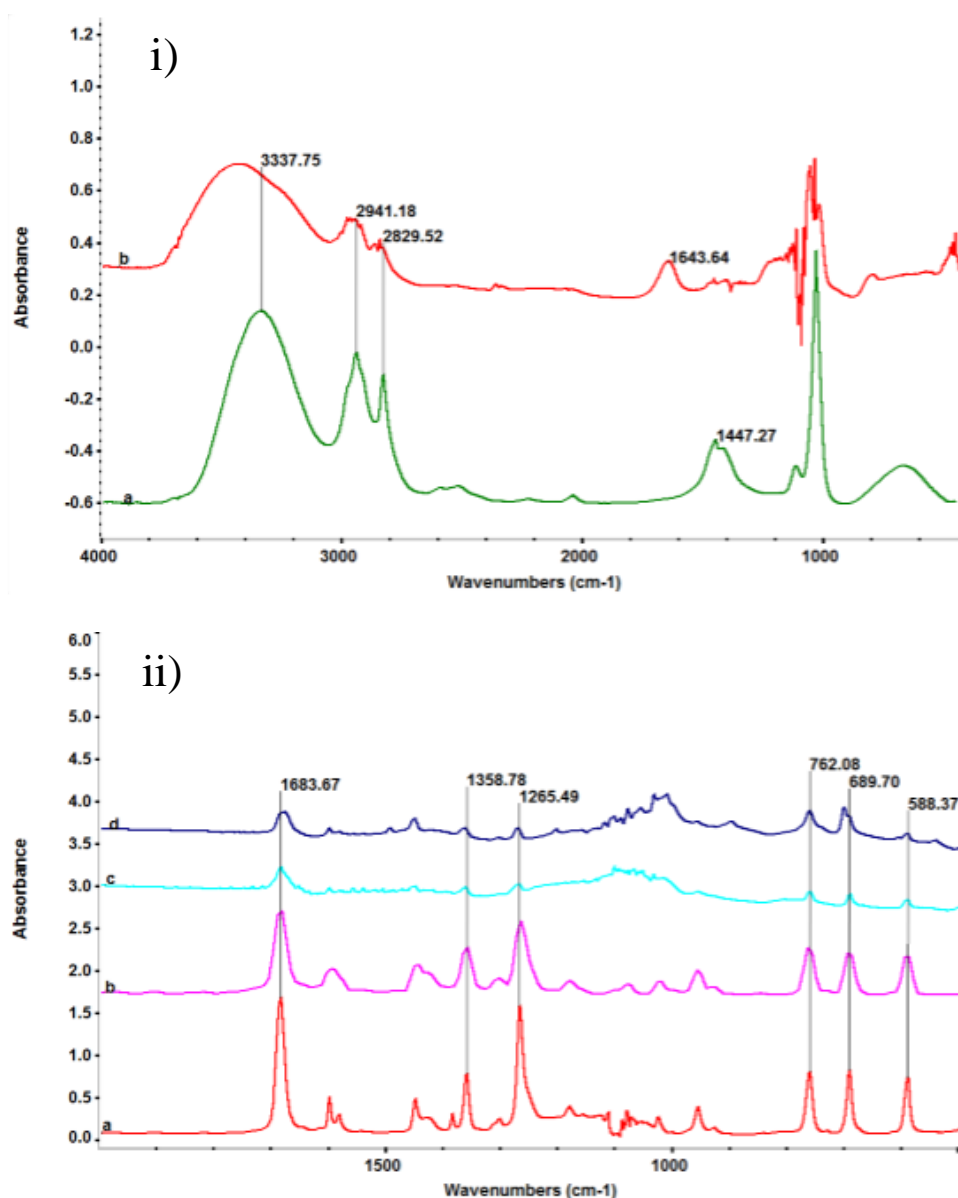


Figure 3.14. FTIR spectra of (i) a) pure methanol, b) methanol adsorbed on catalyst, (ii) a) AP adsorbed on catalyst, b) pure AP, c) catalyst filtered after 1 h reaction time and d) final reaction mixture adsorbed on reduced catalyst (all spectra are subtracted spectra from fresh reduced catalyst, except pure methanol and pure AP)

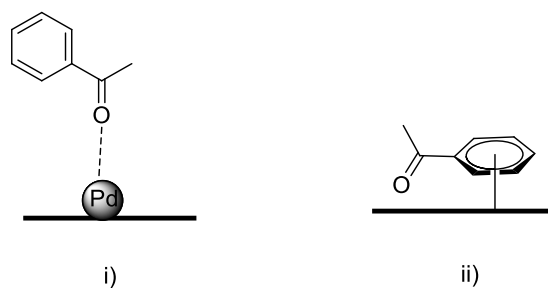


Figure 3.15. Possible bonding modes of AP adsorption on catalyst i) η^1 configuration and ii) X-sensitive benzene mode

Considering all above observations, the hydrogenation of AP using 1P20WS catalyst can be attributed to the facile activation of hydrogen on Pd site and simultaneous adsorption of AP on support through aromatic ring and activation of carbonyl group by surface hydroxyl group. Based on the FTIR study the proposed mechanism for the AP hydrogenation is shown in Figure 3.16. Initially methanol gets dissociative adsorbed on WO_3 center to give W-OMe and W-O-H (B). Hydrogen gets activated on reduced palladium center (C). As observed previously also, Pd on acidic supports leads to activation of hydrogen under ambient conditions [42, 43]. Subsequently AP gets adsorbed on catalyst surface (D). Acetophenone gets activated through aromatic ring on acidic sites via X-sensitive mode whereas carbonyl group gets activated through hydrogen bonding with hydroxyl groups. Subsequent transfer of proton from surface hydroxyl group and hydride from Pd center leads to reduction of carbonyl group to alcohol followed by liberation of PE from catalyst surface.

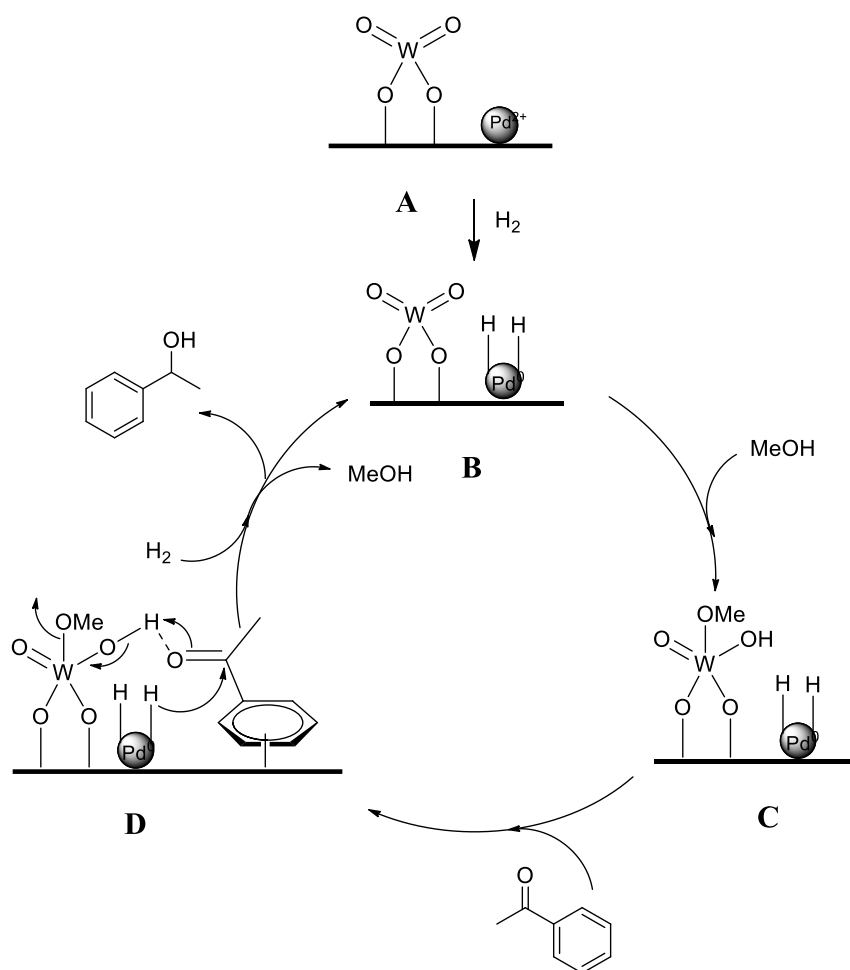


Figure 3.16. Plausible mechanism of AP hydrogenation on 1P20WS catalyst

3.5 Conclusions

1%Pd supported on acidic 20% WO₃/SiO₂ has proved to be highly efficient catalyst for hydrogenation of acetophenone and substituted acetophenone under ambient conditions. 20% WO₃/SiO₂ has provided maximum acidity for supporting palladium, which formed nano sheets of Pd (111) of 12-18 nm size. The acidic support enabled very high dispersion of Pd (36%) leading to very high catalytic activity for hydrogenation at room temperature and atmospheric pressure. 1P20WS catalyst gave 92% acetophenone conversion with 76% yield of 1-phenylethanol. The recycle studies revealed oligomerisation of the product 1-phenylethanol on catalyst surface leading to catalyst deactivation, which was substrate specific. Same catalyst

when used for styrene hydrogenation could be recycled very efficiently up to three cycles without loss in the catalytic activity. The mechanistic studies using FTIR revealed the activation of solvent methanol by dissociation on WO_3 moiety to form $\text{CH}_3\text{O-W-}$ and -W-O-H and activation of acetophenone through aromatic ring. The carbonyl group of acetophenone gets activated due to hydrogen bonding with W-OH formed by dissociation of MeO-H . Thus $\text{Pd-WO}_3/\text{SiO}_2$ has proved to be very efficient hydrogenation catalyst due to synergistic effect of palladium and acidity of the support.

3.6 References

1. L. Liu, A. Corma, *Chem. Rev.*, **2018**, 118, 4981-5079.
2. A. Baiker, *Chem. Soc. Rev.*, **2015**, 44, 7449–7464.
3. D. Wang, D. Astruc, *Chem. Rev.*, **2015**, 115, 6621-6686.
4. X. Zhang, W. Shi, Y. Li, W. Zhao, S. Han, and W. Shen, *ACS Catal.*, **2023**, 13, 4030–4041.
5. A. Saraeian, G. Gupta, R. Johnson, R. W. Dorn, A. M. Kauffmann, H. Bateni, J-P. Tessonnier, L. T. Roling, A. J. Rossini, B. H. Shanks, *ACS Sustainable Chem. Eng.*, **2022**, 10, 7759–7771.
6. X. Liu, M. Wang, X. Ren, M. Guo, C. Li, H. Li, Q. Yang, *ACS Catal.*, **2022**, 12, 6618–6627.
7. S. Lin, J. Liu, L. Ma, *React. Chem. Eng.*, **2022**, 7, 1126–1135.
8. R. K. Marella, V. R. Madduluri, T. Yu, K. Venkateswarlu, J. V. S. Kumar, M. Sreenivasan, S. K. Lakkaboyana, *Mol. Catal.*, **2021**, 507, 111561-111572.
9. D. C. Costa, A. L. Soldati, G. Pecchi, J. F. Bengoa, S. G. Marchetti, V. Vetere. *Nanotechnology*, **2018**, 29, 215702-215713.

10. M. A. Villalba, M. T.M. Koper, *J. Phys. Chem.*, **2020**, 124, 25884–25891.
11. G.F. Santori, A.G. Moglioni, V. Vetere, G.Y. Moltrasio Iglesias, M.L. Casella, O.A. Ferretti, *Appl. Catal. A: Gen.*, **2004**, 269, 215–223.
12. C. Chen, H. Chen, W. Cheng, *Appl. Catal. A: Gen.*, **2003**, 248, 117–128.
13. L. Cervený, Z. Belohlav, M.N.H. Hamed, *Res. Chem. Intermed.*, **1996**, 22, 15–22.
14. M. Casagrande, L. Storaro, A. Talon, M. Lenarda, R. Frattini, E. Rodriguez-Castellon, P. Maireles-Torres, *J. Mol. Catal. A: Chem.*, **2002**, 188, 133–139.
15. M.A. Aramendi'a, V. Borau, J.F. Go' mez, A. Herrera, C. Jime' nez, J.M. Marinas, *J. Catal.*, **1993**, 140, 335-343.
16. A. Drelinkiewicz, A. Waksmundzka, W. Makowski, J.W. Sobczak, A. Krol, A. Zieba, *Catal. Lett.*, **2004**, 94, 143–156.
17. M. Bejblova, P. Zamostny, L. Cervený, J. Cejka, *Collect. Czech. Chem. Commun.*, **2003**, 68, 1969–1984.
18. J. M. Bonnier, J.P. Damon, J. Masson, *Appl. Catal.*, **1988**, 42, 285–297.
19. J. Masson, S. Vidal, P. Cividino, P. Fouilloux, J. Court, *Appl. Catal. A Gen.*, **1993**, 99, 147–159.
20. N. Oku, M. Ishino, Proces for prodcing α -phenyl ethyl alcohol, US006046369A, 1998.
21. M.V. Rajashekharan, I. Bergault, p. Fouilloux, H. Delmas, and R.V. Chaudhari, *Catal. Today*, **1999**, 48, 83–92.
22. D. C. Costa, A. L. Soldati , J. F. Bengoa , S. G. Marchetti , V. Vetere, *Heliyon*, **2019**, 5, 01859.
23. R. V. Malyala, C. V. Rode, M. Arai, S. G. Hegde, R. V. Chaudhari, *Appl. Catal A Gen.*, **2000**, 193, 71–86.

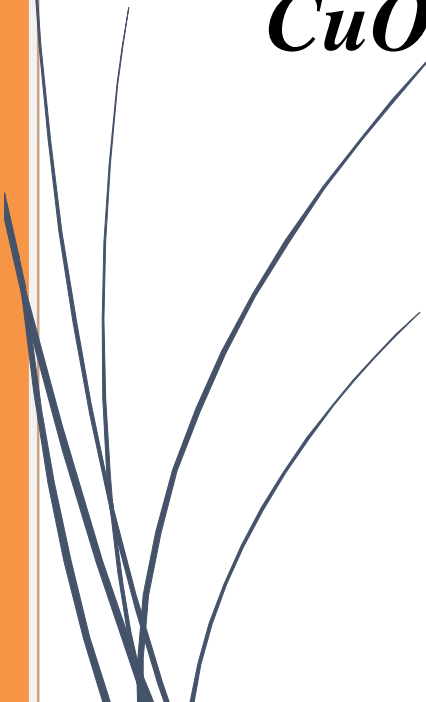
24. N.M. Bertero, A.F. Trasarti, C.R. Apesteguía, A.J. Marchi, *Appl. Catal. A Gen.*, **2011**, 394, 228–238.
25. Y. Xiang, Y. Lv, T. Xu, X. Li, J. Wang, *J. Mol. Catal. A: Chemical*, **2011**, 351, 70–75.
26. Y. Gou, X. Liang, B. Chen, *Catal. Today*, **2013**, 216, 200–204.
27. M. Chen, N. Maeda, A. Baiker, J. Huang, *ACS Catal.*, **2018**, 8, 6594–6600.
28. M. Sudhakar, V.V. Kumar, G. Naresh, M. L. Kantam, S. Bhargava, A. Venugopal, *Appl. Catal. B*, **2016**, 180, 113–120.
29. N. Thakar, T. J. Schildhauer, W. Buijs, F. Kapteijn, J. A. Moulijn, *J. Catal.*, **2007**, 248, 249–257.
30. H. Yoshida, Y. Onodera, S. Fujita, H. Kawamori, M. Arai, *Green Chem.*, **2015**, 17, 1877–1883.
31. M.V. Rajashekharam, R.V. Chaudhari, *Chem. Eng. Sci.*, **1996**, 51, 1663–1672.
32. N. M. Bertero, C. R. Apesteguía, A. J. Marchi, *Appl. Catal. A: General*, **2008**, 349, 100–109.
33. H. Liu, G. Lu, Y. Guo, Y. Wang, Y. Guo, *Catal. Commun.*, **2009**, 10, 1324–1329.
34. N. Hiyoshi, O. Sato, A. Yamaguchi, M. Shirai, *Chem. Commun.*, **2011**, 47, 11546–11548.
35. S. Fujita, Y. Onodera, H. Yoshida, M. Arai, *Green Chem.*, **2016**, 18, 4934–4940.
36. H.-B. Cho, B. U. Lee, C.-H. Ryu, T. Nakayama, Y.-H. Park, *Korean J. Chem. Eng.*, **2013**, 30, 306–313.
37. G. D. Yadav, R. K. Mewada, *Catal. Today*, **2012**, 198, 330–337.
38. J. Wang, Y. Wang, G. Chen, Z. He, *Catalysts*, **2018**, 8, 309, <https://doi.org/10.3390/catal8080309>

39. X. B. Zhang, W. N. Lu, J. L. Wang, B. H. Liao, Y. H. Qin, Ya J Zhang, B. Zhang, Su An Xin, *Catal. Commun.*, **2019**, 119, 124–128.
40. M. D. Argyle, C. H. Bartholomew, *Catalysts*, **2015**, 5, 145–269.
41. Q. Ge, M. Gutowski, *Top. Catal.*, **2015**, 58, 655–664.
42. V. R. Acham, A. V. Biradar, M. K. Dongare, E. Kemnitz, S. B. Umbarkar, *ChemCatChem.*, **2014**, 6, 3182–3191.
43. R. S. Kokane, V. R. Acham, A. B. Kulal, E. Kemnitz, M. K. Dongare, S. B. Umbarkar, *Chem. Select.*, **2017**, 1–11.



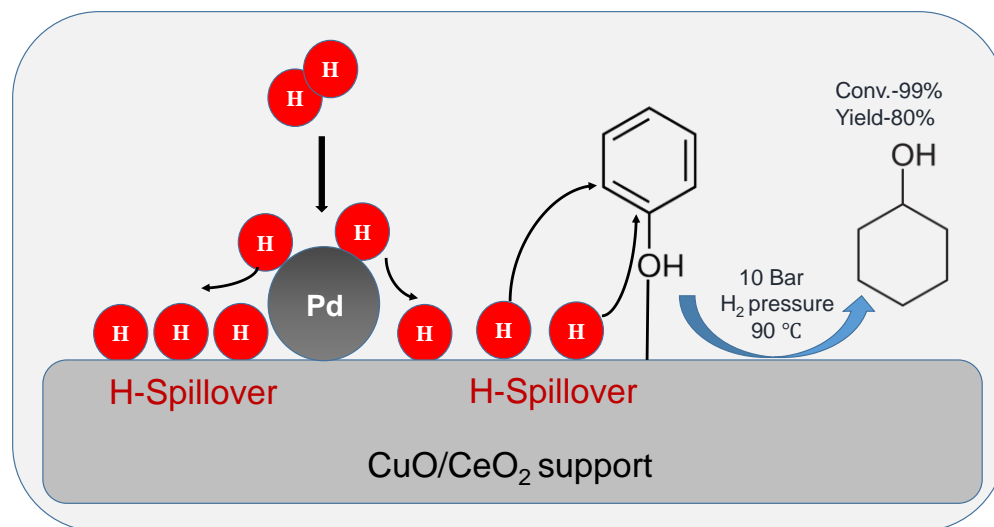
Chapter 4

*Phenol hydrogenation to
cyclohexanol catalysed by
palladium supported on
CuO/CeO₂*



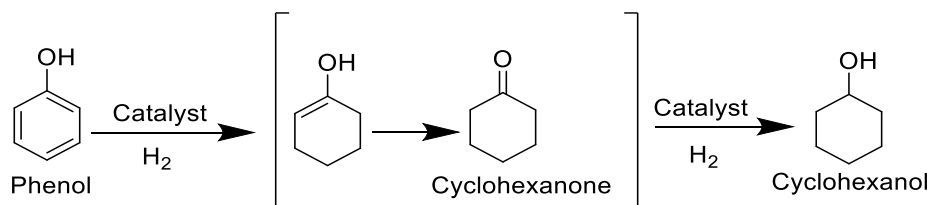
Abstract

Hydrogenation of phenol to cyclohexanone and cyclohexanol is an important reaction in production of nylon-6, nylon-66 and in petroleum industry. Liquid phase phenol hydrogenation over Pd-CuO/CeO₂ was carried out under mild conditions. Palladium impregnated over CuO/CeO₂ synthesized by co-precipitation method showed excellent catalytic activity for phenol hydrogenation (99% conversion with 80% cyclohexanol yield) at 90 °C and 10 bar H₂ pressure in water. Commercial 10%Pd/C showed only 8% phenol conversion under identical conditions. The detailed characterization revealed significant improvement in surface area of ceria after addition of CuO and decrease in crystallite size with creation of defects in CeO₂ lattice. XPS analysis showed Pd loading on CuO/CeO₂ to cause hydrogen spillover on the surface leading to increase in the oxygen vacancies. The interaction of phenol with catalyst surface studied by detailed FTIR analysis, revealed activation of phenol on oxygen vacancy of ceria as phenoxide ion with perpendicular orientation of aromatic ring on catalyst surface.



4.1 Introduction

Selective phenol hydrogenation is an important reaction in the industry as well as in the academia to obtain raw materials (cyclohexanone and cyclohexanol) for the production of adipic acid, caprolactam, nylon-6, nylon-66, and KA oil in petroleum industrial chemistry [1, 2]. Especially cyclohexanol derivatives are important value-added chemical intermediates, in pharmaceuticals, pesticides, plasticizers, cosmetics, surfactants, paint, and used as industrial solvents. Furthermore, cyclohexanol is also an excellent oxygenate additive in enhanced multi-component diesel fuel used to improve emissions. Commercially cyclohexanol is obtained by two routes, first, the oxidation of cyclohexane and another is the hydrogenation of phenol. The oxidation method requires high temperature and high pressure with a low yield of product and also complicated recovery steps [3]. Hydrogenation of phenol involves a two-step reaction, in which first phenol hydrogenates to cyclohexanone and then to cyclohexanol as shown in Scheme 4.1 [4, 5].



Scheme 4.1. Hydrogenation of phenol.

Generally, the hydrogenation of phenol is carried out in the gas phase as well as the liquid phase [6-9]. The former requires high temperature which leads to the formation of coke resulting in the catalyst deactivation [10, 11]. The liquid phase hydrogenation is preferred because; of low temperatures, which leads to saving the energy of the process [12, 13]. Both precious metals, as well as non-precious metals, have been reported for this reaction [12, 14-18]. Huang et al. reported a high-performance PdRu/MNS (mesoporous silica nanoparticles) bimetallic catalyst

for the hydrogenation of phenol to cyclohexanol in dichloromethane solvent [19]. It was found that the addition of Ru, improves the Pd dispersion and assists the electronic interaction between the Ru and Pd, which contribute to improving the catalytic activity. Yi et al. reported 3% palladium supported on γ -Al₂O₃ catalyst with complete phenol conversion (100%) and 100% selectivity of cyclohexanol at 60 °C, 20 MPa H₂ Pressure in 12 h, and 0.05 mol% Pd loading [20]. Li et al. reported a series of 1Co-1Ni@NC catalysts with 100% phenol conversion and 99% cyclohexanol selectivity in IPA at 100 °C and 0.8 MPa H₂ pressure in 12 h [18]. Different transition metals supported on carbon like Rh/C, Ru/C, Pt/C, and Pd/C were synthesized and tested for phenol hydrogenation under scCO₂ conditions. Among these Rh/C was found to be an optimum catalyst at 55 °C, 10 MPa H₂ and 10 MPa CO₂ pressure. 10% Ni/SiO₂ catalyst was highly active for phenol hydrogenation at 200 °C, 1 MPa H₂ pressure within 4 h [21]. Even though the precious metal catalysts have given the good conversion of phenol and selectivity to cyclohexanone or cyclohexanol, the risk in supply and high price of noble metals obstructed to accomplishment industrialization. The non-noble metal based catalysts showed poor catalytic activity and required harsh reaction conditions.

Recently to get the selectively hydrogenated product at a lower cost as compared to another noble metal based catalysts, Pd-based catalysts are widely used though with higher catalyst loading [12, 14, 22-24]. It is necessary to develop a catalyst that works under mild reaction conditions with lower noble metal loading and can be easily recyclable without metal leaching. One of the best options to increase the catalytic activity is to tune the electronic properties of the active metal as well as the support by adding second metal to the catalyst. Ceria has been widely used as a catalyst or as support because of its high reactivity and availability. The ceria has high oxygen storage capacity, a high concentration of oxygen vacancies, and also the potential to easily switch

between Ce^{3+} and Ce^{4+} [25]. In addition, the catalytic activity of CeO_2 could be significantly increased by adding other metal ions, such as Cu^{2+} [26, 27]. The doping of copper ions into ceria lattice leads to crystal lattice distortion which is attributed to the replacement of copper ions in the ceria lattice. Further this leads to partial $\text{Ce}^{4+}/\text{Ce}^{3+}$ reduction and increase in the oxygen vacancies in the lattice. There have been only a few reports of the phenol hydrogenation on ceria-based catalysts. The groups of Inagaki and Scire have reported the vapor phase reaction over palladium supported on high surface area ceria with 80% conversion at 180 °C and 40% conversion at 160 °C, respectively [28]. Li et al. have reported the liquid-phase process using 0.43 mol % Ce-doped Pd nanospheres with a hollow chamber, getting 82% cyclohexanone yield at 10 bar of H_2 and 80 °C [13]. There are several publications where enhancement in the hydrogenation activity due to oxygen vacancies have been reported [29, 30]. Avgouropoulos et al. have prepared CuO/CeO_2 catalyst with varying $\text{CuO}/(\text{Cu}+\text{Ce})$ molar ratios- 0.10, 0.15, 0.25, 0.35, 0.50 and 0.75 by conventional citrate method or the hydrothermal-citrate method. Very high dispersion of CuO on CeO_2 , up to a 0.35 molar ratio was reported [31]. Also previously our group prepared CuO/CeO_2 catalyst with varying amount of CuO out of these 30% CuO/CeO_2 gives good conversion of CO to CO_2 . Hence we have prepared 30% CuO/CeO_2 . Herein, we used CuO/CeO_2 as support to disperse the palladium and evaluated its performance for the selective hydrogenation of phenol to cyclohexanol in the liquid phase at low temperature and H_2 pressure.

4.2 Experimental Section

4.2.1 Materials

Palladium acetate was obtained from Molychem India, copper acetate from Lobachemie, and cerium nitrate from Himedia. Phenol, 25% aq. ammonium hydroxide solution and the solvent (acetonitrile) of HPLC grade were obtained from Thomas Baker chemicals, India. All the

chemicals are used as such without further purification.

4.2.2 Catalyst Preparation

The CuO/CeO₂ support with 30 wt% CuO was synthesized by the co-precipitation method using cerium nitrate as the cerium precursor and copper acetate as the copper precursor and named as CC. The typical synthesis procedures for CC are described below.

(a) Synthesis of 30% CuO/CeO₂

30% CuO/CeO₂ (CC) was synthesized by the following procedure. 10.4 g copper acetate was dissolved in 215 ml distilled water in a 1 lit beaker. In another beaker, 53.1 g cerium nitrate was dissolved in 380 ml distilled water. Copper acetate solution was added to the cerium nitrate solution with constant stirring. To this solution dil. NH₄OH (5%) solution was added till the pH of the solution reached 9. This mixture was aged for 12 h. The resultant precipitate was filtered, washed with water, air-dried, and further calcined at 500 °C in a muffle furnace for 5 h.

(b) Synthesis of 1%Pd/ CuO/CeO₂

For 1% palladium loading, 5 g CC was dispersed in 50 ml methanol. To this slurry, palladium acetate (0.105 g) dissolved in mixture of 10 ml methanol and 10 ml acetone was added drop wise with constant stirring. The slurry was stirred for 2 h and then the solvent was evaporated. The dried powder was calcined at 250 °C in a muffle furnace for 5 h. The catalysts with different palladium loading such as 0.5, 1, and 2 wt% on CC was prepared by varying palladium acetate quantity and following the similar procedure as above. The catalysts were named as 0.5PCC, 1PCC, and 2PCC respectively.

4.2.3 The catalysts characterization

(a) Acidity measurement

The NH₃-TPD experiments were performed using a Micromeritics Autochem 2910 instrument.

Approximately ~100 mg of the sample was placed in a quartz reactor, and pretreated in a flow of He gas at 500 °C for 1 h (ramp rate of 10 °C /min) and further cooled to 100 °C. The NH₃ gas (5% NH₃-95% He, 50mL/min) was passed over the catalyst at 100 °C, followed by evacuation at 100 °C for 3 h. Then, the desorbed NH₃ was measured from 100 °C to 800 °C with a heating rate of 5 °C/min in the flow of He as carrier gas at a flow rate of 30mL/min until ammonia desorbed completely.

(b) X-ray Diffraction analysis

All the synthesized catalysts were characterized by X-ray diffraction method using PAN analytical X'Pert Pro Dual Goniometer diffractometer. The diffractometer consists of X'celerator solid state detector with CuK α ($\lambda=1.5406\text{\AA}$, 40kV, 30mA) radiation and a Ni filter. The X-ray diffraction pattern of the sample was collected in the range of $2\theta = 20-80^\circ$ with a step size of 0.02° and a scan rate of 4° min^{-1} .

(c) BET surface area measurements

The Brunauer–Emmett–Teller (BET) specific surface area of the catalyst was determined by the N₂ sorption method at -196 °C, using Auto-sorb Quanta Chrome equipment. The sample was pretreated at 200 °C under a vacuum prior to N₂ adsorption.

(d) Raman spectroscopy

The Raman spectra of the catalysts were recorded on an HR 800 LabRAM infinity spectrometer (HORIBA Jobin Yvon) equipped with a liquid N₂ detector and a He–Ne laser supplying the excitation line at 632 nm with a power of 1–10 mW and with a resolution of 0.35 cm⁻¹.

(e) XPS analysis

X-ray photoelectron spectroscopy (XPS) measurements for all the catalysts were carried

out using a Thermo K-alpha spectrometer using micro-focused and monochromatic Al K α radiation with energy 1486.6 eV. The samples were degassed at 300K for 4 h in a vacuum chamber. Charge compensation was done with the help of an electron flood gun. The calibration is done with respect to binding energy (BE) values by referring to the standard C 1s peak (284.6 eV) of contaminant carbon.

(f) Electron microscopy

The morphology of the samples was determined using scanning electron microscopy (SEM) on an FEI quanta 200 3D dual beam ESEM instrument having thermionic emission tungsten filament in the 3 nm range at 30 kV. The particle size was determined using transmission electron microscopy (TEM) and analysis was done on a Tecnai G2-20 FEI instrument operating at an accelerating voltage of 300 kV. Before analysis, the powder samples were ultrasonically dispersed in isopropanol, and deposited on a carbon-coated copper grid, dried in the air before TEM analysis.

(g) FTIR spectroscopy

To study the mechanism of phenol hydrogenation on PCC catalyst, the Fourier transform infrared (FTIR) spectra of the samples were recorded on Perkin Elmer Spectrum Two spectrophotometer with a resolution of 4 cm⁻¹ in the range of 4000-400 cm⁻¹ in ATR mode.

4.2.4 Catalytic activity

The catalytic hydrogenation of phenol was performed in a 300 mL high-pressure Parr reactor. The reactor was charged with a known quantity of catalyst, 40 mL of solvent (distilled water), and phenol. Before starting the reaction the reactor was purged with the hydrogen three times, then the reactor was filled with desired pressure of hydrogen (10 bar H₂). The reactor was heated to the required temperature of the reaction (90 °C). Once the temperature was attained the

stirring of the reactor was started and the reaction was carried out for 2-5 h. After completion of the reaction the stirring was stopped, and the reactor was cooled to room temperature. The reactor was depressurized and the analysis of the reaction mixture was carried out. The analysis was done using HPLC (Agilent 1260 Infinity) equipped with a C18 column (250 mm × 4.6 mm × 5 μm) and RI detector at 40 °C, using acetonitrile and deionized (DI) (80%) water and (20%) acetonitrile as a mobile phase. Conversion of phenol was calculated based upon the HPLC by external calibration method, where substrate conversion = [moles of substrate redacted]/[Initial moles of substrate used] × 100. The product identification was carried out by comparing authentic standard samples in HPLC.

4.3. Results and Discussions

4.3.1 Catalyst synthesis

The catalyst support 30% CuO/CeO₂ (CC) was prepared by co-precipitation method using cerium nitrate and copper acetate as precursors. Palladium was loaded by impregnation method by changing the Pd loading from 0.5, 1 to 2 wt%.

4.3.2 Catalyst Characterization

(a) Acidity of support

The total acidity and acid strength of the support (CC), 1%Pd/CeO₂, 1PCC, and CeO₂ were determined by NH₃-TPD analysis which is shown in Table 4.1 and Figure 4.1. The results showed that CeO₂ and 1%Pd/CeO₂ catalyst exhibited two peaks one narrow peak around 250 °C corresponding to weak acidity and other broad peak centred at 450 °C corresponding to moderate acidity. Total acidity for CeO₂ and 1%Pd/CeO₂ catalyst was 0.136 and 0.184 mmol/g respectively. The total acidity of ceria increased after loading of palladium which can be attributed to the Lewis acidic nature of palladium. While CC and 1PCC showed two narrow peaks

one around 200 °C corresponding to weak acidity and other at 800 °C attributed to very strong acidity. The total acidity for CC and 1PCC was 0.166 and 0.191 mmol /g. The area under peak and its position is directly related to the number of acidic sites and its strength respectively. It was concluded that CC and 1PCC were more acidic than the CeO₂ and 1%Pd/CeO₂ catalysts. This may be due to incorporation of CuO into CeO₂ lattice. The quantitative data of NH₃-TPD is given in Table 4.1. Palladium also contributes to the acidity due to Lewis acidic nature of palladium. Hence 1%Pd/CeO₂ and 1PCC showed more acidity than CeO₂ and CC respectively.

Table 4.1. Acidity of the catalysts as determined by NH₃-TPD

Sr. No.	Catalyst	Acidity (mmol /g)
1	CeO ₂	0.136
2	1%Pd/CeO ₂	0.184
3	CC	0.166
4	1PCC	0.191

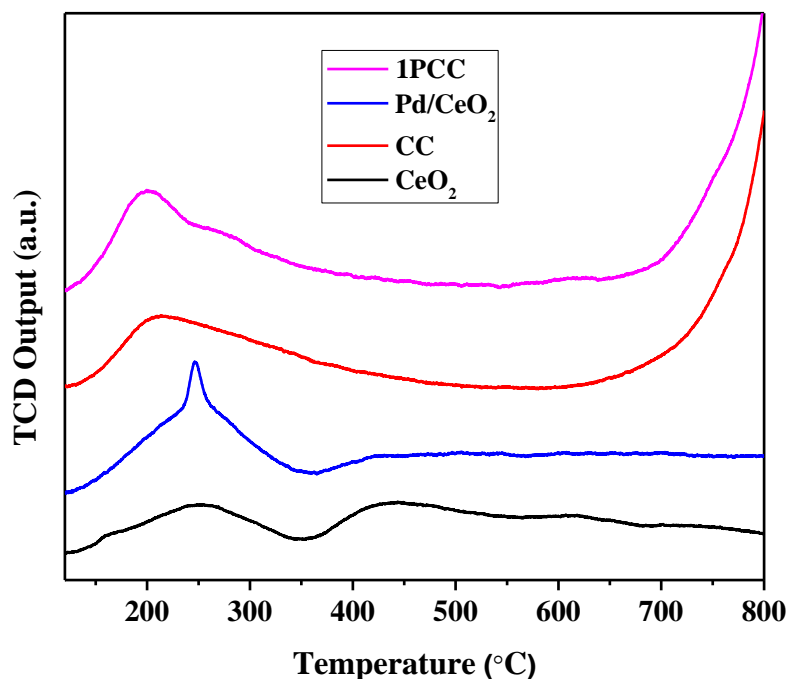


Figure 4.1. NH₃-TPD for CeO₂, 1%Pd/CeO₂, CC and 1PCC

(b) X-ray diffraction studies

The XRD pattern for CC with different palladium loading showed sharp peaks indicating highly crystalline nature of the catalysts (Figure 4.2.). Sharp peaks at 28.5, 33.1, 47.5, 56.3, 59.1, 69.4, 76.6, 79.0, and 88.3 ° correspond to (111), (200), (220), (311), (222), (400), (331), (420) and (422) planes respectively of the cubic crystalline structure of CeO₂ (JCPDS no. 81-0792). In all the samples very small peaks at 35.47 and 38.63° corresponding to (111) and (200) reflections of monoclinic CuO have been observed. The broadening of diffraction peaks in CC (support) and PCC catalysts indicate small crystallite size [32]. The average crystallite size of CeO₂ was determined from the CeO₂ (111) peak using Scherer's equation for pure CeO₂ and CC support. For pure CeO₂, the crystallite size was found to be 13.81nm which decreased to 7.59 nm for CC. This result indicates that the addition of Cu (II) ions inhibits the crystal growth of ceria, which is in accordance with the previous reports [33, 34]. The CuO/CeO₂ catalyst have synthesized with

different CuO/(Cu+Ce) molar ratios: 0.10, 0.15, 0.25, 0.35, 0.50, and 0.75. CuO was observed to disperse extremely well on CeO₂, reaching a 0.35 molar ratio [31]. The lattice parameters for cubic crystal structure calculated from the XRD data was found to be 5.41 for CeO₂ and 5.40 for CC. The ionic radii of Ce⁴⁺ in CeO₂ is 101 pm and for Cu²⁺ in CuO is 73 pm. The minor decrease in lattice parameter indicates lattice substitution of few Ce⁴⁺ ions with Cu²⁺ ions. This also contributes to the decrease of CeO₂ crystallite size. No peak for palladium was observed due to low palladium loading and high dispersion.

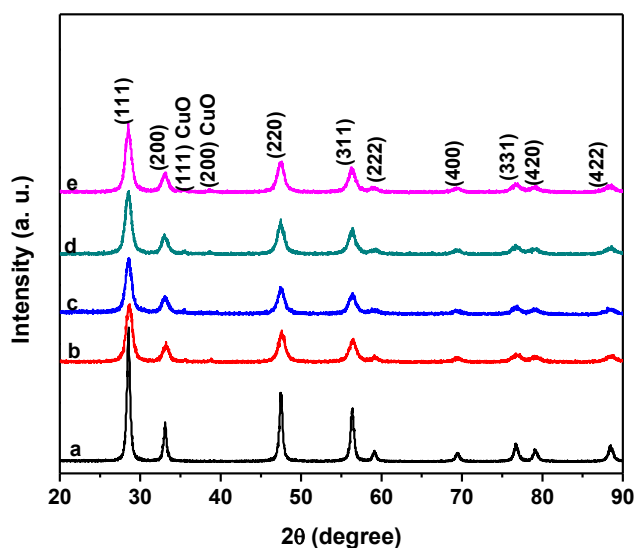


Figure 4.2. XRD patterns of (a) CeO₂, (b) CC, (c) 0.5PCC, (d) 1PCC and (e) 2PCC

(c) BET surface area analysis

The BET surface area of all the catalysts was determined by the N₂ adsorption/desorption method. The surface area, average pore size, pore volume, and metal dispersion of the catalysts are given in Table 4.2. The BET results are in agreement with the XRD data, which shows that after Cu loading the crystallite size of CeO₂ decreases. In principle, the surface area increases with decreasing crystallite size of the sample. Here the surface area of CeO₂ is 33 m²/g, which after the addition of Cu increased to 61 m²/g. The surface area of support was found to affect by

Pd loading. There is a decrease in surface area with increasing palladium loading, such as 57, 56, and 52 m²/g, respectively, for 0.5, 1, and 2% Pd loading. However, there is no specific trend observed in the pore size and pore volume of these catalysts. The adsorption-desorption isotherms of all the Pd-loaded catalysts are shown in Figure 4.3, which showed the type IV isotherm pattern for all the catalysts. Very high Pd dispersion on support with redox properties (52% for 1PCC) was observed which is in agreement with our previous work [35]. The metal dispersion was calculated from the CO chemisorption.

Table 4.2. Surface properties of the CC catalysts

Sr. No.	Catalyst	Elemental composition			Surface area (m ² /g)	Pore size (Å)	Pore volume (cc/g)
		wt% [#]					
		Pd	Cu	Ce			
1	1%Pd/CuO	-	-	-	8	92	0.20
2	CeO ₂	-	-	-	33	16	0.17
3	1%Pd/CeO ₂	-	-	-	28	27	0.19
4	CC	-	11	72	61	27	0.83
5	0.5PCC	0.20	11	77	57	28	0.81
6	1PCC	0.61	9	70	56	27	0.78
7	2PCC	1.35	9	63	52	28	0.73

[#] from EDAX

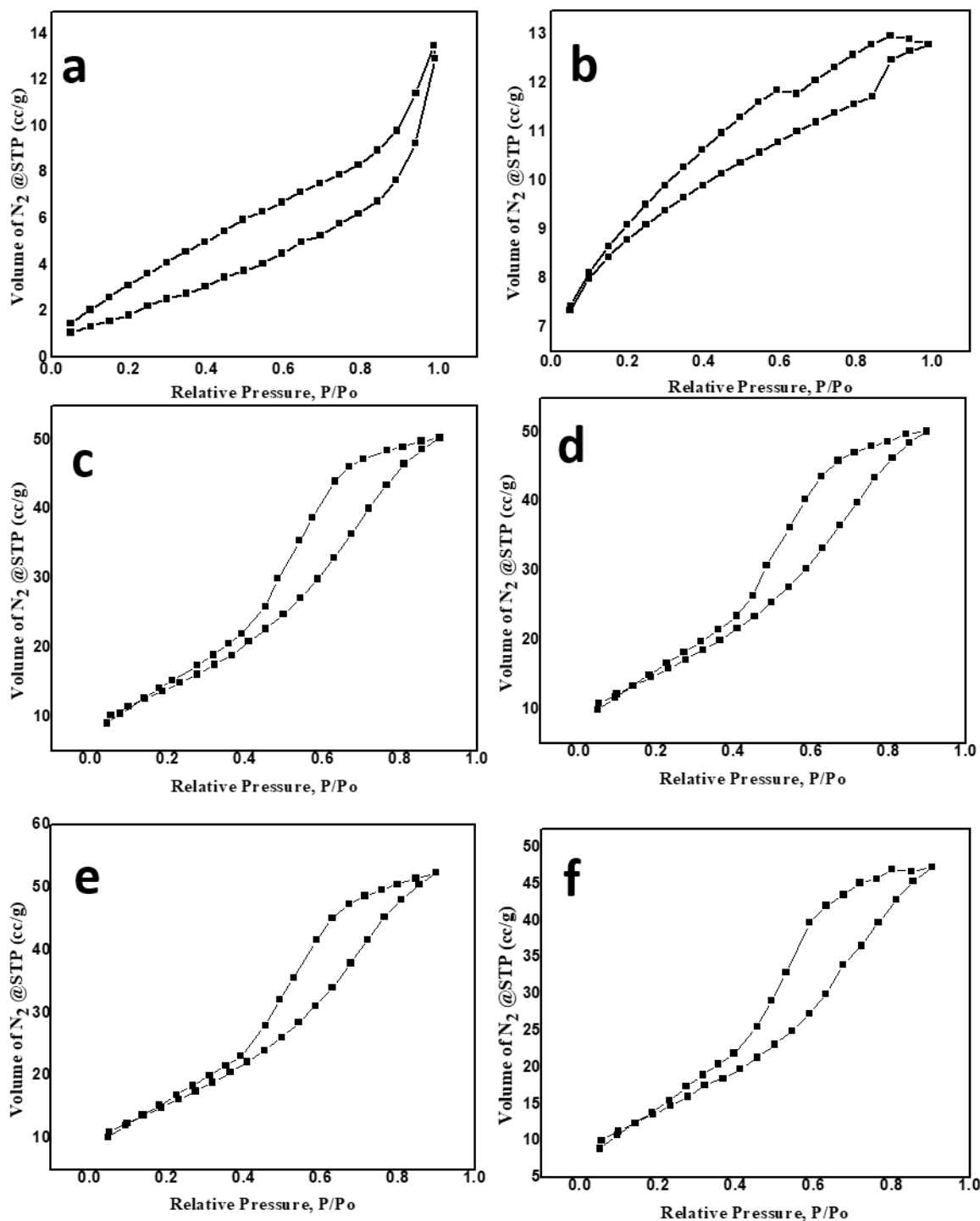


Figure 4.3. BET surface area analysis of (a) 1%Pd/CuO, (b) 1%Pd/CeO₂, (c) CC, (d) 0.5PCC, (e) 1PCC, and (f) 2PCC

(d) Raman spectroscopy

To study the effect of CuO doping in CeO₂ lattice, Raman analysis was carried out, and the results are shown in Figure 4.4. The spectrum of CuO showed peaks at 290 and 340 cm⁻¹, attributed to the fundamental active Raman vibration modes A_g and B_{1g} of CuO respectively [36]. The CC and 1PCC do not show peaks around 290 and 340 cm⁻¹, indicating that CuO is highly dispersed or incorporated in the CeO₂ lattice. The CeO₂, CC and 1PCC catalysts showed a strong peak around 463 cm⁻¹, for the triply degenerate F_{2g} vibration mode in cubic fluorite structure of CeO₂. In CC and 1PCC this peak showed a red shift compared to pure CeO₂. This peak shift to a lower wavenumber in Raman analysis may be due to (i) distortions in the CeO₂ lattice due to the addition of Cu, and/or (ii) the reduction in crystallite size. This is in agreement with the XRD analysis [37, 38].

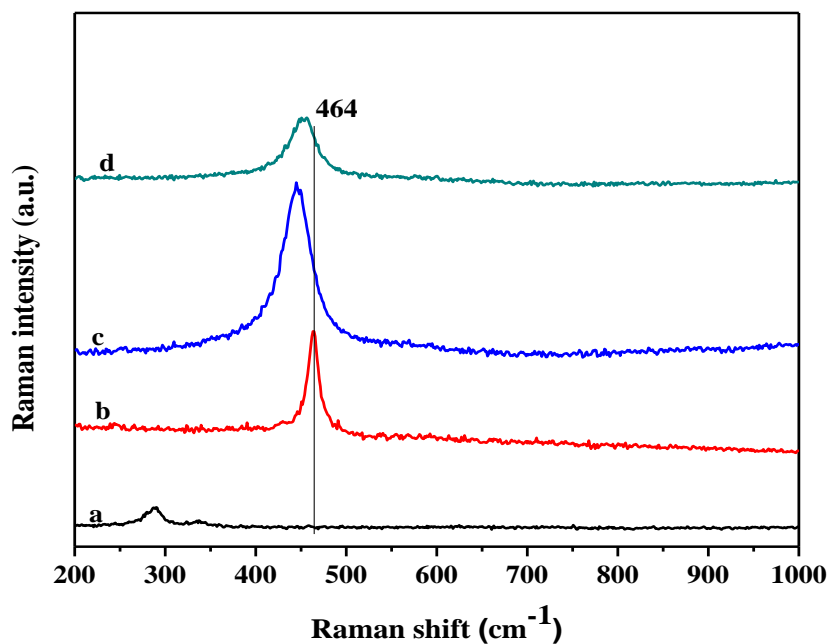


Figure 4.4. Raman spectra of (a) CuO, (b) CeO₂, (c) CC, and (d) 1PCC.

(e) X-ray Photoelectron Spectroscopy

To further analyse the surface composition and electronic state of elements of catalysts,

the XPS spectroscopic analysis was performed. The XPS spectra of Ce 3d and O 1s for CeO₂, CC, and 1PCC (pre-reduced) catalysts are given in Figure 4.5. The result showed that Ce 3d XPS spectra contain multiple doublets related to the spin-orbit split of 3d_{3/2} and 3d_{5/2}, labelled as u and v. For CeO₂ only six peaks could be distinguished, u (902.2 eV), u'' (908.2 eV), and u''' (917.4 eV) of Ce 3d_{3/2} and v (883.5 eV), v'' (889.1 eV), and v''' (899.2 eV) of Ce 3d_{5/2} belong to Ce⁴⁺ [39]. While in CC and PCC, along with the above six peaks additional two peaks were observed u' (903.5 eV) and v' (884.9 eV) attributed to Ce³⁺. The relative concentration of Ce³⁺ was calculated by $Ce^{3+} = Ce^{3+}/(Ce^{3+} + Ce^{4+})$ formula and shown in Table 3.

The O 1s spectra for CeO₂, CC, and 1PCC (reduced) are shown in Figure 4.5 (b). The spectrum for CeO₂ showed two peaks, the one at higher energy is attributed to the adsorbed oxygen or hydroxide and the lower energy peak attributed to the lattice oxygen of metal oxides. The O 1s spectra of CC and 1PCC showed three peaks at 529, 531, and 532 eV. These peaks are labelled as O_α, O_β and O_γ respectively. The peak at 531 eV is attributed to the presence of Ce³⁺ surface defect or defect oxide. The relative amount of O_β species on the surface was calculated by $O_{\beta}/(O_{\alpha} + O_{\beta} + O_{\gamma})$ formula and shown in Table 4.3. The Cu 2p spectra for CuO, CC and 1PCC are shown in Figure 4.5 (c). The spectra showed that the peak at 934.0 eV is attributed to Cu²⁺ component with satellite peak at 942.0 eV. It also showed peak at 932.0 eV corresponding to Cu⁺ or Cu⁰ state of copper. The spectrum of CuO showed strong satellite peaks while spectra of CC and 1PCC showed weak satellite peaks may be due to interaction with CeO₂. The results indicated that Cu addition into CeO₂ creates defects in the CeO₂ lattice. These results are in agreement with the XRD, BET and Raman data. The 1PCC catalyst showed more defects which may be due to higher concentration of Ce⁺³ present. The hydrogen spillover on the reducible catalyst surface may lead to higher Ce⁺³ concentration. The Pd 3d spectrum of 1PCC is given in Figure 4.5(d).

The spectrum showed the peak at 335 eV for Pd 3d_{5/2} attributed to metallic palladium (Pd⁰). This indicates that on reduction all Pd²⁺ get reduced to Pd⁰.

Table 4.3. XPS data for CeO₂, CC and 1PCC

Sr. No.	Catalyst	Ce(III) % of total Ce present	O vacancy %
1	CeO ₂	-	-
2	CC	10.2	26.9
3	1PCC	18	37.7

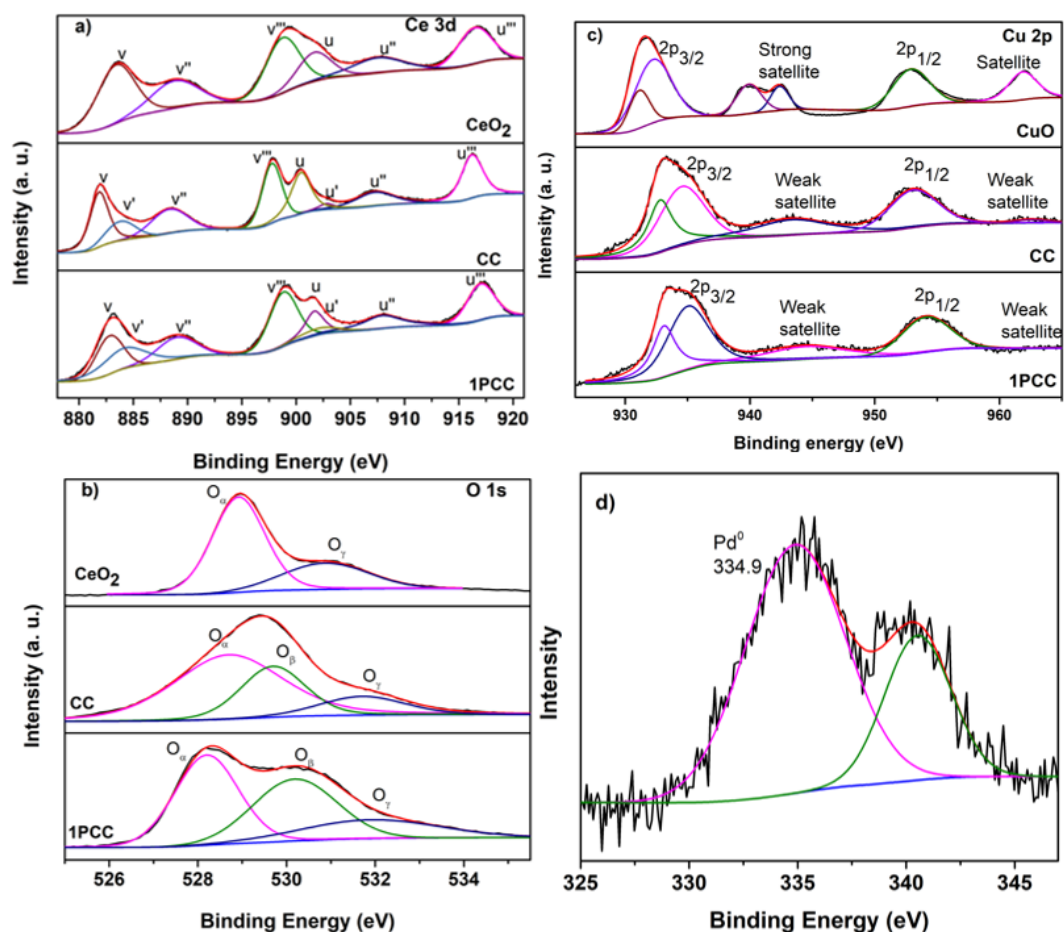


Figure 4.5. XPS spectra of 1PCC (a) Ce 3d (b) O 1s (c) Cu 2p and d) Pd 3d

(f) Electron microscopic analysis

To study morphology and the compositional homogeneity of catalysts, SEM and EDAX analysis was carried out. The SEM images indicate almost identical morphology for all catalysts (Figure 4.6). The CC showed non-uniform particle size distribution with some bigger particles and some smaller particles of 1-4 μm with no specific shape. No significant change in the morphology and particle size was observed after Pd loading. Elemental analysis determined by EDAX is given in Table 4.2. The microstructural characteristics were determined by TEM analysis and the images of CC and PCC are shown in Figure 4.7. This revealed an average particle size of 8-9 nm. The high resolution TEM image for 1PCC catalyst is shown in Figure 4.7e. The palladium, ceria and copper oxide particles were distinguished by d spacing values. The characteristics d spacing value for palladium particles were found to be 0.23nm which corresponds to the (111) plane of Pd [40]. The d spacing value of 0.32nm is attributed to (111) plane of cubic ceria [41]. The d spacing value of 0.22nm is assigned to (200) plane of CuO [42]. The SAED (selected area electron diffraction) pattern is shown in Figure 4.7(f). The image shows distinct four diffraction rings for the cubic ceria crystal corresponding to (111), (200), (220) and (311) planes which is in agreement with XRD data [41].

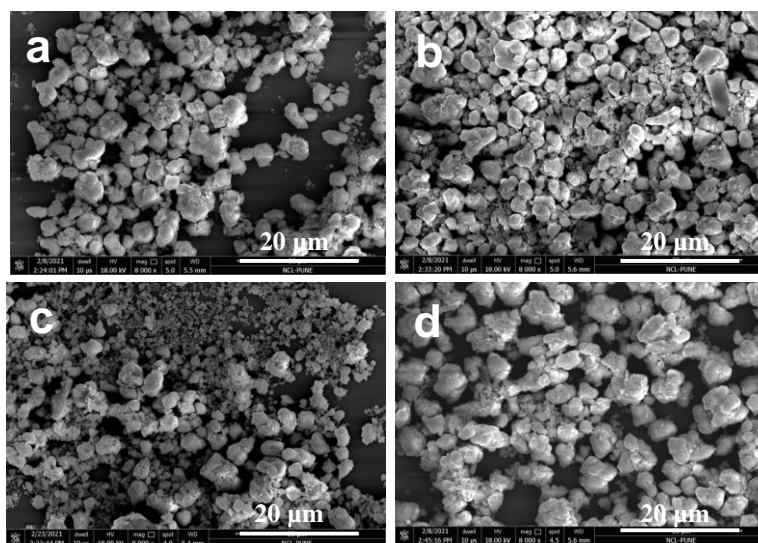


Figure 4.6. SEM image of catalyst a) CC, b) 0.5PCC, c) 1PCC, and d) 2PCC

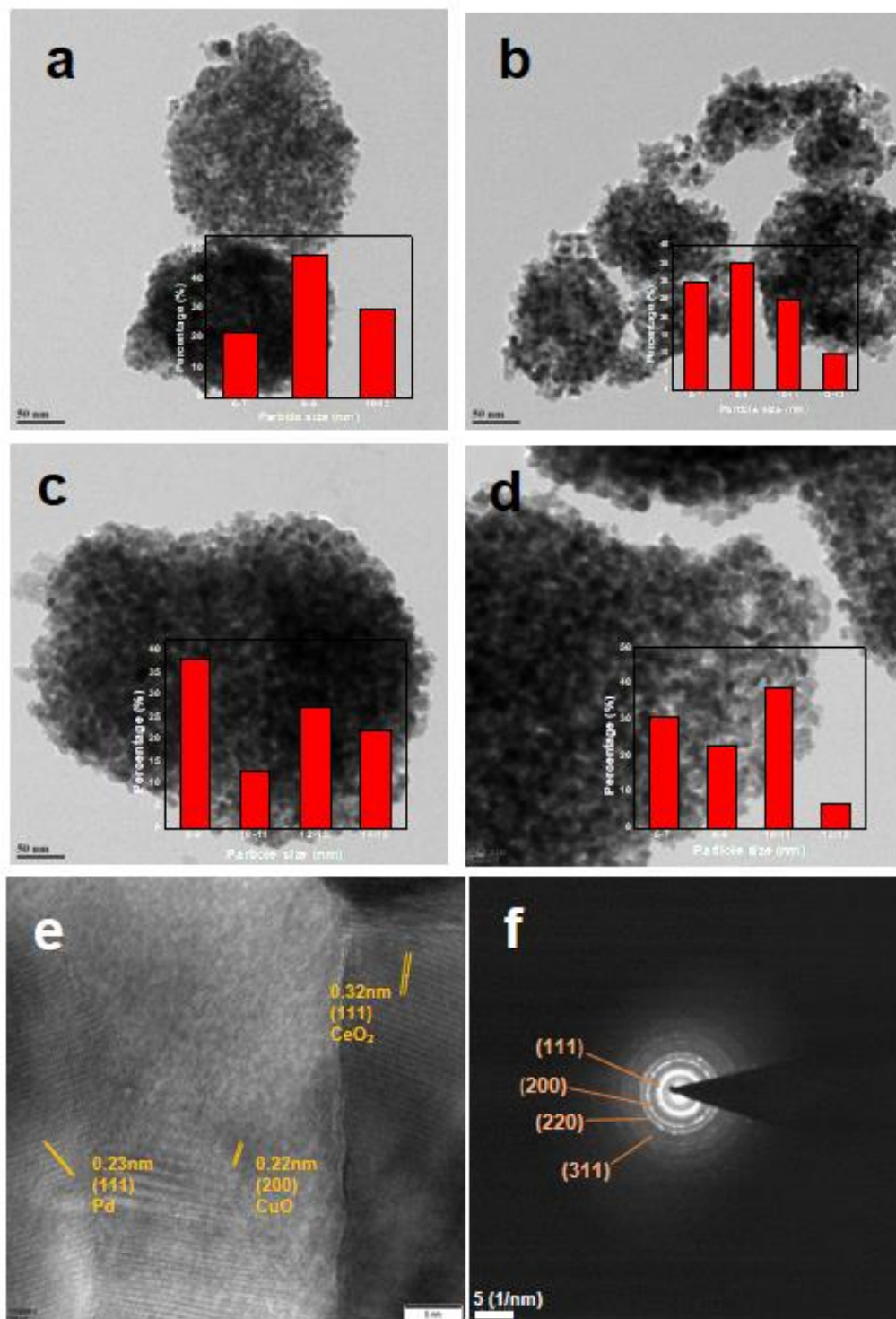


Figure 4.7. TEM image of catalyst a) CC, b) 0.5PCC, c) 1PCC, and d) 2PCC, e) High resolution TEM image of 1PCC, and f) SAED pattern of 1PCC catalyst.

4.3.2 Catalytic activity for phenol hydrogenation

a) Catalyst screening and time profile study

The hydrogenation of phenol was carried out using 1PCC catalyst having 1% palladium loading synthesized by the impregnation method. The reaction was carried out in water at 90 °C and 10 bar H₂ pressure. The hydrogenation of phenol gave benzene and cyclohexane as undesired by-products, apart from cyclohexanone and cyclohexanol (Scheme 4.2). To understand the effect of each component of the catalyst, the reaction was carried out using CuO, CeO₂, support (CC), and the catalyst with 1% palladium loaded separately on CuO (1%Pd/CuO) and CeO₂ (1%Pd/CeO₂) (Table 4.4). For comparison the commercial catalyst 10%Pd/C was also evaluated under identical conditions. There was no conversion of phenol observed with CuO and CeO₂ whereas, only 6% and 1% phenol conversion was obtained with CC and 1%Pd/CuO after 5 h. The catalyst 1%Pd/CeO₂ and 1PCC showed almost 99% phenol conversion after 5 h with 49% and 80% cyclohexanol yield respectively. The higher activity of the catalyst may be attributed to the hydrogen spillover in the case of 1%Pd/CeO₂ and 1PCC catalyst. Hydrogen spillover is well-known in reducible oxides which are used as supports for noble metals [43]. Here CeO₂ is the reducible oxide in both catalysts which improves reaction rate in case of 1%Pd/CeO₂ and 1PCC due to the hydrogen spillover from Pd to CeO₂. The hydrogen molecule adsorbs and dissociates on Pd metal and spills over to CeO₂ causing the reduction of Ce⁴⁺ to Ce³⁺. This increases the availability of H₂ on the catalyst surface. Hence the rate of hydrogenation is high in case of 1%Pd/CeO₂ and 1PCC. The yield of cyclohexanol is higher (80%) for 1PCC; this may be due to contribution of Cu²⁺ for hydrogenation. The addition of CuO to CeO₂ has enhanced the surface area of support contributing to better dispersion of palladium compared to only CeO₂. Because of the high dispersion of Pd (more active site), the rate of hydrogenation is more leading to over

hydrogenation of cyclohexanone to cyclohexanol. The commercial 10%Pd/C catalyst under identical reaction conditions, gave only 8% phenol conversion with 8% yield of cyclohexanol. The catalyst loading for commercial catalyst was 2% with respect to phenol so as to keep Pd loading same as that of 1PCC. The time on stream study of the reaction showed that the conversion of phenol and yield of cyclohexanol increases gradually with time as shown in Figure 4.8.

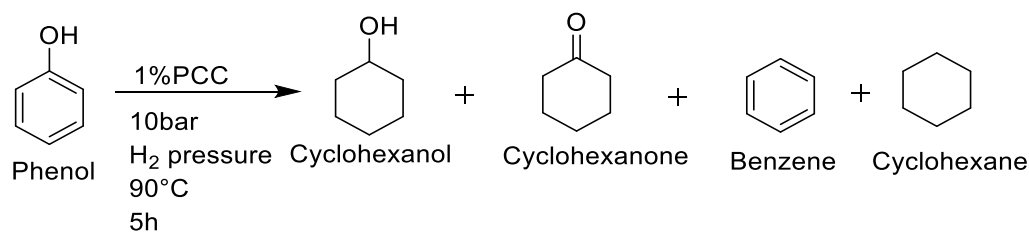
Table 4.4. Catalyst screening for phenol hydrogenation

Sr. No.	Catalyst	Conv. %	Yield of Cyclohexanone (%)	Yield of Cyclohexanol (%)	Other product [#] %
1	CuO	NR	-	-	-
2	CeO ₂	NR	-	-	-
3	CC	5	0	3	2
4	1%Pd/CuO	1	0	1	0
5	1%Pd/CeO ₂	99	41	49	9
6	1PCC	99	9	80	10
7	10%Pd/C ^b	8	-	8	-

Reaction conditions- phenol (0.800 g), 20 wt % catalyst w.r.t. substrate, 40 ml solvent (water),

10 bar H₂ pressure, temp-90 °C, time-5 h; [#] other products: benzene+cyclohexane, ^b 2 wt %

catalyst w.r.t. substrate, NR: No reaction.



Scheme 4.2. Hydrogenation of phenol on 1PCC catalyst

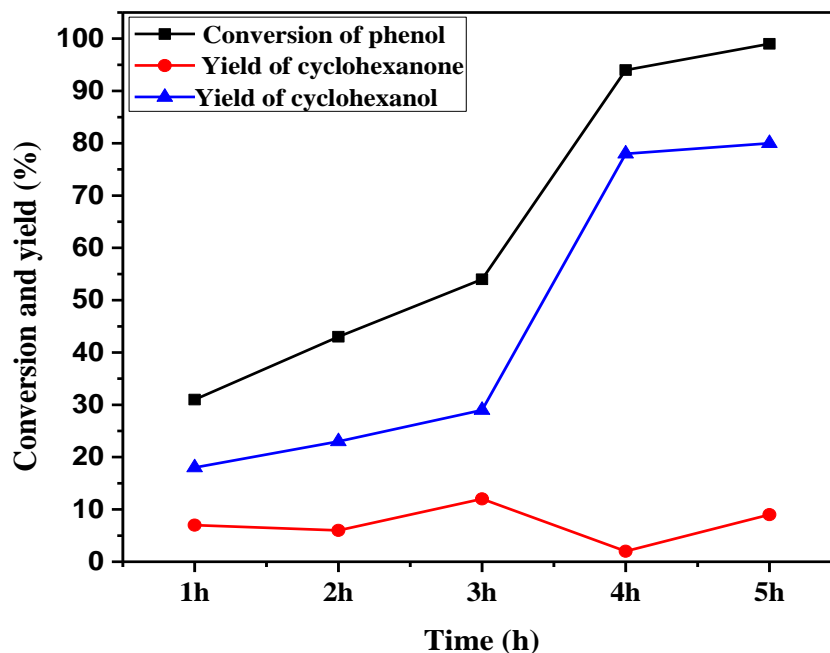


Figure 4.8. The conversion of phenol with time

Reaction condition- phenol (0.800 g), 20 wt % catalyst w.r.t. substrate, 40 ml solvent (water), 10 bar H₂ pressure, temp-90°C.

b) Effect of temperature on phenol hydrogenation

The effect of temperature was studied for phenol hydrogenation at 30 °C (room temperature), 60 °C and 90 °C and the results are shown in Figure 4.9. At 30 °C temperature, only 18% conversion of phenol was obtained after 5 h with 10% cyclohexanol yield. The conversion of phenol increased with temperature. At 60 °C, 92% conversion while at 90 °C almost 99% conversion of phenol was obtained with 75% and 80% yield of cyclohexanol respectively. The rate of reaction increases at a high temperature because it increases the number of high-energy collisions.

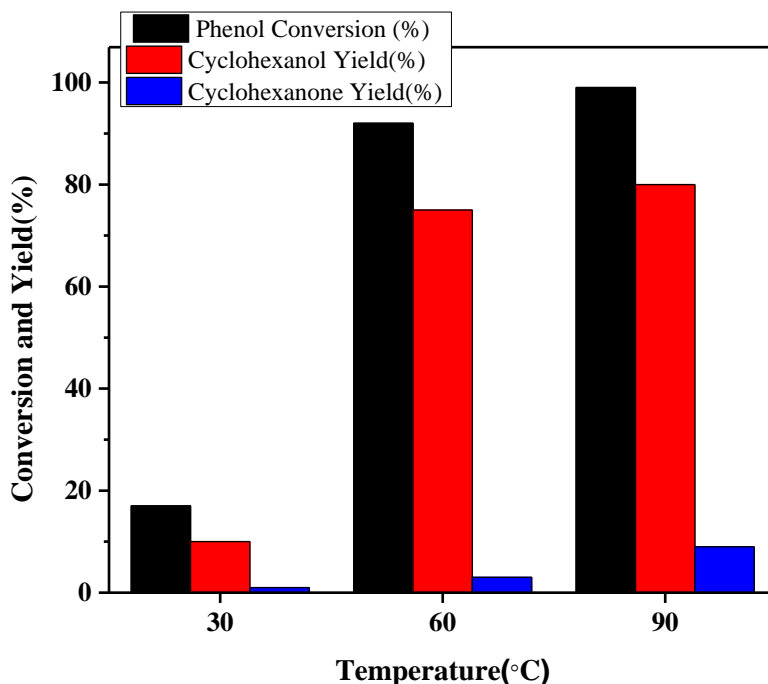


Figure 4.9. Effect of temperature on phenol hydrogenation

Reaction condition- phenol (0.800 g), 20 wt % catalyst w.r.t. substrate, 40 ml solvent (water), 10 bar H₂ pressure, and time-5h.

c) Effect of pressure on phenol hydrogenation

Table 4.5, depicts the effect of H₂ pressure on the hydrogenation of phenol and the yield of cyclohexanol by varying H₂ pressure from 5 to 15 bar. The result showed that there is a linear relationship of H₂ pressure with the phenol conversion and cyclohexanol yield. The phenol conversion and cyclohexanol yield increased from 86 to 99% and 65 to 80% with increase in the pressure from 5 to 10 bar respectively after 5 h while at 15 bar H₂ pressure 99% conversion was obtained with 82% yield of cyclohexanol after 1 h. With increase in H₂ pressure the time required for 99% phenol conversion decreased from 5 h for 10 bar pressure to 1 h for 15 bar pressure. It is well known that at high H₂ pressure the solubility of hydrogen increases leading to more availability of H₂ on the catalyst surface thus increasing the rate of hydrogenation. As there was

a minor difference in the yield of cyclohexanol at 10 and 15 bar H₂ pressure, we used 10 bar H₂ pressure for further optimisation.

Table 4.5. Effect of pressure on phenol hydrogenation

Sr. No.	Pressure bar	Time h	Conv. %	Yield of Cyclohexanone	Yield of Cyclohexanol	Other product [#] %
1	5	2	38	13	19	6
		5	86	11	65	10
2	10	2	42	6	23	13
		5	99	9	80	10
3	15	1	99	3	82	14
		2	99	1	84	14
		5	99	0	86	13

Reaction condition- phenol (0.800 g), 20 wt % catalyst w.r.t. substrate, 40 ml solvent (water), temp-90 °C and time-5h; # other products-benzene and cyclohexane.

d) Effect of catalyst loading on phenol hydrogenation

To study the effect of the amount of catalyst on phenol hydrogenation, reactions were performed at different catalyst loadings such as 10, 20, and 30 wt% with respect to phenol (Figure 4.10). With increase in the catalyst loading from 10 to 20 to 30 wt %, the phenol conversion increased from 35%, 42%, to 99% with cyclohexanol yield of 15%, 23%, and 82% respectively after 2 h. For 20 wt% catalyst loading 99% conversion with 80% yield of cyclohexanol was obtained after 5 h while 30wt% catalyst showed 90% yield of cyclohexanol after 5 h. The increase in the catalyst led to increase in the number of active sites contributing to the higher conversion.

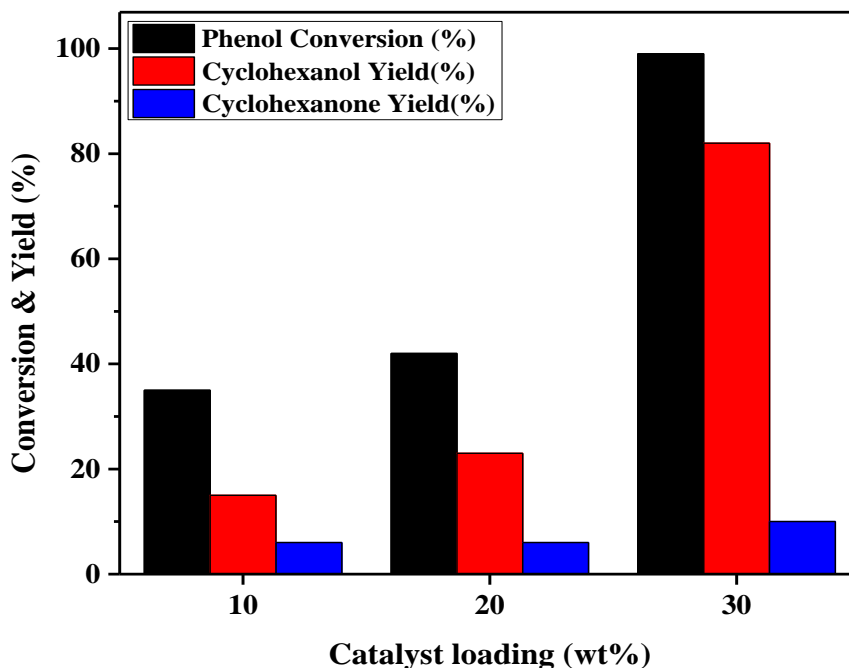


Figure 4.10. Catalyst loading effect on phenol hydrogenation

Reaction condition- phenol (0.800 g), PCC catalyst, 40 ml solvent (water), 10 bar H₂ pressure, temp-90°C and time-2h.

e) Effect of Pd loading on phenol hydrogenation

To study the effect of Pd loading on phenol hydrogenation, varying Pd loaded (0.5, 1, and 2 wt%) CuO/CeO₂ catalysts were tested for phenol hydrogenation and results are shown in Table 4.6. As Pd loading was increased, the phenol conversion and cyclohexanol yield also increased due to increase in the active sites in the reaction medium. As Pd loading increased from 0.5% to 2% the cyclohexanol yield increased from 41% to 88% after 5 h.

The important previous reports on the phenol hydrogenation are described in Table 4.7. Comparison of the present results with previous literature revealed that when non-noble metals are used for phenol hydrogenation the harsh reaction condition were used due to poor catalytic activity of non-noble metals. Non-noble metals such as Ni and Co were mostly used, but it required almost 70 to 200 °C temperature and 10 to 30 bar H₂ pressure. The precious metal

catalysts have given the good conversion of phenol and selectivity to cyclohexanol, but amount of catalyst required for reaction is high. In present work with just 10 wt% catalyst w.r.t phenol gave 99% conversion with 80% yield of cyclohexanol.

Table 4.6. Pd loading effect on phenol hydrogenation

Sr. No.	Pd loading	Time h	Conv. %	Yield of Cyclohexanone	Yield of Cyclohexanol	Other products [#] %
1	0.5PCC	2	20	3	7	10
		5	68	15	41	12
2	1PCC	2	42	6	23	13
		5	99	9	80	10
3	2PCC	2	93	5	80	8
		5	99	1	88	10

Reaction condition- phenol (0.800 g), 20 wt % catalyst w.r.t. substrate, 40 ml solvent (water), 10 bar H₂ pressure, temp-90 °C; [#] other products-benzene and cyclohexane.

Table 4.7. Literature survey for hydrogenation of phenol

Sr. No.	Catalyst	Amount Of catalyst	Solvent	Temp °C	Pressure bar	Time h	Conv. of phenol	Select. Cyclohexanol	Ref.
1	3 wt. % Pd/- Al ₂ O ₃	0.056 mmol pd	Water	60	20	12	100	99	[20]
2	CoO _x @CN	-	Water	150	30	16	99	98	[44]
3	Raney Ni	25 wt%	Water	70	20	2	100	100	[45]
4	20% Ni/CNT	10 wt%	IPA	220	-	1	100	95	[46]
5	10% Ni/SiO ₂	20wt%	Water	200	10	4	100	100	[21]
6	1Co-1Ni@NC	40 mol%	IPA	100	8	12	100	99	[18]
7	NiCo/Mg _x Ni _y O	10 wt%	Hexane	150	20	2.5	99	99	[47]
8	5RuO ₂ -MCM-41	33 wt%	Water	100	10	12	100	100	[48]
9	22% Ni/γ-Al ₂ O ₃	5 wt%	-	140	30	2	63	96	[49]

10	5% Rh/C	3 wt%	-	55	10bar H ₂ 10bar CO ₂	4	53	83	[50]
11	5% Pd/C	5 mol %	Water	100	10	2	55	100	[51,5 2]
12	1% Pd/CeO ₂	5 mol %	Hexane	35	~1	4	94	9	[53]
13	Pd spheres (~26nm)	0.05 mmol pd	Water	90	5	20	100	82	[54]
14	1% PCC	20 wt%	Water	90	10	5	99	80	Present work

f) Catalyst recycles study

To understand the catalyst stability and reusability, 1PCC catalyst was recycled for three cycles under optimized reaction conditions (phenol (0.800 g), 20 wt % catalyst w.r.t. substrate, 40 ml water, 10 bar H₂ pressure, temp 90 °C, time 2 h). The recycle was carried out at lower conversion to understand if any leaching takes place. After each run, the catalyst was separated by centrifugation, washed with methanol and water, dried at 100 °C, and used for the next catalytic run. Similarly the catalyst was recycled for three cycles and the results are shown in Figure 4.11. The results confirmed that the catalyst was stable and there was no decrease in the phenol conversion and cyclohexanol yield even after third cycle. The strong metal support interaction due to acidic nature of support led to efficient recycle of the catalyst. The palladium interacts strongly with acidic support due to which no leaching of the palladium in the reaction mixture was observed. This is in agreement with our previous results where Pd supported on acidic MgF₂ was used for hydrogenation of various organics with no Pd leaching [35]. Additionally, the ICP-AES analysis of the final reaction mixture was carried out to check the metal (Pd) leaching. The result showed no palladium leaching in the reaction mixture. Additionally the detailed

characterisation of the used catalyst was compared with fresh catalyst to confirm the integrity of the catalyst during catalytic hydrogenation.

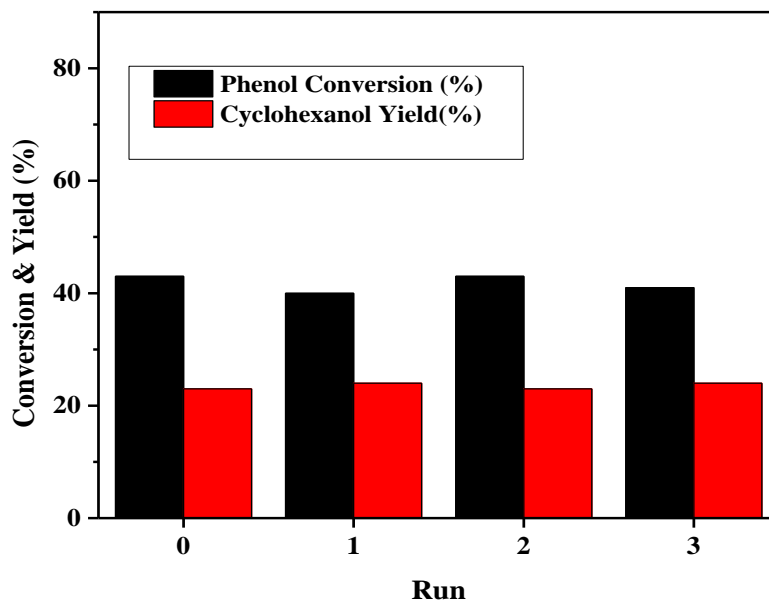


Figure 4.11. Recycle study of phenol hydrogenation

Reaction condition- phenol (0.800 g), 20 wt % catalyst w.r.t. substrate, 40 ml solvent (water),
10 bar H₂ pressure, temp 90°C, and time 2 h.

4.4. Characterization of the used catalyst

4.4.1. Powder X-ray diffraction (PXRD) analysis

The XRD analysis of fresh and used PCC catalyst is shown in Figure 4.12. The diffraction pattern of the used PCC catalyst does not indicate any changes as compared to the diffraction pattern of a fresh PCC catalyst and it completely matched the pattern of the cubic crystalline structure of CeO₂.

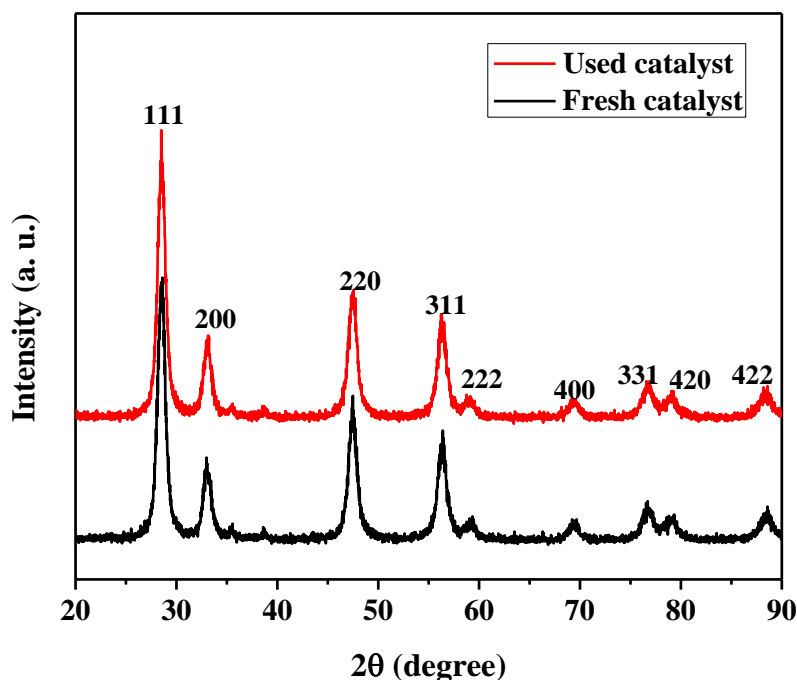


Figure 4.12. XRD pattern of fresh and used 1PCC catalyst

4.4.2 BET surface area measurements

The BET analysis of fresh and used catalysts is shown in Figure 4.13 and Table 4.8. The surface area of the fresh catalyst was 56 m²/g which decreased marginally to 53 m²/g for used catalyst with almost no change in pore size and pore volume. The elemental composition as determined by EDAX was also similar for fresh and used catalyst as evident from Table 4.8 which confirms no leaching of palladium in the reaction mixture.

Table 4.8. Surface characterization of fresh and used 1PCC catalyst

Sr. No.	Catalyst	Element composition by EDAX			Surface area (m ² /g)	Pore size (Å)	Pore volume (cc/g)
		Pd	Cu	Ce			
1	Fresh-1PCC	0.61	9	70	56	27	0.78
2	Used- 1PCC	0.63	10	70	53	29	0.78

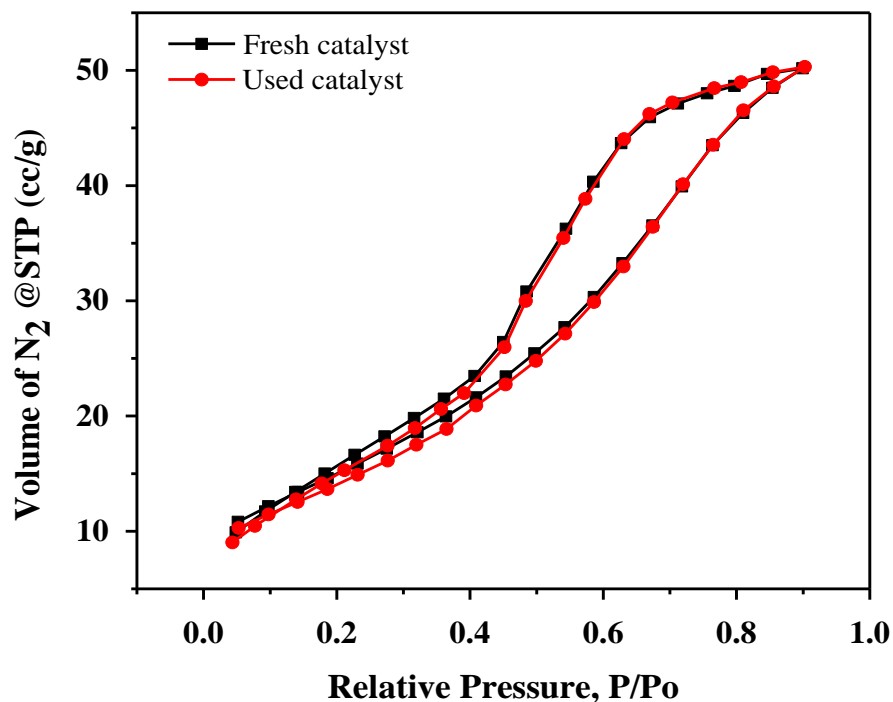


Figure 4.13. BET surface area analysis of fresh and used 1PCC catalyst

4.4.3. TEM analysis of fresh and used catalyst

The TEM analysis of the fresh and spent catalyst as shown in Figure 4.14 indicated only marginal change in the particle size distribution in fresh and used catalyst. The maximum particles are in the range of 8-9 nm for fresh and used catalysts.

The detailed characterisation of fresh and used catalyst revealed no change in the catalyst composition and morphology under reaction conditions.

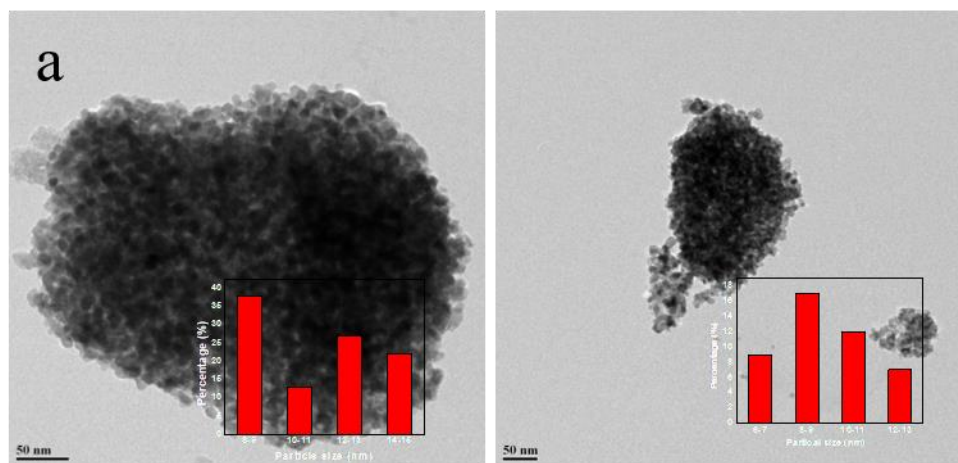


Figure 4.14. TEM images of (a) fresh and (b) used 1PCC catalyst

4.5. Plausible Mechanism

To study the mechanism of phenol hydrogenation over a 1PCC catalyst the detailed FTIR analysis was performed by analysing the interaction of phenol over the catalyst surface. To understand the interaction of adsorbed phenol with catalyst components, the FTIR spectra of phenol adsorbed on all prepared (CuO, CeO₂, CC, 1%Pd/CuO, 1%Pd/CeO₂, and 1PCC (Pd based catalysts were pre-reduced)) catalysts were recorded. The data was compared with authentic phenol as shown in Figure 4.15. The FTIR spectrum of authentic phenol showed peaks at 3274 cm⁻¹ for -OH stretching vibration, 1219 cm⁻¹ for C-O stretching vibration, and at 689, 747, 809 cm⁻¹ for C-H stretching vibration of *ortho*, *meta*, and *para* C-H respectively. The Figure showed decrease in the relative intensity of -OH stretching vibration at 3274 cm⁻¹ for free phenol in spectra of phenol adsorbed on CeO₂, CC, 1%Pd/CuO, 1%Pd/CeO₂ and it disappeared in the spectrum of phenol adsorbed on 1PCC catalyst. It means when phenol is adsorbed on a catalyst, it dissociates into phenoxide ion and proton.

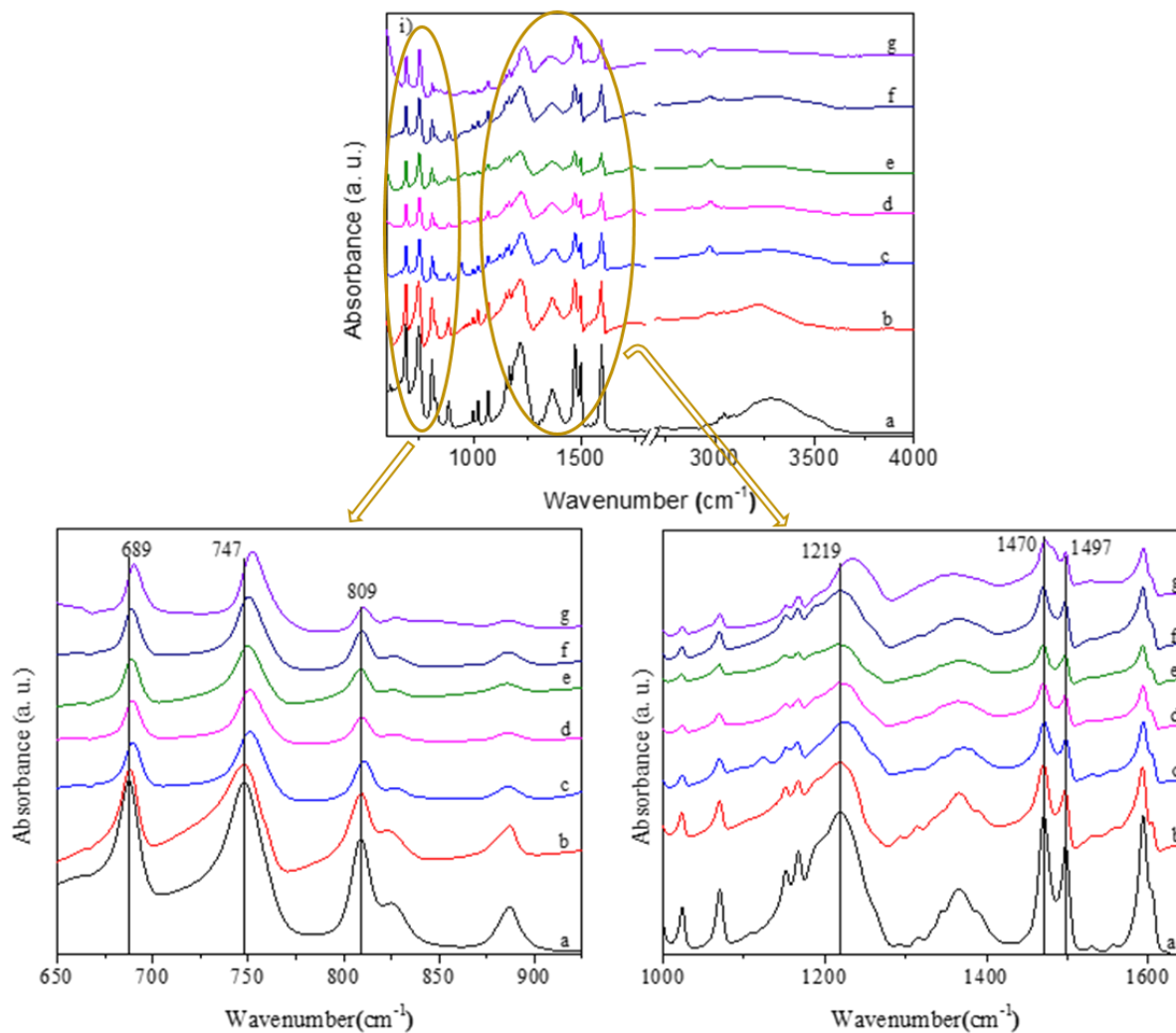
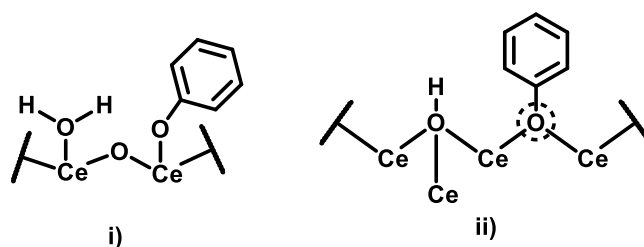


Figure 4.15. FTIR spectra in the range i) 600 to 4000 cm^{-1} , ii) 650 to 900 cm^{-1} , and iii) 1100 to 1660 cm^{-1} : of a) authentic phenol, and phenol adsorbed on b) CuO, c) CeO₂, d) CC, e) 1%Pd/CuO, f) 1%Pd/CeO₂ and g) 1PCC

The results also showed that an intense peak at 1219 cm^{-1} for C-O stretching vibration of authentic phenol is shifted from 1225 to 1234 cm^{-1} in phenol adsorbed on catalysts, and this is attributed to C-O-Ce bond formation. The C-O-Ce bond formation results in electron withdrawal from the phenoxy group toward the cerium ion and leads to C-O bond shortening resulting in the increase in frequency. Nelson and group reported hydrogenation of phenol on 1%Pd/CeO₂ catalyst, and showed that phenol adsorbed onto cerium cation in a dissociative manner with

different modes as shown in Scheme 4.3 [53]. The active site for hydrogenation of phenol on 1%Pd/CeO₂ catalyst was shown to be coordinatively unsaturated cerium cations. Figure 4.15(c) shows spectrum of phenol adsorbed on only CeO₂ and it shows similar shift in C-O bond stretching vibration as in 1PCC. However the shift is smaller compared to 1PCC. The spectrum of phenol adsorbed on 1PCC catalyst showed higher shift (to 1234 cm⁻¹) for peak at 1219 cm⁻¹ for C-O stretching vibration, it may be attributed to higher Ce(III) (coordinatively unsaturated cerium cations) and hence, more oxygen vacancies due to CuO addition and also hydrogen spillover from Pd to catalyst surface. This might be one of the reasons for efficient hydrogenation of phenol on 1PCC catalyst due facile activation of phenol. The higher hydrogenation efficiency of 1PCC catalyst is also reflected in the highest cyclohexanol yield compared to 1%Pd/CeO₂ where equal selectivity for cyclohexanol and cyclohexanone is obtained, though the phenol conversion is same (Table 4.4). Hence the FTIR studies explains the higher hydrogenation efficiency of 1PCC catalyst compared to 1%Pd/CeO₂.



Scheme 4.3. Dissociative adsorption of phenol onto catalyst (i) adjacent to a surface hydroxyl, and (ii) at an oxygen vacancy

The spectra also showed no shift in C=C aromatic ring vibration (1594 and 1498 cm⁻¹), however a shift was observed in aromatic C-H bending vibration (688 to 690 and 748 to 752 cm⁻¹) in spectra of phenol adsorbed on all catalyst except CuO. The difference in the peak shift *-o*, *-m* and *-p* C-H bending vibration clearly indicate perpendicular orientation of aromatic ring with respect to catalyst surface. In case of parallel orientation of the aromatic ring, significantly higher shift in

all *-o*, *-m* and *-p* C-H bending vibration with almost similar shift is expected. From this, it can be concluded that when phenol adsorbs on the catalyst the aromatic ring orientation is perpendicular to the catalyst surface to lower the electronic interaction with the surface as shown in Scheme 4.4 [28]. For the spectrum of phenol adsorbed on CuO no shift was observed in aromatic C-H bending vibration, while in the spectrum of phenol adsorbed on 1%Pd/CuO peaks were shifted from 688 to 689 and 748 to 750 cm^{-1} . This indicates that Pd metal also helps to activate the phenol molecule to some extent.



Scheme 4.4. Adsorption of phenol onto catalyst i) perpendicular orientation and ii) parallel orientation

From all above discussion, the plausible mechanism for phenol hydrogenation on 1PCC catalyst is shown in Figure 4.16. In 1PCC (**A**) under hydrogen atmosphere, Pd^{+2} gets reduced to Pd^0 . Along with reduction of Pd the hydrogen molecule gets activated to H and due to spillover effect the hydrogen atoms migrates on the surface (**B**). Under reducing atmosphere the number of oxygen vacancies also increase which are known to improve the hydrogenation efficiency. Subsequently phenol molecule gets activated on CuO/CeO₂ surface on oxygen vacancy leading to dissociation of phenol to phenoxide ion with perpendicular orientation of aromatics ring with respect to catalyst surface (**C**). The transfer of hydrogen atoms under high pressure to aromatic ring leads to hydrogenation of the aromatic ring forming the product cyclohexanol. Thus the oxygen vacancies generated in the CuO/CeO₂ support have helped activation of phenol on the support and activation of hydrogen on Pd center along with spillover effect, has led to

significantly high efficiency of the catalyst for phenol hydrogenation.

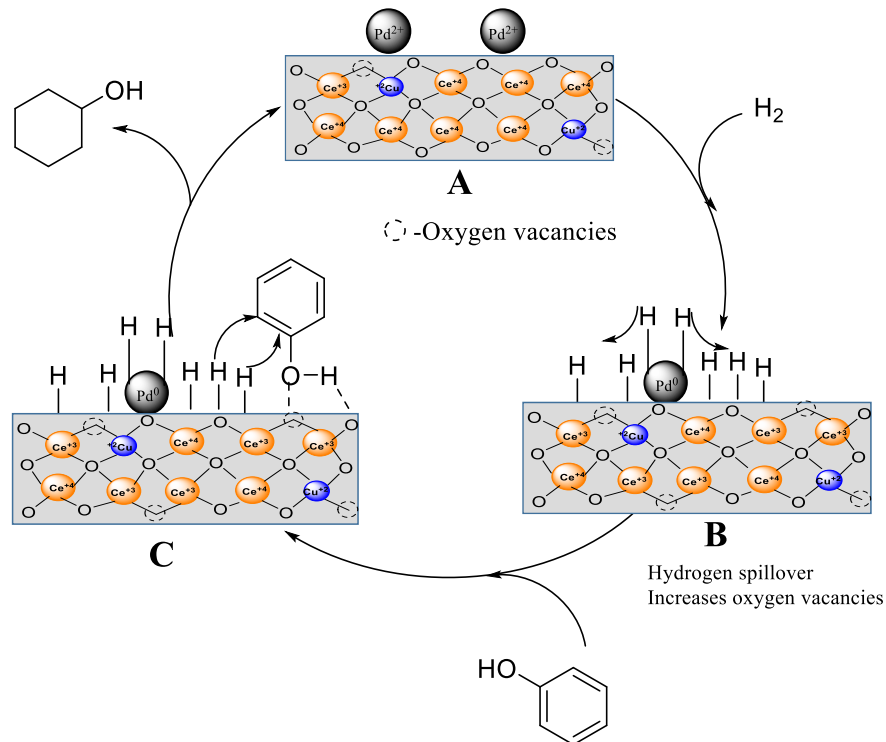


Figure 4.16. Plausible Mechanism of phenol hydrogenation over PCC catalyst

4.6. Conclusion

CuO/CeO₂ has been used as acidic support with redox properties for palladium to prepare an efficient hydrogenation catalyst. Palladium supported on CuO/CeO₂ with different palladium loading has been synthesized by the impregnation method. The detailed analysis showed addition of CuO into CeO₂ to reduce the size of CeO₂ crystallite by inhibiting the crystalline growth of cerianite and also the insertion of some Cu ions into the CeO₂ lattice which leads to the reduction of crystal parameters. The surface area of CeO₂ (33 m²/g) increased significantly after CuO incorporation (61 m²/g). The XPS analysis confirmed high oxygen vacancies due to hydrogen spillover in reduced IPCC catalyst. This leads to more hydrogen availability for reaction and also the activation of phenol. The PCC catalyst has shown excellent catalytic activity for phenol hydrogenation under milder reaction conditions (10 bar H₂ pressure, and

90°C) in an aqueous medium with very high conversion (98%) and a high cyclohexanol yield (80%). The detailed FTIR studies proved perpendicular orientation of aromatic ring of phenol on catalyst surface after activation of phenol as phenoxide on oxygen vacancy of PCC catalyst.

4.7 References

1. Y. Xiang, L. Ma, C. Lu, Q. Zhang, X. Li, *Green Chem.*, **2008**, 10, 939–943.
2. Y. Xiang, L. Kong, P. Xie, T. Xu, J. Wang, X. Li, *Ind. Eng. Chem. Res.*, **2014**, 53, 2197–2203.
3. C. J. Lin, S.H. Huang, N. C. Lai, C. M. Yang, *ACS Catal.*, **2015**, 5, 4121–4129.
4. M. Chatterjee, H. Kawanami, M. Sato, A. Chatterjee, T. Yokoyama, T. Suzuki, *Adv. Synth. Catal.*, **2009**, 351, 1912–1924.
5. V.Z. Fridman, A.A. Davydov, *J. Catal.*, **2000**, 195, 20–30.
6. M. A. Ali, A. Abutaleb, *Catal. Lett.*, **2022** 152, 1555–1581.
7. G. Xue, L. Yin, S. Shao, G. Li, *Nanotechnology*, **2022**, 33, 072003.
8. H. Chen, J. Sun, *J. Ind. Eng. Chem.*, **2021**, 94, 78–91.
9. H. Li, T. She, G. Chen, M. Sun, L. Niu, G. Bai, *Mol. Catal.*, **2021**, 504, 111493–111500.
10. Y. Nakagawa, M. Ishikawa, M. Tamura, K. Tomishige, *Green Chem.*, **2014**, 16, 2197–2203.
11. L. Wang, J. Zhang, X. Yi, A. Zheng, F. Deng, C. Chen, Y. Ji, F. Liu, X. Meng, F.-S. Xiao, *ACS Catal.*, **2015**, 5, 2727–2734.
12. Y. Wang, J. Yao, H. Li, D. Su, M. J. Antonietti, *J. Am. Chem. Soc.*, **2011**, 133, 2362–2365.
13. H. Li, J. Liu, S. Xie, M. Qiao, W. Dai, Y. Lu, H. Li, *Adv. Funct. Mater.*, **2008**, 18, 3235–3241.

14. H. Liu, T. Jiang, B. Han, S. Liang, Y. Zhou, *Science*, **2009**, 326, 1250–1252.
15. H. Zhang, A. Han, K. Okumura, L. Zhong, S. Li, S. Jaenicke, G.K. Chuah, *J. Catal.*, **2018**, 364, 354–365.
16. H. Zhou, B. Han, T. Liu, X. Zhong, G. Zhuang, J. Wang, *Green Chem.*, **2017**, 19, 3585–3594.
17. S. Kuklin, A. Maximov, A. Zolotukhina, E. Karakhanov, *Catal. Commun.*, **2016**, 73, 63–68.
18. A. Li, K. Shen, J. Chen, Z. Li, Y. Li, *Chem. Eng. Sci.*, **2017**, 166, 66–76.
19. C. Huang, X. Yang, H. Yang, P. Huang, H. Song, S. Liao, *Appl. Surf. Sci.*, **2014**, 315, 138–143.
20. J. Yi, Y. Luo, T. He, Z. Jiang, J. Li, C. Hu, *Catalysts*, **2016**, 6, 12.
21. J. He, X.-H. Lu, Y. Shen, R. Jing, R.-F. Nie, D. Zhou, Q.-H. Xia, *Mol. Catal.*, **2017**, 440, 87–95.
22. J. Matshwele, K. Mmusi, V. Vishwanathan, *Sreyas Int. J. Sci. Technol.*, **2019** 3, 1–6.
23. P. Claus, H. Berndt, C. Mohr, J. Radnik, E.-J. Shin, M. A. Keane *J. Catal.*, **2000**, 192, 88–97.
24. E. Diaz, A.F. Mohedano, L. Calvo, M. A. Gilarranz, J.A. Casas, J.J. Rodriguez, *Chem. Eng. J.*, **2007**, 131, 65–71.
25. S. A Lermontov, A. N. Malkova, L. L. Yurkova, A. Y. Baranchikov, V. K. Ivanov, *Nanosyst. Physics. Chem. Math.*, **2013**, 4, 690–695.
26. T. S. Cam, T. A. Vishnievskaya, V. I. Popkov, *Rev. Adv. Mater. Sci.*, **2020**, 59, 131–143.
27. X. Zhang, H. Wang, X. Jiang, H. Sun, Z. Qu, *Catal. Sci. Technol.*, **2019**, 9, 2968–2981.
28. S. Velu, M. P. Kapoor, S. Inagaki, K. Suzuki, *Appl. Catal. A*, **2003**, 245, 317–331.

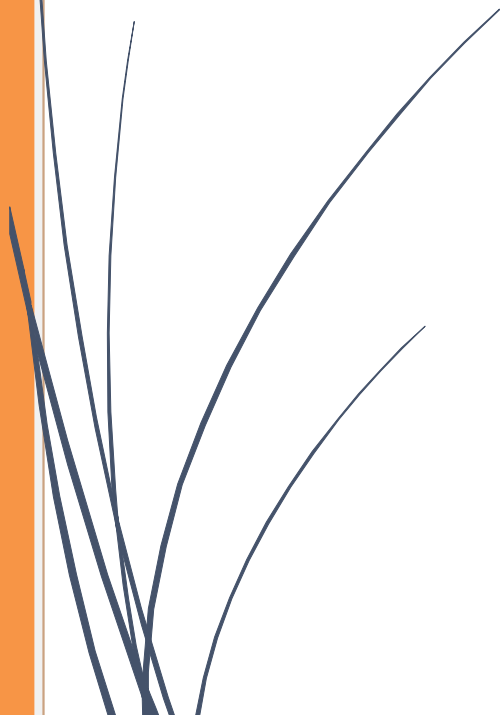
29. J. Wang, Y. Zhang, X. Xu, M. Bao, *ACS Appl. Mater. Interfaces*, **2023**, doi.org/10.1021/acsami.2c21272.
30. A. Hezam, K. Namratha, Q. A. Drmosh, D. Ponnamma, J. Wang, S. Prasad, M. Ahamed, C. Cheng, K. Byrappa, *ACS Appl. Nano Mater*, **2020**, 3, 138–148.
31. G. Avgouropoulos, T. Ioannides, *Appl. Catal. B*, **2006**, 67, 1–11.
32. L. Yin, Y. Wang, G. Pang, Y. Kolytyn, A. Gedanken, *J Colloid Interface Sci.*, **2002**, 246, 78-84.
33. M. Jobbagy, F. Mariño, B. Schönbrod, G. Baronetti, *Chem. Mater.*, **2006**, 18, 1945–1950.
34. X. Wang, J. A. Rodriguez, J. C. Hanson, D. Gamarra, A. Martínez- Arias, M. Fernández-García, *J. Phys. Chem.*, B **2006**, 110, 428-434.
35. V. R. Acham, A. V. Biradar, M. K. Dongare, E. Kemnitz, S. B. Umbarkar, *ChemCatChem*, **2014**, 6, 3182–3191.
36. M. Chuai, X. Chen, K. Zhang, J. Zhang, M. Zhang, *J. Mater. Chem. A*, **2019**, 7, 1160-1167.
37. Z. V. Popovic, Z. Dohcevic-Mitrovic, A. Cros, A. Cantarero, *J. Phys.: Condens. Matter*, **2007**, 19, 496209-496218.
38. F. Zhang, S. W. Chan, J. E. Spanier, E. Apak, Q. Jin, R. D. Robinson, I. P. Herman, *Appl. Phys. Lett.*, **2002**, 80, 127-129.
39. M. Mittal, A. Gupta, O.P. Pandey, *Sol. Energy*, **2018**, 165, 206–216.
40. S. Penner, D. Wang, B. Jenewein, H. Gabasc, B. Klötzer, A. Knop-Gericke, R. Schlögl, K. Hayek, *J. Chem. Phys.*, **2006**, 125, 094703-094715.
41. V. Perala, D. Devaiah, J. Deshetti, D. Mukherjee, V. Muga, B. M. Reddy, *Catal. Lett.*,

- 2020, 150, 948–962.
42. D. Zhang, N. Yin, C. Jiang, B. Xia, *J Mater Sci: Mater Electron* **2017**, 28, 2763–2768.
43. R. Prins, *Chem. Rev.* **2012**, 112, 2714-2738.
44. Z. Weia, Y. Lib, J. Wangb, H. Lib, Y. Wang, *Chin. Chem. Lett.*, **2018**, 29, 815–818.
45. M. Kennema, I. B. Castro, F. Meemken, R. Rinaldi, *ACS Catal.*, **2017**, 7, 2437–2445.
46. C. Chen, P. Liu, M. Zhou, B. K. Sharma, J. Jiang, *Energies*, **2020**, 13, 846-859.
47. J. Donga, X Wena, T. Zhua, J. Qina, Z. Wua, L. Chenb, G. Bai, *Mol. Catal.*, **2020**, 485, 110846-110854.
48. K.J. Betsy, A. Lazar, C.P. Vinod, *Nano-Struct. Nano-Objects*, **2018**, 13, 36–43.
49. S. Bin, C. Wen-wen, K. Qing-yang, *J. Fuel Chem. Technol.*, **2015**, 43, 1252-1257.
50. C. V. Rode, U. D. Joshi, O. Sato, M. Shirai, *Chem Commun.*, **2003**, 15, 1960–1961.
51. M. Li, Y. Li, L. Jia, Y. Wang, *Catal. Commun.*, **2018**, 103, 88-91.
52. M. P. Wiesenfeldt, Z. Nairoukh, T. Dalton, F. Glorius, *Angew. Chem. Int. Ed.*, **2019**, 58, 10460-10476.
53. N. C. Nelson, J. S. Manzano, A. D. Sadow, S. H. Overbury, I. I. Slowing, *ACS Catal.* **2015**, 5, 2051–2061.
54. G. Porwal, S. Gupta, S. Sreedhala, J. Elizabeth, T. S. Khan, M. A. Haider, C. P. Vinod, *ACS Sustain. Chem. Eng.*, **2019**, 7, 17126–17136.

An orange vertical bar runs down the left side of the page. A horizontal orange arrow points to the right, overlapping the vertical bar, and contains the text 'Chapter 5'.

Chapter 5

*Summary
and
Conclusion*



Abstract

The thesis primarily outlines the synthesis of a palladium supported on acidic and active mixed oxide catalyst and its catalytic uses in the reduction of different functional groups. These catalysts worked under milder reaction conditions. The important outcomes are highlighted in this chapter, which also provides a concise overview of the findings. This chapter discusses the results from earlier chapters and provides a summary of the whole thesis.

Chapter 1: Introduction

This chapter presents a broad overview of heterogeneous catalysis, with a particular focus on Pd-based catalyst and its recent advancements. The results of a literature review on several Pd supported catalytic systems employed in hydrogenation processes are discussed. The importance of metal support interaction and role of support are explained in detail. After the detailed literature survey, at the end of chapter the purpose and goals of the thesis are presented.

Chapter-2: Pd-WO₃/SiO₂: Synthesis, Characterization and Its Catalytic Applications For Hydrogenation Of Cinnamaldehyde Under Milder Conditions

This chapter deals with synthesis, detailed characterizations of Pd-WO₃/SiO₂ and its catalytic applications for hydrogenation of cinnamaldehyde. Catalysts were prepared by wet impregnation method with different Pd loading (0.1, 0.5, to 2 wt %). The support (WO₃/SiO₂) with varying WO₃ loading (10, 15, and 20 wt%,) were synthesized by sol-gel method and calcined at 500 °C. The calcined support was dispersed in methanol. To this slurry palladium acetate solution in methanol-acetone (1:1) was added drop wise. After drying the mixture, the final catalysts were calcined at 250 °C and characterized by various techniques such as XRD, BET, FTIR, SEM, TEM, and XPS. The detailed characterization showed that Pd particles were well dispersed on acidic support (WO₃/SiO₂) due to strong metal support interaction as observed in previous work. The catalyst 1%Pd-WO₃/SiO₂ has shown very high efficiency for hydrogenation of cinnamaldehyde with 99% conversion and 70% hydrocinnamyl alcohol selectivity at 60 °C and 3 bar H₂ pressure. Selective hydrogenation to hydrocinnamyl alcohol is due the high dispersion and large particle size of Pd on WO₃/SiO₂ acidic support. The catalyst was recycled up to three runs without losing catalytic activity. To study the mechanistic aspects FTIR analysis was done. The results showed that adsorption of cinnamaldehyde on 1%Pd-WO₃/SiO₂ catalyst through C=O group subsequently reacts with hydrogen atoms which dissociates on reduced Pd on WO₃/SiO₂ catalyst and transferred to saturated products.

Chapter 3: Pd-WO₃/SiO₂: Efficient Acidic Catalyst For Hydrogenation Of Acetophenone Under Ambient Conditions

This chapter deals with catalytic applications of 1% Pd-WO₃/SiO₂ catalyst for hydrogenation of acetophenone. The 1-phenylethanol is an important compound in pharmaceutical and fragrance industry. It can be obtained by acid-catalyzed hydration of styrene or hydrogenation of acetophenone. The former one is environmentally not suitable due to mineral acids used in the process. To extend the application of 1% Pd-WO₃/SiO₂ catalyst, it was used to hydrogenate acetophenone to 1-phenylethanol. The catalyst showed good catalytic activity with 92% conversion of acetophenone and 76% yield for 1-phenylethanol under ambient conditions (10 ml/min H₂ bubbling at RT). The high catalytic activity was attributed to the high dispersion of Pd on WO₃/SiO₂ acidic support due to strong metal-support interaction. Variation in support acidity showed increase in catalytic activity with increase in the support acidity. 1-Phenylethanol on acid catalyst undergo oligomerisation which caused catalyst deactivation. TGA analysis of used catalyst confirmed the adsorption of oligomers. At lower conversion catalyst showed recyclability up to 5 runs. Mechanistic study by FTIR spectroscopy, showed dissociative activation of methanol on WO₃ moiety to form CH₃O-W and W-O-H and activation of acetophenone by hydrogen bonding with W-OH.

Chapter-4: Pd-CuO/CeO₂: Synthesis, Characterization and Its Catalytic Applications for Selective Hydrogenation of Phenol to Cyclohexanol Under Ambient Conditions

This chapter deals with synthesis, detailed characterizations of Pd-CuO/CeO₂ and its catalytic applications for hydrogenation of phenol. The reduction of phenol into cyclohexanone or cyclohexanol is an important reaction in chemical industry to synthesize nylon-6 & nylon-66 and KA oil in petroleum industry. In present chapter the support (30%CuO/CeO₂) was prepared by co-precipitation method. This support after calcination was used to disperse palladium metal. This catalyst (Pd-CuO/CeO₂) was used for liquid phase hydrogenation of phenol in an autoclave at 10 bar H₂ pressure and 60 °C. All prepared catalysts were characterized by

different techniques (NH₃-TPD, XRD, BET, Raman spectroscopy, XPS, TEM, and SEM). The XRD analysis revealed that the addition of CuO to CeO₂ decreases the size of CeO₂ crystallite due to the Cu (II) ions inhibiting the crystalline growth of ceria. XRD analysis also showed reduction in crystal parameters which attributed to insertion of some smaller Cu ions into the CeO₂ lattice. BET and Raman analysis was in agreement with XRD analysis. The surface area of CeO₂ (33 m²/g) increased almost two fold in CuO/CeO₂ (61 m²/g). XPS analysis showed that Pd loading on CuO/CeO₂ caused hydrogen spillover on the catalyst which leads to an increase in oxygen vacancies in CeO₂ lattice. Hydrogen spillover leads to increase the hydrogen availability on the catalyst surface which lead to Pd-CuO/CeO₂ catalyst showing good catalytic activity for phenol hydrogenation (99% phenol conversion with 80% selectivity for cyclohexanol) at 90 °C and 10 bar H₂ pressure after 5h.

ABSTRACT

Name of the Student: Kasabe Mirabai Madhukar
Faculty of Study: Chemical science
AcSIR academic centre/CSIR Lab: CSIR-NCL
Name of the Supervisor(s): Dr. S. B. Umbarkar

Registration No.:10CC17J26032
Year of Submission: 2023

Title of the thesis: Palladium based catalysts for hydrogenation of various functional groups

Supported metal nanoparticles are increasingly dominant in heterogeneous catalysis and serve a critical role in catalysing several chemical reactions that are significant to the industry. The logical designing of a catalyst would include understanding how a molecule interacts with each other to get the desired product. The different properties of metal and support in heterogeneous catalysts give the catalytic trends in the reaction. More specifically, the strength of the metal-support interaction can affect the catalytic performance. We can control metal NPs size and its dispersion on support with the help of metal support interaction. In this thesis, we have prepared a palladium based catalyst by impregnation method on two mixed metal oxides namely WO_3/SiO_2 and CuO/CeO_2 . These metal oxides are acidic additionally CuO/CeO_2 has redox nature and showed good metal support interaction with palladium metal.

Palladium supported on 20% WO_3/SiO_2 (high acidic), formed nano sheets of Pd (111) of 12-18 nm size. The significantly high dispersion of Pd (36%) due to the acidic support which resulted in a high catalytic activity for hydrogenation of cinnamaldehyde and acetophenone to hydrocinnamyl alcohol and 1-phenyl ethanol respectively under milder condition. Also, due to strong metal support interaction there is no palladium leaching during reaction. Hence catalyst showed good recyclability in the case of cinnamaldehyde hydrogenation. In the case of acetophenone, the product 1-phenyl ethanol undergo polymerization/oligomerisation on acidic surface and adsorbs on the catalyst leading to the deactivation of the catalyst. But at lower conversion catalyst could be recycled. The process optimisation was done with a 1%Pd- WO_3/SiO_2 catalyst by varying parameters, including temperature, solvent, catalyst loading, and Pd loading for hydrogenation of both the substrates.

1%Pd- CuO/CeO_2 catalyst has shown efficient catalytic activity for phenol hydrogenation to cyclohexanol under milder reaction conditions of 10bar H_2 pressure and 90°C temperature with 20 wt% catalyst loading. The activity of this catalyst is also attributed to good metal support interaction and reducibility of CeO_2 . Due to the reducibility of CeO_2 , the catalyst showed a hydrogen spillover mechanism and increasing oxygen vacancies in the CeO_2 lattice, which is responsible for activating the phenol molecule. These lead to increase the yield of product.

We have successfully prepared Pd-based catalysts and used for the hydrogenation of different functional groups. Selected hydrogenation reactions are industrially important.

List of publication(s) in SCI Journal(s) (published & accepted) emanating from the thesis work

- **Mirabai M. Kasabe**, Deepa K. Dumbre, Mohan K. Dongare, and Shubhangi B. Umbarkar, Pd-WO₃/SiO₂: efficient acidic catalyst for hydrogenation of acetophenone under ambient conditions. *Catalysis in Green Chemistry and Engineering*, 2021, 4(2):1–28.
- **Mirabai M. Kasabe**, Vaibhav R. Kotkar, Mohan K. Dongare, and Shubhangi B. Umbarkar, Phenol hydrogenation to cyclohexanol catalysed by palladium supported on CuO/CeO₂, *Chem Asian J.*, 2023, e202300119

List of publication(s) in SCI Journal(s) (published&accepted) other than thesis

- A.B. Kulal, **M. M. Kasabe**, P. Jadhav, M.K. Dongare, S.B. Umbarkar, Hydrophobic WO₃/SiO₂ catalyst for the nitration of aromatics in liquid phase. *Applied Catalysis A: General*, 2019, 574, 105-113.
- Shweta Mehta, **Mirabai M. Kasabe**, Shubhangi B. Umbarkar, and Kavita Joshi Methanol decomposition to formaldehyde on ZnO: from computation to experiments (manuscript to be submitted)

List of the papers with abstract presented (oral/ poster) at national/international conference/seminars with details

- 1] Demonstrated “Eco-friendly Ganesh Jalabhishek” in the Bharat Vigyan Sammelan – 2017 which was held at Fergusson College during 13th May 2017.

Abstract:

Ganesh Utsav is ten-day festival involves bringing Ganesh idols at homes for worship in most of states in India. During this traditional immersion of Ganesh idols in water, those made of clay easily dissolve, but idols made of Plaster of Paris (POP) pose a problem. POP has very low solubility in water, making it hard to dissolve, leading to increased water hardness and pollution. To address these issues, NCL-Pune, Pune Municipal Corporation, and Cummins India collaborated to find a solution. They propose using ammonium bicarbonate (commonly known as baking soda) to disintegrate POP idols. The chemical reaction between Plaster of Paris and ammonium bicarbonate results in the formation of ammonium sulphate, calcium carbonate, carbon dioxide, and water. The byproducts of this reaction have practical applications. Ammonium sulphate can be used as fertilizer for crops, plants, and lawns, while calcium carbonate (lime) can be utilized in the production of chalk, bricks, and paint industries. This approach offers an eco-friendly method to celebrate the festival without harming water bodies and the environment.

- 2] Presented a poster entitled “Pd on acidic support for hydrogenation of acetophenone at ambient conditions” during National Science Day Celebrations at CSIR-National Chemical Laboratory, Pune, India, February 2020.

Abstract:

Pd supported on WO_3/SiO_2 acidic support is useful catalyst for hydrogenation of acetophenone to 1-phenyl ethanol under ambient conditions. To study the effect of support acidity on catalyst activity, we have prepared catalysts with 1% Pd loading on 10% WO_3/SiO_2 (1P10WS) and 15% WO_3/SiO_2 (1P15WS) and 20% WO_3/SiO_2 (1P20WS). Results showed that the conversion increases with acidity of support, conversion of acetophenone 79% and selectivity of 1-phenyl ethanol 94% is achieved by 1P20WS catalyst in 4h. The catalysts were characterized by XRD, FTIR, BET, SEM, TEM, XPS and TGA.

- 3] Demonstrated “Eco-friendly Ganesh Jalabhishek” for One Week One Lab program at CSIR-National Chemical Laboratory, Pune, India during 22-27 May 2023.

Abstract: See the abstract for entry (1).

List of the conference/ workshops attended

- 1) The Annual Students’ Conference 2018, organized by NCL Research Foundation & CSIR-NCL, Pune
- 2) International Conference on structural and inorganic chemistry, ICSIC-II, March 2019, IISER, Pune.
- 3) The Annual Students’ Conference 2021, organized by NCL Research Foundation & CSIR-NCL, Pune.

Pd-WO₃/SiO₂: EFFICIENT ACIDIC CATALYST FOR HYDROGENATION OF ACETOPHENONE UNDER AMBIENT CONDITIONS

Mirabai M. Kasabe,^{1,2} Deepa K. Dumbre,¹ Mohan K. Dongare,^{1,3} & Shubhangi B. Umbarkar^{1,2,*}

¹Catalysis Division, CSIR-National Chemical Laboratory, Pune, India

²Academy of Scientific and Innovative Research, CSIR, Ghaziabad, India

³Malati Fine Chemicals Pvt. Ltd., 4/ADurvankurdarshan Society, Pune, India

*Address all correspondence to: Shubhangi B. Umbarkar, Catalysis Division, CSIR-National Chemical Laboratory, Pune-411008, India; Tel.: +91 02025902044, E-mail: sb.umbarkar@ncl.res.in

Original Manuscript Submitted: 2/6/2021; Final Draft Received: 6/23/2021

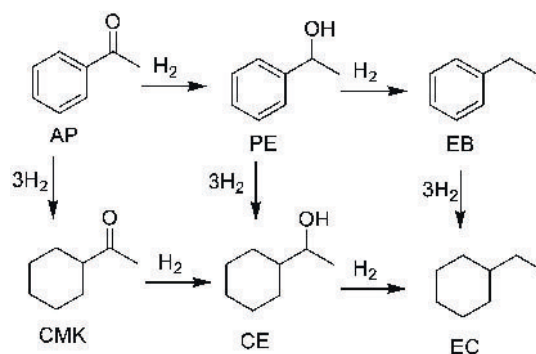
Selective hydrogenation of acetophenone to 1-phenylethanol is an important reaction in the pharmaceutical and fragrance industries. In-house prepared 1% Pd-WO₃/SiO₂ acidic catalyst showed very high efficiency for acetophenone hydrogenation under ambient conditions with 79% conversion and 94% selectivity for 1-phenylethanol. The detailed characterization revealed formation of Pd nano sheets (12–18 nm) on acidic support leading to very high Pd dispersion (36%). Selective hydrogenation has been correlated to the high dispersion of Pd on WO₃/SiO₂ acidic support and the milder reaction conditions. Variation in support acidity showed an increase in catalytic activity with an increase in the support acidity. Detailed Fourier-transform infrared spectroscopy analysis revealed dissociative activation of methanol on WO₃ moiety to form CH₃O-W and W-O-H and activation of acetophenone by hydrogen bonding with W-OH. Because of oligomerization of 1-phenylethanol on the catalyst surface, no recycling was possible. The catalyst deactivation was substrate specific. The same catalyst could be efficiently recycled for styrene hydrogenation under ambient conditions.

KEY WORDS: acetophenone, acidic support, hydrogenation, palladium, WO₃/SiO₂

1. INTRODUCTION

Hydrogenation is an important organic reaction, which has valuable industrial applications in the production of fine chemicals, flavors, agrochemicals, fragrances, and pharmaceutical industries (Cervený, 1986; Bauer and Garbe, 1988; Rylander, 1985; Liu and Corma, 2018; Baiker, 2015; Wang and Astruc, 2015). Catalytic hydrogenation of acetophenone (AP) to produce 1-phenylethanol (PE) is specifically very important due to the applications of PE as a perfumery chemical, and it is also an important building block for styrene monomer (Liu and Corma, 2018; Baiker, 2015; Wang and Astruc, 2015). This reaction includes different side reactions, such as the ring hydrogenation, hydrogenolysis of the produced alcohol to an aromatic saturated compound. The possible products of AP hydrogenation are shown in Scheme 1. The carbonyl hydrogenation gives PE and ethylbenzene (EB) as possible products, and ring hydrogenation gives cyclohexyl methyl ketone (CMK), cyclohexyl ethanol (CE), and ethyl cyclohexane (EC).

Generally, hydrogenation of AP has been investigated over both noble and non-noble transition metals, such as Pd, Pt, Rh, Ru, Ni, Cu, Ag, and Co with different supports, such as Al₂O₃, SiO₂, zeolites, NiO, CNTs (carbon nano tubes), and a polymer matrix under different liquid- or gas-phase reaction conditions (Santori et al., 2004; Chen et al., 2003; Cervený et al., 1996; Casagrande et al., 2002; Aramendia et al., 1993; Drelinkiewicz et al., 2004; Bejblova et al., 2003; Bonnier et al., 1988; Masson et al., 1993). Commercially, this reaction is carried out in liquid phase using supported Ni or Raney Ni doped with Cr or Co catalysts (Rajashekharam et al., 1999). Among the non-noble



SCHEME 1: Possible products of acetophenone hydrogenation

metals, Ni-based catalysts are widely studied for AP hydrogenation. In 2019, Costa et al. reported a 5% NiP/MSNS (mesoporous silica nano spheres) catalyst for AP hydrogenation with 30% conversion and 95% selectivity for PE at 80°C and 10 bar H₂ pressure (Costa et al., 2019). Under ambient conditions, non-noble metal-based catalysts give very poor conversion of AP because of lower catalytic activity of metals under such mild conditions. If the temperature and pressure is increased to increase conversion of AP, then variable quantities of by-products, such as CMK, CE, and EC, are obtained because of reduction of the phenyl ring at high pressure and temperature (Malyala et al., 2000; Bertero et al., 2011). Although on noble metals such as Pt, Rh, and Ru, hydrogenation can occur under ambient reaction conditions, the high cost of the noble metals is an issue of concern along with selectivity for the desired product due to undesired by-product formation (Santori et al., 2004; Chen et al., 2003; Cervený et al., 1996; Casagrande et al., 2002). Pt-based catalysts hydrogenate both the carbonyl group as well as the phenyl ring of AP with an identical rate; hence, similar quantities of PE and CMK are formed, which further hydrogenate to CE (Santori et al., 2004; Chen et al., 2003). Ruthenium-based catalysts are known to reduce mostly the phenyl ring of AP, and hence it gives lower selectivity for PE (Cervený et al., 1996; Casagrande et al., 2002). Palladium is reported for selective hydrogenation of AP to PE and EB under ambient reaction conditions with relative low cost (Aramendia et al., 1993; Drelinkiewicz et al., 2004; Cejka et al., 2003). Xiang et al. (2011) has shown the selectivity difference between hydrogenation of AP over Pd supported on carbon nanotubes and commercial activated carbons. The yield of PE for a Pd/CNTs catalyst (94.2%) was significantly higher than Pd/ACs (47.9%) at 60°C (Xiang et al., 2011). Gou et al. (2013) achieved higher conversion (80–92%) by applying shape-controlled phenomenon for Pd supported on sheetlike NiO catalysts at 80°C and 1.5 MPa pressure of H₂ in 3 h (Gou et al., 2013). In addition, Chen et al. (2018) reported an excellent study of tunable acidity, which is essential for developing more efficient catalysts in terms of Pd/silica–alumina for greener chemical processes.

Previously, we synthesized palladium supported on magnesium hydroxyl fluoride Pd-MgF_{2-x}(OH)_x catalysts, which showed very high efficiency for selective hydrogenation of various olefins/nitro-aromatics under ambient conditions (Acham et al., 2014; Kokane et al., 2017). The high activity was attributed to the acidity of the support, which enhanced metal-support interaction and high Pd dispersion thus leading to activation of hydrogen under ambient conditions. To study the effect of different acidic supports with tunable acidity on Pd dispersion, metal-support interaction and in turn on hydrogenation activity, we prepared a series of WO₃/SiO₂ solid acid catalysts by a simple sol-gel method with varying WO₃ loading for supporting Pd and its activity for AP hydrogenation.

2. EXPERIMENTAL SECTION

2.1 Materials

All the reagents, such as palladium acetate, ammonium meta-tungstate (AMT), ethyl silicate-40 (ES-40), and acetophenone, and all the solvents (methanol, ethanol, ethyl acetate, toluene, and hexane) of AR grade quality were procured from Molychem India, Chemplast, Chennai, Sigma Aldrich, and Thomas Baker Chemicals, India, and used as such without further purification.

2.2 Catalyst Preparation

The support WO₃/SiO₂ (WS) with different WO₃ loadings (10, 15, and 20 wt% WO₃ loading on SiO₂) was synthesized by a previously reported method (Kulal et al., 2016), using ES-40 as silica precursor and AMT as WO₃ precursor, respectively, by the sol-gel technique. Subsequently, palladium (0.1, 0.5, 1, and 2%) was loaded on the WS support by a simple impregnation method. The typical synthesis procedure for 20% WO₃/SiO₂ (20WS) and 1% Pd20WS (1P20WS) is described in Sections 2.2.1 and 2.2.2.

2.2.1 Synthesis of 20WS

AMT (5.31 g) was dissolved in 10 mL distilled water and added dropwise into dry IPA solution (35 ml) of ES-40 (50.0 g) with constant stirring. To this solution, 3 mL dil. NH₄OH (2.5%) solution was added and stirred until the formation of a white gel. This resultant gel was air dried and calcined at 500°C in air for 5 h.

2.2.2 Synthesis of 1P20WS

The support 20WS (5 g) was dispersed in 50 mL of methanol. A solution of palladium acetate (0.105 g) in a mixture of methanol (10 mL) and acetone (10 mL) was added dropwise to the slurry of 20WS with constant stirring. This slurry was stirred for 2 h. The solvent was removed on a rotary evaporator. The solid was dried at 100°C and calcined at 250°C in air for 5 h. Similarly, all the catalysts with different palladium loadings (0.1, 0.5, and 2%) supported on 20WS were prepared. Similarly, 1% Pd loaded catalysts on 10WS and 15WS support were prepared. The nomenclature for the catalysts is specified in Table 1.

2.3 Catalysts Characterization

2.3.1 X-Ray Diffraction Analysis

All the synthesized catalysts were characterized by the X-ray diffraction (XRD) method using a PAN analytical X'Pert Pro Dual Goniometer diffractometer. The diffractometer consisted of an X'celerator solid state detector with CuK α ($\lambda = 1.5406 \text{ \AA}$, 40 kV, 30 mA) radiation and a Ni filter. The X-ray diffraction pattern of the sample was collected in the range of $2\theta = 20\text{--}80 \text{ deg}$ with a step size of 0.02 deg and a scan rate of 4 deg min⁻¹.

2.3.2 BET Surface Area Measurements

The Brunauer–Emmett–Teller (BET) specific surface area of the catalyst was determined by the N₂ sorption method at -196°C, using Auto-sorb Quanta Chrome equipment. The sample was pretreated at 200°C under vacuum prior to N₂ adsorption.

TABLE 1: Nomenclature of all xPdyWO₃/SiO₂ catalysts

Sr. No.	Catalyst Name	Wt% of Pd, <i>x</i>	Wt% of WO ₃ , <i>y</i>
1	0.1P20WS	0.1	20
2	0.5P20WS	0.5	20
3	1P20WS	1	20
4	2P20WS	2	20
5	1P15WS	1	15
6	1P10WS	1	10

2.3.3 Chemisorption Studies

The chemisorption study of H₂ was carried out using a Qudrasorb instrument. The catalyst sample (0.15 g) was pretreated at 250°C with 10°C min⁻¹ heating rate, for 2 h. The catalyst was reduced at 400°C in hydrogen for 2 h. The analysis was carried out at 30°C, with the help of stoichiometry of 1:2 of palladium and H₂.

2.3.4 Fourier Transform Infrared Spectroscopic Studies

The Fourier transform infrared (FTIR) spectra of the samples were recorded on a Thermo Nicolet Nexus 670 IR instrument using a deuterated triglycine sulfate detector (DTGS). The KBr pellet method was used for preparation of samples with a resolution of 4 cm⁻¹ in the range of 4000 to 40,000 cm⁻¹ and 100 scans.

2.3.5 X-Ray Photoelectron Spectroscopy Analysis

X-ray photoelectron spectroscopy (XPS) measurements for all the catalysts were carried out using a Thermo K-alpha spectrometer using micro-focused and monochromatic Al K α radiation with energy 1486.6 eV. The samples were degassed at 300 K for 4 h in a vacuum chamber. Charge compensation was done with the help of an electron flood gun. The calibration was done with respect to binding energy (BE) values by referring standard C 1 s peak (284.6 eV) of contaminant carbon.

2.3.6 Electron Microscopy

The morphology of the samples was determined using a scanning electron microscopy (SEM) on a FEI quanta 200 3D dual beam ESEM instrument having a thermionic emission tungsten filament in the 3 nm range at 30 kV. The particle size was determined using transmission electron microscopy (TEM) and analysis was done on a Tecnai G2-20 FEI instrument operating at an accelerating voltage of 300 kV. Before analysis, the powder samples were ultrasonically dispersed in isopropanol, and deposited on a carbon-coated copper grid, dried in air before TEM analysis.

2.4 Catalytic Activity

2.4.1 Hydrogenation of Acetophenone

The catalytic hydrogenation of AP was carried out in a 50 mL two necked round bottom flask at room temperature and 1 atm pressure of H₂. Initially, the catalyst (1P20WS) (0.1 g) was reduced *in situ* in methanol (15 mL) by bubbling H₂ (10 mL/min) for 15 min before each catalytic reaction. Then, AP (1 g, 8.3 mmol) was added to the flask. The reaction mixture was stirred at room temperature with H₂ gas continuously bubbling through the reaction mixture. The reaction was monitored by Gas chromatography (GC) using a GC-Perkin Elmer equipped with a HP-FFAP column (30 m \times 0.25 mm \times 1 μ m) and flame ionization detector (FID). Conversion of AP was calculated based on the GC-FID results, where substrate conversion = (moles of substrate reacted)/(initial moles of substrate used) \times 100 and the selectivity of products was calculated by (total moles of the product formed)/(total moles of substrate converted) \times 100. The product identification was carried out by comparing authentic standard samples in GC and GCMS.

2.4.2 Catalyst Recyclability

The catalyst recycle study was carried out using 1P20WS catalyst for AP hydrogenation under optimized reaction conditions [1 g AP, 0.1 g catalyst, 15 mL methanol as solvent, bubbling H₂, at room temperature (27°C) for 4 h]. After completion of the reaction, the catalyst was separated from the reaction mixture by centrifugation. Then, the catalyst was washed with methanol for two to three times and dried in an oven at 60°C. This dried catalyst was used for further recycle study of the catalyst.

2.4.3 Recycle Study for Styrene Hydrogenation

Recycle study for styrene hydrogenation was carried out using 1P20WS catalyst under similar conditions [1 g styrene, 0.1 g catalyst, 15 mL methanol as solvent, bubbling H₂, at room temperature (27°C) for 4 h]. After completion of the reaction, the catalyst was separated from the reaction mixture by centrifugation. Then, the catalyst was washed with methanol for two to three times and dried in an oven at 60°C. This dried catalyst was used for further recycle study of the catalyst.

2.4.4 Leaching Test

The leaching of Pd in the reaction mixture under the identical reaction conditions was analyzed by the filtration and ICP methods. AP (1 g) and catalyst (0.1 g) were stirred in 15.0 mL of methanol solvent by bubbling H₂ at room temperature (27°C) for 2 h after reducing the catalyst. After 2 h, the catalyst was separated from the reaction mixture by centrifugation and the reaction mixture was further allowed to react under identical reaction conditions without catalyst. ICP-AES analysis of the reaction mixture was carried out to detect any palladium leaching in the reaction.

3. RESULTS AND DISCUSSIONS

3.1 Catalyst Characterization

A series of Pd-WO₃/SiO₂ (PWS) catalysts with Pd loading ranging from 0.1 to 2 wt% on 20% WO₃/SiO₂ (20WS) were prepared by the wet impregnation method using palladium acetate as the palladium precursor. To study the effect of support acidity on catalyst activity, we also prepared catalysts with 1% Pd loading on 10% WS and 15% WS. The acid strength of the WO₃/SiO₂ supports with varying WO₃ loading is shown in Table 2 (Kulal et al., 2016). Increase in the acidity from 0.34 to 0.56 mmol NH₃/g was observed with an increase in the WO₃ loading from 10 to 20%, with maximum acidity for 20WS (0.56 mmol/g) (Kulal et al., 2016).

3.1.1 X-Ray Diffraction Studies

The XRD pattern of all the prepared catalysts were analyzed for its crystalline phases, and the information is provided in Fig. 1. The XRD pattern showed all the characteristic peaks for monoclinic crystalline WO₃ phases, at 23.1, 23.6, 24.2, 26.6, 28.8, and 33.5 deg corresponding to (002), (020), (220), and (202) planes. The XRD patterns also indicate the crystalline nature of the WO₃ phase with an underlying broad peak for amorphous silica centered at 24 deg. The intensities and positions of the peaks are in accordance with the literature (JCPDS No. 43-1035). However, no peaks

TABLE 2: Surface properties of the PWS catalysts

Catalyst	Surface Area (m ² /g)	Pore Size (Å)	Pore Volume (cc/g)	Pd Dispersion (%)	NH ₃ Desorbed (mmol/g)
10WS	553	20	0.56	—	0.34
1P10WS	489	16	0.38	33	—
15WS	438	44	0.96	—	0.35
1P15WS	394	30	0.59	37	—
20WS	289	36	0.53	—	0.56
0.1P20WS	278	26	0.35	40	—
0.5P20WS	274	22	0.30	38	—
1P20WS	264	24	0.31	36	—
2P20WS	255	15	0.34	33	—

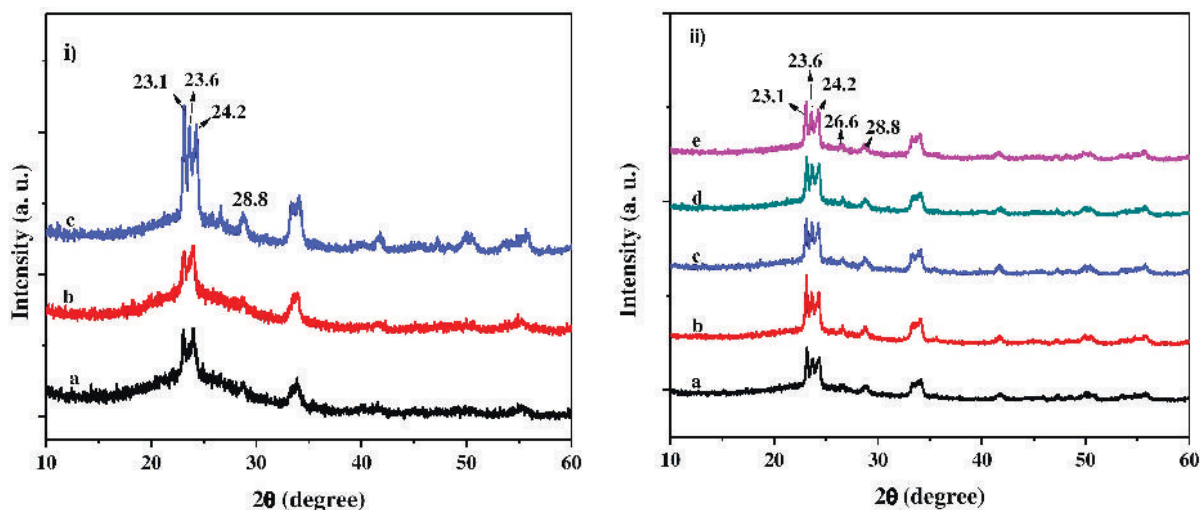


FIG. 1: XRD spectra of (i.a) 1P10WS, (i.b) 1P15WS, and (i.c) 1P20WS; (ii.a) 20WS, (ii.b) 0.1P20WS, (ii.c) 0.5P20WS, (ii.d) 1P20WS, and (ii.e) 2P20WS

corresponding to the palladium were observed in the XRD spectra of the catalysts, even for 2% Pd loading, probably due to low palladium loading and high dispersion on the support.

3.1.2 BET Surface Area Analysis

The surface area of the support and metal dispersion of the Pd loaded catalysts was determined using the BET method, which is given in Table 2. The surface area for the supports decreased with increasing WO_3 loading from $553 \text{ m}^2/\text{g}$ for 10WS to $289 \text{ m}^2/\text{g}$ for 20WS. Similarly, there was a decrease in surface area from $289 \text{ m}^2/\text{g}$ with increasing palladium loading, such as 278, 274, 264, and $255 \text{ m}^2/\text{g}$, respectively, for 0.1P20WS, 0.5P20WS, 1P20WS, and 2P20WS catalysts. There was no specific trend observed in pore size and pore volume. The adsorption-desorption isotherms of all the Pd loaded catalysts are shown in Fig. 2, which show a type IV isotherm pattern for all the catalysts. The metal dispersion was calculated from the H_2 chemisorptions. Very high Pd dispersion on acidic support (Table 2) was observed; 0.1P20WS showed maximum Pd dispersion of 40% followed by 0.5P20WS (38%), 1P15WS (37%), and 1P20WS (36%).

3.1.3 Fourier Transform Infrared Spectroscopy

The FTIR spectra were studied for PWS catalysts using the KBr pellet method (Fig. 3). A very strong band between 1300 and 1000 cm^{-1} for Si-O-Si appeared mainly due to asymmetric stretching, symmetric stretching, and bending vibrations; whereas, $\text{W}=\text{O}_t$ and W-O-W stretching were observed as weak bands at 959 and 806 cm^{-1} . The bands at 467 cm^{-1} are assigned to O-Si-O bending vibrations. The band at 1630 cm^{-1} can be attributed to surface hydroxyl groups.

3.1.4 X-Ray Photoelectron Spectroscopy

XPS was utilized to detect the electronic state of palladium in fresh, activated (reduced in H_2 atmosphere) and used catalysts [Fig. 4(a)]. A palladium 3d core level spectrum of the catalyst with the binding energy (BE) of the $\text{Pd}3d_{5/2}$ peaks at 335.1 eV , corresponding to metallic palladium; whereas, $\text{Pd}3d_{3/2}$ peaks at 336.7 and 336.4 eV , corresponding to Pd^{+2} phases, was observed in the fresh and used catalysts, respectively, indicating presence of both $\text{Pd}(0)$ and $\text{Pd}(+2)$. However, only metallic palladium species ($\text{Pd}3d_{5/2}$ at 335.1 eV) were observed in the activated catalyst, due to complete reduction of Pd^{2+} to Pd^0 , in the presence of hydrogen under ambient conditions. This indicates very

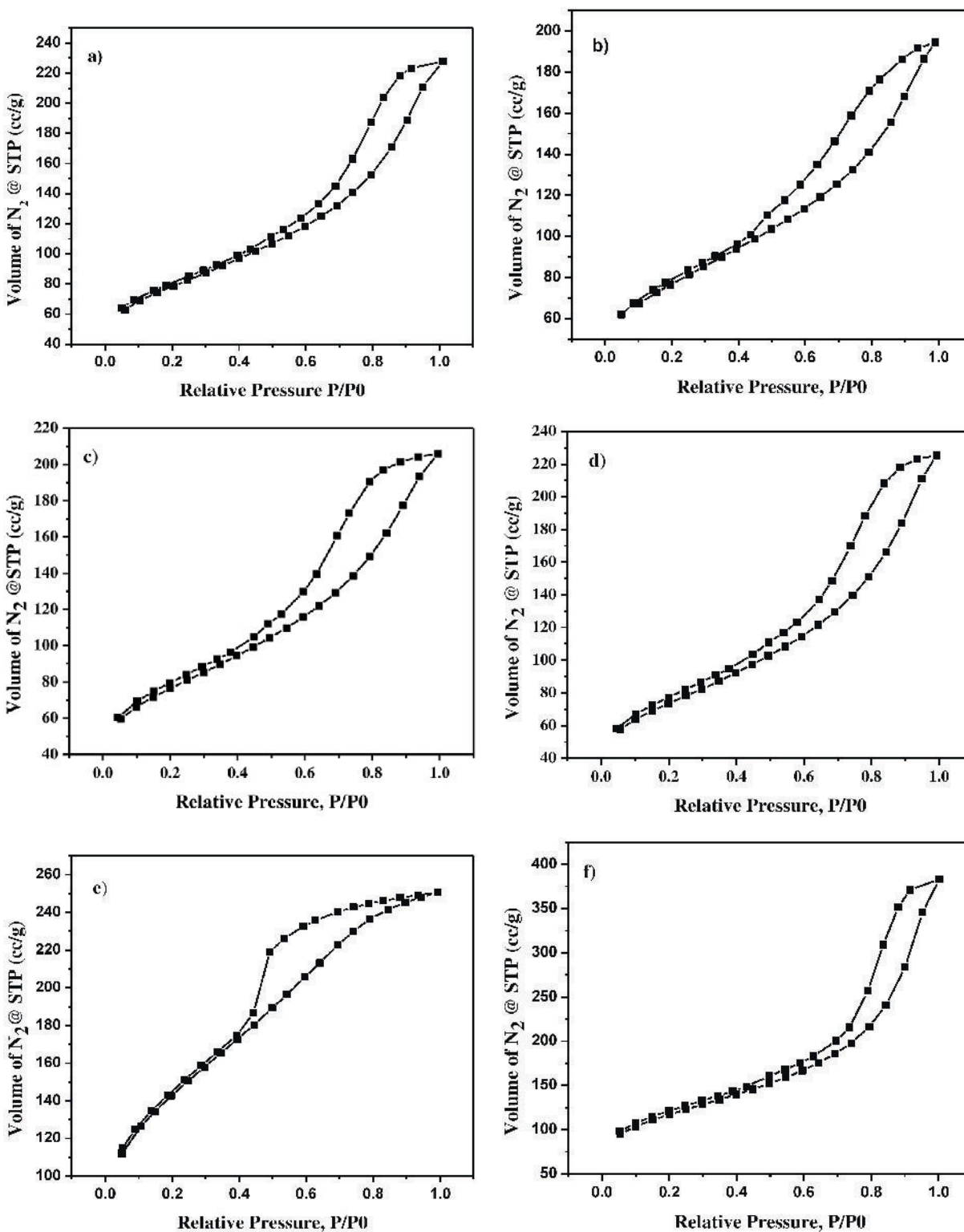
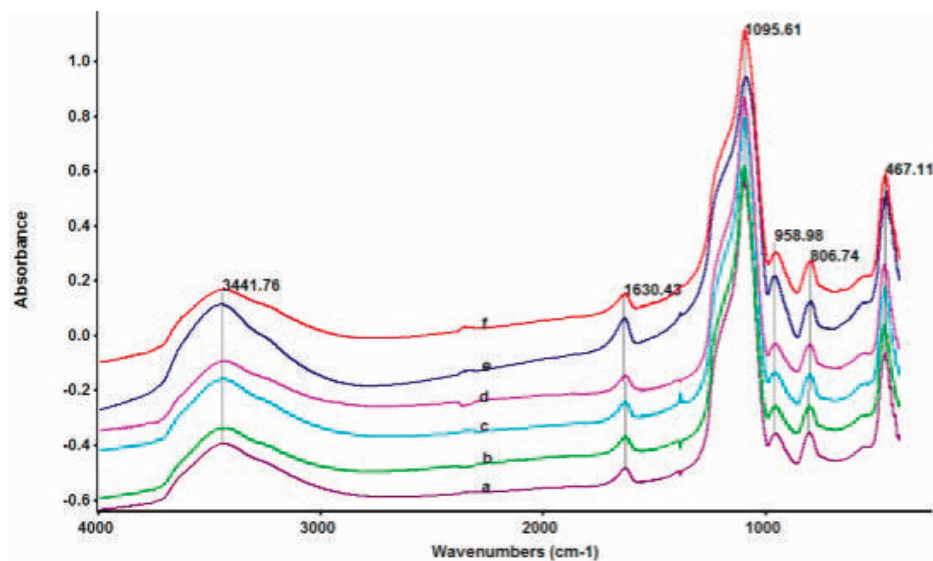
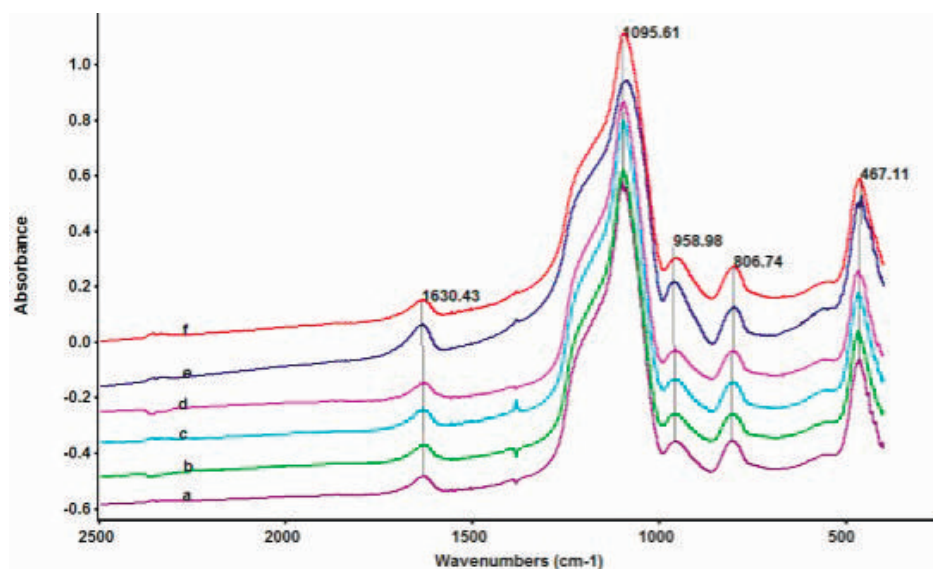


FIG. 2: BET surface area analysis of (a) 0.1P20WS, (b) 0.5P20WS, (c) 1P20WS, (d) 2P20WS, (e) 1P10WS, and (f) 1P15WS



(i)



(ii)

FIG. 3: FTIR spectra of all PWS catalyst in the range of (i) 400 to 40,000 cm^{-1} and (ii) 400 to 2500 cm^{-1}

facile reduction of Pd (+2) to Pd (0) at room temperature and atmospheric pressure. Figure 4(b) represents the W4f core level spectra, where a doublet can be deconvoluted into a pair of peaks with binding energies at 35.1–35.7 eV for W 4f_{7/2} and 37.3–37.8 eV for W 4f_{5/2}, respectively. These peaks can be attributed to +6 oxidation state of tungsten by comparing to earlier literature (Wagner et al., 1991).

3.1.5 TEM Analysis

The palladium particle size was determined using TEM analysis (Figs. 5–9). The catalyst prepared by the impregnation method showed very high dispersion of the palladium particles. Most of the Pd particles were found to be in the

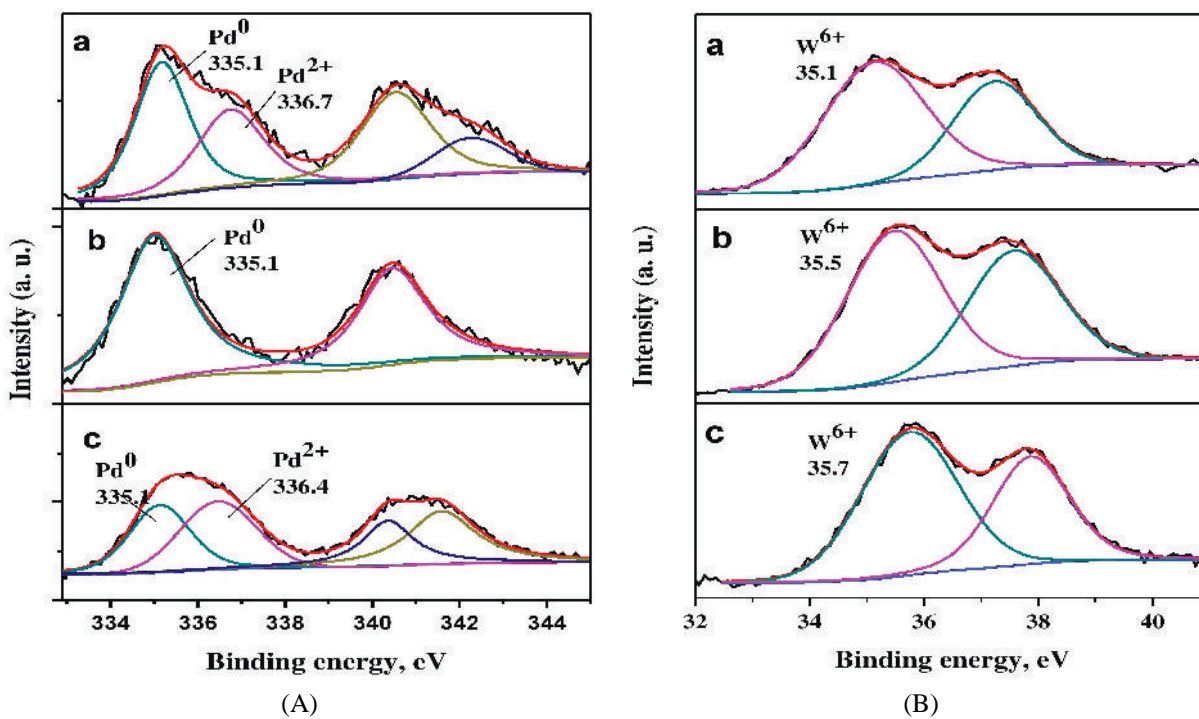


FIG. 4: XPS spectra related to (A) Pd3d and (B) W4f of (a) fresh, (b) activated, and (c) used catalyst

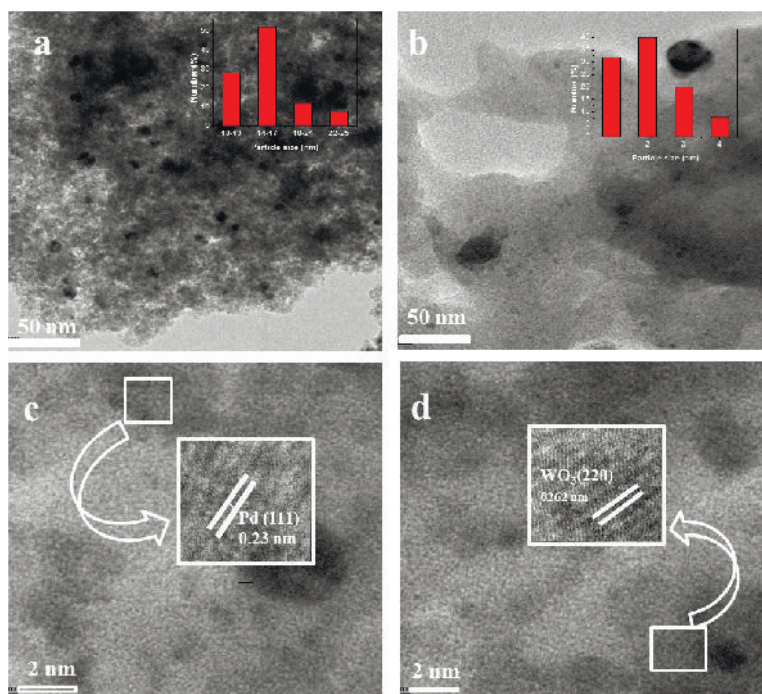


FIG. 5: TEM images of PWS catalyst

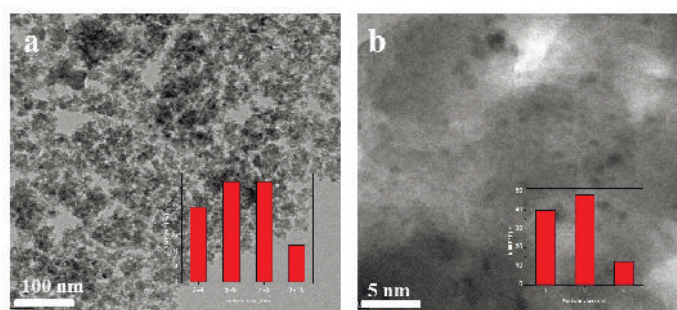


FIG. 6: TEM images of 0.1P20WS catalyst

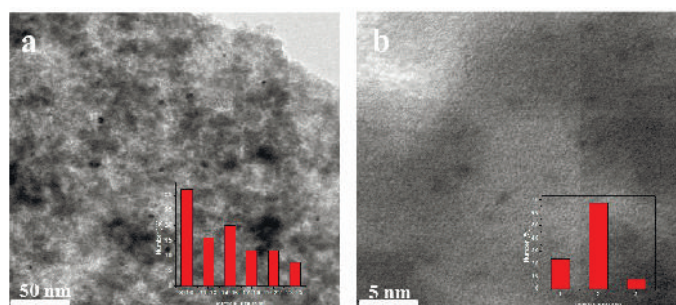


FIG. 7: TEM images of 0.5P20WS catalyst

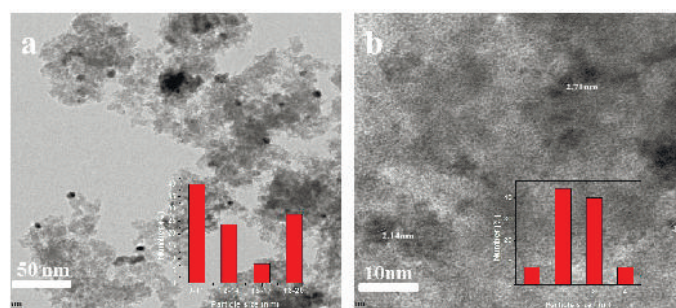


FIG. 8: TEM images of 2P20WS catalyst

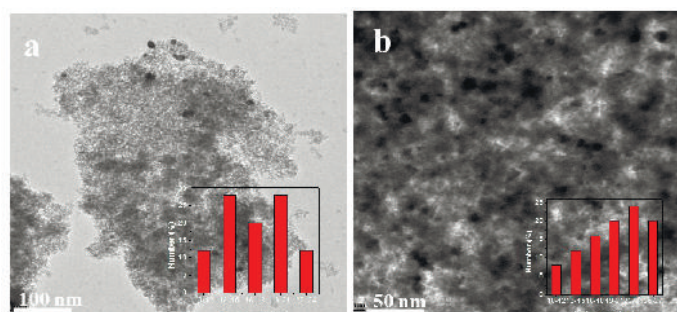


FIG. 9: TEM images of (a) 1P10WS and (b) 1P15WS catalyst

range of 12–18 nm though the particle size distribution, ranged up to 25 nm. The tungsten and palladium particles were distinguished by characteristics d spacing values. Palladium nanoparticles were found to be in the (111) plane as confirmed by characteristics d spacing of 0.23 nm (Yu et al., 2009). The particle size distribution is given in the inset of Figs. 5–9. The particle size distribution ranges over 5–25 nm; however, maximum particles are in the range of 12–18 nm.

As previously reported by Kulal et al. (2016), the formation of very small particles of WO₃ (2–5 nm) dispersed on SiO₂ are formed due to the sol gel preparation method. The loaded palladium has formed nano sheets on WS support, as confirmed from Fig. 5(c). The catalysts showed very high metal dispersion (36%) compared to the literature reports. Palladium dispersion on commercial carbon of a very high surface area (1400 m²/g) was reported to be only 30% for 1% Pd loading (Chary et al., 2007). The Pd (3%) dispersed on a high surface area carbon (844 m²/g) used for nitrobenzene hydrogenation showed only 12.4% Pd dispersion (Turáková et al., 2015). The high metal dispersion can be attributed to the formation of palladium nano sheets on the surface. This observation is in agreement with our previous work where Pd nano sheet formation was observed on acidic MgF_{2-x}(OH)_x support (Acham et al., 2014).

3.1.6 SEM Analysis

SEM images of all the prepared catalysts are shown in Fig. 10. All the catalysts showed almost similar morphology and particle size with some particles in the range of 10–20 μ m and some very small particles of < 5 μ m. Elemental analysis of catalysts carried out by the EDAX technique is presented in Table 3.

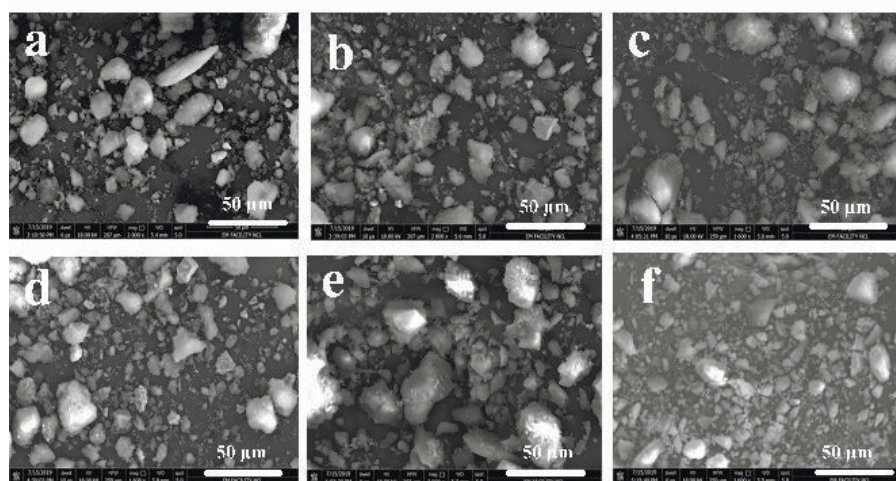


FIG. 10: SEM images of (a) 0.1P20WS, (b) 0.5P20WS, (c) 1P20WS, (d) 2P20WS, (e) 1P10WS, and (f) 1P15WS

TABLE 3: Elemental composition of catalysts by EDAX

Entry	Catalyst	Elemental Composition (%)			
		Pd	W	Si	O
1	0.1P20WS	0.22	4.17	37.49	58.12
2	0.5P20WS	0.32	2.86	35.46	61.36
3	1P20WS	1.43	6.20	35.29	57.08
4	2P20WS	1.62	14.06	24.71	59.62
5	1P10WS	0.78	6.68	30.63	61.73
6	1P15WS	0.97	16.50	36.18	46.73

3.2 Catalytic Activity for Acetophenone Hydrogenation

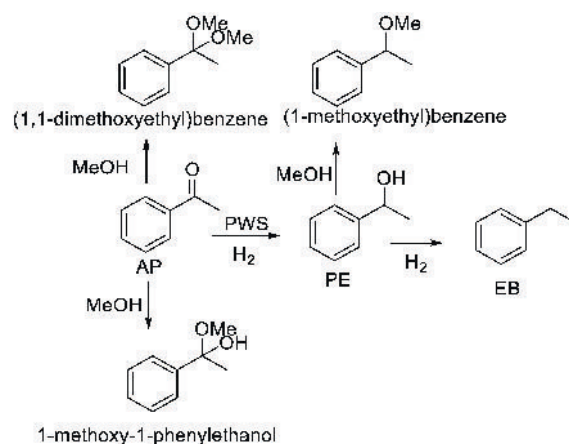
3.2.1 Catalyst Screening

Initially, the catalytic activity of 1% Pd loaded on different supports (WS with different WO₃ loading) for AP hydrogenation was evaluated at room temperature and atmospheric hydrogen pressure (8–10 mL/min) in methanol solvent. For comparison, blank reaction without a catalyst as well as 1% Pd loaded separately on SiO₂ and WO₃ was also carried out. As expected, the blank reaction gave a very poor conversion (~ 1%) after 5 h (Table 4, entry 1), indicating necessity of the catalyst for AP hydrogenation under ambient conditions. The AP conversion after 5 h was 92, 45, and 26% for 1P20WS, 1P15WS, and 1P10WS, respectively; whereas, the PE yield was 76, 25, and 15%, respectively. This trend in conversion and yield is in accordance with the acidity of the support. The acidity trend for the support is as follows: 20WS > 15WS > 10WS (Table 2). The very high activity under ambient condition of the catalysts can be attributed to the very high Pd dispersion on acidic support. This observation is in agreement with our previous results for hydrogenation of styrene under ambient conditions using 1% Pd/MgF_x(OH)_{2-x}, where very high activity was attributed to very high Pd dispersion (48%) and formation of Pd nano sheets on acidic MgF_x(OH)_{2-x} support (Acham et al., 2014). Similarly in the case of PWS catalysts, Pd nano-sheet formation was observed on WS support (Figs. 5–9), explaining the high activity of the catalyst for hydrogenation of AP under ambient conditions. To study the contribution of individual SiO₂ and WO₃ in the catalytic activity, 1% Pd loaded separately on SiO₂ and WO₃ was used for AP hydrogenation under identical conditions and indeed the difference in the activity was observed. Though the conversion after 5 h was almost similar, 24 and 23% (Table 4, entry 5 and 6) for Pd/SiO₂ and Pd/WO₃, respectively, the PE yield was significantly different. PE yield was 12 and 6% for Pd/WO₃ and Pd/SiO₂, respectively, confirming the role of acidity in catalytic activity. In the hydrogenation reaction using PWS catalysts, apart from PE other products formed were EB and hemiketal and ketal of AP as well as methyl ether of PE, as shown in Scheme 2. Ethylbenzene formation can be explained by sequential dehydration of PE to styrene and subsequent hydrogenation. Palladium is well known for a dehydration reaction (Sudhakar et al., 2016). The reaction solvent used was methanol; hence, acid catalyzed hemiketal and ketal formation with AP takes place in the presence of acidic WS support. Similarly, acid catalyzed etherification of PE takes place with solvent methanol leading to undesired by-product formation. The reaction was monitored with time to study the concentration time profile.

TABLE 4: AP hydrogenation using series of PWS catalysts

Sr. No.	Catalyst	Time (h)	Conv. (%)	% Yield of			TON	TOF (h ⁻¹)
				PE	EB	Others		
1	Blank	5	1	< 1	—	—	—	—
2	1P20WS	1	42	14	< 1	—	—	1102
		5	92	76	7	2	2374	—
3	1P15WS	1	29	5	< 1	3	—	471
		5	45	25	1	4	707	—
4	1P10WS	1	15	3	—	1	—	454
		5	26	15	< 1	3	776	—
5	Pd/SiO ₂	1	16	1	—	—	—	248
		5	24	6	—	—	372	—
6	Pd/WO ₃	1	8	4	—	—	—	313
		5	23	12	—	—	983	—

Reaction conditions: 1 g AP (8.3 mmol), 10 wt% catalyst with respect to substrate, 15 ml solvent (methanol), 1 atm H₂ pressure, and RT.



SCHEME 2: Acetophenone hydrogenation products using PWS catalysts

3.2.2 Concentration Time Profile for Acetophenone Hydrogenation

The AP hydrogenation was monitored with time to follow the change in PE yield with AP conversion (Fig. 11). The results showed that, initially with an increase in AP conversion, only PE was formed. After 300 min, the AP conversion increased further, though with a decrease in PE yield with a corresponding increase in EB formation due to dehydration of PE and subsequent hydrogenation to EB. However, the decrease in PE yield (~ 10%) did not match with the corresponding increase in the yield of EB (~ 2%). This may be due to the possibility of polymerization of PE on the catalyst surface (Thakar et al., 2007). To confirm the oligomerization of PE, a control experiment was performed for hydrogenation of PE under identical reaction conditions and the results showed (Table 5) that, after 5 h, the PE conversion was 35% with 7% yield of EB and 1% other products. These results confirmed oligomerization of PE on the catalyst surface under reaction conditions.

It was also observed that, initially up to 1 h of reaction time, the total yield of all the products was significantly lower than the conversion. This could be due to strong physisorption of AP on the catalyst surface. The initial difference in conversion and yield may be attributed to the induction period, during which only acetophenone adsorption

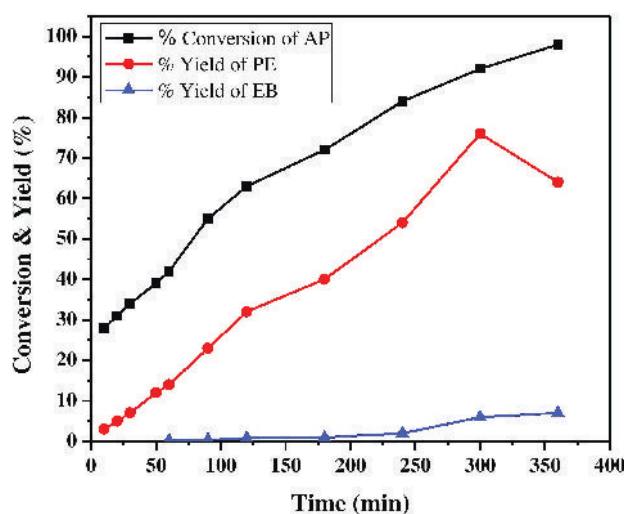


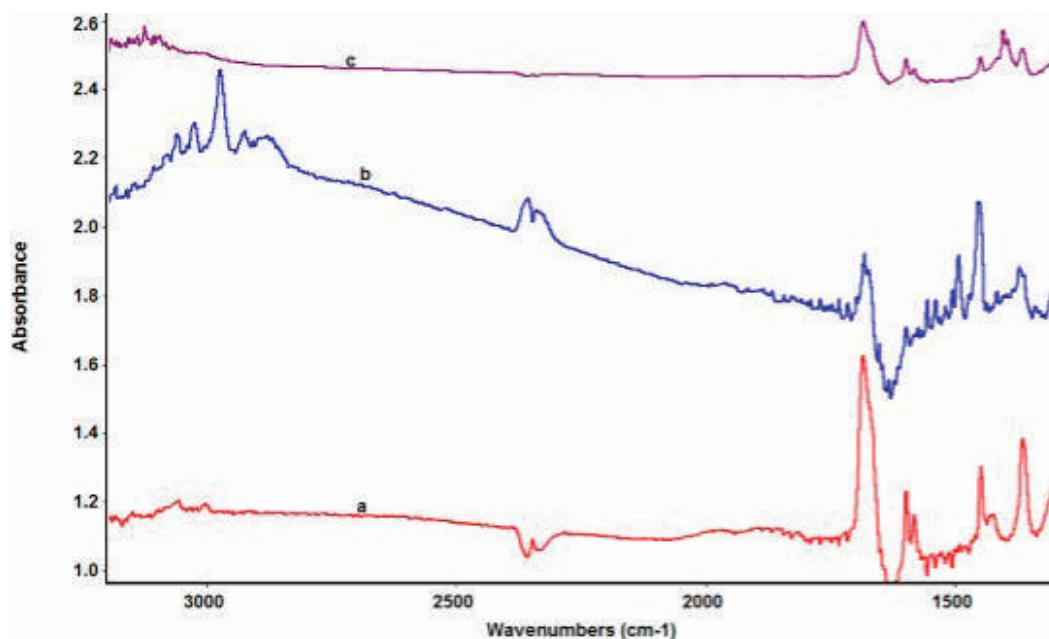
FIG. 11: Time on stream analysis for AP hydrogenation

TABLE 5: Hydrogenation of PE using 1P20WS catalyst

Sr. No.	Time (h)	Conv. (%)	Yield (%) EB	Yield (%) Other
1	1	7	1	< 2
2	2	9	3	< 1
3	3	13	4	< 1
4	4	26	5	< 1
5	5	35	7	< 1

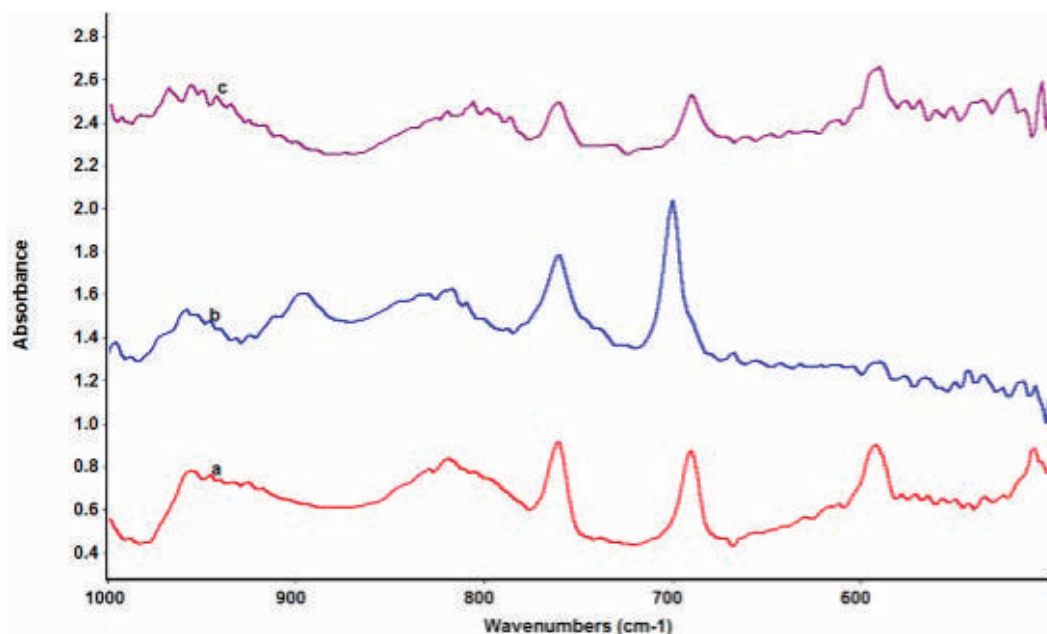
Reaction conditions: 1 g PE, 10 wt% 1P20WS catalyst with respect to PE, Methanol-15 ml, 1-atm H₂ pressure, and RT.

onto the catalyst surface was observed. Later, the yield of the products increased with an increase in the conversion. To confirm this fact, the catalyst was separated from the reaction after 1 h and characterized by FTIR and TGA analysis (Figs. 12 and 13). Indeed, the FTIR spectrum clearly showed the presence of carbonyl and aromatic peaks for AP at 1683 and 800–900 cm⁻¹, respectively, as shown in Fig. 12. Additionally, only support, 20WS, was subjected to the identical reaction conditions for 5 h and the FTIR was recorded after filtration. The spectrum [Fig. 12(ii.c)] also showed the presence of strongly adsorbed AP, indicating the acidic nature of the support to contribute to the adsorption of the AP on the catalyst surface. The TGA analysis (Fig. 13) also indicated weight loss and the presence of exotherm in the catalyst separated after 1 and 5 h, indicating the presence of physisorbed organics on the catalyst surface. Hence, the concentration-time profile along with FTIR and TG/DTA analysis of the catalyst separated after 1 and 5 h indicated an initial adsorption of AP on the catalyst surface and later the oligomerization of PE on the catalyst surface, giving rise to a difference in the AP conversion and total yield of the products as analyzed by GC.



(i)

FIG. 12.



(ii)

FIG. 12: FTIR spectra of PWS catalysts in the range of (i) 1300 to 3200 cm⁻¹ and (ii) 500 to 1000 cm⁻¹, and (a) 1P20WS catalyst isolated from reaction mixture after 1 h after subtraction of the fresh 1P20WS catalyst, (b) 1P20WS catalyst isolated from reaction mixture after 5 h after subtraction of reduced 1P20WS catalyst, and (c) support (WO₃/SiO₂) isolated after 5 h reaction time after subtraction of fresh support

3.2.3 Effect of Solvent

The effect of different solvents on AP conversion and PE yield was studied using a range of polar (methanol, ethanol) and nonpolar solvents (hexane, toluene), and the results are shown in Fig. 14. In the case of polar solvents, the conversion was 92 and 65% for methanol and ethanol with 78 and 58% PE yield, respectively. In the case of nonpolar solvents such as hexane and toluene, AP conversion was 67 and 37%; however, PE yield was significantly lower for both solvents with 42 and 30%, respectively. A very high AP conversion was obtained in polar solvents with the better yield of PE as compared to the nonpolar solvents. This may be due to a high dipole moment, high dielectric constant, and also high hydrogen donor ability of polar solvents (Yoshida et al., 2015). High AP conversion and PE yield was observed in the case of methanol solvent. This may be attributed to the polarization and activation of the C = O bond. In the case of the protic solvent, due to the hydrogen bonding the chances of hydrogenolysis of C-OH reduces, which leads to the higher yield of PE compared to EB. In the case of nonpolar solvents, as they have a low dipole moment and no hydrogen donor ability, the catalytic activity is low compared to the polar solvents. Because there is no possibility of hydrogen bonding, this may further lead to the hydrogenolysis of the C-OH bond faster than the polar solvents, resulting in a high yield of EB compared to the polar solvents.

3.2.4 Effect of Catalyst Loading

The effect of catalysts loading on AP conversion and PE yield was studied (Fig. 15). It is very clear from the results that, with an increase in the catalyst loading gradually from 5 to 10 wt%, the PE conversion after 5 h increased from 68 to 92%; whereas for 15% catalyst loading, an almost 98% conversion was achieved in only 3 h. The PE yield increased from 28 to 78% for 5 and 10 wt% catalyst loading, respectively; however, a further increase in the catalyst loading to 15%, decreased the PE yield to 52% with formation of 4% EB, 1% each of methyl ether of PE, ketal, and hemiketal. This decrease in the PE yield with an increase in the catalyst loading to 15% may be attributed to the

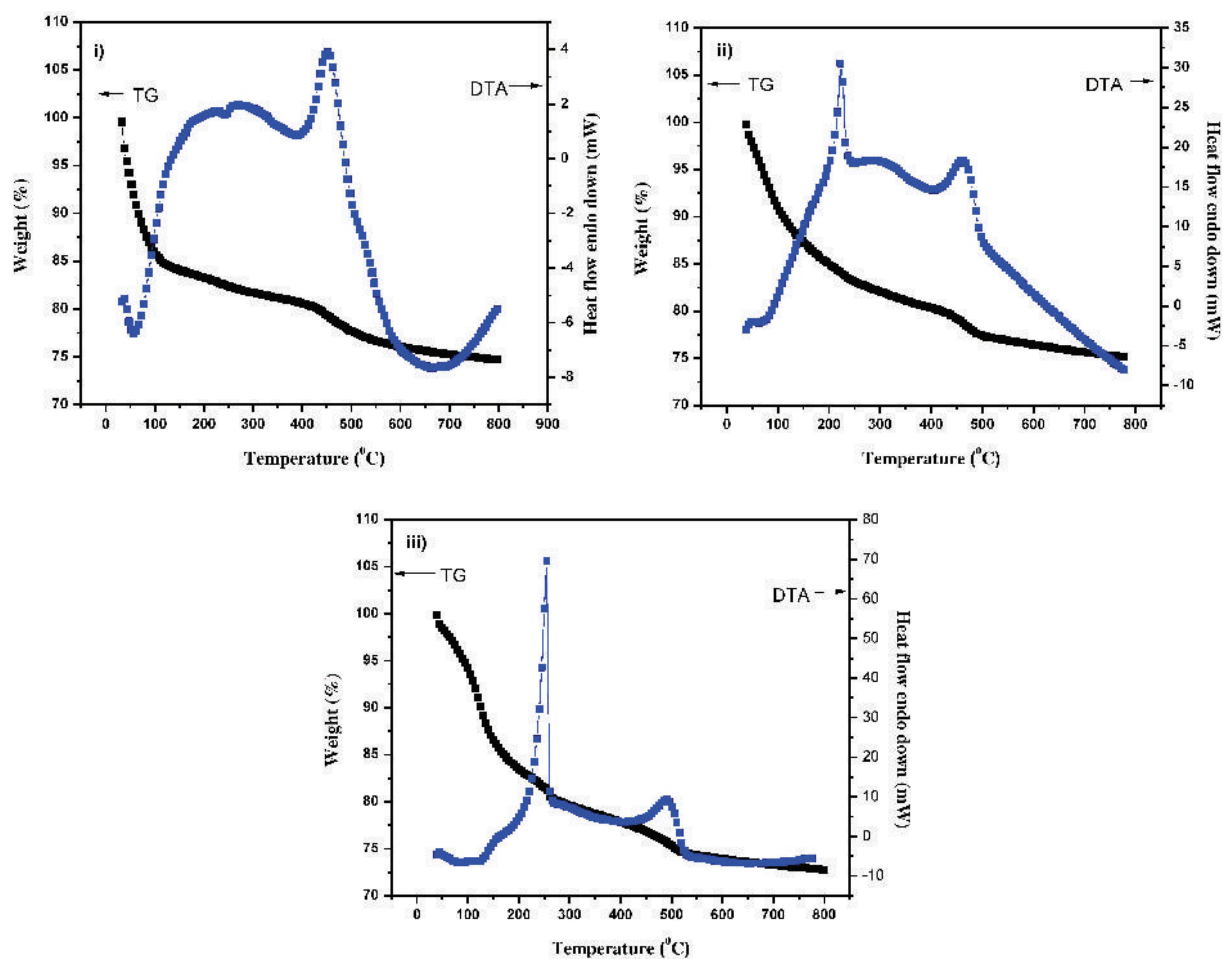


FIG. 13: TG/DTA curves of 1P20WS (i) fresh catalyst, (ii) catalyst isolated after 1 h, and (iii) used catalyst

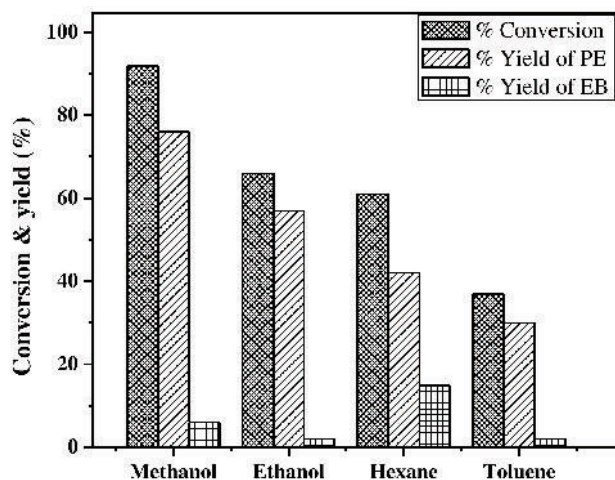


FIG. 14: Effect of solvent on AP hydrogenation

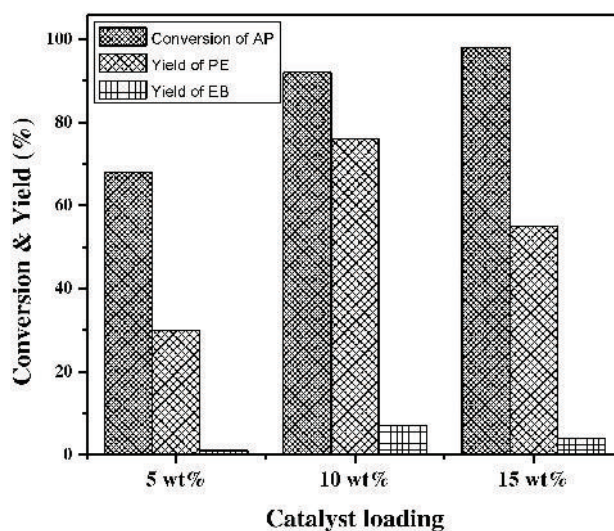


FIG. 15: Effect of catalyst loading on AP hydrogenation

higher oligomerization of PE on the catalyst surface. As, the conversion and yield was maximum for 10 wt% catalyst loading, further optimization was carried out using the same catalyst loading (10 wt% with respect to AP).

3.2.5 Effect of Palladium Loading

The effect of Pd loading on 20WS support was studied for AP hydrogenation, and the results are summarized in Table 6. When Pd loading was gradually increased from 0.1 to 1% on 20WS support, there was a gradual increase in AP conversion from 30 to 92 % and yield of PE from 5 to 76% after 5 h. When Pd loading was further increased to 2%, there was increase in the conversion (96%); however, with a decrease in the PE yield (72%) after 3 h. This can be attributed to accelerated dehydration of PE to styrene (3%) and subsequent hydrogenation to EB (5%) due to high Pd loading. Recent reports confirmed that palladium is responsible for dehydration reactions (Sudhakar et al., 2016).

TABLE 6: Effect of palladium loading on AP hydrogenation using Pd20WS catalyst

Sr. No.	Palladium Loading	Time (h)	Conv. (%)	% Yield of			TON	TOF (h ⁻¹)
				PHE	EB	Others		
1	0 (WS)	1	11	—	—	2	—	—
		5	18	—	—	4	—	—
2	0.1%	1	25	1	—	2	—	6111
		5	30	5	—	4	6746	—
3	0.5%	1	33	4	—	2	—	2222
		5	49	31	—	3	3252	—
4	1%	1	42	14	1	—	—	1102
		5	92	76	7	2	2374	—
5	2%	1	46	28	1	1	—	647
		3	96	72	5	11	1359	—

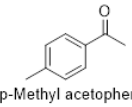
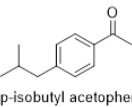
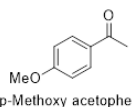
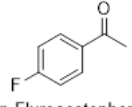
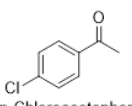
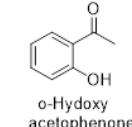
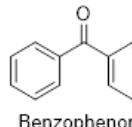
Reaction condition: 1g AP (8.3 mmol), 10 wt% catalyst with respect to substrate, 15 ml solvent (methanol), 1 atm H₂ pressure, and RT.

Acid catalyzed (20WS) etherification of PE with methanol (8%) was also observed, leading to a further decrease in the PE yield.

3.2.6 Effect of Different Substituents on Acetophenone

To establish the wider applicability of the catalyst, hydrogenation of various substituted acetophenones, including some industrially important substrates, was carried out using 1P20WS catalyst in methanol solvent (Table 7) under optimized conditions. The rate of hydrogenation was affected by electronic and steric effects of substituents on aromatic ring. The rate of hydrogenation was higher for AP with the electron donating groups than for the unsubstituted AP except for 2-hydroxy acetophenone. The hydrogenation of *p*-methyl acetophenone was very fast, with a 34%

TABLE 7: Hydrogenation of different substituted AP using 1P20WS catalyst

Sr. No.	Substrate	Time (h)	Conv. (%)	% Selectivity of Product			TON	TOF (h ⁻¹)
				Phenyl Ethanol	Ethyl Benzene	Other		
1	 p-Methyl acetophenone	1	34	97	3	—	—	728
		5	96	86	10	4	2056	—
2	 p-isobutyl acetophenone	1	18	100	—	—	—	301
		5	82	91	8	1	1371	—
3	 p-Methoxy acetophenone	1	19	63	11	26	—	371
		5	95	43	39	18	1855	—
4	 p-Fluoroacetophenone	1	16	100	—	—	—	340
		5	80	97	3	—	1698	—
5	 p-Chloroacetophenone	1	30	23	53	24	—	572
		5	73	22	53	25	1392	—
6	 o-Hydroxy acetophenone	5	No reaction	—	—	—	—	—
7	 Benzophenone	1	6	83	—	17	—	97
		5	19	88	—	12	307	—

Reaction conditions: Substrate (8.3 mmol), 10 wt% catalyst with respect to substrate, 15 ml solvent (methanol), 1 atm H₂ pressure, RT, and time 5 h.

conversion after 1 h with 97% selectivity for 1-(4-methyl phenyl) ethanol with high TOF 728 h⁻¹ (Table 7, entry 1). As the steric effect of the alkyl substituted group increased, the rate of hydrogenation decreased. Hence, the rate of hydrogenation of *p*-alkyl acetophenone over 1P20WS decreased in order *p*-Me > *p*-*i*-Bu (Table 7, entry 1 and 2). Hydrogenation of 4-isobutyl acetophenone gives 1-(4-isobutyl phenyl) ethanol, which is an intermediate in the synthesis of the ibuprofen drug. This drug is used as a nonsteroidal and anti-inflammatory drug to reduce swelling and inflammation.

Nickel-based catalysts have been reported previously for this hydrogenation, however, at high temperature (100–140°C) and high pressure (2–6 MPa) (Rajashekharam and Chaudhari, 1996); whereas using the present catalyst, the hydrogenation of 4-isobutyl acetophenone could be achieved under ambient conditions with an 82% conversion and 91% selectivity after 4 h with very high TOF of 301 h⁻¹ (Table 7, entry 2). In the case of *p*-methoxyacetophenone, a 95% conversion was obtained after 5 h, but with a lower selectivity (43%) for corresponding PE (Table 7, entry 3). Due to the electron donating effect of the *p*-methoxy group, along with dehydration of PE to EB, it also gave methyl ether of corresponding PE, decreasing the selectivity for desired product.

In the case of *para*-fluoro and *para*-chloroacetophenone, the conversion obtained was 80 and 73%, respectively (Table 7, entries 4 and 5). However, the selectivity for corresponding PE was very low in case of *para*-chloroacetophenone; due to facile Pd catalyzed hydro dechlorination. Generally, palladium-based catalysts are well known for hydro-dehalogenation. The hydrogenation of *p*-chloroacetophenone gave only 22% 1-(4-chloro phenyl) ethanol along with 53% dechlorinated EB and acetophenone. There was no conversion in the case of *ortho*-hydroxyacetophenone. This may be due to *ortho*-steric effect of the -OH group and/or higher stability of the substrate due to intramolecular hydrogen bonding (Table 7, entry 6). The hydrogenation of benzophenone was also carried out using 1P20WS catalyst, however with very slow rate, may be due to steric effect of two phenyl ring in molecule. It gave only 19% conversion of benzophenone with 88% selectivity for biphenyl methanol after 4 h (Table 7, entry 7).

There are several reports published on hydrogenation of AP using different transition metal-based catalysts, and some of the work is summarized in Table 8. From the literature reports, it is very clear that hydrogenation of AP is carried out at higher temperatures and/or high pressures. For hydrogenation under milder conditions, high noble metal loading was needed. Copper supported on a SiO₂ catalyst is reported for 100% conversion of AP at high temperature and pressure (Bertero et al., 2008). Platinum supported on alumina with 1 wt% platinum loading has shown good catalytic activity for hydrogenation of AP at room temperature and atmospheric pressure (Liu et al., 2009). Although Pt/Al₂O₃ has provided very high conversion of AP, significantly higher cost of platinum is an issue of concern. Palladium supported on carbon (Hiyoshi et al., 2011; Fujita et al., 2016) and carbon nanotubes (Xiang et al., 2011) has shown very high catalytic activity for AP hydrogenation at lower temperature and pressure within a short period of time, however at high palladium loading (up to 5%). Sodium promoted 5% Pd/C catalyst has shown 100% AP conversion with 96.4% selectivity for PE at 20 bar hydrogen pressure and 70°C (Cho et al., 2013). Hydrogenation of AP with a 97% conversion and 100% selectivity at very high temperature (160°C) and 10 bar pressure has been reported using an Ag-OMS-2 catalyst (Yadav and Mewada, 2012). Pd/NiO catalyst has yielded only 19% conversion (Gou et al., 2013) for hydrogenation of AP. Ni- and Co-based catalysts required high temperature (80–180°C) and high pressures (10–30 bar) for hydrogenation of AP (Costa et al., 2019; Wang et al., 2018; Zhang et al., 2019). Compared to the literature report, the present catalyst 1P20WS has provided efficient AP hydrogenation under ambient conditions. The hydrogenation of AP was carried out at atmospheric pressure and room temperature using 1P20WS catalyst with very high conversion (92%) and PE yield (76%). The high catalytic activity of the PWS catalyst can be correlated to very high surface area, mesoporous nature, and high acidity of the catalyst leading to formation of Pd nano sheets and, in turn, very high Pd dispersion on the catalyst surface.

3.2.7 Recycle Study

The recyclability of the 1P20WS catalyst was tested for AP hydrogenation and the results are shown in Fig. 16. The AP conversion for the fresh catalyst was 95%, which decreased to 60% for the second use with a simultaneous decrease in the PE yield from 78 to 49% (recycle 1). The results showed non-recyclability of the 1P20WS catalyst for AP hydrogenation. To understand the reason for catalyst deactivation, Pd leaching was analyzed by ICP and the used catalyst was additionally characterized in detail.

TABLE 8: Literature survey for hydrogenation of AP

Sr. No.	Catalyst	Solvent	Temp. (°C)	Pressure	Time (min)	Conv. (%)	Sel. PE (%)	Refs.
1	6.8% Cu/SiO ₂	Isopropanol	90	20 bar (total) 18.7 (H ₂)	300	100	> 99	Bertero et al., 2008
2	1% Pt/Al ₂ O ₃	Methanol	RT	0.6 MPa	24 h	89	98	Liu et al., 2009
3	5% Pd/C	H ₂ O/CO ₂	40	3 MPa	45	100	95	Hiyoshi et al., 2011
4	3% Pd/CNTs	Ethanol	60	10 ml/min	240	95	97	Xiang et al., 2011
5	15% Ag-OMS-2	Isopropanol	160	10 bar	180	97	100	Yadav and Mewada, 2012
6	1% Pd/NiO	Ethanol	80	1.3 MPa	180	19	92	Gou et al., 2013
7	5% Pd/C	Water in presence of CO ₂	80	CO ₂ -1 MPa H ₂ -4 MPa	60	80	100	Fujita et al., 2016
8	5 wt% Pd/SA (amorphous silica–alumina)	n-hexane	60	—	5	12	100	Chen et al., 2018
9	Na-5% Pd/C	Ethanol	30–70	20 bar	2–9 h	100	96.4	Cho et al., 2013
10	80% Ni ₂ P/Al ₂ O ₃	33.3 wt% AP in ethanol	180	3 MPa	H ₂ /AP 5 (molar ratio)	100	95.6	Wang et al., 2018
11	5% NiP/MSNS	n-heptane	80	1 MPa	—	30	95	Costa et al., 2019
12	16.7% Co/Mordernite	Water	100	2 MPa	360	99.9	100	Zhang et al., 2019
13	1P20WS	Methanol	RT	10 ml/min	300	92	76 (yield)	Present work

3.2.8 Leaching Test and ICP Analysis of Reaction Mixture

After completion of 50% reaction, the catalyst was filtered and the reaction mixture without the catalyst was allowed to react further for 4 h under identical reaction conditions (Fig. 17). Even after an additional 4 h reaction, there was no increase in the conversion indicating no Pd leaching in the reaction. Additionally, ICP analysis of the reaction mixture indicated no Pd in the liquid reaction mixture, confirming almost no leaching of the Pd from the catalyst surface (0.53 ppm). Hence, the used catalyst was further characterized in detail to understand the cause of deactivation.

3.3 Characterization of Used Catalyst

3.3.1 XRD Analysis

The powder XRD spectra of fresh and used catalysts are shown in Fig. 18. No change in the diffraction pattern of the used catalyst was observed compared to the fresh catalyst. However, the intensity of the WO₃ peaks in the used catalyst decreased compared to the fresh catalyst, indicating a more amorphous nature of the used catalyst.

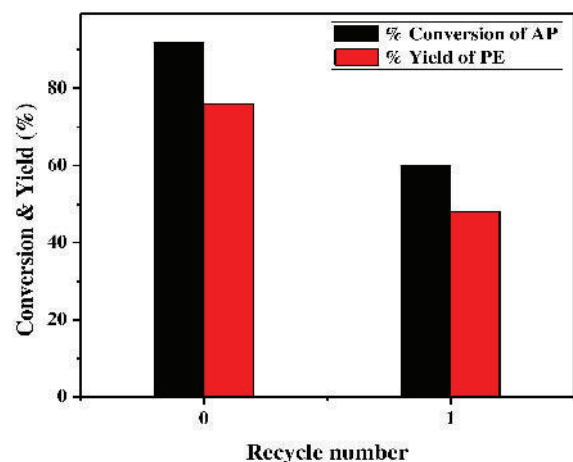


FIG. 16: Recycle study of 1P20WS catalyst for acetophenone hydrogenation

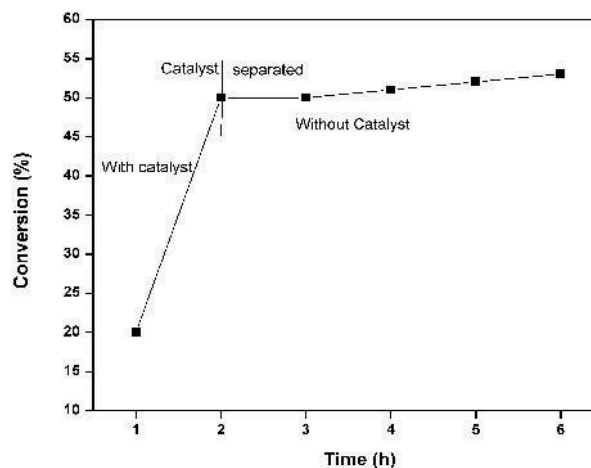


FIG. 17: Conversion of AP after filtration of catalyst

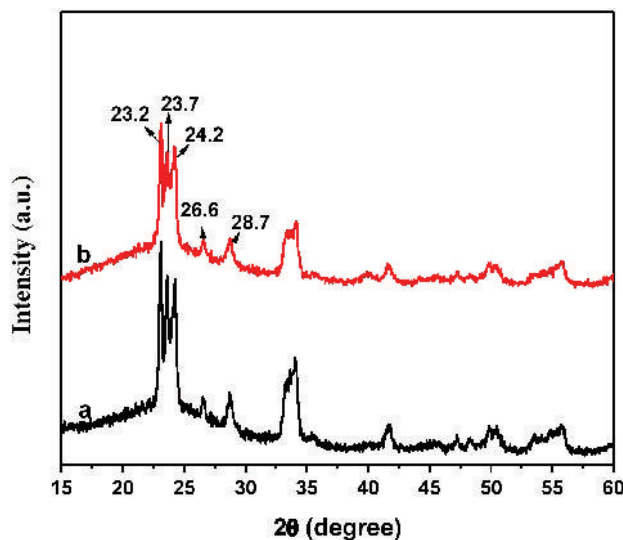


FIG. 18: XRD pattern of (a) fresh and (b) used 1P20WS catalysts

3.3.2 High-Resolution TEM Analysis

The high-resolution TEM (HRTEM) analysis of the fresh and used catalyst is presented in Figs. 19 and 20. The HRTEM image showed no change in the particle size of the fresh and used catalyst. The particle size was found to be in the range of ~ 12–15 nm. Also, no change in the elemental composition in the fresh and used catalyst was observed, confirming no leaching of Pd in the reaction mixture.

3.3.3 Thermogravimetry and Differential Thermal Analysis

The thermogravimetry (TG) and differential thermal analysis (DTA) (TG/DTA) curves of the fresh and used catalysts are shown in Fig. 13. The results showed the total weight loss in the fresh and used catalysts to be about 25 and 27 wt%, respectively. However, the weight loss in the temperature range of 30–100°C for physisorbed water was 13.9 and 5.7%, respectively, for fresh and used catalysts, indicating higher physisorbed water on the fresh catalyst.

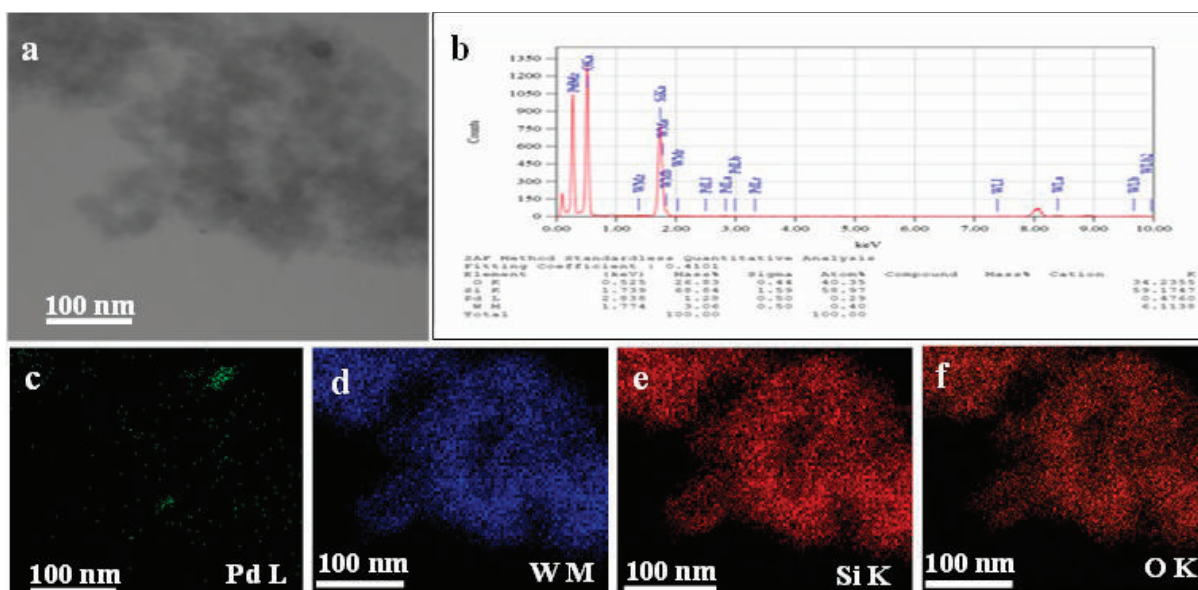


FIG. 19: HRTEM data of fresh 1P20WS catalyst

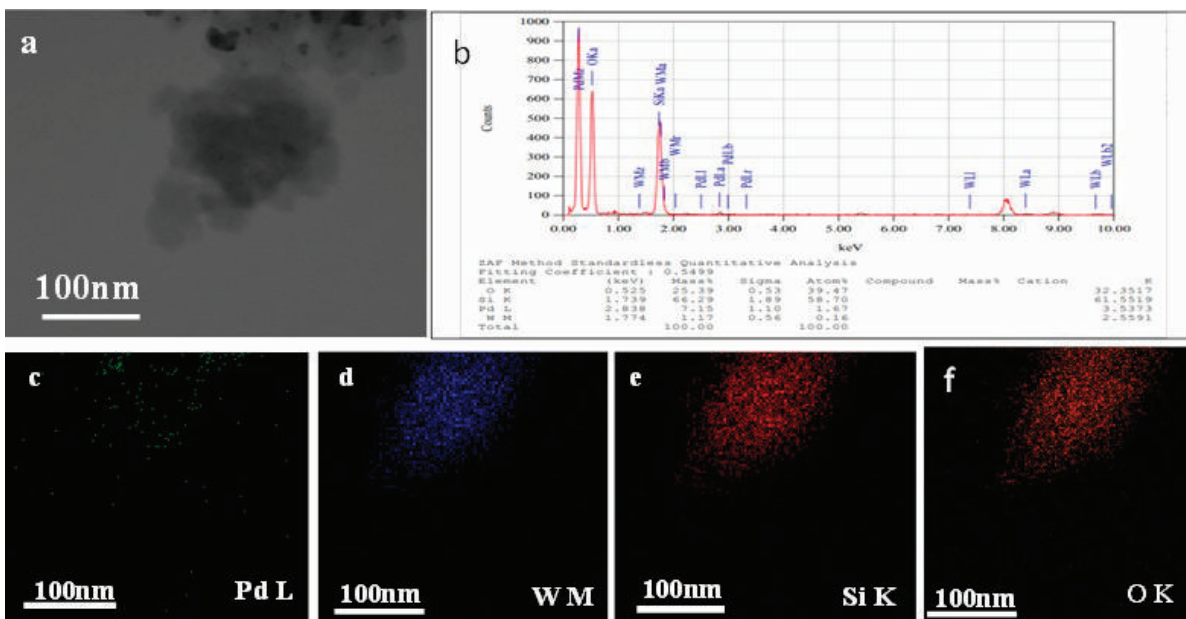


FIG. 20: HRTEM data of used 1P20WS catalyst

The weight loss in the temperature range of 100–250°C for physisorbed organics was significantly higher for the used catalyst (12.5%) compared to the fresh catalyst (3.3%), indicating strong adsorption of organic moieties like reactant/products on the catalyst surface contributing to catalyst deactivation. This is also supported by the highly intense exotherm observed in DTA analysis at 256°C for the used catalyst (heat flow 70 mW) compared to the fresh catalyst (heat flow 4 mW), confirming combustion of organics at that temperature.

From abovementioned characterization of the used catalyst, it is clear that there is no change in the morphology of the used catalyst. In a review article by Argyle and Bartholomew (2015), different reasons for catalyst deactivation

were discussed. One of the reasons was strong chemisorption of species on catalytic sites, which block active sites for catalytic reaction. TGA of the used catalyst showed strong adsorption of the reactant and products on the catalyst contributing to the catalyst deactivation. In the present case, the oligomerisation of the PE was also confirmed by hydrogenation of PE under identical conditions, where a significant difference in PE conversion and product yield was observed on the catalyst surface, as shown in Table 5. To confirm that, the deactivation and non-recyclability of the 1Pd20WS catalyst is substrate-specific for only AP hydrogenation due to the tendency of the product PE to undergo oligomerization on the catalyst surface, and this catalyst was used for hydrogenation of styrene and a subsequent recycle study (see Table 9). The results clearly indicated very high efficiency of the catalyst 1Pd20WS for recycle in hydrogenation of styrene to EB. Hence, this catalyst can be recycled efficiently for the hydrogenation reactions where the substrate, product, or intermediate does not adsorb very strongly or oligomerize on the catalyst surface.

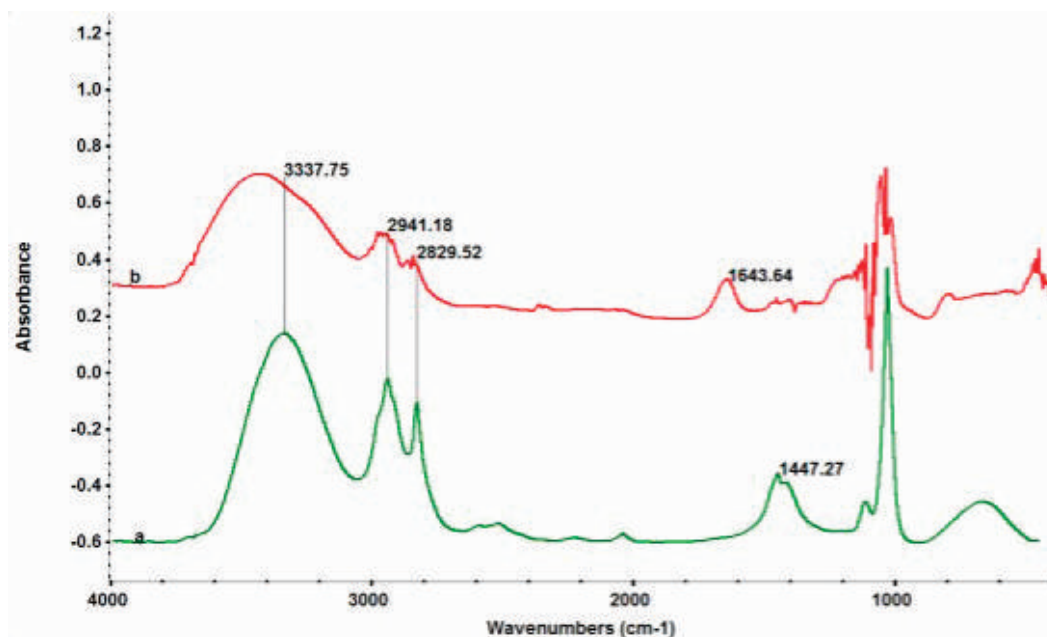
3.4 Mechanistic Study of AP Hydrogenation on 1P20WS Catalyst

The mechanism of AP hydrogenation over the 1P20WS catalyst was studied by analyzing interaction of reactant/product, solvent methanol, and reaction mixture on the catalyst (pre-reduced in hydrogen) surface. To study the interaction of adsorbed species on the catalyst surface, all spectra were reported after subtraction of the neat catalyst (reduced). A drop of methanol, AP, or final reaction mixture was added on the catalyst wafer, and the FTIR spectrum was recorded. All FTIR spectra are shown in Fig. 21. The FTIR spectrum of pure methanol [Fig. 21(a)] showed peaks at 1447 and 3338 cm⁻¹ for bending and stretching vibrations of the Me-O-H group, respectively. The spectrum of methanol adsorbed on the catalyst surface showed the disappearance of peak at 1447 cm⁻¹ with appearance of peak at 1643 cm⁻¹, which can be attributed to formation of surface hydroxyl groups [Fig. 21(b)]. The appearance of a broad peak centred around 3500 cm⁻¹ also indicated the formation of surface hydroxyl groups by dissociation of the MeO-H bond to form MeO- and surface-OH groups. This means that methanol adsorbed dissociatively on the WO₃ group to form W-OMe and W-OH (Ge and Gutowski, 2015). To find out the interaction of AP with the catalyst surface, AP was adsorbed on the catalyst (pre-reduced) wafer and the FTIR spectrum was recorded. The difference spectrum was compared to authentic AP [Fig. 21(ii.a)]. Also, the FTIR spectrum of the catalyst filtered after 1 h reaction time [Fig. 21(ii.c)] was recorded. The final reaction mixture was adsorbed on the catalyst wafer [Fig. 21(ii.d)] and compared to the authentic AP spectrum [Fig. 21(ii.b)]. There was no shift observed in the spectrum of the adsorbed AP in the carbonyl region on the catalyst surface [Fig. 21(ii.a)] compared to the authentic AP, indicating no direct activation of AP on the catalyst surface through the carbonyl group. However, the catalyst filtered after 1 h [Fig. 21(ii.c)] and final reaction mixture [Fig. 21(ii.d)] showed a shift in two peaks, i.e., 1265–1270 cm⁻¹ and 1359–1365 cm⁻¹ [Figs. 21(ii.c) and 21(ii.d)]. Chen et al. (2018) reported that the band at 1697 cm⁻¹ is attributed to the stretching vibration of AP when adsorbed on Pd by η¹ coordination [Fig. 22(i)]; whereas, AP adsorbed on the catalyst surface by the X-sensitive benzene mode [Fig. 22(ii)] showed a band at 1276 cm⁻¹. The band at 1365 cm⁻¹ is attributed to a bending mode of CH₃. This clearly indicated the adsorption of AP on the catalyst surface through an aromatic ring and not through the carbonyl group. The spectrum of the final reaction mixture also showed a very marginal shift in carbonyl and from 1683 to 1680 cm⁻¹. The marginal shift may be due to activation of the carbonyl group of AP by surface hydroxyl groups through hydrogen bonding.

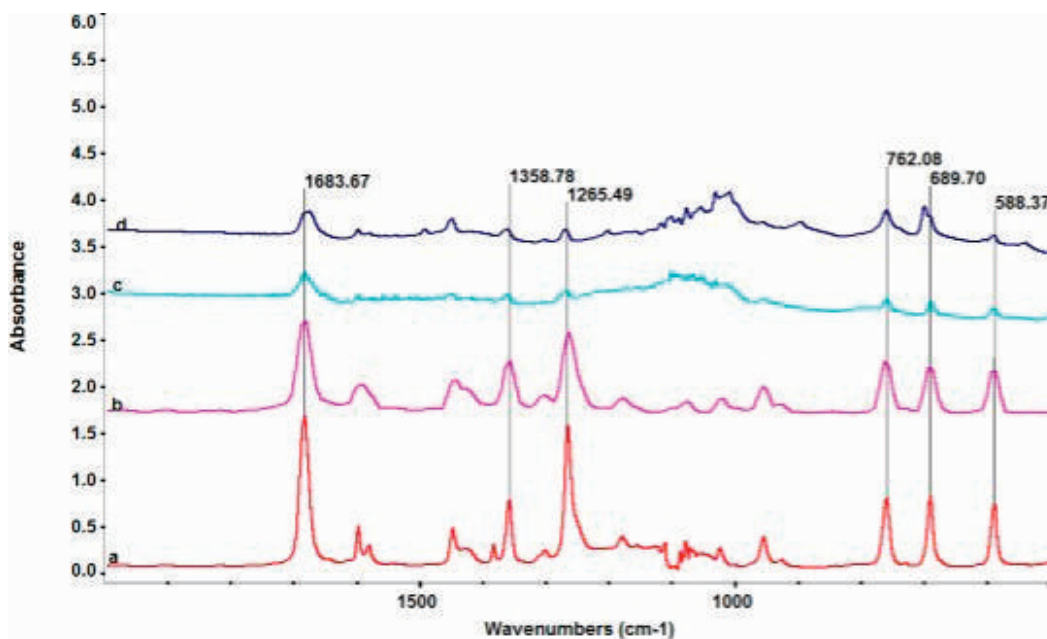
TABLE 9: Recycle study of 1Pd20WS for styrene hydrogenation

Sr. No.	Run	Conv. (%)	Selectivity (%) EB
1	0	81	100
2	1	80	100
3	2	81	100
4	3	81	100

Reaction conditions: 1g styrene, 10 wt% catalyst (1Pd20WS) with respect to substrate, 15 ml solvent (methanol), 1-atm H₂ pressure, RT, and time 4 h.



(i)



(ii)

FIG. 21: FTIR spectra of (i.a) pure methanol, (i.b) methanol adsorbed on catalyst, (ii.a) AP adsorbed on catalyst, (ii.b) pure AP, (ii.c) catalyst filtered after 1 h reaction time, and (ii.d) final reaction mixture adsorbed on reduced catalyst

Considering all above observations, the hydrogenation of AP using the 1P20WS catalyst can be attributed to the facile activation of hydrogen on the Pd site and simultaneous adsorption of AP on support through the aromatic ring and activation of the carbonyl group by the surface hydroxyl group. On the basis of the FTIR study, the proposed mechanism for the AP hydrogenation is shown in Fig. 23. Initially, methanol gets dissociatively adsorbed on the

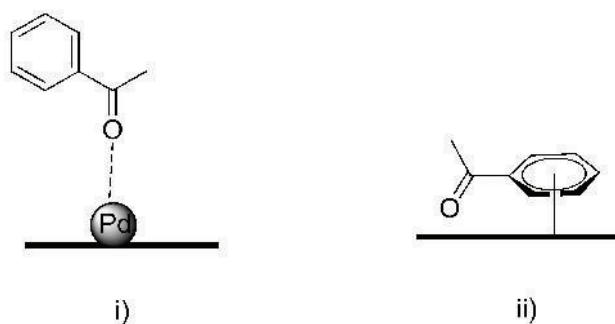


FIG. 22: Possible bonding modes of AP adsorption on catalyst (i) η^1 configuration and (ii) X-sensitive benzene mode

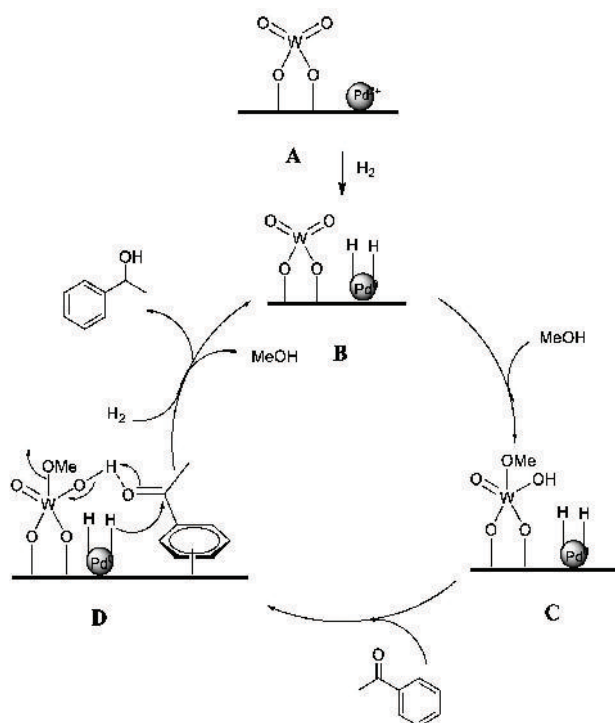


FIG. 23: Plausible mechanism of AP hydrogenation on 1P20WS catalyst

WO₃ center to give W-OMe and W-O-H (B). Hydrogen gets activated on the reduced palladium center (C). As observed previously also, Pd on acidic supports leads to activation of hydrogen under ambient conditions (Acham et al., 2014; Kokane et al., 2017). Subsequently, AP gets adsorbed on the catalyst surface (D). Acetophenone gets activated through aromatic ring on acidic sites via X-sensitive mode; whereas, the carbonyl group gets activated through hydrogen bonding with hydroxyl groups. Subsequent transfer of proton from surface hydroxyl group and hydride from Pd center leads to reduction of carbonyl group to alcohol followed by liberation of PE from the catalyst surface.

4. CONCLUSIONS

1% Pd supported on acidic 20% WO₃/SiO₂ has proved to be highly efficient catalyst for hydrogenation of acetophenone and substituted acetophenones under ambient conditions. 20% WO₃/SiO₂ has provided maximum acidity for

supporting palladium, which formed nano sheets of Pd (111) of 12–18 nm size. The acidic support enabled very high dispersion of Pd (36%), leading to very high catalytic activity for hydrogenation at room temperature and atmospheric pressure. The 1Pd20WS catalyst gave 92% acetophenone conversion with 76% yield of 1-phenylethanol. The recycle studies revealed oligomerization of the product 1-phenylethanol on the catalyst surface, leading to catalyst deactivation, which was substrate-specific. The same catalyst when used for styrene hydrogenation could be recycled very efficiently up to three cycles without loss in the catalytic activity. The mechanistic studies using FTIR revealed the activation of solvent methanol by dissociation on WO_3 moiety to form $\text{CH}_3\text{O-W-}$ and -W-O-H and activation of acetophenone through the aromatic ring. The carbonyl group of acetophenone gets activated due to hydrogen bonding with W-OH formed by dissociation of MeO-H . Thus, $\text{Pd-WO}_3/\text{SiO}_2$ has proved to be a very efficient hydrogenation catalyst due to the synergistic effect of palladium and acidity of the support.

REFERENCES

- Acham, V.R., Biradar, A.V., Dongare, M.K., Kemnitz, E., and Umbarkar, S.B., Palladium Nanoparticles Supported on Magnesium Hydroxide Fluorides: A Selective Catalyst for Olefin Hydrogenation, *ChemCatChem*, vol. **6**, pp. 3182–3191, 2014.
- Aramendia, M.A., Borau, V., Gomez, J.F., Herrera, A., Jimenez, C., and Marinas, J.M., Reduction of Acetophenones over Pd/AlPO_4 Catalysts. Linear Free Energy Relationship (LFER), *J. Catal.*, vol. **140**, pp. 335–343, 1993.
- Argyle, M.D. and Bartholomew, C.H., Heterogeneous Catalyst Deactivation and Regeneration: A Review, *Catalysts*, vol. **5**, pp. 145–269, 2015.
- Baiker, A., Crucial Aspects in the Design of Chirally Modified Noble Metal Catalysts for Asymmetric Hydrogenation of Activated Ketones, *Chem. Soc. Rev.*, vol. **44**, pp. 7449–7464, 2015.
- Bauer, K. and Garbe, D., *Ullmann's Encyclopedia*, 3rd ed., Vol. A11, VCH, New York, pp. 141–152, 1988.
- Bejblova, M., Zamostny, P., Cerveny, L., and Cejka, J., Hydrogenation and Hydrogenolysis of Acetophenone, *Collect. Czech. Chem. Commun.*, vol. **68**, pp. 1969–1984, 2003.
- Bertero, N.M., Apesteagua, C.R., and Marchi, A.J., Catalytic and Kinetic Study of the Liquid-Phase Hydrogenation of Acetophenone over Cu/SiO_2 Catalyst, *Appl. Catal. A*, vol. **349**, pp. 100–109, 2008.
- Bertero, N.M., Trasarti, A.F., Apesteagua, C.R., and Marchi, A.J., Solvent Effect in the Liquid-Phase Hydrogenation of Acetophenone over Ni/SiO_2 : A Comprehensive Study of the Phenomenon, *Appl. Catal. A*, vol. **394**, pp. 228–238, 2011.
- Bonnier, J.M., Damon, J.P., and Masson, J., New Approach to Skeletal Nickel Catalysts Catalytic Properties of the Nickel-Chromium System, *Appl. Catal.*, vol. **42**, pp. 285–297, 1988.
- Casagrande, M., Storaro, L., Talon, A., Lenarda, M., Frattini, R., Rodriguez-Castellon, E., and Maireles-Torres, P., Liquid Phase Acetophenone Hydrogenation on $\text{Ru}/\text{Cr}/\text{B}$ Catalysts Supported on Silica, *J. Mol. Catal. A*, vol. **188**, pp. 133–139, 2002.
- Cerveny, L., Belohlav, Z., and Hamed, M.N.H., Catalytic Hydrogenation of Aromatic Aldehydes and Ketones over Ruthenium Catalysts, *Res. Chem. Intermed.*, vol. **22**, pp. 15–22, 1996.
- Cerveny, L., Ed., *Catalytic Hydrogenation* Elsevier Amsterdam, 1986.
- Chary, K.V.R., Naresh, D., Vishwanathan, V., Sadakane, M., and Ueda, W., Vapour Phase Hydrogenation of Phenol over Pd/C Catalysts: A Relationship between Dispersion, Metal Area and Hydrogenation Activity, *Catal. Commun.*, vol. **8**, pp. 471–477, 2007.
- Chen, C., Chen, H., and Cheng, W., Study of Selective Hydrogenation of Acetophenone on Pt/SiO_2 , *Appl. Catal. A*, vol. **248**, pp. 117–128, 2003.
- Chen, M., Maeda, N., Baiker, A., and Huang, J., Hydrogenation of Acetophenone on $\text{Pd}/\text{Silica-Alumina}$ Catalysts with Tunable Acidity: Mechanistic Insight by In Situ ATR-IR Spectroscopy, *ACS Catal.*, vol. **8**, pp. 6594–6600, 2018.
- Cho, H.-B., Lee, B.U., Ryu, C.-H., Nakayama, T., and Park, Y.H., Selective Hydrogenation of 4-Isobutylacetophenone over a Sodium-Promoted Pd/C Catalyst, *Korean J. Chem. Eng.*, vol. **30**, pp. 306–313, 2013.
- Costa, D.C., Soldati, A.L., Bengoa, J.F., Marchetti, S.G., and Vetere, V., Phosphorus as a Promoter of a Nickel Catalyst to Obtain 1-Phenylethanol from Chemoselective Hydrogenation of Acetophenone, *Heliyon*, vol. **5**, p. e01859, 2019.
- Drelinkiewicz, A., Waksmundzka, A., Makowski, W., Sobczak, J.W., Krol, A., and Zieba, A., Acetophenone Hydrogenation on Polymer-Palladium Catalysts. The Effect of Polymer Matrix, *Catal. Lett.*, vol. **94**, pp. 143–156, 2004.

- Fujita, S., Onodera, Y., Yoshida, H., and Arai, M., Selective Hydrogenation of Acetophenone with Supported Pd and Rh Catalysts in Water, Organic Solvents, and CO₂-Dissolved Expanded Liquids, *Green Chem.*, vol. **18**, pp. 4934–4940, 2016.
- Ge, Q. and Gutowski, M., A Comparative Study of Methanol Adsorption and Dissociation over WO₃(001) and ReO₃(001), *Top. Catal.*, vol. **58**, pp. 655–664, 2015.
- Gou, Y., Liang, X., and Chen, B., Catalytic Hydrogenation of Acetophenone over Shape Controlled Pd Catalysts Supported on Sheet-Like NiO, *Catal. Today*, vol. **216**, pp. 200–204, 2013.
- Hiyoshi, N., Sato, O., Yamaguchi, A., and Shirai, M., Acetophenone Hydrogenation over a Pd Catalyst in the Presence of H₂O and CO₂, *Chem. Commun.*, vol. **47**, pp. 11546–11548, 2011.
- Kokane, R.S., Acham, V.R., Kulal, A.B., Kemnitz, E., Dongare, M.K., and Umbarkar, S.B., Palladium Supported on Fluorinated Magnesium Hydroxide: An Efficient Catalyst for Hydrogenation under Ambient Conditions, *Chem. Select.*, vol. **2**, pp. 10618–10627, 2017.
- Kulal, A.B., Dongare, M.K., and Umbarkar, S.B., Sol–Gel Synthesised WO₃ Nanoparticles Supported on Mesoporous Silica for Liquid Phase Nitration of Aromatics, *Appl. Catal. B*, vol. **182**, pp. 142–152, 2016.
- Liu, H., Lu, G., Guo, Y., Wang, Y., and Guo, Y., Synthesis of Mesoporous Pt/Al₂O₃ Catalysts with High Catalytic Performance for Hydrogenation of Acetophenone, *Catal. Commun.*, vol. **10**, pp. 1324–1329, 2009.
- Liu, L. and Corma, A., Metal Catalysts for Heterogeneous Catalysis: From Single Atoms to Nanoclusters and Nanoparticles, *Chem. Rev.*, vol. **118**, pp. 4981–5079, 2018.
- Malyala, R.V., Rode, C.V., Arai, M., Hegde, S.G., and Chaudhari, R.V., Activity, Selectivity and Stability of Ni and Bimetallic Ni–Pt Supported on Zeolite Y Catalysts for Hydrogenation of Acetophenone and Its Substituted Derivatives, *Appl. Catal. A*, vol. **193**, pp. 71–86, 2000.
- Masson, J., Vidal, S., Cividino, P., Fouilloux, P., and Court, J., Selective Hydrogenation of Acetophenone on Chromium Promoted Raney Nickel Catalysts: II. Catalytic Properties in the Hydrogenation of Acetophenone, Determination of the Reactivity Ratios as Selectivity Criteria, *Appl. Catal. A*, vol. **99**, pp. 147–159, 1993.
- Rajashekharam, M.V. and Chaudhari, R.V., Kinetics of Hydrogenation of P-Isobutyl Acetophenone Using a Supported Ni Catalyst in a Slurry Reactor, *Chem. Eng. Sci.*, vol. **51**, pp. 1663–1672, 1996.
- Rajashekharam, M.V., Bergault, I., Fouilloux, P., Delmas, H., and Chaudhari, R.V., Hydrogenation of Acetophenone Using a 10% Ni Supported on Zeolite Y Catalyst: Kinetics and Reaction Mechanism, *Catal. Today*, vol. **48**, pp. 83–92, 1999.
- Rylander, P., *Hydrogenation Methods*, Academic Press, London, pp. 66–75, 1985.
- Santori, G.F., Moglioni, A.G., Vetere, V., Moltrasio Iglesias, G.Y., Casella, M.L., and Ferretti, O.A., Hydrogenation of Aromatic Ketones with Pt- and Sn-Modified Pt Catalysts, *Appl. Catal. A*, vol. **269**, pp. 215–223, 2004.
- Sudhakar, M., Kumar, V.V., Naresh, G., Kantam, M.L., Bhargava, S., and Venugopal, A., Vapor Phase Hydrogenation of Aqueous Levulinic Acid over Hydroxyapatite Supported Metal (M = Pd, Pt, Ru, Cu, Ni) Catalysts, *Appl. Catal. B*, vol. **180**, pp. 113–120, 2016.
- Thakar, N., Schildhauer, T.J., Buijs, W., Kapteijn, F., and Moulijn, J.A., Evaluation of Deactivation Mechanisms of Pd-Catalyzed Hydrogenation of 4-Isobutylacetophenone, *J. Catal.*, vol. **248**, pp. 249–257, 2007.
- Turáková, M., Salmi, T., Eränen, K., Wärna, J., Murzin, D.Y., and Králik, M., Liquid Phase Hydrogenation of Nitrobenzene, *Appl. Catal. A*, vol. **499**, pp. 66–76, 2015.
- Wagner, C.D., The NIST X-Ray Photoelectron Spectroscopy Database, NIST Technical Note 1289, 1991.
- Wang, D. and Astruc, D., The Golden Age of Transfer Hydrogenation, *Chem. Rev.*, vol. **115**, pp. 6621–6686, 2015.
- Wang, J., Wang, Y., Chen, G., and He, Z., Highly Loaded and Dispersed Ni₂P/Al₂O₃ Catalyst with High Selectivity for Hydrogenation of Acetophenone, *Catalysts*, vol. **8**, p. 309, 2018.
- Xiang, Y., Lv, Y., Xu, T., Li, X., and Wang, J., Carbon Nanotubes and Activated Carbons Supported Catalysts for Phenol In Situ Hydrogenation: Hydrophobic/Hydrophilic Effect, *J. Mol. Catal. A*, vol. **351**, pp. 70–75, 2011.
- Yadav, G.D. and Mewada, R.K., Selective Hydrogenation of Acetophenone to 1-Phenyl Ethanol over Nanofibrous Ag-OMS-2 Catalysts, *Catal. Today*, vol. **198**, pp. 330–337, 2012.
- Yoshida, H., Onodera, Y., Fujita, S., Kawamori, H., and Arai, M., Solvent Effects in Heterogeneous Selective Hydrogenation of Acetophenone: Differences between Rh/C and Rh/Al₂O₃ Catalysts and the Superiority of Water as a Functional Solvent, *Green Chem.*, vol. **17**, pp. 1877–1883, 2015.

Yu, Y., Zhao, Y., Huang, T., and Liu, H., Shape-Controlled Synthesis of Palladium Nano Crystals by Microwave Irradiation, *Pure Appl. Chem.*, vol. **81**, pp. 2377–2385, 2009.

Zhang, X.B., Lu, W.N., Wang, J.L., Liao, B.H., Qin, Y.H., Zhang, Y.-J., Zhang, B., and Xin, S.A., Selective Catalytic Hydrogenation of Acetophenone To 1-Phenylethanol over Co/Mordenite in Water, *Catal. Commun.*, vol. **119**, pp. 124–128, 2019.

Phenol Hydrogenation to Cyclohexanol Catalysed by Palladium Supported on CuO/CeO₂

Mirabai M. Kasabe,^[a, b] Vaibhav R. Kotkar,^[a] Mohan K. Dongare,^[a, c] and Shubhangi B. Umbarkar^{*[a, b]}

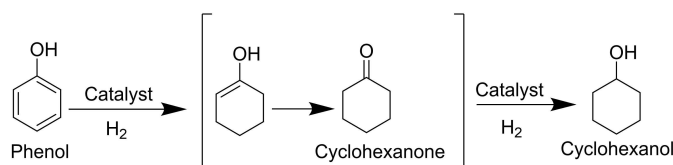
Abstract: Hydrogenation of phenol to cyclohexanone/cyclohexanol is an important reaction in production of nylon-6, nylon-66 and in petroleum industry. Liquid phase phenol hydrogenation over Pd-CuO/CeO₂ was carried out under mild conditions. Palladium impregnated over CuO/CeO₂ synthesized by co-precipitation method showed excellent catalytic activity for phenol hydrogenation (99% conversion with 80% cyclohexanol yield) at 90 °C and 10 bar H₂ pressure in water. Commercial 10%Pd/C showed only 8% phenol conversion under identical conditions. The detailed characterization

revealed significant improvement in surface area of ceria after addition of CuO and decrease in crystallite size with creation of defects in CeO₂ lattice. XPS analysis showed Pd loading on CuO/CeO₂ to cause hydrogen spillover on the surface leading to increase in the oxygen vacancies. The interaction of phenol with catalyst surface studied by detailed FTIR analysis, revealed activation of phenol on oxygen vacancy of ceria as phenoxide ion with perpendicular orientation of aromatic ring on catalyst surface.

Introduction

Selective phenol hydrogenation is an important reaction in the industry as well as in the academia to obtain raw materials (cyclohexanone and cyclohexanol) for the production of adipic acid, caprolactam, nylon-6, nylon-66, and KA oil in petroleum industrial chemistry.^[1–2] Especially cyclohexanol derivatives are important value-added chemical intermediates, in pharmaceuticals, pesticides, plasticizers, cosmetics, surfactants, paint, and as industrial solvents. Furthermore, cyclohexanol is also an excellent oxygenated additive in enhanced multi-component diesel fuel which improves emissions. Commercially cyclohexanol is obtained by two routes, first, the oxidation of cyclohexane and another is the hydrogenation of phenol. The oxidation method requires high temperature and high pressure with a low yield of product and also complicated recovery steps.^[3] Hydrogenation of phenol involves a two-step reaction, in which first phenol hydrogenates to cyclohexanone and then to cyclohexanol as shown in Scheme 1.^[4–5]

Generally, the hydrogenation of phenol is carried out in the gas phase as well as the liquid phase.^[6–9] The former requires



Scheme 1. Hydrogenation of phenol.

high temperature which leads to the formation of coke resulting in the catalyst deactivation.^[10–11] The liquid phase hydrogenation is preferred because; of low temperatures, which leads to saving the energy of the process.^[12–13] Both precious metals, as well as non-precious metals, have been reported for this reaction.^[12,14–18] Huang et al. reported a high-performance PdRu/MNS (mesoporous silica nanoparticles) bimetallic catalyst for the hydrogenation of phenol to cyclohexanol in dichloromethane solvent.^[19] It was found that the addition of Ru, improves the Pd dispersion and assists the electronic interaction between the Ru and Pd, which contribute to improving the catalytic activity. Yi et al. reported 3% palladium supported on γ -Al₂O₃ catalyst with complete phenol conversion (100%) and 100% selectivity of cyclohexanol at 60 °C, 20 MPa H₂ Pressure in 12 h, and 0.05 mol% Pd loading.^[20] Li et al. reported a series of 1Co-1Ni@NC catalysts with 100% phenol conversion and 99% cyclohexanol selectivity in IPA at 100 °C and 0.8 MPa H₂ pressure in 12 h.^[18] Different transition metal supported on carbon like Rh/C, Ru/C, Pt/C, and Pd/C were synthesized and tested for phenol hydrogenation under scCO₂ conditions. Among these Rh/C was found to be a optimum catalyst at 55 °C, 10 MPa H₂ and 10 MPa CO₂ pressure. 10% Ni/SiO₂ catalyst was highly active for phenol hydrogenation at 200 °C, 1 MPa H₂ pressure within 4 h.^[21] Even though the precious metal catalysts have given the good conversion of phenol and selectivity to cyclohexanone or cyclohexanol, the risk in supply and high

[a] M. M. Kasabe, V. R. Kotkar, Dr. M. K. Dongare, Dr. S. B. Umbarkar
Catalysis Division, CSIR-National Chemical Laboratory,
Pune-411008 (India)

[b] M. M. Kasabe, Dr. S. B. Umbarkar
Academy of Scientific and Innovative Research,
CSIR, Ghaziabad – 201002 (India)
E-mail: sb.umbarkar@ncl.res.in

[c] Dr. M. K. Dongare
Malati Fine Chemicals Pvt. Ltd.,
4/A Durvankur Darshan Society,
Pune-411008 (India)

Supporting information for this article is available on the WWW under
https://doi.org/10.1002/asia.202300119

This manuscript is part of a joint special collection highlighting the chemistry research from CSIR Institutes in India.

price of noble metals obstructed to accomplishment industrialization. The non-noble metal based catalysts showed poor catalytic activity and required harsh reaction conditions.

Recently to get the selectively hydrogenated product at a lower cost as compared to another noble metal based catalysts, Pd-based catalysts are widely used though with higher catalyst loading.^[12,14,22-24] It is necessary to develop a catalyst that works under mild reaction conditions with lower noble metal loading and can be easily recyclable without metal leaching. One of the best options to increase the catalytic activity is to tune the electronic properties of the active metal as well as the support by adding second metal to the catalyst. Ceria has been widely used as a catalyst or as support because of its high reactivity and availability. The ceria has high oxygen storage capacity, a high concentration of oxygen vacancies, and also the potential to easily switch between Ce^{3+} and Ce^{4+} .^[25] In addition, the catalytic activity of CeO_2 could be significantly increased by adding other metal ions, such as Cu^{2+} .^[26-27] The doping of copper ions into ceria lattice leads to crystal lattice distortion which is attributed to the replacement of copper ions in the ceria lattice. Further this leads to partial Ce^{4+}/Ce^{3+} reduction and increase in the oxygen vacancies in the lattice. There have been only a few reports of the phenol hydrogenation on ceria-based catalysts. The groups of Inagaki and Scire have reported the vapor phase reaction over palladium supported on high surface area ceria with 80% conversion at 180 °C and 40% conversion at 160 °C, respectively.^[28] Li et al. have reported the liquid-phase process using 0.43 mol% Ce-doped Pd nanospheres with a hollow chamber, getting an 82% cyclohexanone yield at 10 bar of H_2 and 80 °C.^[13] There are several publications where enhancement in the hydrogenation activity due to oxygen vacancies have been reported.^[29-30] Addition of several metal oxides to ceria is known to improve oxygen vacancies and oxygen transport capacity of ceria.^[26-28] Hence we have prepared CuO/CeO_2 with improved oxygen vacancies and used as support for palladium for phenol hydrogenation. Herein, we used CuO/CeO_2 as support to disperse the palladium and evaluated its performance for the selective hydrogenation of phenol to cyclohexanol in the liquid phase at low temperature and H_2 pressure.

Results and Discussion

Catalyst synthesis

The catalyst support 30% CuO/CeO_2 (CC) was prepared by co-precipitation method using cerium nitrate and copper acetate as precursors. Palladium was loaded by impregnation method by changing the Pd loading from 0.5, 1 to 2 wt%.

Catalyst Characterization

Acidity of support

The total acidity and acid strength of the support (CC), 1%Pd/ CeO_2 , 1PCC, and CeO_2 were determined by NH_3 -TPD analysis which is shown in Table 1 and Figure S1. The results showed that CeO_2 and 1%Pd/ CeO_2 catalyst exhibited two peaks one narrow peak around 250 °C corresponding to weak acidity and other broad peak centred at 450 °C corresponding to moderate acidity. Total acidity for CeO_2 and 1%Pd/ CeO_2 catalyst was 0.136 and 0.184 mmol/g respectively. The total acidity of ceria increased after loading of palladium which can be attributed to the Lewis acidic nature of palladium. While CC and 1PCC showed two narrow peaks, one around 200 °C corresponding to weak acidity and other at 800 °C attributed to very strong acidity. The total acidity for CC and 1PCC was 0.166 and 0.191 mmol /g. The area under peak and its position is directly related to the number of acidic sites and its strength respectively. It concluded that CC and 1PCC were more acidic than the CeO_2 and 1%Pd/ CeO_2 catalysts. This may be due to incorporation of CuO into CeO_2 lattice. The quantitative data of NH_3 -TPD is given in Table 1. Palladium also contributes to the acidity due to Lewis acidic nature of Palladium. Hence 1%Pd/ CeO_2 and 1PCC showed more acidity than CeO_2 and CC respectively.

Powder X-ray diffraction analysis

The XRD pattern for CC with different palladium loading showed sharp peaks indicating highly crystalline nature of the catalysts (Figure 1.). Sharp peaks at 28.5, 33.1, 47.5, 56.3, 59.1, 69.4, 76.6, 79.0, and 88.3° correspond to (111), (200), (220), (311), (222), (400), (331), (420) and (422) planes respectively of the cubic crystalline structure of CeO_2 (JCPDS no. 81-0792). In all the samples very small peaks at 35.47 and 38.63° corresponding to (111) and (200) reflections of monoclinic CuO have been observed. The broadening of diffraction peaks in CC (support) and PCC catalysts indicate small crystallite size.^[31] The average crystallite size of CeO_2 was determined from the CeO_2 (111) peak using Scherer's equation for pure CeO_2 and CC support. For pure CeO_2 , the crystallite size was found to be 13.81 nm which decreased 7.59 nm for CC. This result indicates that the addition of Cu (II) ions inhibits the crystal growth of ceria, which is in accordance with the previous reports.^[32-33] Avgouropoulos et al. have prepared CuO/CeO_2 catalyst with varying $CuO/(Cu+Ce)$ molar ratios (0.10, 0.15, 0.25, 0.35, 0.50 and 0.75) by conventional citrate method or the hydrothermal-

Table 1. NH_3 desorbed mmol/g.

Sr. No.	Catalyst	Acidity [mmol/g]
1	CeO_2	0.136
2	1%Pd/ CeO_2	0.184
3	CC	0.166
4	1PCC	0.191

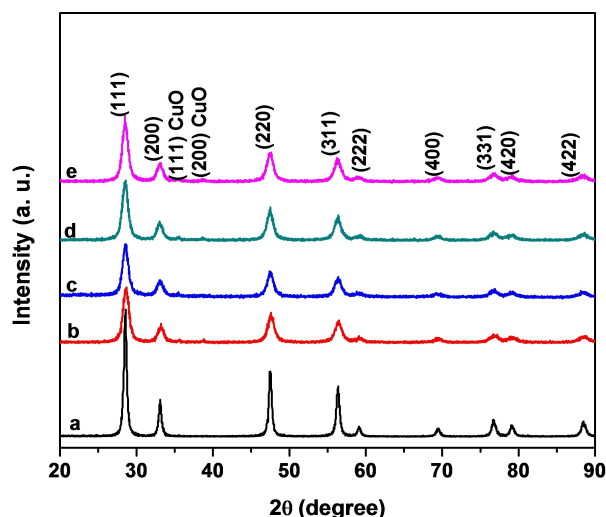


Figure 1. XRD patterns of (a) CeO₂, (b) CC, (c) 0.5PCC, (d) 1PCC and (e) 2PCC.

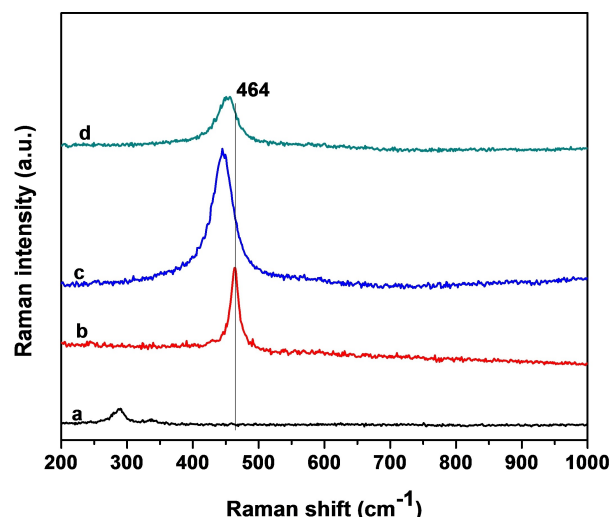


Figure 2. Raman spectra of (a) CuO, (b) CeO₂, (c) CC, and (d) 1PCC.

citrate method. Very high dispersion of CuO on CeO₂ up to a 0.35 molar ratio was reported.^[34] The lattice parameters for cubic crystal structure calculated from the XRD data was found to be 5.41 for CeO₂ and 5.40 for CC. The ionic radii of Ce⁴⁺ in CeO₂ is 101 pm and for Cu²⁺ in CuO is 73 pm. The minor decrease in lattice parameter indicates lattice substitution of few Ce⁴⁺ ions with Cu²⁺ ions. This also contributes to the decrease of CeO₂ crystallite size. No peak for palladium was observed due to low palladium loading and high dispersion.

BET surface area analysis

The BET surface area of all the catalysts was determined by the N₂ adsorption/desorption method. The surface area, average pore size, pore volume, and metal dispersion of the catalysts are given in Table 2. The BET results are in agreement with the XRD data, which shows that after Cu loading the crystallite size of CeO₂ decreases. In principle, the surface area increases with decreasing crystallite size of the sample. Here the surface area of CeO₂ is 33 m²/g, which after the addition of Cu increased to 61 m²/g. The surface area of support was found to affect by Pd loading. There is a decrease in surface area with increase in palladium loading, such as 57, 56, and 52 m²/g, respectively, for 0.5, 1, and 2% Pd loading. However, there is no specific trend

observed in the pore size and pore volume of these catalysts. The adsorption-desorption isotherms of all the Pd-loaded catalysts are shown in Figure S2, which showed the type IV isotherm pattern for all the catalysts. Very high Pd dispersion on acidic support (52% for 1PCC) was observed which is in agreement with our previous work.^[35] The metal dispersion was calculated from the CO chemisorption.

Raman spectroscopy

To study the effect of CuO doping in CeO₂ lattice, Raman analysis was carried out, and the results are shown in Figure 2. The spectrum of CuO showed peaks at 290 and 340 cm⁻¹, attributed to the fundamental active Raman vibration modes A_g and B_{1g} of CuO respectively.^[36] The CC and 1PCC do not show peaks around 290 and 340 cm⁻¹, indicating that CuO is highly dispersed or incorporated in the CeO₂ lattice. The CeO₂, CC and 1PCC catalysts showed a strong peak around 463 cm⁻¹, for the triply degenerate F_{2g} vibration mode in cubic fluorite structure of CeO₂. In CC and 1PCC this peak showed a red shift compared to pure CeO₂. This peak shift to a lower wavenumber in Raman analysis may be due to (i) distortions in the CeO₂ lattice due to the addition of Cu, and/or (ii) the reduction in crystallite size. This is in agreement with the XRD analysis.^[37–38]

Table 2. Surface properties of the CC catalysts[a] from EDAX.

Sr. No.	Catalyst	Elemental composition wt % ^a			Surface area [m ² /g]	Pore size [Å]	Pore volume [cc/g]
		Pd	Cu	Ce			
1	1%Pd/CuO	–	–	–	8	92	0.20
2	CeO ₂	–	–	–	33	16	0.17
3	1%Pd/CeO ₂	–	–	–	28	27	0.19
4	CC	–	11	72	61	27	0.83
5	0.5PCC	0.20	11	77	57	28	0.81
6	1PCC	0.61	9	70	56	27	0.78
7	2PCC	1.35	9	63	52	28	0.73

X-ray Photoelectron Spectroscopy

To further analyse the surface composition and electronic state of elements of catalysts, the XPS spectroscopic analysis was performed. The XPS spectra of Ce 3d and O 1s for CeO₂, CC, and 1PCC (pre-reduced) catalysts are given in Figure 3. The result showed that Ce 3d XPS spectra contain multiple doublets related to the spin-orbit split of 3d_{3/2} and 3d_{5/2}, labelled as u and v. For CeO₂ only six peaks could be distinguished, u (902.2 eV), u'' (908.2 eV), and u''' (917.4 eV) of Ce 3d_{3/2} and v (883.5 eV), v'' (889.1 eV), and v''' (899.2 eV) of Ce 3d_{5/2} belong to Ce⁴⁺.^[39] While in CC and PCC, along with the above six peaks additional two peaks were observed u' (903.5 eV) and v' (884.9 eV) attributed to Ce³⁺. The relative concentration of Ce³⁺ was calculated by $Ce^{3+} = Ce^{3+}/(Ce^{3+} + Ce^{4+})$ formula and shown in Table 3.

The O 1s spectra for CeO₂, CC, and 1PCC (reduced) are shown in Figure 3(b). The spectrum for CeO₂ showed two peaks, the one at higher energy is attributed to the adsorbed oxygen or hydroxide and the lower energy peak attributed to the lattice oxygen of metal oxides. The O 1s spectra of CC and 1PCC showed three peaks at 529, 531, and 532 eV. These peaks are labelled as O_α, O_β, and O_γ respectively. The peak at 531 eV is attributed to the presence of Ce³⁺ surface defect or defect oxide. The relative amount of O_β species on the surface was calculated by $O_{\beta}/(O_{\alpha} + O_{\beta} + O_{\gamma})$ formula and shown in Table 3. The Cu 2p spectra for CuO, CC and 1PCC are shown in Figure 3(c). The spectra showed that the peak at 934.0 eV is

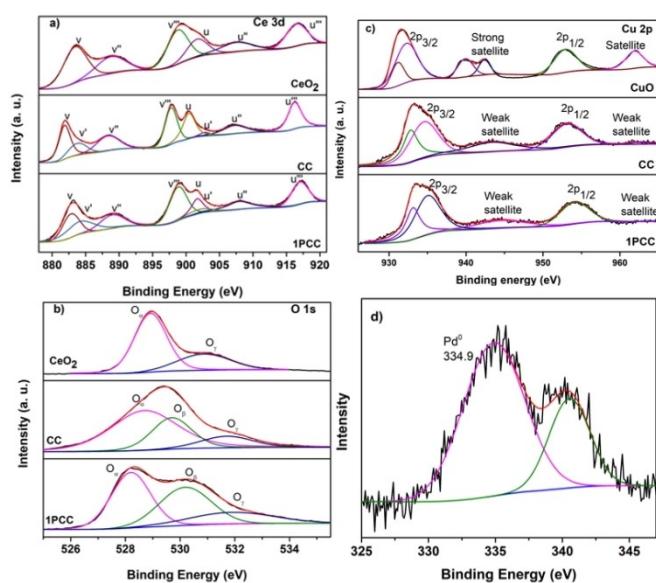


Figure 3. XPS spectra of (a) Ce 3d (b) O 1s (c) Cu 2p and d) Pd 3d.

Table 3. XPS data measured for CeO ₂ , CC and 1PCC.			
Sr. No.	Catalyst	Ce(III) % of total Ce present	O vacancy [%]
1	CeO ₂	–	–
2	CC	10.2	26.9
3	1PCC	18	37.7

attributed to Cu²⁺ component with satellite peak at 942.0 eV. It also showed peak at 932.0 eV corresponding to Cu⁺ or Cu⁰ state of copper. The spectrum of CuO showed strong satellite peaks while spectra of CC and 1PCC showed weak satellite peaks may be due to interaction with CeO₂.

The results indicated that Cu addition into CeO₂ creates defects in the CeO₂ lattice. These results are in agreement with the XRD, BET and Raman data. The 1PCC catalyst showed more defects which may be due to higher concentration of Ce⁺³ present. The hydrogen spillover on the reducible catalyst surface may lead to higher Ce⁺³ concentration. The Pd 3d spectrum of 1PCC is given in Figure 3(d). The spectrum showed the peak at 335 eV for Pd 3d_{5/2} attributed to metallic palladium (Pd⁰). This indicates that on reduction all Pd²⁺ get reduced to Pd⁰.

Electron microscopic analysis

To study morphology and the compositional homogeneity of catalysts, SEM and EDAX analysis was carried out. The SEM images indicate almost identical morphology for all catalysts (Figure S3). The CC showed non-uniform particle size distribution with some bigger particles and some smaller particles of 1–4 μm with no specific shape. No significant change in the morphology and particle size was observed after Pd loading. Elemental analysis determined by EDAX is given in Table 2. The microstructural characteristics were determined by TEM analysis and the images of CC and PCC are shown in Figure 4. This revealed an average particle size of 8–9 nm. The high resolution TEM image for 1PCC catalyst is shown in Figure 4e. The palladium, ceria and copper oxide particles were distinguished by *d* spacing values. The characteristic *d* spacing value for palladium particles were found to be 0.23 nm which corresponds to the (111) plane of Pd.^[40] The *d* spacing value of 0.32 nm is attributed to (111) plane of cubic ceria.^[41] The *d* spacing value of 0.22 nm is assigned to (200) plane of CuO.^[42] The SAED (selected area electron diffraction) pattern is shown in Figure 4f. The image shows distinct four diffraction rings for the cubic ceria crystal corresponding to (111), (200), (220) and (311) planes which is in agreement with XRD data.^[41]

Catalytic activity for phenol hydrogenation

Catalyst screening and time profile study

The hydrogenation of phenol was carried out using 1PCC catalyst having 1% palladium loading synthesized by the impregnation method. The reaction was carried out in water at 90 °C and 10 bar H₂ pressure. The hydrogenation of phenol gave benzene and cyclohexane as undesired by-products, apart from cyclohexanone and cyclohexanol (Scheme 2). To understand the effect of each component of the catalyst, the reaction was carried out using CuO, CeO₂, support (CC), and the catalyst with 1% palladium loaded separately on CuO (1%Pd/CuO) and CeO₂ (1%Pd/CeO₂) (Table 4). For comparison the commercial

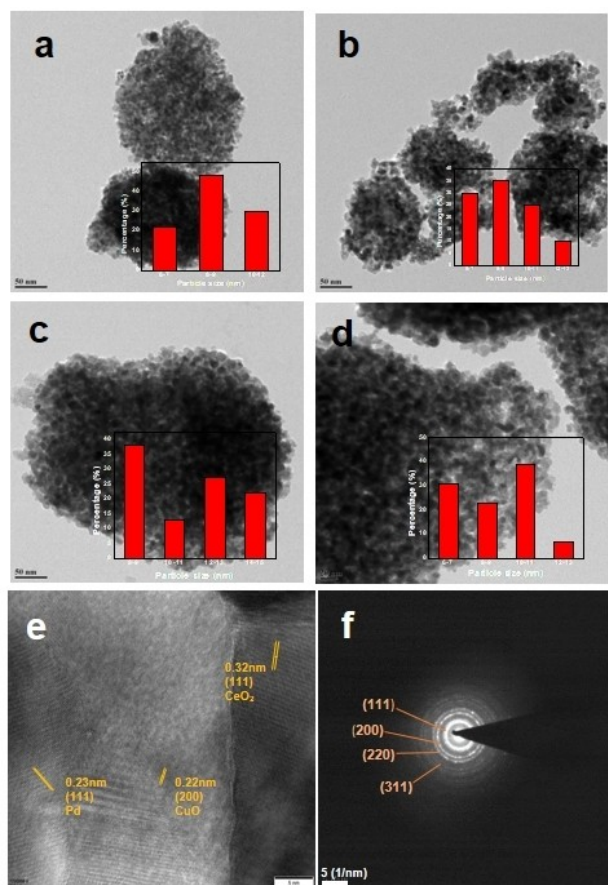
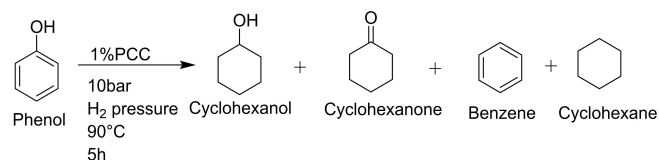


Figure 4. TEM image of catalyst a) CC, b) 0.5PCC, c) 1PCC, and d) 2PCC, e) High resolution TEM image of 1PCC, and f) SAED pattern of 1PCC catalyst.



Scheme 2. Hydrogenation of phenol

catalyst 10%Pd/C was also evaluated under identical conditions. There was no conversion of phenol observed with CuO and CeO₂ whereas, only 6% and 1% phenol conversion was

obtained with CC and Pd/CuO after 5 h. The catalyst Pd/CeO₂ and 1PCC showed almost 99% phenol conversion after 5 h with 49% and 80% cyclohexanol yield respectively. The higher activity of the catalyst may be attributed to the hydrogen spillover in the case of Pd/CeO₂ and 1PCC catalyst. Hydrogen spillover is well-known in reducible oxides which are used as supports for noble metals.^[43] Here CeO₂ is the reducible oxide in both catalysts which improves reaction rate in case of Pd/CeO₂ and 1PCC due to the hydrogen spillover from Pd to CeO₂. The hydrogen molecule adsorbs and dissociates on Pd metal and spills over to CeO₂ causing the reduction of Ce⁴⁺ to Ce³⁺. This increases the availability of H₂ on the catalyst surface. Hence the rate of hydrogenation is high in case of Pd/CeO₂ and 1PCC. The yield of cyclohexanol is higher (80%) for 1PCC; this may be due to contribution of Cu²⁺ for hydrogenation. The addition of CuO to CeO₂ has enhanced the surface area of support contributing to better dispersion of palladium compared to only CeO₂. Because of the high dispersion of Pd (more active site), the rate of hydrogenation is more leading to over hydrogenation of cyclohexanone to cyclohexanol. The commercial 10%Pd/C catalyst under identical reaction conditions, gave only 8% phenol conversion with 8% yield of cyclohexanol. The catalyst loading for commercial catalyst was 2% with respect to phenol so as to keep Pd loading same as that of 1PCC. The time on stream study of the reaction showed that the conversion of phenol and yield of cyclohexanol increases gradually with time as shown in Figure 5.

Effect of temperature on phenol hydrogenation

The effect of temperature was studied for phenol hydrogenation at 30 °C (room temperature), 60 °C and 90 °C and the results are shown in Figure 6. At 30 °C temperature, only 18% conversion of phenol was obtained after 5 h with 10% cyclohexanol yield. The conversion of phenol increased with temperature. At 60 °C, 92% conversion while at 90 °C almost 99% conversion of phenol was obtained with 75% and 80% yield of cyclohexanol respectively. The rate of reaction increases at a high temperature because it increases the number of high-energy collisions.

Table 4. Catalyst screening for phenol hydrogenation.

Sr. No.	Catalyst	Conv. [%]	Yield of Cyclohexanone	Yield of Cyclohexanol	Other product ^a [%]
1	CuO	–	–	–	–
2	CeO ₂	–	–	–	–
3	CC	5	0	3	2
4	1%Pd/CuO	1	0	1	0
5	1%Pd/CeO ₂	99	41	49	9
6	1PCC	99	9	80	10
7	10%Pd/C ^b	8	–	8	–

Reaction conditions-phenol (0.800 g), 20 wt % catalyst w.r.t. substrate, 40 ml solvent (water), 10 bar H₂ pressure, temp 90 °C, time 5 h; [a] other products: benzene + cyclohexane, [b] 2 wt % catalyst w.r.t. substrate.

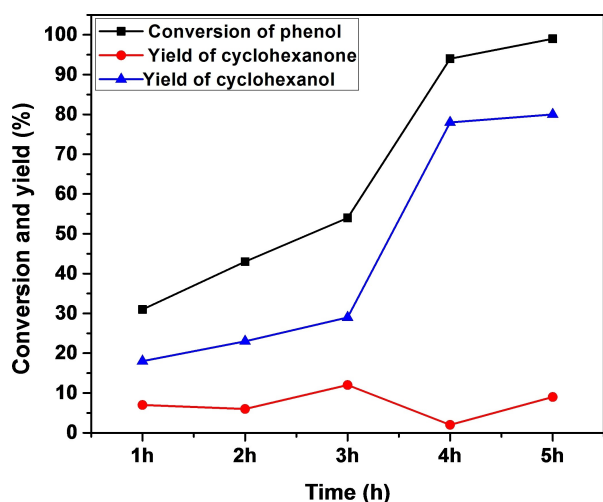


Figure 5. The conversion of phenol with time. Reaction condition- phenol (0.800 g), 20 wt% catalyst w.r.t. substrate, 40 ml solvent (water), 10 bar H₂ pressure, temp 90 °C.

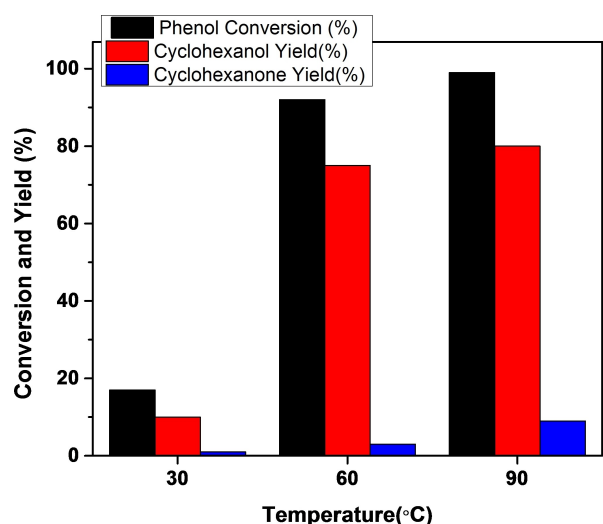


Figure 6. Effect of temperature on phenol hydrogenation. Reaction condition- phenol (0.800 g), 20 wt% catalyst w.r.t. substrate, 40 ml solvent (water), 10 bar H₂ pressure, and time 5 h.

Effect of pressure on phenol hydrogenation

Table 5, depicts the effect of H₂ pressure on the hydrogenation of phenol and the yield of cyclohexanol by varying H₂ pressure from 5 to 15 bar. The result showed that there is a linear relationship of H₂ pressure with the phenol conversion and cyclohexanol yield. The phenol conversion and cyclohexanol yield increased from 86 to 99% and 65 to 80% with increase in the pressure from 5 to 10 bar respectively after 5 h while at 15 bar H₂ pressure 99% conversion was obtained with 82% yield of cyclohexanol after 1 h. With increase in H₂ pressure the time required for 99% phenol conversion decreased from 5 h for 10 bar pressure to 1 h for 15 bar pressure. It is well known that at high H₂ pressure the solubility of hydrogen increases leading to more availability of H₂ on the catalyst surface thus increasing the rate of hydrogenation. As there was a minor difference in the yield of cyclohexanol at 10 and 15 bar H₂ pressure, we used 10 bar H₂ pressure for further optimisation.

Effect of catalyst loading on phenol hydrogenation

To find out the role of the amount of catalyst on phenol hydrogenation, reactions were performed at different catalyst loadings such as 10, 20, and 30 wt% with respect to phenol (Figure S4). With increase in the catalyst loading from 10 to 20 to 30 wt%, the phenol conversion increased from 35%, 42%, to 99% with cyclohexanol yield of 15%, 23%, and 82% respectively after 2 h. For 20 wt% catalyst loading 99% conversion with 80% yield of cyclohexanol was obtained after 5 h while 30 wt% catalyst showed 90% yield of cyclohexanol after 5 h. The increase in the catalyst led to increase in the number of active sites contributing to the higher conversion.

Effect of Pd loading on phenol hydrogenation

To study the effect of Pd metal loading on phenol hydrogenation, varying Pd loaded (0.5, 1, and 2 wt%) CuO/CeO₂ catalysts were tested for phenol hydrogenation and results are shown in Table 6. As Pd loading was increased, the phenol conversion and cyclohexanol yield also increased due to increase in the active sites in the reaction medium. As Pd

Table 5. Effect of pressure on phenol hydrogenation.

Sr. No.	Pressure bar	Time [h]	Conv. [%]	Yield of Cyclohexanone	Yield of Cyclohexanol	Other product ^a [%]
1	5	2	38	13	19	6
		5	86	11	65	10
2	10	2	42	6	23	13
		5	99	9	80	10
3	15	1	99	3	82	14
		2	99	1	84	14
		5	99	0	86	13

Reaction condition- phenol (0.800 g), 20 wt% catalyst w.r.t. substrate, 40 ml solvent (water), temp 90 °C and time 5 h; [a] other products-benzene and cyclohexane.

Table 6. Pd loading effect on phenol hydrogenation.

Sr. No.	Pd loading	Time [h]	Conv. %	Yield of Cyclohexanone	Yield of Cyclohexanol	Other products ^a [%]
1	0.5PCC	2	20	3	7	10
		5	68	15	41	12
2	1PCC	2	42	6	23	13
		5	99	9	80	10
3	2PCC	2	93	5	80	8
		5	99	1	88	10

Reaction condition- phenol (0.800 g), 20 wt% catalyst w.r.t. substrate, 40 ml solvent (water), 10 bar H₂ pressure, temp 90 °C; [a] other products-benzene and cyclohexane.

loading increased from 0.5% to 2% the cyclohexanol yield increased from 41% to 88% after 5 h.

The important previous reports on the phenol hydrogenation are listed in Table 7. Comparison of the present results with previous literature revealed that when non-noble metals are used for phenol hydrogenation the harsh reaction condition were used due to poor catalytic activity of non-noble metals. Non-noble metals such as Ni and Co were mostly used, but it required almost 70 to 200 °C temperature and 10 to 30 bar H₂ pressure. The precious metal catalysts have given the good conversion of phenol and selectivity to cyclohexanol, but amount of catalyst required for reaction is high. In present work with just 10 wt% catalyst w.r.t phenol gave 99% conversion with 80% yield of cyclohexanol.

Catalyst recycles study

To understand the catalyst stability and reusability, 1PCC catalyst was recycled for three cycles under optimized reaction conditions (phenol (0.800 g), 20 wt% catalyst w.r.t. substrate, 40 ml water, 10 bar H₂ pressure, temp 90 °C, time 2 h). The recycle was carried out at lower conversion to understand if any leaching takes place. After each run, the catalyst was separated by centrifugation, washed with methanol and water, dried at 100 °C, and used for the next catalytic run. Similarly the catalyst was recycled for three cycles and the results are shown in Figure 7. The results confirmed that the catalyst was stable and there was no decrease in the phenol conversion and cyclohexanol yield even after third cycle. The strong metal support interaction due to acidic nature of support led to efficient recycle of the catalyst. The palladium interacts strongly with acidic support due to which no leaching of the palladium in the reaction mixture was observed. This is in agreement with our previous results where Pd supported on acidic MgF₂ was used for hydrogenation of various organics with no Pd leaching.^[35] Additionally, the ICP-AES analysis of the final reaction mixture was carried out to check the metal (Pd) leaching. The result showed no palladium leaching in the reaction mixture. Additionally the detailed characterisation of the used catalyst was compared with fresh catalyst to confirm the integrity of the catalyst during catalytic hydrogenation.

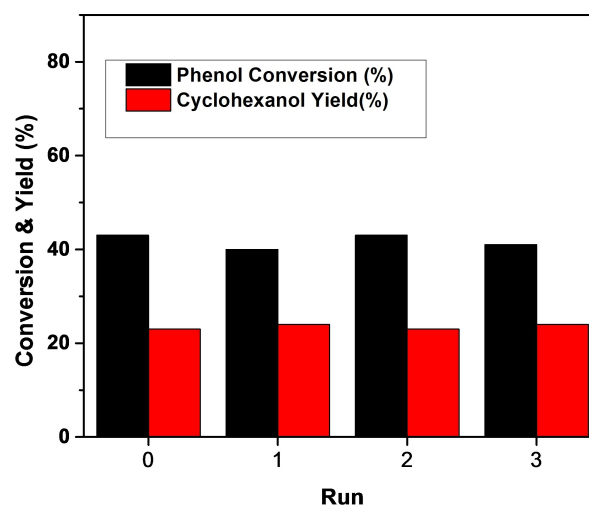


Figure 7. Recycle study of phenol hydrogenation. Reaction condition-phenol (0.800 g), 20 wt% catalyst w.r.t. substrate, 40 ml solvent (water), 10 bar H₂ pressure, temp 90 °C, and time 2 h.

Characterization of the used catalyst

Powder X-ray diffraction (PXRD) analysis

The XRD analysis of fresh and used PCC catalyst is shown in Figure 8. The diffraction pattern of the used PCC catalyst does not indicate any changes as compared to the diffraction pattern of a fresh PCC catalyst and it completely matched the pattern of the cubic crystalline structure of CeO₂.

BET surface area measurements

The BET analysis of fresh and used catalysts is shown in Figure 9 and Table 8. The surface area of the fresh catalyst was 56 m²/g which decreased marginally to 53 m²/g for used catalyst with almost no change in pore size and pore volume. The elemental composition as determined by EDAX was also similar for fresh and used catalyst as evident from Table 7 which confirms no leaching of palladium in the reaction mixture.

Table 7. Literature survey for hydrogenation of phenol.

Sr. No.	Catalyst	Amount of catalyst wrt substrate	Solvent	Temp [°C]	Pressure bar	Time, h	Conv. of phenol	Select. cyclohexanol	Ref.
1	3 wt. % Pd/-Al ₂ O ₃	0.056 mmol pd	Water	60	20	12	100	99	[20]
2	CoO _x /CN	-	Water	150	30	16	99	98	[44]
3	Raney Ni	25 wt%	Water	70	20	2	100	100	[45]
4	20% Ni/CNT	10 wt%	Isopropanol	220	-	1	100	95	[46]
5	10%Ni/SiO ₂	20 wt%	Water	200	10	4	100	100	[21]
6	1Co-1Ni@NC	40 mol%	IPA	100	8	12	100	99	[18]
7	NiCo/Mg ₂ Ni ₂ O	10 wt%	n-hexane	150	20	2.5	99	99	[47]
8	5RuO ₂ -MCM-41	33 wt%	Water	100	10	12	100	100	[48]
9	22% Ni/γ-Al ₂ O ₃	5 wt%	-	140	30	2	63	96	[49]
10	5% Rh/C	3 wt%	-	55	10 bar H ₂ 10 bar CO ₂	4	53	83	[50]
11	5% Pd/C	5 mol%	Water	100	10	2	55	100	[51,52]
12	1% Pd/CeO ₂	5 mol%	Hexane	35	~1	4	94	9	[53]
13	Pd spheres (~26 nm) 1% PCC	0.05 mmol pd	Water	90	5	20	100	82	[54]
14	1% PCC	20 wt%	Water	90	10	5	99	80	Present work

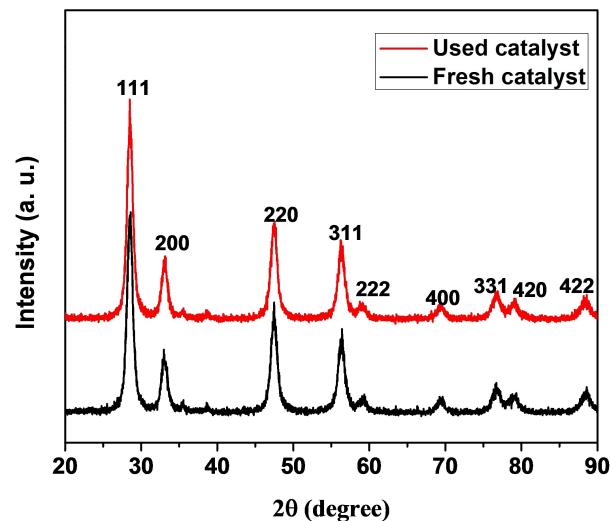


Figure 8. XRD pattern of fresh and used PCC catalyst.

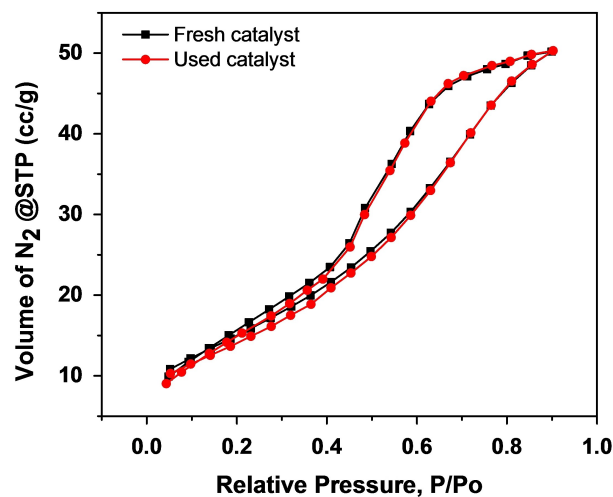


Figure 9. BET surface area analysis of the pattern of fresh and used PCC catalyst.

TEM analysis of fresh and used catalyst

The TEM analysis of the fresh and spent catalyst as shown in Figure 10 indicated only marginal change in the particle size

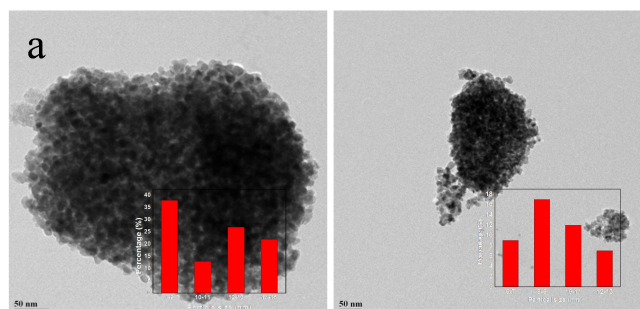


Figure 10. TEM images of (a) fresh PCC, (b) used PCC.

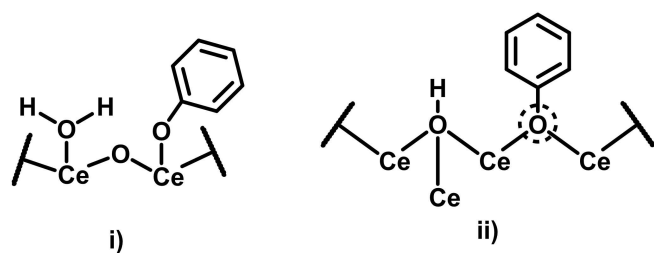
Sr. No.	Catalyst	Element composition by EDAX			Surface area [m ² /g]	Pore size [Å]	Pore volume [cc/g]
		Pd	Cu	Ce			
1	Fresh-PCC	0.61	9	70	56	27	0.78
2	Used- PCC	0.63	10	70	53	29	0.78

distribution in fresh and used catalyst. The maximum particles are in the range of 8–9 nm for fresh and used catalysts.

The detailed characterisation of fresh and used catalyst revealed no change in the catalyst composition and morphology under reaction conditions.

Plausible Mechanism

To study the mechanism of phenol hydrogenation over a 1PCC catalyst the detailed FTIR analysis was performed by analysing the interaction of phenol over the catalyst surface. To understand the interaction of adsorbed phenol with catalyst components, the FTIR spectra of phenol adsorbed on all prepared (CuO, CeO₂, CC, 1%Pd/CuO, 1%Pd/CeO₂, and 1PCC (Pd based catalysts were pre-reduced)) catalysts were recorded. The data was compared with authentic phenol as shown in Figure 15. The FTIR spectrum of authentic phenol showed peaks at 3274 cm⁻¹ for –OH stretching vibration, 1219 cm⁻¹ for C–O stretching vibration, and at 689, 747, 809 cm⁻¹ for C–H stretching vibration of *ortho*, *meta*, and *para* C–H respectively. The Figure showed decrease in the relative intensity of -OH stretching vibration at 3274 cm⁻¹ for free phenol in spectra of phenol adsorbed on CeO₂, CC, 1%Pd/CuO, 1%Pd/CeO₂ and it disappeared in the spectrum of phenol adsorbed on 1PCC catalyst. It means when phenol is adsorbed on a catalyst, it dissociates into phenoxide ion and proton. The results also showed that an intense peak at 1219 cm⁻¹ for C–O stretching vibration of authentic phenol is shifted from 1225 to 1234 cm⁻¹ in phenol adsorbed on catalysts, and this is attributed to C–O–Ce bond formation. The C–O–Ce bond formation results in electron withdrawal from the phenoxy group toward the cerium ion and leads to C–O bond shortening resulting in the increase in frequency. Nelson and group reported hydrogenation of phenol on Pd/CeO₂ catalyst, and showed that phenol adsorbed onto cerium cation in a dissociative manner with different modes as shown in Scheme 3.^[53] The active site for



Scheme 3. Dissociative adsorption of phenol onto catalyst (i) adjacent to a surface hydroxyl, and (ii) at an oxygen vacancy.

hydrogenation of phenol on Pd/CeO₂ catalyst was shown to be coordinatively unsaturated cerium cations. Figure 11(c) shows spectrum of phenol adsorbed on only CeO₂ and it shows similar shift in C–O bond stretching vibration as in 1PCC. However the shift is smaller compared to 1PCC. The spectrum of phenol adsorbed on 1PCC catalyst showed higher shift (to 1234 cm⁻¹) for peak at 1219 cm⁻¹ for C–O stretching vibration, it may be attributed to higher Ce(III) (coordinatively unsaturated cerium cations) and hence, more oxygen vacancies due to CuO addition and also hydrogen spillover from Pd to catalyst surface. This might be one of the reasons for efficient hydrogenation of phenol on 1PCC catalyst due facile activation of phenol. The higher hydrogenation efficiency of 1PCC catalyst is also reflected in the highest cyclohexanol yield compared to 1Pd/CeO₂ where equal selectivity for cyclohexanol and cyclohexanone is obtained, though the phenol conversion is same (Table 3). Hence the FTIR studies explains the higher hydrogenation efficiency of 1PCC catalyst compared to 1Pd/CeO₂.

The spectra also showed no shift in C=C aromatic ring vibration (1594 and 1498 cm⁻¹), however a shift was observed in aromatic C–H bending vibration (688 to 690 and 748 to 752 cm⁻¹) in spectra of phenol adsorbed on all catalyst except CuO. The difference in the peak shift *-o*, *-m* and *-p* C–H bending vibration clearly indicate perpendicular orientation of aromatic ring with respect to catalyst surface. In case of parallel orientation of the aromatic ring, significantly higher shift in all

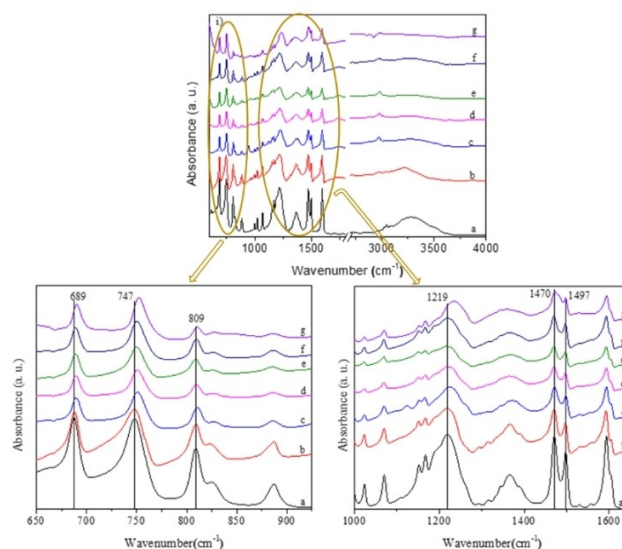
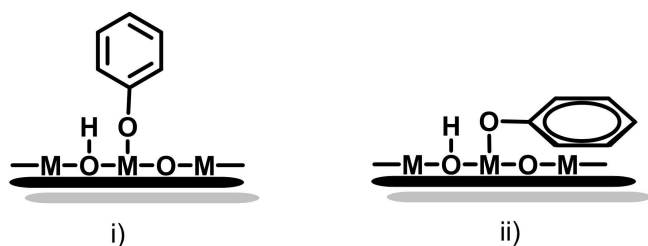


Figure 11. FTIR spectra in the range of i) 600 to 4000 cm⁻¹, ii) 650 to 900 cm⁻¹, and iii) 1100 to 1660 cm⁻¹: of a) authentic phenol, and phenol adsorbed on b) CuO, c) CeO₂, d) CC, e) 1%Pd/CuO, f) 1%Pd/CeO₂ and g) 1PCC.

-o, -m and -p -C-H bending vibration with almost similar shift is expected. From this, it can be concluded that when phenol adsorbs on the catalyst the aromatic ring orientation is perpendicular to the catalyst surface to lower the electronic interaction with the surface as shown in Scheme 4.^[26] For the spectrum of phenol adsorbed on CuO no shift was observed in aromatic C-H bending vibration, while in the spectrum of phenol adsorbed on Pd/CuO peaks were shifted from 688 to 689 and 748 to 750 cm^{-1} . This indicates that Pd metal also helps to activate the phenol molecule to some extent.

From all above discussion, the plausible mechanism for phenol hydrogenation on 1PCC catalyst is shown in Figure 12. In Pd-CuO/CeO₂ (A) under hydrogen atmosphere, Pd⁺² gets reduced to Pd⁰. Along with reduction of Pd the hydrogen molecule gets activated to H and due to spillover effect the hydrogen atoms migrates on the surface (B). Under reducing atmosphere the number of oxygen vacancies also increase which are known to improve the hydrogenation efficiency. Subsequently phenol molecule gets activated on CuO/CeO₂ surface on oxygen vacancy leading to dissociation of phenol to phenoxide ion with perpendicular orientation of aromatics ring with respect to catalyst surface (C). The transfer of a hydrogen atoms under high pressure to aromatic ring leads to hydrogenation of the aromatic ring forming the product cyclohexanol. Thus the oxygen vacancies generated in the CuO/CeO₂ support have helped activation of phenol on the support and



Scheme 4. Adsorption of phenol onto catalyst i) perpendicular orientation and ii) parallel orientation.

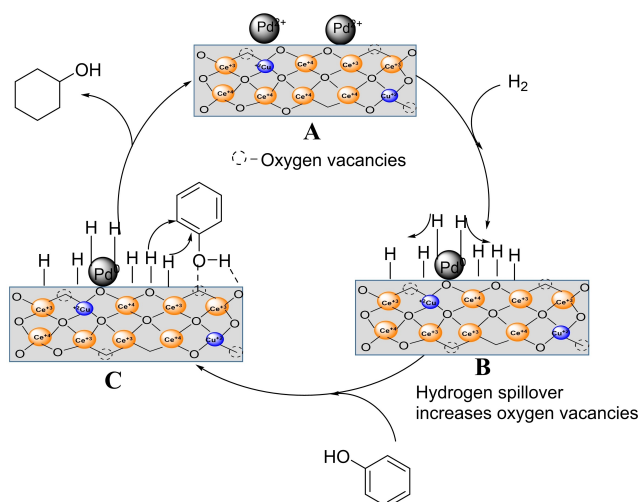


Figure 12. Plausible Mechanism of phenol hydrogenation over PCC catalyst.

activation of hydrogen on Pd centre along with spillover effect, has led to significantly high efficiency of the catalyst for phenol hydrogenation.

Conclusion

CuO/CeO₂ has been used as acidic support with redox properties for palladium to prepare an efficient hydrogenation catalyst. Palladium supported on CuO/CeO₂ with different palladium loading has been synthesized by the impregnation method. The detailed analysis showed addition of CuO into CeO₂ to reduce the size of CeO₂ crystallite by inhibiting the crystalline growth of cerianite and also the insertion of some Cu ions into the CeO₂ lattice which leads to the reduction of crystal parameters. The surface area of CeO₂ (33 m^2/g) increased significantly after CuO incorporation (61 m^2/g). The XPS analysis confirmed high oxygen vacancies due to hydrogen spillover in reduced 1PCC catalyst. This leads to more hydrogen availability for reaction and also the activation of phenol. The PCC catalyst has shown excellent catalytic activity for phenol hydrogenation under milder reaction conditions (10 bar H₂ pressure, and 90 °C) in an aqueous medium with very high conversion (99%) and a high cyclohexanol yield (80%). The detailed FTIR studies proved perpendicular orientation of aromatic ring of phenol on catalyst surface after activation of phenol as phenoxide on oxygen vacancy of PCC catalyst.

Acknowledgements

MMK acknowledges CSIR for research fellowship. SERB is greatly acknowledged for financial assistance (SPG/2021/004654). The help from Mr. R. S. Gholap and Mr. S. B. Deo for SEM/TEM and XPS analysis is gratefully acknowledged.

Conflict of Interests

The authors declare no conflict of interest.

Data Availability Statement

The data that support the findings of this study are available on request from the corresponding author. The data are not publicly available due to privacy or ethical restrictions.

Keywords: Cyclohexanol · Hydrogen spillover · Oxygen vacancies · Pd-CuO/CeO₂ · Phenol hydrogenation

- [1] Y. Xiang, L. Ma, C. Lu, Q. Zhang, X. Li, *Green Chem.* **2008**, *10*, 939–943.
- [2] Y. Xiang, L. Kong, P. Xie, T. Xu, J. Wang, X. Li, *Ind. Eng. Chem. Res.* **2014**, *53*, 2197–2203.
- [3] C. J. Lin, S. H. Huang, N. C. Lai, C. M. Yang, *ACS Catal.* **2015**, *5*, 4121–4129.

- [4] M. Chatterjee, H. Kawanami, M. Sato, A. Chatterjee, T. Yokoyama, T. Suzuki, *Adv. Synth. Catal.* **2009**, *351*, 1912–1924.
- [5] V. Z. Fridman, A. A. Davydov, *J. Catal.* **2000**, *195*, 20–30.
- [6] M. A. Ali, A. Abutaleb, *Catal. Lett.* **2022**, *152*, 1555–1581.
- [7] G. Xue, L. Yin, S. Shao, G. Li, *Nanotechnology* **2022**, *33*, 072003.
- [8] H. Chen, J. Sun, *J. Ind. Eng. Chem.* **2021**, *94*, 78–91.
- [9] H. Li, T. She, G. Chen, M. Sun, L. Niu, G. Bai, *J. Mol. Catal.* **2021**, *504*, 111493–111500.
- [10] Y. Nakagawa, M. Ishikawa, M. Tamura, K. Tomishige, *Green Chem.* **2014**, *16*, 2197–2203.
- [11] L. Wang, J. Zhang, X. Yi, A. Zheng, F. Deng, C. Chen, Y. Ji, F. Liu, X. Meng, F.-S. Xiao, *ACS Catal.* **2015**, *5*, 2727–2734.
- [12] Y. Wang, J. Yao, H. Li, D. Su, M. J. Antonietti, *J. Am. Chem. Soc.* **2011**, *133*, 2362–2365.
- [13] H. Li, J. Liu, S. Xie, M. Qiao, W. Dai, Y. Lu, H. Li, *Adv. Funct. Mater.* **2008**, *18*, 3235–3241.
- [14] H. Liu, T. Jiang, B. Han, S. Liang, Y. Zhou, *Science* **2009**, *326*, 1250–1252.
- [15] H. Zhang, A. Han, K. Okumura, L. Zhong, S. Li, S. Jaenicke, G. K. Chuah, *J. Catal.* **2018**, *364*, 354–365.
- [16] H. Zhou, B. Han, T. Liu, X. Zhong, G. Zhuang, J. Wang, *Green Chem.* **2017**, *19*, 3585–3594.
- [17] S. Kuklin, A. Maximov, A. Zolotukhina, E. Karakhanov, *Catal. Commun.* **2016**, *73*, 63–68.
- [18] A. Li, K. Shen, J. Chen, Z. Li, Y. Li, *Chem. Eng. Sci.* **2017**, *166*, 66–76.
- [19] C. Huang, X. Yang, H. Yang, P. Huang, H. Song, S. Liao, *Appl. Surf. Sci.* **2014**, *315*, 138–143.
- [20] J. Yi, Y. Luo, T. He, Z. Jiang, J. Li, C. Hu, *Catalysts* **2016**, *6*, 12.
- [21] J. He, X.-H. Lu, Y. Shen, R. Jing, R.-F. Nie, D. Zhou, Q.-H. Xia, *J. Mol. Catal.* **2017**, *440*, 87–95.
- [22] J. Matshwele, K. Mmusi, V. Vishwanathan, *Sreyas Int. J. Sci. Technol.* **2019**, *3*, 1–6.
- [23] P. Claus, H. Berndt, C. Mohr, J. Radnik, E.-J. Shin, M. A. Keane, *J. Catal.* **2000**, *192*, 88–97.
- [24] E. Diaz, A. F. Mohedano, L. Calvo, M. A. Gilarranz, J. A. Casas, J. J. Rodriguez, *Chem. Eng. J.* **2007**, *131*, 65–71.
- [25] S. A. Lermontov, A. N. Malkova, L. L. Yurkova, A. Y. Baranchikov, V. K. Ivanov, *Nanosyst.: Phys. Chem. Math.* **2013**, *4*, 690–695.
- [26] T. S. Cam, T. A. Vishnievskaia, V. I. Popkov, *Rev. Adv. Mater. Sci.* **2020**, *59*, 131–143.
- [27] X. Zhang, H. Wang, X. Jiang, H. Sun, Z. Qu, *Catal. Sci. Technol.* **2019**, *9*, 2968–2981.
- [28] S. Velu, M. P. Kapoor, S. Inagaki, K. Suzuki, *Appl. Catal. A* **2003**, *245*, 317–331.
- [29] J. Wang, Y. Zhang, X. Xu, M. Bao, *ACS Appl. Mater. Interfaces.* **2023**, doi.org/10.1021/acsami.2c21272.
- [30] A. Hezam, K. Namratha, Q. A. Drmish, D. Ponnamma, J. Wang, S. Prasad, M. Ahamed, C. Cheng, K. Byrappa, *ACS Appl. Nano Mater.* **2020**, *3*, 138–148.
- [31] L. Yin, Y. Wang, G. Pang, Y. Kolytyn, A. Gedanken, *J. Colloid Interface Sci.* **2002**, *246*, 78–84.
- [32] M. Jobbagy, F. Mari'no, B. Sch'ombrod, G. Baronetti, *Chem. Mater.* **2006**, *18*, 1945–1950.
- [33] X. Wang, J. A. Rodriguez, J. C. Hanson, D. Gamarra, A. Martínez-Arias, M. Fernández-Garíá, *J. Phys. Chem. B* **2006**, *110*, 428–434.
- [34] G. Avgouropoulos, T. Ioannides, *Appl. Catal. B* **2006**, *67*, 1–11.
- [35] V. R. Acham, A. V. Biradar, M. K. Dongare, E. Kemnitz, S. B. Umbarkar, *ChemCatChem* **2014**, *6*, 3182–3191.
- [36] M. Chuai, X. Chen, K. Zhang, J. Zhang, M. Zhang, *J. Mater. Chem. A* **2019**, *7*, 1160–1167.
- [37] Z. V. Popovic, Z. Dohcevic-Mitrovic, A. Cros, A. Cantarero, *J. Phys. Condens. Matter* **2007**, *19*, 496209–496218.
- [38] F. Zhang, S. W. Chan, J. E. Spanier, E. Apak, Q. Jin, R. D. Robinson, I. P. Herman, *Appl. Phys. Lett.* **2002**, *80*, 127–129.
- [39] M. Mittal, A. Gupta, O. P. Pandey, *Sol. Energy* **2018**, *165*, 206–216.
- [40] S. Penner, D. Wang, B. Jenewein, H. Gabasc, B. Klötzer, A. Knop-Gericke, R. Schlögl, K. Hayek, *J. Chem. Phys.* **2006**, *125*, 094703–094715.
- [41] V. Perala, D. Devaiah, J. Deshetti, D. Mukherjee, V. Muga, B. M. Reddy, *Catal. Lett.* **2020**, *150*, 948–962.
- [42] D. Zhang, N. Yin, C. Jiang, B. Xia, *J. Mater. Sci. Mater. Electron.* **2017**, *28*, 2763–2768.
- [43] R. Prins, *Chem. Rev.* **2012**, *112*, 2714–2738.
- [44] Z. Weia, Y. Lib, J. Wangb, H. Lib, Y. Wang, *Chin. Chem. Lett.* **2018**, *29*, 815–818.
- [45] M. Kennema, I. B. Castro, F. Meemken, R. Rinaldi, *ACS Catal.* **2017**, *7*, 2437–2445.
- [46] C. Chen, P. Liu, M. Zhou, B. K. Sharma, J. Jiang, *Energies* **2020**, *13*, 846–859.
- [47] J. Donga, X. Wena, T. Zhua, J. Qina, Z. Wua, L. Chenb, G. Bai, *J. Mol. Catal.* **2020**, *485*, 110846–110854.
- [48] K. J. Betsy, A. Lazar, C. P. Vinod, *Nano-Struct. Nano-Objects* **2018**, *13*, 36–43.
- [49] S. Bin, C. Wen-wen, K. Qing-yang, *J. Fuel Chem. Technol.* **2015**, *43*, 1252–1257.
- [50] C. V. Rode, U. D. Joshi, O. Sato, M. Shirai, *Chem. Commun.* **2003**, *15*, 1960–1961.
- [51] M. Li, Y. Li, L. Jia, Y. Wang, *Catal. Commun.* **2018**, *103*, 88–91.
- [52] M. P. Wiesenfeldt, Z. Nairoukh, T. Dalton, F. Glorius, *Angew. Chem. Int. Ed.* **2019**, *58*, 10460–10476; *Angew. Chem.* **2019**, *131*, 10570–10586.
- [53] N. C. Nelson, J. S. Manzano, A. D. Sadow, S. H. Overbury, I. I. Slowing, *ACS Catal.* **2015**, *5*, 2051–2061.
- [54] G. Porwal, S. Gupta, S. Sreedhala, J. Elizabeth, T. S. Khan, M. A. Haider, C. P. Vinod, *ACS Sustainable Chem. Eng.* **2019**, *7*, 17126–17136.

Manuscript received: February 11, 2023
Revised manuscript received: April 16, 2023
Accepted manuscript online: April 24, 2023
Version of record online: May 2, 2023